THE SYNTHESIS, ELECTROCHEMICAL, SPECTROSCOPIC, AND PHOTOPHYSICAL CHARACTERISATION OF RUTHENIUM(II) POLYPYRIDYL COMPLEXES CONTAINING QUINONE/HYDROQUINONE MOIETIES.

By

Tia E. Keyes, G.R.S.C.

A Thesis presented to Dublin City University for the degree of Doctor of Philosophy.

Supervisor Dr. Johannes G. Vos.

School of Chemical Sciences
Dublin City University.

November 1994.

Dedicated to the memory of Da Murray.

This thesis is submitted in fulfilment of the requirements for Doctor of Philosophy by research and thesis. It not been submitted as an exercise for a degree at this or any other university . Except as otherwise indicated, this work has been carried out by the author alone.

Tia E. Keyes.

Acknowledgements

I would like to extend my sincerest thanks to my supervisor Dr. Han Vos for his encouragement and guidance over the past three years. His very generous assistance and huge patience in the final hectic preparations of this manuscript are greatly appreciated.

Sincerest thanks also are due to the other members of the Vos research group, Helen, Karen, Frances, Miriam, Dave, Margeret S., Noel and Andy for their friendship and support. Special thanks are due to Helen Hughes for her help early on and in particular for her crash course on instrumentation. Also thanks to Frances Weldon who kept me sane in the final hectic stages of putting this thesis together.

Thanks to my other fellow postgraduates for their friendship and encouragement, Mary P. Mary M., Fiona, Eithne, Pat, Mark, James, James, Shane, Cormack, Farmer, Ciaran, Margaret H. to name but a few. Thanks to the members of the Dr. Conor Long research group for their help with the laser, especially Conor himself, Mary P., Ciara, and Charley.

Thanks to the technical staff without whose support my work would have been impossible. Many thanks to Mick Burke, Paraic James and Damien McGuirk for their work on the nmr. Thanks to Prof. Albert Pratt for his discussion early on in my thesis on protecting groups, and also to Dr. P. Kenny for his advice, and also for some of the mass spectra reported here.

Thanks to the project students who helped me Andre, Stefan, and Jorn.

I wish to express my gratitude to those in The Queens University of Belfast from whom I received help and hospitality, Dr. J.J. Mc Garvey, Dr. Stephen Bell and Tanya Martin for the Raman spectroscopy. Prof. Ken Seddon , for his help on my co-crystals and molecular modelling, many thanks to both Prof. Seddon and Harvey for putting me up in Belfast and for all the cheese and soda farls. Thanks are also due to Dr. Francesco Barigelletti for his kindness during our stay in Italy.

Thanks to Forbairt for their financial support.

Finally thanks to my "non-chemical" friends, Gemma, Audrey, Fiona, Karen, Colette, Mark (of course) Niamh, Kieran and all the lads for their continued friendship and support over the years.

Most important of all, thanks to my Parents Kay and Emmet for their encouragement and support (financial and otherwise) down through the years and also to my grandparents.

Abstract.

The synthesis and characterisation of photophysical, electrochemical and photochemical properties of ruthenium(II) polypyridyl containing hydroquinone triazole or pyrazole moieties are described. The characterisations described involve, HPLC, ^{1}Hnmr, UV/vis/NIR spectroscopy, fluorimetry, electrochemistry, spectroelectrochemistry, laser flash photolysis, and resonance Raman spectroscopy.

In the main chapter of this thesis the investigation of a series of Ru(II) complexes bound to pyridyltriazole ligands bridged to pendent electroactive phenol, hydroquinone and quinone moieties is described. A novel synthesis for oxidation of the hydroquinone containing complex is described, employing benzeneselininc acid which, in a one pot reaction under very mild conditions, the hydroquinone may be completely oxidised without concomitant oxidation of the quinone. None of the complexes described exhibit intramolecular electron transfer from any of the electroactive groups under neutral conditions. This was associated with endoergonic ΔG values for intramolecular electron transfer in these complexes under neutral conditions. At high pH however, intramolecular electron transfer was observed in all complexes containing the electroctive aryl groups. This was associated with intramolecular hole transfer from the Ru(III)* to the phenolate, semiquinone or anionic hydroquinone formed from these ligands at high pH. This electron transfer is ranges around 2 x10^6 s-1 in neutral acetonitrile, it is therefore rather a slow transfer, however, the resulting charge separated state is stable over several microseconds. The electron transfer processes also persist at cryogenic temperatures, and outside the glass phase are largely temperature independent. These complexes were therefore described as simple abiotic models for photosynthesis, this is particularly the case for the hydroquinone containing complex, which also exhibits an electrochemically induced intramolecular proton transfer verified by electrochemical and spectroelectrochemical measurements.

In the second part of this thesis the synthesis and characterisation of mononuclear and dinuclear O,N coordinated Ru(II) complexes to hydroquinonepyrazole and phenolpyridyltriazole were described. The mononuclear complexes exhibit intense, broad range, visible absorbances, with λ_{max} tailing to 800 nm, they are photostable, luminescent and electroactive. Luminescence in complexes bound via O,N are normally rare.

The dinuclear O,N coordinated complexes produced stable mixed valence states. These mixed valence states exhibit class II behaviour, i.e. weakly coupled, electronic communication between the metal centres. This interaction is particularly weak in the complex bridged by the phenolpyridyltriazole, which shows an intervalence transition of unusually high energy. Most interestingly, this complex, which is luminescent in the (II)-(II) state exhibits increased luminescence in the mixed valence state, whereby it appeared that the unoxidised N,N coordinated side of this complex became isolated from the Ru(III)O,N side of the complex in the excited state.

Finally, a novel synthesis for the deuteration of bipyridyl was described, this synthesis is a one pot, high yield reaction, that was considerably easier than that available in current literature. The properties of complexes containing deuterated bpy are described and the value of employing deuteration as a means of ascertaining the position of the LUMO was discussed.

Table of Contents **Page**

Chapter 3 N,N coordinated complexes: The influence of substituted phenyl groups on the photophysical and photochemical properties of mononuclear Ru(II) complexes containing pyridyl-1,2,4-triazole ligands.

Chapter 4 O, N coordinated complexes: Mononuclear Ruthenium (II) complexes bound via O and N to phenolpyridyltriazoles and hydroquinone pyrazole ligands.

Chapter 5 O,N coordinated complexes: Dinuclear complexes O, N bound to symmetric hydroquinone pyrazole ligands and asymmetric phenolpyridyl ligands.

Chapter 6 The influence of bipyridyl deuteration on the excited state properties of Ru(II) polypyridyl mixed ligand complexes.

Chapter 1

Introduction.

1.1 General introduction.

The earth only intercepts a small portion of the total radiative energy produced by the sun, yet over a period of one year the earth receives approximately 1.3 x 10^{16} joules of solar energy per square mile [1]. Considering the total surface area of the earth this means that this energy exceeds the total present requirement by over 50,000 times. With this in mind researchers over the last 25 years have made a concerted effort at determining a means of harnessing this potent natural resource. One of the most interesting possibilities lies in the complex physiophotochemical process of photosynthesis, whereby a means of mimicking the unit functions of this process is sought. The common aim of such work is the creation of an antenna device capable of fulfilling the same role as the chlorophyll photosensitizers, that is, light absorption over a wide visible spectrum range ultimately leading to efficient charge separation. There have emerged two approaches to this problem, the first is the creation of "biomimetic" species which as the name suggests involves molecular assemblies of structure reminiscent of that found in nature, for example, the porphyrins, carotenoids and quinones [2]. The second approach deals with assemblies comprised of "abiotic" units the biggest success story of which has been the ruthenium-polypyridine chromophores, which this report deals with in the form of the $Ru(bpy)_2$ unit, which itself has provided the basis for a myriad of diverse photoactive complexes.

1.2 Photochemical molecular devices and supramolecular assemblies.

A photochemical molecular device is defined as an assembly of molecular components capable of performing light induced functions, such as vectorial electron transfer, migration of electronic energy, and switching on/off of receptor ability. Such complex functions require a complex array of multifunctional components, a supramolecular structure for example. Such complex multifunctional devices exist in nature, the obvious example being the photosynthetic machinery in certain bacteria or the more complex case of green plants [3]. The increasing interest in development of means of artificially replicating photosynthesis, or creating other optically electronic materials for example, photosensitive receptor molecules which may be used as substrate selective optical signal generation [4], has resulted in unprecedented growth in the area of "supramolecular photochemistry" [5-8].

1.2.1 PMDs capable of light induced electron and energy transfer.

The microstructure of the photosynthetic membrane generates vectorial electron transfer along an organised chain of relays that rapidly transfer the photoexcited electron to the ultimate acceptor and a stable charge separated state. Some of the microstructural functions of the photosynthetic apparatus may be simulated by supramolecular assemblies.

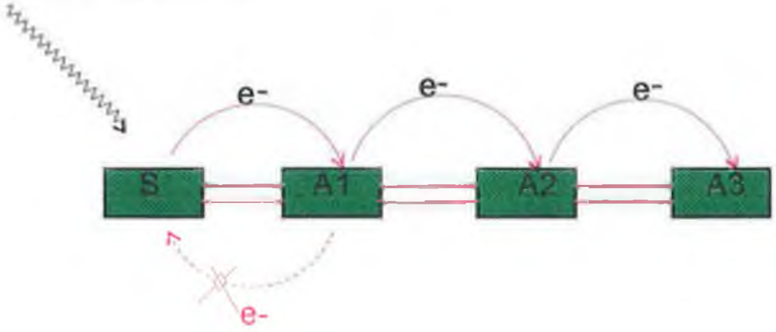

Figure 1: Assembly model exhibiting vectorial electron transfer.

Figure 1.1 shows an assembly model for light energy conversion, this consists of a sensitizer species S, possessing suitable redox, ground and excited state properties, linked to a series of relay species, i.e. a series of electron acceptors A_X along a redox gradient. Following sensitization via light absorption, an electron is transferred from the excited sensitizer to the relays until charge separation has been accomplished via oxidation of the sensitizer and reduction of the final acceptor. Such vectorial electron transfer has been accomplished in artificial molecular assemblies such as triad porphyrin quinone and quinone-porphyrin-carotenoid supramolecules [9,10]. Such assemblies consist of the three fundamental components of a photochemical molecular device (PMD), these are, the active components, which in photoinduced electron transfer machinery are the sensitizer, the donor and acceptor moieties. The perturbing components, used to modify the properties of the active components, such as substituents on the active components, or spectator ligands in metal complex assemblies. Finally, connecting components, these connectors may take no active part in the transfer process but must be conducive to electron transfer, in other words they must produce a certain degree of orbital continuity to the assembly between active components as well as possessing the correct structural attributes. Design of a supramolecular assembly which may act as a PMD requires careful choice of active and connecting components, since vectorial electron transfer requires the correct "downhill" progression of redox potentials to prevent charge recombination, but also more subtle considerations such as spatial arrangement of components and distances separating donor and acceptor [11] are important in determining the degree of efficiency of electron transfer.

During the course of the last decade, two approaches have emerged for imitation of the photosynthetic process. The first is a bio-mimetic strategy, in which the molecular components of the supramolecular assembly are structurally reminiscent of those found in nature. The most important example of such an approach is the multi-functional porphyrin based compounds [12-15]. Probably the foremost exponents of this approach have been Gust and Moore, who produced the prototypical quinone-porphyrin-carotenoid triad shown in figure 1.2 in 1984 [12].

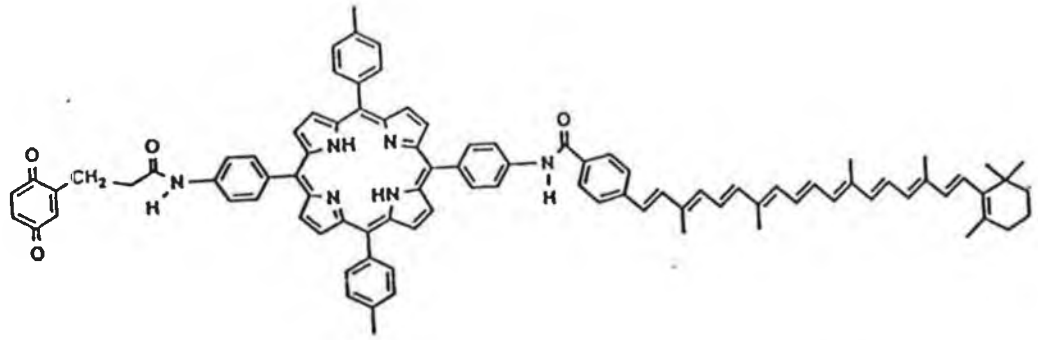

Figure 1.2 Structure of the quinone-porphyrin-carotenoid triad investigated by Gust and Moore [12].

This structure proved capable of photo-induced electron transfer and creation of a relatively stable charge separated state. Since the creation of this triad there have been many spectacular synthetic successes in developing porphyrin compounds which exhibit increased efficiency of photoinduced charge separation. The most important has been the multi-metallo-porphyrins [13], which have shown impressive charge separation properties. A particularly distinctive set of poly-porphyrin are the entwined bisporphyrins. Sauvage and co-workers for example produced an assembly involving two identical zinc/gold bisporphyrins assembled into a tetramer by coordination of the pendent 1,10-phenanthroline moieties to a Cu(II) cation [14]. This biomimetic assembly exhibits rates of electron transfer to charge separation of 3.33×10^{11} s^{-1}, which considerably exceeds that of the single unentwined bisporphyrin. Charge recombination occurs at 1.1×10^{9} s^{-1} since the copper complex mediates the forward transfer but not the reverse, thereby stabilising the charge separated state.

The second approach is abiotic whereby reproduction of some of the unit functions of the photosynthetic process are attempted in deliberately abiological species. This area is expansive, ranging from the use of PMDs containing multi component systems consisting of small organic chromophores such as the early examples of charge separation exhibited by J.W. Verhoeven and coworker's carbazole/tetrachlorophthalimde pair [15]. Microheterogeneous assemblies containing organic macrostructures such as micelles [16] or polymers [17,18] bound to photoactive components. Such systems show increased rates of electron transfer and charge separation which is associated with slow back-transfer as a result of isolation of the charge separated species after transfer to different regions of the assembly. One of the most interesting examples of this behaviour was demonstrated by Ottolenghi and coworkers where incredibly long lived charge separation was achieved on this basis. Whereby pyrene (donor) and methylviologen (acceptor) were immobilised in a sol-gel matrix and employing a mobile charge carrier, N,N'-tetramethylene-2,2'-bipyridinium bromide, electrons were shuttled between the donor/acceptor in the glass resulting in redox photoproducts which were reported to stable over a remarkable 4 hours [19].

Since this thesis encompasses only the area of Ru(II) chemistry, supramolecular systems based on this and other transition metals are of greatest relevance. The approach to the problem of designing photoactive PMDs based on transition metal complexes is based on the linking of a photoactive centre to a donor and acceptor group via a spacer. A frequent manifestation of this system is where the photoactive species plays the dual role of chromophore and terminal donor or acceptor. The choice of donor and acceptor will, as was described, be dictated by the redox potentials of these species. For kinetic reasons the energy of the ultimate charge separated state should be as high as possible, as long as this is compatible with the considerations involving the spectral properties of the photoactive centre. In order to ensure slow back electron transfer, this transfer should occur in the Marcus inverted region (see section 1.6). Some very interesting assemblies involving the

$Ru(bpy)_2$ chromophore have been produced which have shown promising results in the regions of vectorial electron and energy transfer. One of the earliest cases of a chromophore quencher assembly of this type was produced by Sprintschnick and coworkers in 1978 [20], where a methylviologen-based moiety is coordinately linked to a Re(I) or Ru(II) complex (see figure 3). Electron transfer occurs between the ^{3}MLCT state of the rhenium/ruthenium chromophore and the pyridinium acceptor unit, demonstrated by the occurrence of a short-lived, red shifted emission from the complex at room temperature.

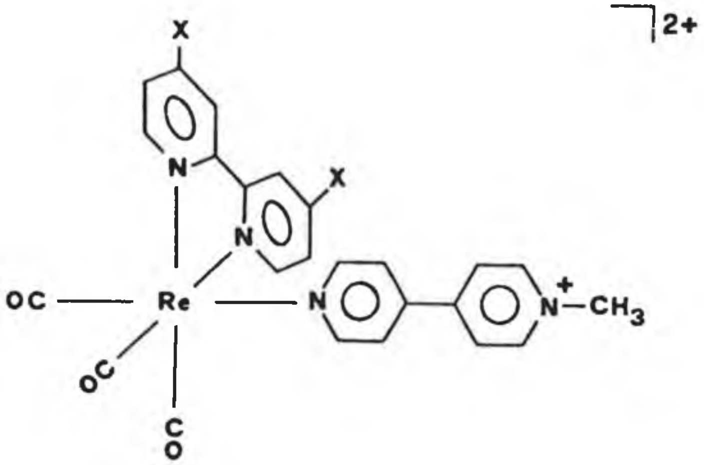

Figure 3 Schematic structure of $[Re^{(I)}(4,4'\text{-}X_2\text{-}bpy)(CO)_3(MQ^+)]^{2+}$ *[20].*

Since then there have been a myriad of such assemblies involving covalently linked $Ru(bpy)_2$ and diaquat complexes, exhibiting varying degrees of electron transfer [21-25]. In addition there have been reports of triad systems in which the ruthenium polypyridyl chromophore is linked directly to both donor and acceptor species. An example of this type of device was produced by Meyer and coworkers in 1987 [26], in which the electron acceptor (viologen)and acceptor (phenothiazine) are covalently linked to the chromophoric $Ru(bpy)_3$ unit. Charge separation in this device was found to last to up to 165ns.

Finally, as a result of the development of the "complexes as metals" and "complexes as ligands" synthetic strategy developed over the last few years mainly by the Italian group under V. Balzani, multinuclear systems have been developed which show promise as devices capable of light induced directional electron and energy transfers. Employing this synthesis complexes containing up to 13 metal centres have been produced [27], and it would appear that there is little limit to the size these complexes can ultimately be. These polynuclear complexes exhibit intense visible absorbance, they are luminescent in both fluid and rigid matrices, and they exhibit a rich electrochemistry. Most importantly, the lowest energy excited state can be controlled synthetically by the nature of the metal or complex employed in a particular building block. Exoergonic energy transfer between metals which share the same bridging unit takes place in these compounds with 100% efficiency [28]. Direction of electronic energy transfer can be completely controlled in these complexes by judicious choice and positioning of chromophoric, luminophoric and redox centres in these compounds.

1.2.2 Photochemically induced water cleavage.

The ultimate aim in the design of assemblies capable of efficient light induced charge separation is the implementation of these units into catalytic molecular apparatus capable of photocleavage of water into O_2 and energy rich H_2. The theoretical approach for achieving this is based on mimicking some of the unit functions of photosynthesis. Water is transparent in the visible region of the spectrum, to wavelengths greater than 185 nm. The aim therefore is to the trap solar radiation in the wavelength region where it is most intense by employing an appropriate antenna molecule, and transmit this energy to water cleavage. In photosynthesis this sensitiser is a group of pigments collectively known as chlorophyll.

The process of photocleavage of water may be described in 4 steps by a flow diagram as in figure 4.

The primary step, as in photosynthesis is photoabsorption whereby the sensitiser S becomes electronically excited.

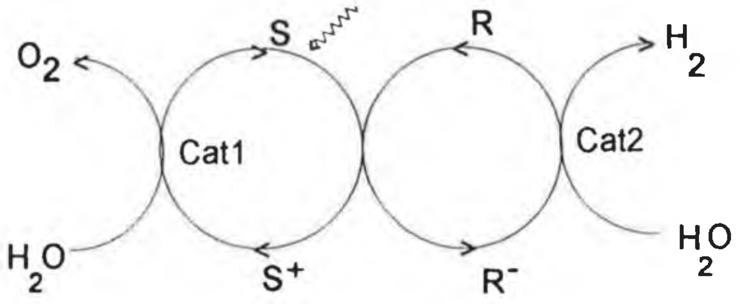

Figure 1.4. Cyclic water photocleavage[18].

The excited state of S is then quenched by electron transfer to a relay of acceptors in a charge separation process exactly as described in figure 1.4. The relay then passes the electron to a suitable catalyst capable of decomposition of water. The final step involves actual decomposition of water.

These processes may be described by the equations 1.1 -1.4

$$S \rightarrow S^* \qquad (1.1)$$

$$S^* + R \rightarrow S^+ + R^- \qquad (1.2)$$

$$2R^- + H_2O \rightarrow 2R + H_2 + 2OH^- \qquad (1.3)$$

$$4S^+ + 2H_2O \rightarrow 4S + O_2 + 4H^+ \qquad (1.4)$$

The success of a potential apparatus will depend on:

1. The selection of a suitable photosensitiser, possessed of broad range of visible absorbance and the correct redox properties in the excited state.
2. Efficient electron transfer leading to a stable charge separated state, with suppression of reverse electron transfer.
3. Continual "dark" redox reactions leading to the decomposition of water.

4. Continuous renewal of both sensitiser and relay (quenching) molecules to their original oxidation states.

Over the last decade a number of model systems have been proposed along these lines. Mainly they have been of three types

(a) Homogenous assemblies relying on liquid/liquid interfaces, such as micelles [29] or vesicles [30].

(b) Heterogeneous systems consisting of combinations of suspended sensitizer and n-type semiconductors loaded with catalyst [31].

(c) Heterogeneous systems relying on band gap excitation of an n-type semiconductor [32].

Employing $[Ru(bpy)_3]^{2+}$ as sensitiser for reasons that will be discussed in section 1.4, as early as 1975 Creutz and Sutin [33] revealed that the excited state of $[Ru(bpy)_3]^{2+}$ is capable of pH dependent reduction of water to dihydrogen. They suggested that photodecompostion of water might be accomplished by exposing an n-type semiconductor connected to electrodes immersed in a buffered solution of $[Ru(bpy)_3]^{2+}$ to light. The electrons injected into the conduction band of the semiconductor would then pass to the working electrode and effect the reduction of water.

The first successful operation of a complete water cleavage cycle employing $[Ru(bpy)_3]^{2+}$ was achieved by Graetzel and coworkers in 1981 [34]. Employing $[Ru(bpy)_3]^{2+}$ as sensitiser and methylviologen as electron relay, light induced injection of electrons into the conduction band of RuO_2 doped TiO_2 catalysed water oxidation. Although this process was inefficient it paved the way to further attempts to optimising the systems employing ruthenium polypyridyl sensitizers. This has lead to the production, by the Graetzel group, of a photovoltaic cell of conversion efficiencies that may be commercially viable [35]. The cell, a nanocrystalline dye sensitized solar cell consists of a condutive (SnO_2) glass slide on which nanometer sized particles of TiO_2 are deposited. The TiO_2 surface is made highly porous by heating and the glass is then dipped into a solution of dye molecules. A monolayer of dye covers the glass through bonding of the dye to the titanium via carboxylate bonds. The dyes employed are in general complexes of $Ru(dcbpy)_2$ (where dcbbpy =2,2'-bipyridine-4,4'-dicarboxylic acid. An electrolyte containing I^- is added to the film where it permeates the membranal pores. A conductive glass coated with Pt or carbon is placed under the dye coated glass as a counter electrode. The cell is illuminated as shown it figure 1.5.

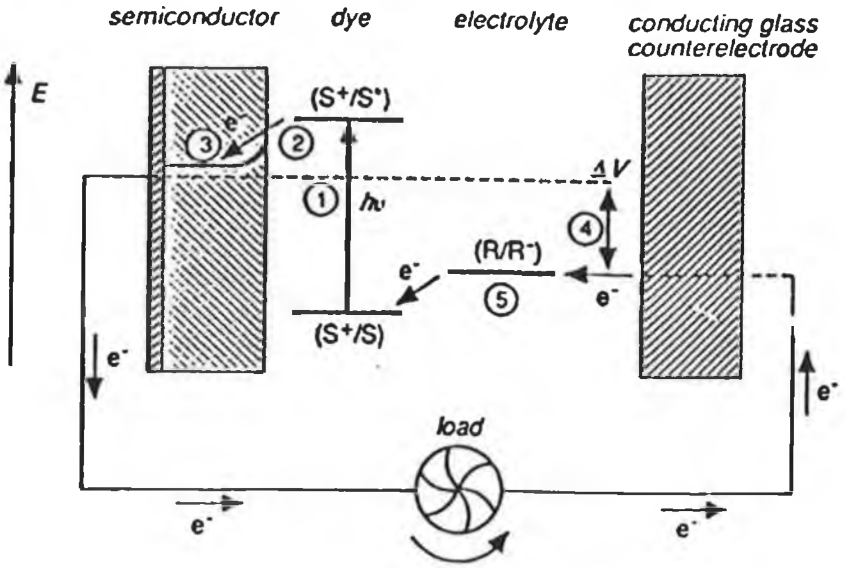

Figure 1.5. Schematic representation of the nanocrystalline dye sensitized solar (Graetzel) cell [35].

The cell operates when light excites the dye and causes electrons to be injected directly into conduction band of the TiO_2 layer. To complete the circut, the electrons lost by the dye to the semiconductor must be regenerated by electron transfer from the iodide species which is itself rereduced at the counter elctrode.

This cell has been shown to possess an overall sunlight to electrical energy conversion of 6-7% in direct sunlight or 11-12% efficiency in diffuse daylight [35]. This implies this device is cheap and easily assembled, it has solar conversion efficiencies approaching those of more conventional solar cells (10-15%).

1.3 Photosynthesis, the ultimate PMD.

1.3.1 General outline of photosynthesis.

Nature has, with the help of evolution, developed a complex series of devices capable of producing the most efficient conversion of electromagnetic to chemical energy.

Photosynthesis may be simplisticly defined by the equation (1.5);

$$6CO_2 + 6H_2O + \text{chlorophyll} + \text{light} \rightarrow C_6H_{12}O_6 \text{ (glucose)} + 6O_2 \quad (1.5).$$

This describes one of the most fundamental processes in the sustainment of life on this planet, since it describes the origin of the food chain from which all living matter either directly or indirectly derives nutrition. Photosynthesis occurs in two discrete phases:

1 Light reactions, where light energy is trapped and employed to generate energy rich ATP (adenosine trineucleotide phosphate) and biological reducing agent NADPH (nicotinamideadenine dincleotide phosphate).

2. Dark reactions, where the reactive intermediates ATP and NADPH are active in the synthesis of carbohydrate from H_2O and CO_2 in what is known as the Calvin cycle. These dark reactions, as the name would suggest, are light independent processes.

In eukaryotes these processes occur in different parts of the cell, the light reactions in the chloroplast and the dark reactions in the stroma. In such species as green plants and cyanobacteria, the light reactions may be further divided into two classes; photosystem I (PSI) in which $NADP^+$ is reduced to NADPH and photosystem II (PSII) in which water is oxidised to produce molecular oxygen.

In prokaryotes, which lack chloroplasts the light reactions occur in the cells plasma or in vesicles called chromatophores.

1.3.2 Elucidation of the mechanism of light absorption and charge separation in purple bacteria.

Two main classes of organism perform photosynthesis, those that evolve oxygen and those that do not, green plants occupy the former classification and photosynthetic bacteria the latter, which is the simpler, better understood mechanism, details of which have emerged over the past two decades [36].

From these studies, strong similarities have been perceived between the structure and operation of the reaction centres of, in particular the photosynthetic purple bacteria (Rb. sphaeroides) and photosystem II in green plants [37]. It is from these two reaction centres related by the evolutionary chain, that the inspiration has come in the development of molecular devices capable of sensitization leading to efficient charge separation, and ultimately the photochemically induced splitting of water [38].

The primary process in the reaction centres of bacteria and PSII is transmembranal charge separation, as in figure 1.6.

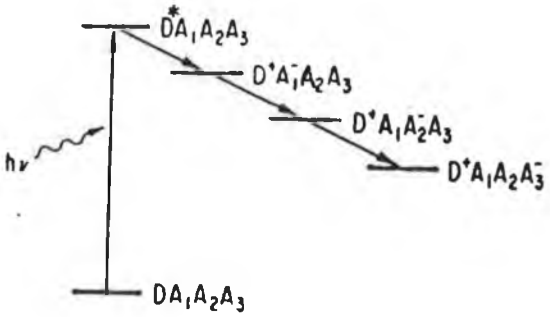

Figure 1.6. Schematic representation of the initial charge separation process in the photosynthetic bacteria, where D = photoactive donor (e.g. chlorophyll), A = acceptor species (e.g. quinone) [36].

These processes will be described concentrating on the reaction centre of purple bacteria, though the same arguments with small modifications are applicable to PSII and other bacteria. The centre consists of a membrane protein containing three subunits titled L, H, and M, plus the following co-factors, four bacteriochlorophyls two bacteriophaeophytons, two quinones, ubiquinones in purple bacteria menaquinones in other species [3], and one high spin non-haem Fe^{2+} figure 1.7.

It was established [39, 40, 41] that the primary donor is a bacteriochlorophyll dimer $(Bchl)_2$, the primary and secondary acceptors are the quinones, Q_A and Q_B, transient intermediate acceptor is the bacteriophaeophyton (Bph). Figure 1.8 depicts the cycle occurring whereby light absorption excites the primary donor dimer $(Bchl)_2$ to $(Bchl)_2^*$, this process is followed by a rapid (10^{10} s^{-1}) electron transfer to the transient intermediate acceptor (Bph) which rapidly transports the electron on to the ubiquinone acceptor Q_A and finally on to Q_B, when charge separation has been accomplished. Electron transfer in photosynthetic reaction centres is stabilised against energy wasting charge recombination for successively long periods via the electrochemical gradient existing between the acceptor species. Subscripts A and B refer to the branches of the reaction centre. Branch B mainly appears to be redundant in the electron transfer process, the reason for this is unclear but it is thought that this side of the redox chain is simply an evolutionary artefact [42], why electron transfer occurs preferentially in chain A is also unknown.

The outcome of the electron transfer steps is, as mentioned, a relatively stable charge separated state with an electron carried on an anion radical $Q_B{\cdot}^-$ and a hole carried on the primary donor dimer $(Bchl)_2$. This hole carrying dimer then proceeds to be reduced by cytochrome c, in order to reinitiate the cycle, and $Q_B{\cdot}^-$ is reduced to its corresponding quinol Q_BH_2, consuming a H^+ which has been transferred across the membrane, this quinol is then exchanged via transmembranal migration with an externally oxidized quinone, the time scale of the entire operation is 1 ms.

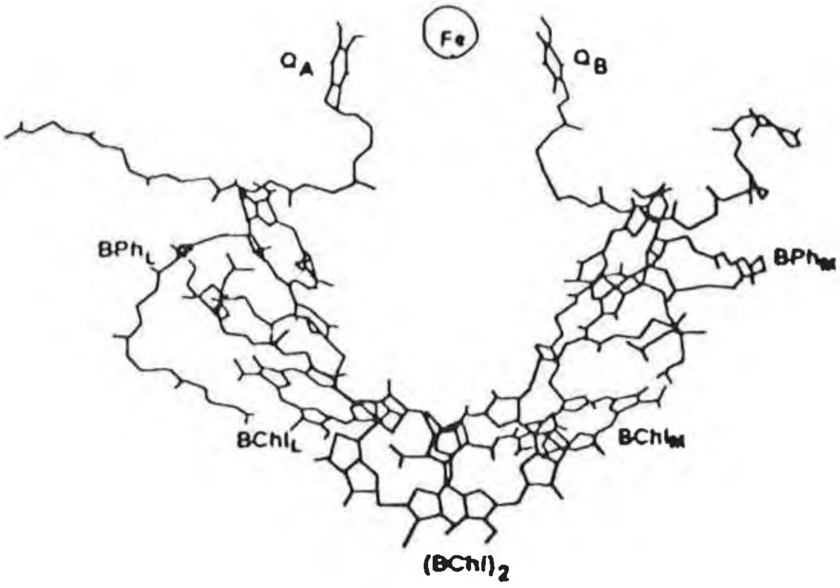

Figure 1.7. Reaction centre of photosynthetic bacteria [3]

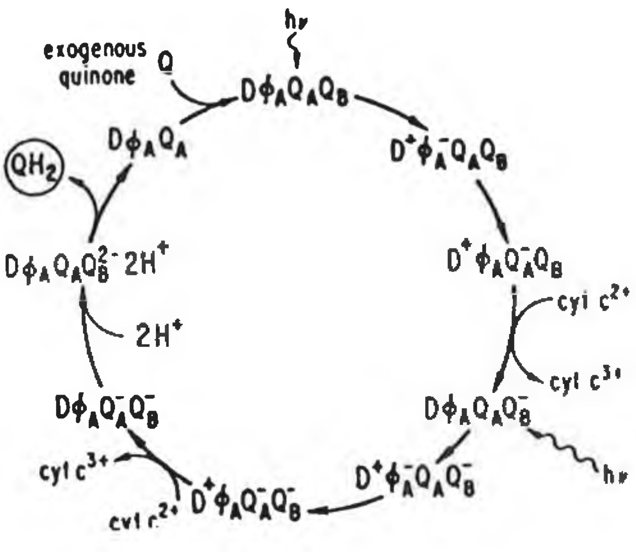

Figure 1.8. Photosynthetic reaction cycle [44].

The quantum yield of the photosynthetic reaction centre is approximately unity, the unidirectionality of the electron transfer is still not well understood from a thermodynamic and kinetic stance, however it is understood to be closely associated with the spatial distribution of the components in the protein matrix [43-45]. This provides intriguing problems for those investigating such relations, and as more is discovered about the influence of various parameters in the photosynthetic device, valuable information is provided for those seeking to obtain vectorial electron transfer and stable charge separation in synthetic analogues of the photosynthetic reaction centre.

The transmembranel exchange of quinol for quinone is a vital step necessary to establish the correct proton gradient for ATP generation, which is a proton catalysed redox process, the mechanism of which is still the subject of much debate [5]. The cyclic electron transfers that constitute photosynthesis operate as part of protonmotive machinery, so that the net result is the formation of a stable difference in the electrochemical potential of the protons on either side of the membrane, it is this potential that is used to drive the ADP ---> ATP reaction. Establishment of this potential is achieved by the flow of electrons in the redox processes which creates an electronic field which in turn polarizes the membrane and a pH gradient is produced across both sides of the membrane see figure 1.9.

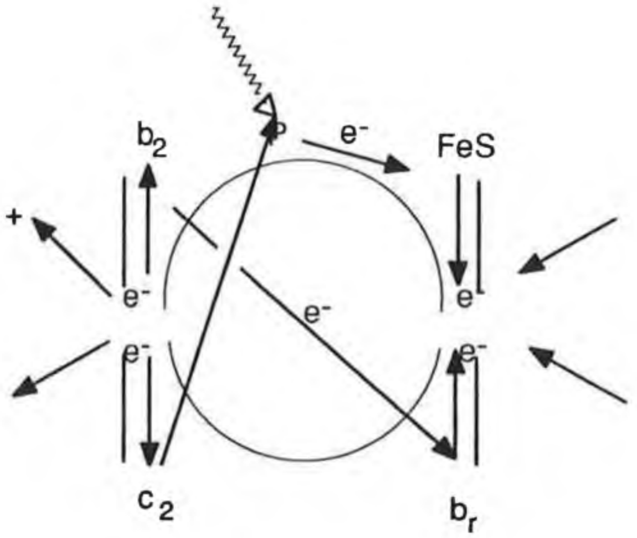

Figure 1.9. Schematic representation of the protonmotive function of the bacterial cytochrome b-c_2 [20].

The pH gradient is a direct result of the transmembranel movement of protons involved semiquinone reduction whereby the proton is abstracted from the aqueous media outside the reaction centre membrane decreasing the pH inside the membrane and increasing pH outside [20]. The replacement of the quinone after reduction is dependent on the movement of protons across the protein residues since the Qb may not detach from the B chain until it is protonated. The mechanism by which the proton transfers to the reduced quinone is not completely understood, but a model was proposed by J.P. Allen and coworkers [21]. This suggests that the protons are transferred from the external aqueous media to the $Q_B{\cdot}^-$ via a chain of protonatable residues, a biochemical pass the parcel. The reaction centre shows two chains of residues that could conceivably form H^+ bridges from the semiquinone to the outside.

1.4 $[Ru(bpy)_3]^{2+}$ the archetypal photosensitizer.

1.4.1 Spectroscopic and photophysical properties of $[Ru(bpy)_3]^{2+}$.

$[Ru(bpy)_3]Cl_2$ was first reported as luminescent in 1959 by Paris and Brandt [46] and since then this molecule has become the building block for an ever expanding array of photoactive molecules of dilating complexity [47].

This prototypical status of $[Ru(bpy)_3]^{2+}$ has arisen out of its unique photophysical and photochemical properties. The absorption spectra of polypyridyl complexes of ruthenium are dominated by a metal to ligand charge transfer (MLCT) band in the visible region [48], as in figure 9.

This corresponds to the following transition

$[Ru(bpy)_3]^{2+}$ -------- $[(bpy)_2Ru^{III}(bpy\cdot^-)]^{2+}$

which is largely singlet in character [49], and is ligand localized on the resonance raman time scale [50]. The absorption band has been analysed statistically into four Gaussian components [51] (figure 1.10). Component Q is attributed to the weak, forbidden ^1d-$^3\pi^*$ transition. No d-d transitions have been assigned, being of low extinction coefficient they are probably obscured by the intense charge transfer bands. Intersystem crossing between ^{1}MLCT and ^{3}MLCT is rapid, estimated to be 5×10^{-10} s^{-1} [52], with an efficiency of unity [39]. Intraligand transitions dominate the UV region of the $[Ru(bpy)_3]^{2+}$ spectrum, intense bipyridyl π–π^* absorbances lie around 185 and 285 nm.

The emission band of $[Ru(bpy)_3]^{2+}$ is assigned as a spin forbidden charge transfer [54], i.e. a phosphorescence from the ^{3}MLCT or $^3d\pi^*$ state, see figure 9. Although long lived (> 0.6 μs in deareated solution [55]), the lifetime of $[Ru(bpy)_3]^{2+}$ is short for a phosphorescent emission and this is associated with heavy atom perturbation of the emitting triplet state. The emission band in $[Ru(bpy)_3]^{2+}$ consists of three closely spaced levels ($\Delta E = 61$ cm^{-1}) in thermal equilibrium. Studies involving resonance

Raman spectroscopy, [56] and E.S.R. [57], suggest strongly that the excited electron in ^{3}MLCT is localized (in fluid media, in rigid media the results are quite different, see chapter 6) on a single bpy moiety on the vibrational timescale. Results from resonance Raman spectroscopy are consistent with the reduction of the symmetry of the complex from D_3 to C_2V. The electron is presumed to reside on the bipyridyl ligand which from electrochemical studies is observed to be most easily reduced, (the LUMO), creating a localised excited state $[Ru^{III}(bpy)_2(bpy^{\cdot -})]^{2+}$ [58, 59]. After intersystem crossing (ISC) deactivation to the ground state may occur by emission or a radiationless transition.

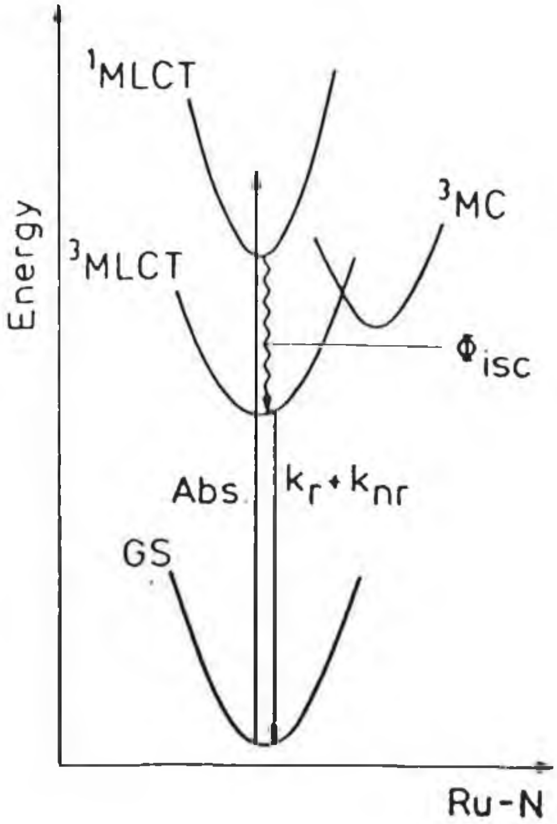

Figure 1.10 Schematic representation of the photophysical pathways of [Ru(bpy)$_3$]$^{2+}$.

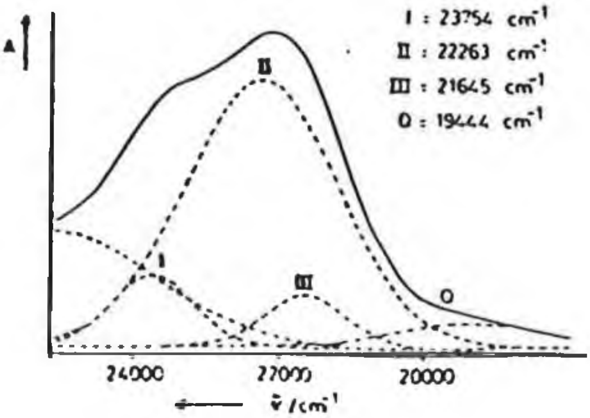

Figure 1.11 Statistical analyses of ^{1}MLCT absorbance of [Ru(bpy)$_3$]$^{2+}$ [63].

One possible route for this radiationless deactivation is thermal population of the triplet metal centered state ^{3}MC ($^3e_g^*$) state (figure 1.10). This state is strongly distorted with respect to ground state nuclear geometry, and on population depletes the emission quantum yield by causing rapid radiationless decay, or more destructively, photodecomposition via cleavage of the Ru-N bond which in the presence of a coordinating species such as Cl^- or NCS^- anions, leads to photosubstitution. Radiationless decay from the ^{3}MC state is rapid despite its triplet state since these are metal centered orbitals and are hence strongly influenced by spin-orbit coupling. The ligand dissociation reactions of $[Ru(bpy)_3]^{2+}$ [60, 61, 62] are a dominant in the photochemistry of this complex yielding quantum yields of photosubstitution as high as 1×10^{-3} [60]. This was a major drawback in their use as photosensitizers, although the Graetzel photovoltaic cell has reduced the need for photostability in its sensitiser [35].

1.4.2 Redox properties of $[Ru(bpy)_3]^{2+}$.

Electrochemistry of ruthenium polypyridyl complexes can provide valuable information on the redox orbitals of a particular electrogenerated species. Collective use of both electrochemistry and spectroscopy can yield a very detailed diagnosis of the orbital nature of the excited state of a complex. Ruthenium is richly endowed with redox orbitals and correspondingly possesses a large number of oxidation states, as many as 10 are known [63], between -2 and +8, with the exception of -1. Electrochemical electron transfer will occur at a coordinated ligand when the ligand possesses one or more low lying unoccupied orbitals for reduction and one or more occupied orbitals of intermediate stability for oxidation, the bipyridyl ligands possess the former. These unsaturated ligands possess unoccupied π^* orbitals making them useful candidates for electrochemical activity. Bipyridine is capable of the following oxidation states, bpy^{2-}, $bpy^{\cdot -}$, bpy and $bpy^{\cdot +}$, the two middle members of this group are those most commonly accessible in normal potential ranges, and are most important in the redox series of $[Ru(bpy)_3]^{2+}$ [64]. In non-aqueous aprotic solvent such as DMF or acetonitrile, four successive reversible one electron waves are observed in the cyclic voltammogram of $[Ru(bpy)_3]^{2+}$. The wave at anodic potential ($E_{1/2}$ = 1.32V vs SCE), corresponds to the metal centred oxidation involving the $\pi_m(t_{2}g)$ orbital [65],

$$[Ru(bpy)_3]^{2+} \rightleftharpoons [Ru^{III}(bpy)_3]^{3+} + e^- \qquad (1.6)$$

and the three couples at cathodic potentials corresponding to [65],

$$[Ru(bpy)_3]^{2+} \rightleftharpoons [Ru(bpy)_2(bpy^{\cdot -})]^{+} \rightleftharpoons [Ru(bpy)(bpy^{\cdot -})_2] \rightleftharpoons [Ru(bpy^{\cdot -})_3]^{-} \qquad (1.8)$$

In the excited state the $[Ru(bpy)_3]^{2+}$ becomes both a stronger oxidant and reductant, and as mentioned, there is an established correlation between electrochemistry and electronic spectroscopy for these complexes [66, 67]. The basis for such correlations is derived from the fact that the lowest energy MLCT transition involves the promotion of an electron from a metal centred π_M orbital to the lowest antibonding "spatially isolated" ligand centered πl^* orbital which bears strong resemblance to the lowest π^* orbital of the free ligand. The metal centered and ligand centered orbitals involved in these charge transfer transitions are also involved in the oxidation and reduction process of the molecule. This correlation is described by an orbital diagram in figure 1.12.

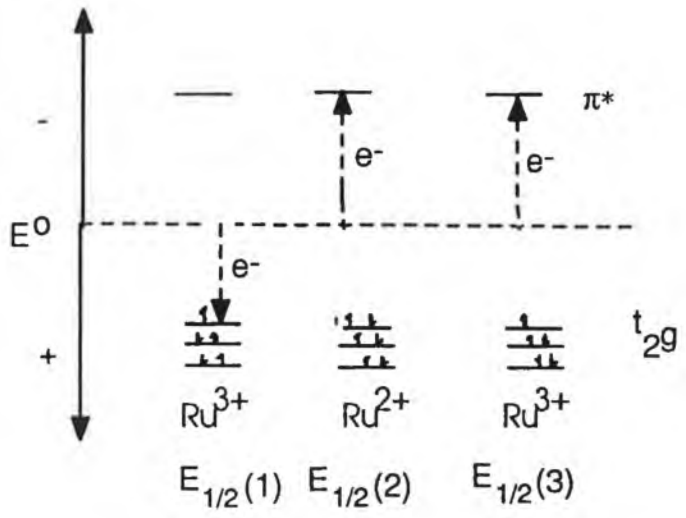

Figure 1.12. Schematic representation of the relation ship between electronic and redox orbitals in $[Ru(bpy)_3]^{2+}$.

The excited state redox potentials may be estimated from a knowledge of ground state redox potentials and the energy of the lowest triplet state $E^{(o\text{-}o)}$, i.e. the emission energy, from [68] Ru(II)*,

$$E^o(Ru^{II*/I}) = E^o(Ru^{II/I}) + E^{(o\text{-}o)} \qquad (1.9)$$

$$E^o(Ru^{III/II*}) = E^o(Ru^{III/II}) - E^{(o\text{-}o)} \qquad (1.10)$$

From these values the efficacy of the complex as reductant or oxidant in excited state can be determined. For $[Ru(bpy)_3]^{2+}$ the Ru*(III)/(II) potential is -0.84V and Ru* (II)/(I) is 0.84V [69], providing this complex with the correct excited state redox properties to oxidise or reduce water, although kinetically, this process would be slow.

In view of these large excited state redox potentials and the fact that $[Ru(bpy)_3]^{2+}$ possess a long-lived excited state, the complex may participate in a range of bimolecular redox or energy transfer processes.

$$*[Ru(bpy)_3]^{2+} + Q \xrightarrow{kq(ox)} [Ru(bpy)_3]^{3+} + Q^- \quad (1.11)$$

$$*[Ru(bpy)_3]^{2+} + Q \xrightarrow{kq(red)} [Ru(bpy)_3]^{+} + Q^+ \quad (1.12)$$

$$*[Ru(bpy)_3]^{2+} + Q \xrightarrow{kq(E)} [Ru(bpy)_3]^{2+} + Q^* \quad (1.13)$$

Where (1.11) represents oxidative quenching, (1.12) reductive quenching, and (1.13) energy transfer. The bimolecular quenching of the excited state of $[Ru(bpy)_3]^{2+}$ has been extensively studied employing such quenching agents metals Eu^{3+} [70] and Cr^{2+}, amines [71], quinones [72], and particularly paraquats such as methylviologen [73].

1.4.3 Temperature dependent lifetimes and photosubstitution processes in $[Ru(bpy)_3]^{2+}$.

Luminescent decay of excited states is a competitive process whereby the quantum yield of emission is actually a measure of the fraction of excited state which undergoes luminescent decay.

$$\Phi_r = k_r / k_r + k_{nr} \qquad (1.14)$$

where k_r is the radiative decay rate, k_{nr} the non-radiative decay rate and Φ_r the quantum yield of emission. This may be related to the lifetime of luminescence, which in

$$\frac{1}{\tau} = k_r + k_{nr} \qquad (1.15)$$

$[Ru(bpy)_3]^{2+}$ shows strong temperature dependence, $1/\tau$ may therefore be expressed as the sum of temperature dependent and independent terms, i.e.

$$\frac{1}{\tau} = k_o + \sum_i k_{nr}(T) \qquad (1.16)$$

where k_{nr} is associated with an Arrhenius activated surface crossing between states (1.17);

$$k_{nr} = A \exp^{-\Delta E/RT} \qquad (1.17)$$

where A and ΔE correspond to the preexponental factor and activation energy for surface crossing respectively.

With inclusion of the vibrational modes critical for k_{nr} that are restricted in frozen or very viscous media at low temperature (1.18) applies.

$$k_{nr} = \frac{B}{1 + \exp[C(1/T - 1/T_B)]} \qquad (1.18)$$

T_B is the temperature centered around the step associated with melting of the frozen matrix, C is related to the smoothness of this step, and B is the value attained k at T >> T_B. Temperature dependent studies of $[Ru(bpy)_3]^{2+}$ reveal the luminescence of this complex originates from 3 close lying ^{3}MLCT states in Boltzmann equilibrium [74-76]. For $[Ru(bpy)_3]^{2+}$ a plot of ln $1/\tau$ vs 1000/T reveals a strong temperature dependent behaviour, with luminescence lifetime decreasing with increasing temperature [77]. This behaviour is particularly prevalent at temperatures above 250K. This has been related to activated surface crossing between ^{3}MLCT and ^{3}MC. Such a process has significant photochemical ramifications, since as described it may lead to cleavage of the Ru-N bond. Detailed photochemical studies reveal that this is indeed the case, since in chlorinated solvents in the presence of ligating species the complex undergoes photosubstitution. The pathway for this reaction has not been unequivocally elucidated but is thought to proceed according to the scheme in figure 1.13 [78, 79]. Thermally activated formation of a d-d state leads to Ru-N cleavage resulting in the formation of a 5-coordinate square pyramidal intermediate. In the absence of a ligating species this will return to the starting compound. When ligating anion is present formation of a monodentate intermediate occurs which eventually leads to loss of this bpy and formation of $[Ru(bpy)_2X_2]$. Alternatively a "self-annealing" process may occur resulting in reformation of $[Ru(bpy)_3]^{2+}$.

Although $[Ru(bpy)_3]^{2+}$ represents a significant step towards an ideal solar sensitiser, it possesses problems which must be overcome. Its restricted visible absorbance range and its lack of photochemical stability mar the complexes aptitude as a sensitiser. It does however mark a starting point, as a result of its remarkable photophysical properties, from which to pursue an ideal.

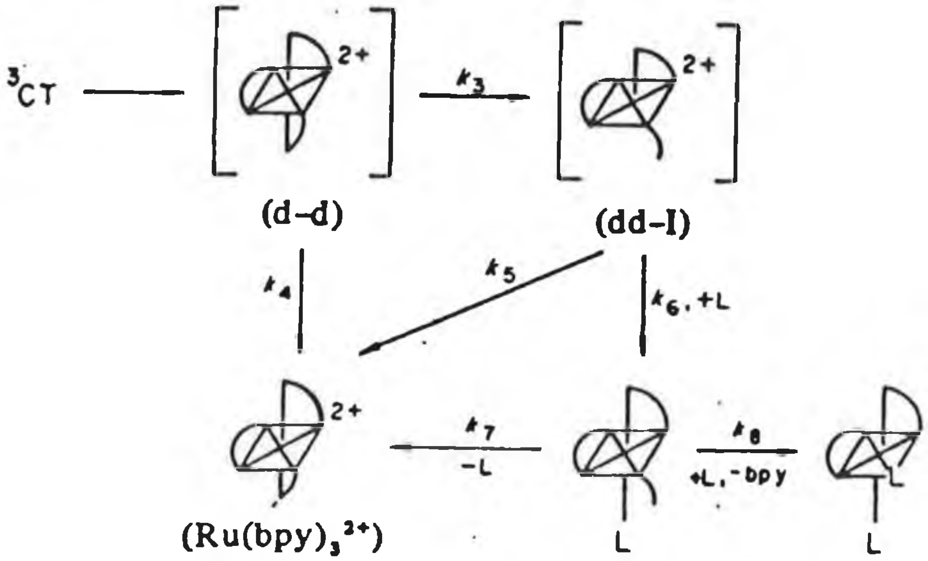

Figure 1.13 Pathway for photocleavage of $[Ru(bpy)_3]^{2+}$ *[79].*

1.5 Tuning of excited state properties in donor acceptor systems.

The photochemical reactions of metal complexes such as $[Ru(bpy)_3]^{2+}$ predominantly involve the lowest excited states of the molecule. These lowest excited states are also responsible for luminescence, therefore by manipulating the LUMO (lowest unoccupied molecular orbital) of the photoactive species one of the photochemical or photophysical pathways may be compelled to dominate.

In d^6 transition metal complexes, for the second and third row transition series the strong field (low spin) ground state configuration is anticipated. Complexes of these metals may be designed to possess radically different types of excited states lowest in energy, accessible with near u.v. or visible radiation.

Figure 1.14 shows a representation of orbital dispositions for strong field nd^6 complexes.

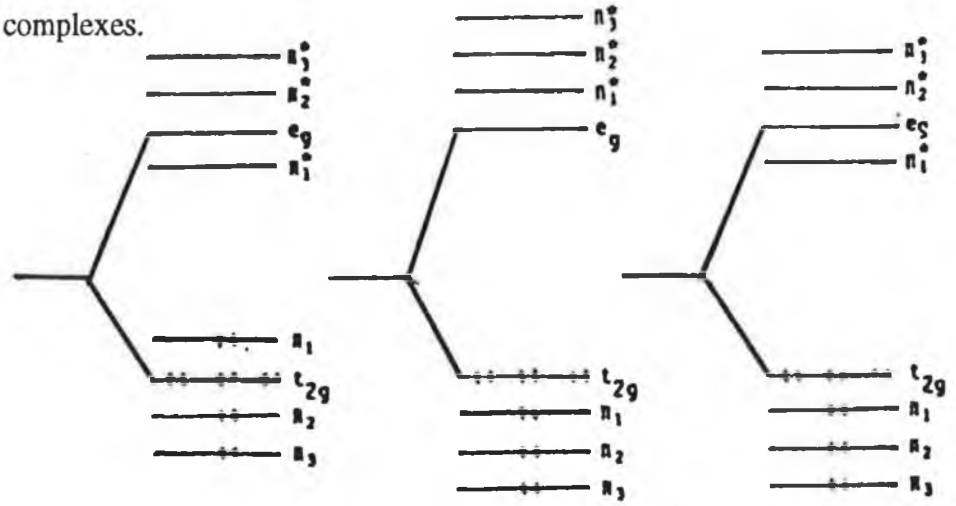

Case A Case B Case C

Figure 13. Orbital dispositions for strong field nd^6 complexes [81].

(a) Intraligand (π-π), lowest energy transition.*

(b) d-d lowest energy transition.

(c) Charge transfer (d-π) lowest energy transition.*

The third case (c) in which dπ^* represents the excited state, is the usual situation for $[Ru(bpy)_3]^{2+}$ and related complexes. In the CT excited state configuration the complex possesses a hole in the t_{2g} orbital with the excited electron residing on the ligand system. In this state the complex is a new chemical species with several additional channels of reaction open to it, radiationless transitions, radiative transitions, and various bimolecular processes.

As mentioned $[Ru(bpy)_3]^{2+}$ is not an ideal photosensitizer by virtue of its photochemical instability and narrow visible absorption range. These problems, may be overcome by judicious manipulation of coordinating ligands. Since population of the distorted ^{3}MC state is responsible for instability, this problem can be tackled by increasing Δ_o, the crystal field splitting parameter. Three main factors influence Δ_o of a particular metal, the electrostatic field generated by the coordinating ligands, L-M σ bonding, since e_g depends on this, and L-M π bonding, which effects the energy of t_{2g} manifold. The energy of the MLCT states are influenced in a similar fashion, and by the ligands and metals redox properties. Since charge transfer is an optical electron transfer, which ultimately results in short lived charge separation, as mentioned in 1.5, solvent properties become important, such as polarity and dielectric constant (see section 1.6).

One of the most common ways of altering excited state properties in ruthenium polypyridyl complexes is to substitute another ligand for a bipyridyl. If a ligand which is a weaker σ donor but better π acceptor than bipyridine (a class a type ligand) is introduced then this ligand may partake directly in the excited state reactions and will alter the excited state properties by decreasing the t_{2g}-^{3}MLCT energy gap, since π^* (LUMO) will reside on this ligand, and also because of the reduced electrostatic field of class a ligands, the Δ_o will be reduced compared with $[Ru(bpy)_3]^{2+}$. The aim in using class a ligands is to isolate ^{3}MC from ^{3}MLCT, though the low d-d splitting may counteract this effect. Alternatively, if the new ligand is a better σ donor and worse π acceptor (class b ligand) than bpy, then this ligand will not become directly involved in the excited state, i.e. it will act as a spectator ligand. Such a ligand on introduction, increases Δ_o and also destabilises t_{2g}, so that the ^{3}MC-^{3}MLCT gap will decrease. The effects of the introduction of different ligand types into Ru polypyridyl complexes is clearly observed in their electronic spectra.

Class a ligands have been extensively studied, examples are bipyrimidines [80], bipyrazines [82] and biquinonlines [83] for which both mono and dinuclear complexes have been studied in which one or all of the bpy ligands are replaced. The most attractive feature of such complexes is that they possess a λ_{max} which is red-shifted by comparison with $[Ru(bpy)_3]^{2+}$ thus making the absorbance range more accessible to the solar spectrum. The second problem, that of photochemical instability, has been less easy to solve by the introduction of class a ligands. This is a result of the stabilisation of the Ru(II) t_{2g} levels, caused by the smaller σ-donation of these ligands, and their propensity for accepting π-backbonding from the metal dπ orbitals. The net effect is smaller Δ_o thus making ^{3}MC state thermally accessible at ambient temperatures. This unfortunately, has been reflected in both the temperature dependent studies and absence of photochemical stability in the majority of these complexes [84]. There have however been some examples of stable complexes containing class a ligands. For example, where the effect of decreasing Δ_o is mitigated by the effect of having ligand based π^* levels at very low energies, thus maintaining a large ^{3}MC-^{3}MLCT gap [85]. More recently, photostability has been attained by combining both class a and b ligands, i.e. biquinolines and triazoles [86].

A number of $Ru(bpy)_2$ complexes of class b type ligand have been examined, such as the imidazoles [87], and the species under study here the triazoles [88, 89, 90] and pyrazoles [91]. Because of their strong σ-donating ability, this class of ligands possess π^* levels of much higher energy than bpy, as a result, in mixed chelate complexes containing both bpy and class b ligands the excited state is always bpy based. This point is illustrated by the trischelate triazole complexes created by Vos and co-workers, which is yellow as opposed to the vibrant orange of $[Ru(bpy)_3]^{2+}$ [92]. The magnitudes of σ and π donating properties of these ligands may be modified by introduction of substituents onto the ligand [93]. Specifically, the triazoles have been a particularly important contribution to the class b ligands, and an interesting property of these species is the asymmetry of the coordination sites of the triazole. Whereby the specific sites chosen affects the magnitude of σ donation "felt" by the metal [94]. Another very important property of triazoles is their acid/base chemistry, the uncoordinated nitrogen of the triazole can undergo protonation and deprotonation, which has a profound effect on the π acceptor and σ donor properties of the ligand. Therefore the class b ligands by virtue of their substituents, coordination mode and for the triazoles specifically, acid/base chemistry are uncommonly versatile ligands, capable with only moderate modification of significantly altering the excited state properties of a complex.

1.6 Photoinduced electron transfer theory.

Electron transfer is a simple, weakly interacting process where no bond making or breaking occurs, rather it involves the movement of an electron from an occupied orbital of one reactant to an unoccupied of the other. Leading to radical ion formation or a charge transfer complex.

The feasibility of electron transfer between an excited state sensitizer and quencher is dictated by the overall free energy change accompanying the reaction, which for efficient mechanism must be exoergonic ($\Delta G < 0$). For bimolecular electron transfer in the ground state the free energy change is related to the ionisation potential (IP_D) of the donor and electron affinity (EA_A) of the acceptor [95] since;

$$\Delta G = IP_D - EA_A \qquad (1.19)$$

Excitation via light absorption reduces the ionisation potential and electron affinity of both donor acceptor as a result

$$IP_D = IP_D - E_{D*} \qquad (1.20)$$

$$EA_A = EA_A + EA_{A*} \qquad (1.21)$$

Therefore if the donor is the excited species then,

$$\Delta G = IP_D - EA_A - E_{A*} \qquad (1.22)$$

In solution the ionisation potential and electron affinity of a donor acceptor pair are related to the redox potentials of the pair, since,

$$IP_D = E(D^{+\cdot}/D) - \Delta G\ (D^{+\cdot}) + \text{constant} \qquad (1.23)$$

$$EA_a = E(A/A^{-\cdot}) + \Delta G\ (A^{-\cdot}) + \text{constant} \qquad (1.24)$$

where $\Delta G(D^{+\cdot})$ and $\Delta G(A^{-\cdot})$ are the individual solvation energies of the ionised donor and acceptor species. Since in solution account must be taken of the coulombic interactions, solvent stabilizations and the effects of charge transfer intermediates formed as a result of electron transfer [96] i.e.

$$\Delta G(D^{+\cdot}) + \Delta G(A^{-\cdot}) = -e^2/2\ (1/r_D + 1/r_A)(1 - 1/\varepsilon) \qquad (1.25)$$

Where r_A and r_D are the radii of donor and acceptor and ε is the dielectric constant of the solvent. This translates into the Weller equation which takes into account the coulombic contribution of the solvent.

$$\Delta G\ (\text{kcal/mol}) = 23.06[\ E(D^{+\cdot}/D) - E(A/A^{-\cdot}) - e^2/\varepsilon d] - E_{D*} \qquad (1.26)$$

Equation 1.26, providing the excited state energy of the reactant and the redox potentials of both species are known, can be utilized to determine whether excited state electron transfer is exoergonic and hence whether it will be possible. For bimolecular electron transfer where the ion pair dissociates completely or in solvents of large dielectric constant the coulombic contribution may be neglected.

For intramolecular electron transfer, estimation of $\Delta G(eV)$ may be obtained from equation (1.27), [97].

$$\Delta G(eV) = \left[E(D^{+} / D) - E(A / A^{\cdot -})\right] - E_{D*} \quad (1.27)$$

In terms of kinetics of electron transfer, there are two treatments, classical and semi-classical the latter integrating quantum dynamical constraints [98]. The first, classical model was devised by Nobel laureate R.A Marcus [99] where the rate constant of electron transfer is expressed in terms reminiscent of conventional transition state theory.

$$k_{el} = v_n\, k \exp(-\Delta G^*/RT) \qquad (1.28)$$

Where v_n is the nuclear frequency factor relating to the vibrational frequency of the critical vibration mode of electron transfer and k is the transmission coefficient, the probability that the reactants on reaching the isoenergetic point actually cross over to form the products. The meanings of the various terms are expressed in terms of an energy profile of reactant A.B and charge separated product $A^{+}.B^{-}$ see figure 1.15.

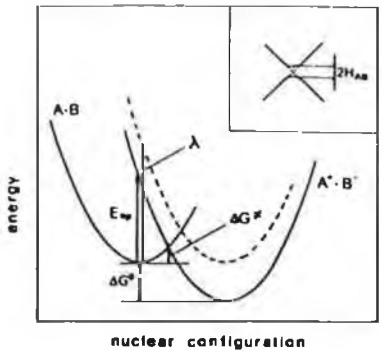

Figure 1.15. Energy profile and kinetic parameters for electron transfer [7].

According to the Franck Condon principle, the distortion of nuclear geometry leading to an isoenergetic point of crossover between reactant and product must be established prior to electron transfer.

When the molecular vibrations of the donor and acceptor required to reach the transition state correspond to an harmonic oscillator model, then the free energy of the transition may be expressed as

$$\Delta G = \frac{\lambda}{4}\left(1 + \frac{\Delta G^{o}}{\lambda}\right)^{2} \quad (1.29)$$

where λ is the total reorganisational energy required for the system to reach the reactant- product intersection. The reorganisational energy is comprised of two components since $\lambda = \lambda_i + \lambda_s$ where λ_i relates to structural changes (such as bond lengths) in the molecule occurring during electron transfer and λ_s relates to the changes in the surrounding media. λ_i may be determined using the molecular vibrational coordinates of the molecule and λ_S was determined [100] by employing dielectric continuum theory. In this way λ_S was found to be

$$\lambda_s = (\Delta e^2)\left[\frac{1}{2a_1} + \frac{1}{2a_2} - \frac{1}{r}\right]\left[\frac{1}{\varepsilon_{op}} - \frac{1}{\varepsilon_s}\right] \qquad (1.30)$$

Where in the simplest interpretation of this model the donor and acceptor are assumed to be spherical with radii a_1 and a_2 at distance (r) from each other. Δe is the charge transferred between them and ε_{op} and ε_S are the solvent optical and static dielectric constants respectively. The term λ_S exhibits the influence of solvent on the free energy of electron transfer.

In the classical limit, the maximum rate of electron transfer achievable is predicted to occur when $-\Delta G = \lambda$.

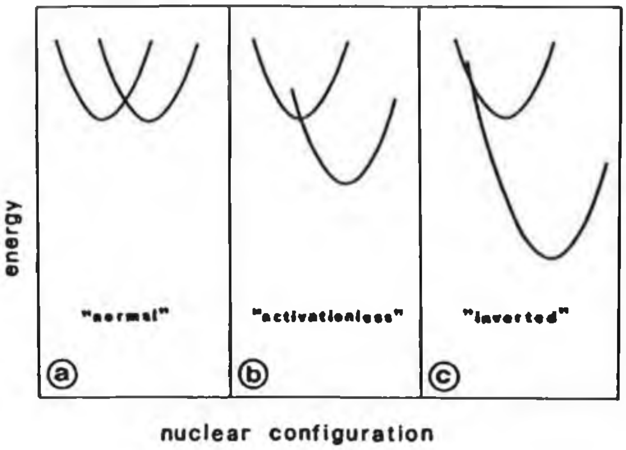

Figure 1.16. Potential energy curve for reactant and product states for an electron transfer process in the Marcus inverted region [7].

One of the key predictions of this theory is that the rate of electron transfer will slow down when ΔG becomes very large (i.e. when $-\Delta G > \lambda$) this effect is known as the Marcus inverted region (see figure 15). Although in dispute originally, experimental evidence for its existence has been increasing, [25, 101, 102]. One of the most interesing applications of the inverted region is in creating species capable of forward electron transfer, with very slow back electron transfer as a result of its $-\Delta G > \lambda$ [25, 102]. The quantum dynamical treatment based on the work of Landau and Zener [103] expresses the rate of electron transfer in the following way;

$$k_{el} = (2\pi/\hbar).H^2{}_{AB}.(FC) \qquad (1.31)$$

Where the rate constant k_{el} is expressed as function of $H^2{}_{AB}$, the electronic coupling matrix, which describes the extent of coupling between the donor and acceptor, and as function of the Franck Condon factor (FC), which is the sum of the products of the orbital overlap integrals of vibrations wavefunctions of solvent and reactant with product. An important influence to emerge in both these treatments is that of distance dependence, on which the components λ and $H^2{}_{AB}$ depend. The occurrence and rate of electron transfer is strongly dependent on the nature of the media intervening A and B in the case of intramolecular electron transfer this implies both the connector molecules and solvent. The π and σ bonds of the spacer will determine $H^2{}_{AB}$. Since in covalently linked donor-acceptor species, mixing of electronic states with connector moieties usually occurs. The electronic coupling matrix is also dependant on the orientations of A and B with respect to one another [104]. Therefore intramolecular photoinduced electron transfer is implicitly dependent on the separation between donor and acceptor, their respective orientations, the molecular structure of the covalent link and the solvent. If the connector is flexible, and particularly if it is long, occurrence and efficiency of electron transfer will be complicated by steric nature of the chain, its length, the solvent dielectric constant and viscosity and the motion of the chain [105]. Whereas with rigid connectors such as the triazolate bridges [106] the situation is simpler.

The effects of distance between donor and acceptor has been the subject of considerable investigation, in particular in porphyrin - quinone [107] pairs separated by rigid spacer molecules, where from fluorescence lifetime studies electron transfer was observed clearly to decrease over increasing distances. The effects of orientation on electron transfer was elegantly highlighted by Sakata and coworkers [107, 108] who demonstrated that in cis and trans isomers of porphyrin - quinone systems the trans bound molecules undergo charge separation, more slowly than cis by one order of magnitude. The authors suggested that this was a result of greater through - space orbital interaction in the trans isomer.

1.7 Scope of this thesis.

The aim of this work is to study the synthesis and properties of Ru(II)bipyridyl complexes N,N and O,N coordinated to substituted class b ligands, triazoles and pyrazoles. This work is part of ongoing research by the Vos research group into the creation of possible solar sensitizer materials based on Ruthenium(II) and Osmium(II) polyimine materials. To date most of the emphasis of this work has been the N,N coordinated triazole containing complexes, which has been very successful in creating photostable, luminescent complexes with unique acid-base [93] and electron transfer properties [106]. Pyrazoles as strong σ-donors have been the subject of some research [91], but have not yet been fully exploited. Phenols, and in particular hydroquinones and quinones are important because of their importance in biological electron transport chains and represent a potentially interesting subject because of their proven ability to quench the excited state of $[Ru(bpy)_3]^{2+}$. This thesis seeks to describe the effect of combining the class b ligands pyrazole and triazole with phenolic, hydroquinone and quinone moieties and in the first instance observe the effects of these species as pendant groups on the properties of the complex. Secondly, to observe the effect of direct coordination of the Ru(II) to the oxygen to create O,N coordinated complexes.

In chapter 2 the experimental methodology employed to characterise the complexes discussed are described. Chapter 3 will discuss the synthesis and properties of a number of N,N coordinated mononuclear complexes containing pyridyltriazole substituted with phenols, hydroquinones and quinone.

In Chapter 3 the synthesis and properties of some mononuclear Ru(II)(bpy)$_2$ complexes containing substituted aryl-pyridyltriazole ligands. Namely phenolic, hydroquinone and quinone moieties. The influence of the hydroxyl and quinone substituents is investigated with respect to unsubstituted aryl containing ligand containing HL5, with emphasis placed on their photophysical and electrochemical properties.

Chapter 4 deals with the synthesis, structural elucidation and photophysical properties of some totally novel Ru(II)(bpy)$_2$ complexes, O,N coordinated to 3-(2-phenol)-5-(pyridin-2-yl)-1,2,4-triazole (H$_2$L2) and pyrazole-hydroquinone ligands H$_2$L7-9. Their potential as photosensitiser material is, in particular assessed.

Chapter 5 examines the synthesis, structural elucidation, and properties of the two dinuclear complexes arising from the ligands H$_2$L2 and H$_2$L8. In particular, the electrochemistry and spectrochemistry is assessed with a view to determining the extent of interaction between the metals centres in these complexes.

Chapter 6 explores the influence of ligand deuteration on the properties of some the complexes discussed in the preceeding chapters. In particular the influence that deuteration bears on the excited state of these species. Bipyridyl deuteration is in particular appraised as a means of determination of the nature and location of the excited state in mixed ligand complexes. Most importantly in this chapter a new, one pot method of bipyridyl deuteration is described.

Finally, two appendices are supplemented to this thesis, the first relating to a novel Bpt-hydroquinone co-crystal formed during the synthesis of H_3L1, and a novel, much simplified, one-pot synthesis of Bpt. The second describes briefly the synthesis, structure and properties of a novel Ru(II)(bpy)$_2$ complex O,O coordinated to H_3L6.

Structures of ligands cited in this thesis.

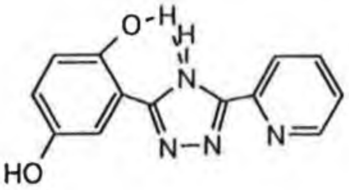

H_3L1

3-(2,5-dihydroxyphenyl)-5-(pyridin-2-yl)-1,2,4-triazole

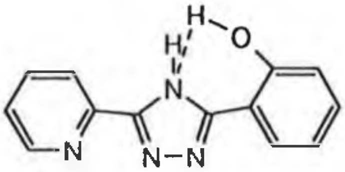

H_2L2

3-(2-phenol)-5-(pyridin-2-yl)-1,2,4-triazol

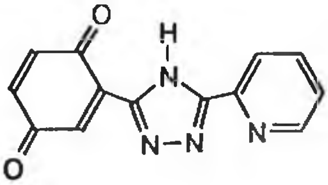

L3

3-(2,5-benzoquinone)-5-(pyridin-2-yl)-1,2,4-triazole

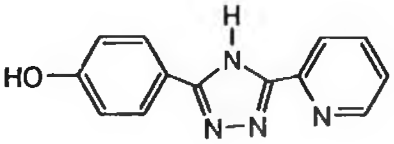

L4

3-(4-phenol)-5-(pyridin-2-yl)-1,2,4-triazol

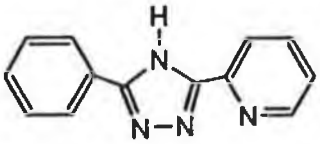

HL5

3-(phenyl)-5-(pyridin-2-yl)-1,2,4-triazole

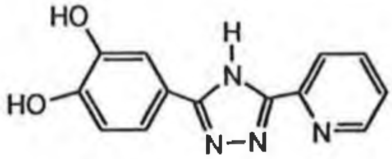

H_3L6

3-(3,4-dihydroxyphenyl)-5-(pyridin-2-yl)-1,2,4-triazole

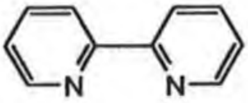

bpy

2,2-Bipyridyl

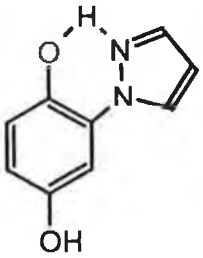

H_2L7

1,4-Dihydroxy-2-pyrazol-1'-ylbenzene

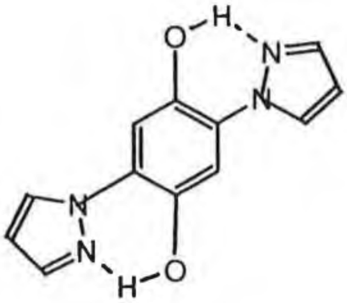

H_2L8

1,4-Dihydroxy-2,5-bis(pyrazol-1'-yl)benzene

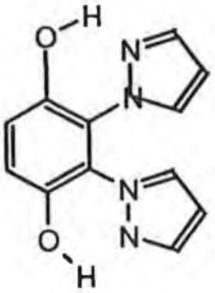

H_2L9

1,4-Dihydroxy-2,3-bis(pyrazol-1'-yl)benzene

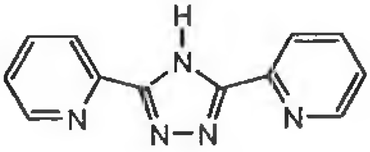

Bpt

3,5-bis(pyridin-2-yl)-1,2,4-triazole

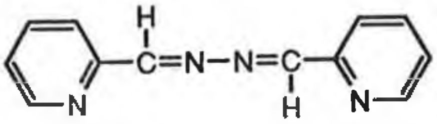

DPA

Bispyridylazine

HQ

Hydroquinone

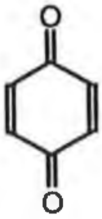

Q

Quinone

1.8 References.

[1] D. K. McDaniels, The Sun: Our future energy source, 2nd ed., 1989, J. Wiley and Sons, N.Y..

[2] M. R. Wasielewski, *Chem. rev.* **1992**, 92, 435.

[3] R. K. Clayton, Photosynthesis; Physical methods and chemical patterns, 1st ed., 1980, Cambridge University Press.

[4] See for instance: J.-P. Konopelski, F. Kotzyba-Hibert, J.-M.. Lehn, J.-P.Desvergne, F. Fages, A. Castellen, H. J. Bouas-Laurent, *J. Chem. Soc., Chem. Comm.*, 1985, 433.

[5] V. Balzani, ed., Supramolecular Photochemistry, NATO ASI Ser.,vol 214, Riedel, Dordrecht, 1987.

[6] J.-M. Lehn, ed., Supramolecular Organic chemistry

[7] V. Balzani, F. Scandola, Supramolecular Photochemistry 1st ed., 1991, Ellis Horwood, G.B..

[8] V. Balzani, *Pure and Appl. Chem.*, 62, 6, 1099, 1990.

[9] D.G. Johnson, M.P Niemczyk, D.W. Minsek, G.P Wiederrecht, W.A Svec, G.L. Gaines III, M.R. Wasielewski, *J. Am. Chem. Soc.*, 115, 5692, 1993.

[10] D. Gust, T.A. Moore, P.A. Liddell, G. A. Nemeth, L.R. Makings, A.L. Moore, D. Barrett, P.J. Pessiki, R.V. Bensasson, M. Rougee, C. Chachaty, F.C. DeSchryver, M. Van der Auweraer, A.R. Hotzwarth, J.S. Connolly, *J. Am. Chem. Soc.*, 109, 846, 1987.

[11] N.S. Hush, *Coord. Chem. Rev.*, 64, 135, 1985.

[12] T.A. Moore, D. Gust, P. Mathis, J.C. Malocq, C. Chachaty, R.V. Bensasson, E. J. Land, D., Doizi, P.A. Liddell, W.R. Lehmen, G.A. Nemeth, A.L. Moore, *Nature*, 307, 307, 630, 1984.

[13] J.L Sessler, M.R. Johnson, T.-Y. Lin, *Tetrahedron*, 45, 4767, 1989.

[14] A.M. Brun, S.J. Atherton, A. Harrimen, V. Haitz, J.P. Sauvage, *J. Am. Chem. Soc.*, 1992.

[15] J.H. Borkent, A.W.J. de Long, J.W. Verhoeven, Th.J. deBoer, *Chem. Phys. Lett.*, 57, 530, 1978.

[16] F. M. el Torki, R.H. Schmehl, W.F. Reed, *J. Chem. Soc., Faraday Trans. I*, 85, 349, 1989.

[17] R.E. Sassoon, *J. Am. Chem. Soc.*, 107, 6133, 1985.

[18] P.M. Ennis, J.M. Kelly, C.M.O'Connell, *J. Chem. Soc., Dalton Trans.*, 2485, 1986.

[19] A. Slama-Schowk, D. Avnir, M. Ottolenghi, *Nature*, 355, 240, 1992.

[20] B.P. Sullivan, H. Abruna, H.O. Finklea, D.J. Salmon, J.K Nagle, T.J. Meyer, H. Spritschnik, *Chem. Phys. Lett.*, 58, 389, 1978.

[21] C.M. Elliott, R.A. Freitag, D.D. Blaney, *J. Am. Chem.* Soc., 107, 4647, 1985.

[22] A. Juris, V. Balzani, F. Barigelletti, S. Campagna, P. Belser, A. von Zelewsky, *Coord. Chem. Rev.* 93, 245, 1988.

[23] C.K. Ryu, R. Wang, R.H. Schmehl, S. Ferrere, M. Ludwikow, J.W. Merkert, C.E.L. Headford, C.M. Elliott, *J. Am. Chem. Soc.*, 114, 430, 1992.

[24] E. Amoyal, M.M. Bahout, *J. Chem. Soc., Dalton Trans.*, 509, 1992.

[25] E. H. Yonemoto, R.L. Riley, Y.I. Kim, S.J. Atherton, R.H. Schmehl, T.E. Mallouk, *J. Am. Chem. Soc.*, 114, 8081, 1992.

[26] E. Danielson, C.M. Elliot, J.W. Merkert, T.J. Meyer, *J. Am. Chem. Soc.*, 109, 2519, 1987.

[27] S. Roffia, M. Marcaccio, C. Paradisi, F. Paolucci, V. Balzani, G. Denti, S. Serroni, S. Campagna, *J. Am. Chem. Soc.*, 32. 3003, 1993.

[28] G. Denti, S. Serroni, S. Campagna, V. Ricevuto, V. Balzani, *Inorg. Chim. Acta,* 182, 127, 1991.

[29] F.M. el Torki, R.H. Schmehl W.F. Reed, *J. Chem. Soc., Faraday Trans. I*, 85, 349, 1989.

[30] V.Y. Shafirovich, A.E. Shilov, *Isr. J. Chem.*, 38, 149,1988.

[31] E. Borgarello, J. Kiwi, E. Pelizzetti, M. Visca, M. Gratzel, *Nature*, 289, 159, 1981.

[32] K. Kalyanasandaram, E. Borgarello, M. Gratzel, *Helv. Chim. Acta*, 64, 362, 1981.

[33] C. Creutz N. Sutin, *Proc. Nat. Acad. Sci.* USA, 72, 8, 2858, 1975.

[34] M. Gratzel, *Acc. Chem. Res.*, 14, 376, 1981.

[35] B. O'Regan, M. Gratzel, *Nature*, 353, 737, 1991.

[36] G. Feher, J.P. Allen, M.Y. Okamura, D. C. Rees, *Nature*, 339, 111, 1989.

[37] J. Barber, B. Anderson, *Nature*, 370, 31, 1994.

[38] M. Gratzel, Photoinduced electron transfer, Part D. Ed. M.A. Fox, M. Chanon, p. 429, Elsevier, N.Y., 1989.

[39] J.D. Mc Elroy, G. Feher, D.C. Maizeral, *Biochim. Biophys. Acta*, 172, 180, 1969.

[40] J.D. McElroy, G Feher, M.Y. Okamura, *Biochim. Biophys. Acta*, 267, 222, 1972,

[41] V.A. Shuvdov, V.A. Klimov, *Biochim. Biophys. Acta*, 440, 587, 1976.

[42] W. W. Parson, Ann. Rev., *Biophys. Bioeng.*, 11, 57, 1982.

[43] A.R. McIntosh, A. Siemiarczuk, J.R. Bolton, M.J.Stillman, A.C.J. Weeden, *J. Am. Chem. Soc.*, 105, 7215, 1983.

[44] C.H. Chang, D.M. Tiede, J. Tang, J.R. Norris, M. Schiffer, *F.E.B.S. Lett.*, 205, 82, 1986.

[45] N. Mataga, A. Karen, T. Okada, S. Nishitani, N. Kurata, Y. Sakata, S. Misumi, *J. Phys. Chem.*, 88, 5138, 1984.

[46] J.P. Paris, W.W. Brandt, *J. Am. Chem. Soc.*, 81, 5001, 1959.

[47] A. Juris, V. Balzani, F. Barigelletti, S. Campagna, P. Belser, A. von Zelewsky, *Coord. Chem. Rev..*, 93, 245, 1988.

[48] D.M. Klassen, G.A. Crosby, *J. Am. Chem. Soc.*, 48, 1853, 1968.

[49] E.M. Kober, T.J. Meyer, *Inorg. Chem.*, 21, 3978, 1982.

[50] S. Umapathy, R.E. Hester, Springer Proc. Phys., Ed. H. Takahashi, 60, 121, 1992.

[51]

[52] F.E. Lytle, D.M. Hercules, *J. Am. Chem. Soc.*, 105, 1067, 1983.

[53] J.N. Demas, G.A. Crosby, *J. Am. Chem. Soc.*, 93, 2841, 1971.

[54] J.N. Demas, G.A. Crosby, *J. Mol. Spect.*, 26, 82, 1968.

[55] Y. Kawanishi, N. Kitamura, Y. Kim, S. Tazuke, Sci. Papers I.P.C.R., 78, 4, 212, 1984.

[56] P.A. Mabrouk, M.S. Wrighton, *Inorg. Chem.*, 25, 526, 1986.

[57] A.G. Motten, K. Hanck, M.K. DeArmond, *Chem. Phys. Lett.*, 79, 3, 541, 1981.

[58] V. Balzani, F. Bolletta, M.T. Gandolfi, M. Maestri, *Chem. Phys. Lett.*, 75, 1, 1978.

[59] T.J. Meyer, Prog. *Inorg. Chem.*, 30, 389, 1983.

[60] J. Van Houten, R.J. Watts, *Inorg. Chem.*, 12, 3381, 1978.

[61] D.V. Pinnick, B. Durham, *Inorg. Chem.*, 23, 3841, 1984.

[62] L.R. Allen, P.R. Craft, B. Durham, J. Walsh, *Inorg. Chem.*, 26, 53, 1987.

[63] E.A. Seddon, K.R. Seddon, The Chemistry of Ruthenium, 1984, Elsevier, Amsterdam.

[64] W.E. Tokel, T. Akuoryan, R.E. Hemingway, A.J. Bard, *J. Am. Chem. Soc.*, 95, 6582, 1973.

[65] D.P. Rillema, G.A. Allen, T.J. Meyer, D. Conrad, *Inorg. Chem.*, 22, 1617, 1983.

[66] E.S. Dodsworth, A.B.P. Lever, *Chem. Phys. Lett.*, 119, 61, 1985.

[67] E.S. Dodsworth, A.B.P. Lever, *Chem. Phys. Lett.*, 2, 124, 1986.

[68] B.K.Ghosh, A. Chakravorty, *Coord. Chem. Rev..*, 95, 239, 1989.

[69] R.J. Watts, *J. Chem. Ed.*, 60, 10, 834, 1983.

[70] J.E. Baggot, M.J. Pilling, *J. Phys. Chem.*, 84, 3-12, 1980. (b) P. Connolly, J.H. Espenson, A. Bakac, *Inorg. Chem.*, 25, 2169, 1986. (c) C-T. Lin, W. Bottcher, M. Chou, C. Creutz, N. Sutin, *J. Am. Chem. Soc.*, 98, 6536, 1976.

[71] N. Kitamura, H-B. Kim, S. Okano, S. Tazuke, *J. Phys. Chem.*, 93, 5750, 1989.

[72] A. Vleck, F. Bolletta, *Inorg. Chim. Acta*, 76, L227, 1983.

[73] G. Jones II, V. Malba, *J. Org. Chem.*, 50, 5776, 1985.

[74] G.D. Harrigan, G.A. Crosby, *J. Phys. Chem.*, 59, 3468, 1973.

[75] G.D. Hagar, R.J. Watts, G.A. Crosby, *J. Am. Chem. Soc.*, 97, 7037, 1975.

[76] G.A. Crosby, W.H. Elfring Jr., *J. Phys. Chem.*, 80, 2206, 1976.

[77] J. Van Houten, R.J. Watts, *J. Am. Chem. Soc.*, 98, 4853, 1976.

[78] J. Van Houten, R.J. Watts, *Inorg. Chem.*, 17, 3381, 1978.

[79] B. Durham, J.V. Casper, J.K. Nagle, T.J. Meyer, *J. Am. Chem. Soc.*, 104, 4803, 1982.

[80] E.V. Dose, L.J. Wilson, *Inorg. Chem.*, 17, 2660, 1978.

[81] G.A. Crosby, *J. Chem. Ed.*, 60, 10, 791, 1983.

[82] G.D. Danzer, K.R. Kincaid, *J. Phys. Chem.*, 94, 3976, 1990.

[83] R.P. Thummel, F. Lefoulon, S. Chirayil, *Inorg. Chem.*, 26, 3072, 1987.

[84] A. Juris, F. Barigelletti, V. Balzani, P. Belser, A. von Zelewsky, *Inorg. Chem.*, 24, 202, 1985.

[85] G.H. Allen, R.P. White, D.P. Rillema, T.J. Meyer, *J. Am. Chem. Soc.*, 106, 2613, 1984.

[86] R. Hage, T. E.Keyes, J. G. Vos, *Inorg. Chim. Acta*, in press.

[87] M.R. McDevitt, Y.Ru, A. W. Addison, *Trans. Met. Chem.*, 18, 197, 1993.

[88] J.G. Vos, J.G. Haasnoot, G. Vos, *Inorg. Chim. Acta*, 71, 155, 1983.

[89] R. Hage, J.G. Haasnoot, J. Reedijk, J.G. Vos, *Inorg. Chim. Acta*, 118, 73, 1986.

[90] B.E, Buchanan, R. Wang, J.G. Vos, R. Hage, J.G. Haasnoot, J. Reedijk, *Inorg. Chem.*, 29, 3263, 1990.

[91] P.J. Steel, E.C. Constable, *J. Chem. Soc., Dalton Trans.*, 1389, 1990.

[92] R. Hage, J.G. Haasnoot, J. Reedijk, J.G. Vos, *Inorg. Chim. Acta*, 118, 73, 1986.

[93] R. Hage, R. Prins, J.G. Haasnoot, J. Reedijk, J.G. Vos, *J. Chem. Soc., Dalton Trans.*, 1389, 1987.

[94] R. Hage, J.G. Haasnoot, H.A. Nieuwenhuis, J. Reedijk, R. Wang, J.G. Vos, *J. Chem. Soc., Dalton Trans.*, 3271, 1991.

[95] M. Chanon, M.D. Hawley, M.A. Fox, Photoinduced Electron Transfer, Part A, Ed. M.A. Fox, M. Chanon, p.2, Elsevier, N.Y., 1988.

[96] D.F. Calef, Photoinduced Electron Transfer, Part A, Ed. M.A. Fox, M. Chanon, p. 362, Elsevier, N.Y. 1988.

[97] Rehm, D; Weller, A., *Isr. J. Chem.*, **1970**, 8, 259.

[98] M.R. Wasielewski, M.P. Niemczyk, W. A. Svec, E.P. Pewitt, *J. Am. Chem. Soc.*, 107, 5562, 1985.

[99] R.A. Marcus, *J. Chem. Phys.*, 24, 966, 1956.

[100] R.A. Marcus, *Faraday Disc. Chem. Soc.*,74, 7, 1982.

[101] (a) W. Worthy, *Chem. Chem. Eng.*, June 4, 1984. (b) G. Grampp, *Angew. Chem. Int. Ed. Eng.*, 32, 5, 691, 1993.

[102] T. Ohno, A. Yoshimura, D.R. Prasad, M. Z. Hoffman, *J. Phys. Chem.*, 95, 4723, 1991.

[103] C. Zener, *Proc. Roy. Soc.* London A, 137, 698, 1932.

[104] P. Chen, M. Curry, T.J. Meyer, *Inorg. Chem.*, 28, 2271, 1989.

[105] M.C. Palazzotto, M.R.V. Sahyun, N. Serpone, D.K. Sharma, *J. Chem. Phys.*, 90, 3373, 1989.

[106] R. Hage, J.G. Haasnoot, H.A. Nieuwenhuis, J. Reedijk, D.J.A DeRidder, J.G. Vos, *J. Am. Chem. Soc.*, 112, 9245, 1990.

[107] Y. Sakata, Y. Hirano, H. Tatemitou, S. Ochiai, H. Shibata, *Tetrahedron*, 45, 4807.

[108] Y. Sakata, H. Tsue, Y. Goto, S. Misumi, T. Asahi, S. Nishikawa, T. Okada, N. Mataga, *Chem. Lett.*, 1307, 1991.

Chapter 2

Experimental Procedures.

Synthetic procedures are described in each chapter. All synthetic reagents were of commercial grade and no further purification was employed, again unless otherwise stated. All solvents employed in spectroscopic measurements were HPLC grade with the exception of ethanol.

2.1 Nuclear Magnetic Resonance spectroscopy.

Both Proton and ^{13}C NMR spectra were carried out on a Bruker AC400 (400 MHz) instrument. The solvents used were either deuterated acetonitrile or acetone for complexes and deuterated dimethyl sulphoxide for ligands. The chemical shifts were recorded relative to TMS.

The 2-D COSY (correlated spectroscopy) experiments involved the accumulation of 128 FIDs (free inductive decays) of 16 scans. Digital filtering was sine-bell squared and the FID was zero filled in the F1 dimension. Acquisition parameters were F1 = $\pm$ 500Hz, F2 = 1000 Hz, and $t_{1/2} = 0.001$ s. The cycle time delay was 2 s.

2.2 Absorption and emission measurements

UV-vis spectra were carried out using either a Shimadzu UV-240 spectrophotometer, Hewlett Packard 8451 photodiode array spectrophotometer or on a Shimadzu 3100 UV-vis/NIR spectrophotometer interfaced with an Elonex PC-433 personal computer. The solvent used was acetonitrile for absorption measurements unless other–wise stated. Extinction coefficients are accurate up to 5%.

Emission measurements were carried out on a Perkin Elmer LS50 luminescence spectrometer interfaced with an Epson PCAX2E personal computer employing Fluorescence Data Manager custom built software. At room temperature, measurements were taken in acetonitrile unless otherwise stated, using an excitation slit width of 5 nm and emission slit of 10 nm. At 77 K an ethanol/methanol 4:1 mixture was used and the excitation and emission slit widths were set to 5 nm. In both absorption and emission spectroscopy deprotonation was achieved using diethylamine or concentrated aqueous ammonia, and protonation using 60% (w/v) perchloric acid. In both cases about 10% acid or base (v/v) was added. Emission spectra were not corrected for photomultiplier response.

Quantum yields of emission, Φ_{em}, were carried out according to the method of optically dilute measurements described by Demas and Crosby [1]. The standard used was $[Ru(bpy)_3]^{2+}$, known to have a quantum yield of 0.028 in aqueous, air equilibrated solution [2]. Normalisation of absorbance intensity was carried out prior to emission measurement and Φ_{em} was determined by employing equation (2.1).

$$\Phi_{em} = 0.028\left(\frac{A_s}{A_{ref}}\right)\left(\frac{n_s}{n_{ref}}\right)^2 \qquad (2.1)$$

Where Φ_{em} is the emission quantum yield, A_s and A_{ref} the integrated areas of the emission band of the sample and reference complex respectively and n_s and n_{ref} are the solvent refractive indices of the sample and reference solutions.

Ground and excited state pK_a values were obtained using the instrumentation described above, whereby ground state pK_as were determined observing intensity changes in absorption as a function of pH. Similarly excited state pK_as (pK_a*) were determined monitoring emission intensity at a fixed wavelength (vide infra) as a function of pH. Most pKas described were carried out in Britton Robinson buffer [2] measuring pH changes using a Phillips PW9421 pH meter. PH was altered by addition of either NaOH or conc. H_2SO_4. For pK_as determined in acetonitrile, the sample was made up in unbuffered acetonitrile, and pH calculated via addition of known amounts of perchloric acid which is known to dissociate completely in acetonitrile [3]. For pKa*s the excitation wavelengths were taken from the isobestic points observed in the pKa measurements. Ground state pKas were determined from the point of inflection of a plot of percentage change in absorbance versus pH, and excited state pKa*s using the pH_i (point of inflection on percentage change in emission intensity vs pH plot) in the excited state lifetime formula, or the Forster cycle equation [4] was employed, in particular in cases where lifetime could not be measured accurately, see chapter 3.

2.3 Luminescent lifetime and temperature dependent luminescent lifetime measurements.

Luminescent lifetimes were carried out on a Q-switched Nd-YAG spectrum laser system. Room temperature measurements were carried out in acetonitrile, unless otherwise stated. At 77K and for temperature dependent studies, measurements were carried out in ethanol/methanol 4:1 (v/v). For all laser work samples were of low concentration i.e. 10^{-4} - 10^{-5}M. Samples were degassed by bubbling dry argon through the sample for at least 20 minutes. Lifetimes conforming to single exponential decays were analysed with modified non-linear programs. Those of multiple exponential regression were analysed using circular reference iteration employing Microsoft Excel. The lifetime errors are estimated to be < 8%.

Temperature dependent studies when carried out on deareated samples were purged with dry argon for 30-40 minutes. Samples were placed in a custom built sample holder inside a Thor C600 nitrogen flow cryostat equipped with a Thor 3030 temperature controller. The temperatures quoted are ± 2K. Standard iterative non linear programs were employed to obtain the variables values for the temperature dependent lifetimes.

2.4 Electrochemistry.

For electrochemistry all organic solvents employed were HPLC grade, dried over molecular sieve. The electrolyte employed was home-made tetraethylammoniumperchlorate. This was prepared by dissolving tetraethylammonium bromide (1M) in water. Perchloric acid (1M) was added dropwise to the solution until precipitation of the white perchlorate ceased. The product was collected by filtration and redissolved in hot water, neutralised, and recrystallised 5 times from hot water.

The working electrode was a 3 mm diameter Teflon shrouded glassy carbon electrode, the reference electrode was a saturated calomel electrode, and auxiliary electrode was a platinum gauze. The electrochemical cell employed was a three electrode cell compartmentalised with glass frits. The analyte was only degassed for use of cathodic potentials, in which case nitrogen or argon was pumped through the solution for 20 minutes prior to the experiment. PH was adjusted using perchloric acid or ammonium hydroxide.

For cyclic voltammetry an EG&G PAR model 362 scanning potentiostat, and a Linseis, model 17100 x-y recorder, at scan rate of 100 mVs^{-1}. For differential pulse polarography an EG&G PAR model 264A polarographic analyser and Linseis model 17100 x-y recorder were used, at scan rate of 10 mVs^{-1}

2.5 Spectroelectrochemistry.

Spectroelectrochemistry was carried out using a home-made Pyrex glass, thin layer cell (1 mm), employing a set up as shown in figure 2.1. The optically transparent working electrode, was a platinum gauze, which inserted fully into the cell.

The auxiliary electrode was a platinum wire and the reference was Ag/AgCl, these were inserted into the sample reservoir on top of the cell. The solvents and electrolyte used were as described for the electrochemistry.

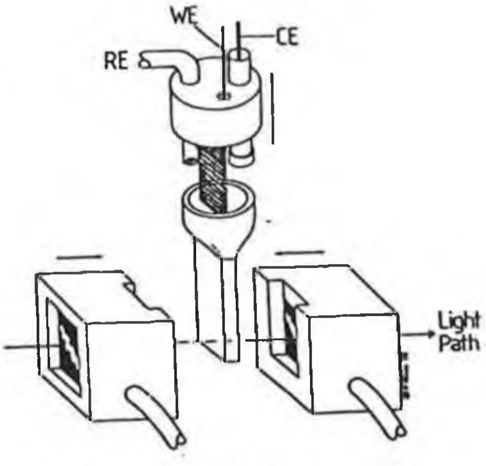

Figure 2.1. Representation of the OTTLE cell employed for spectroelectrochemistry.

The working electrode was held at the required potential for 30 minutes prior to commencement of spectral scan and was maintained throughout the measurement using an EG&G PAR model 362 scanning potentiostat.

For absorption spectroelectrochemistry, the absorption spectra were obtained on a Shimadzu UV-240 spectrophotometer or Shimadzu 3100 UV-vis/NIR spectrophotometer interfaced with an Elonex PC-433 personal computer. For emission spectroelectrochemistry the emission spectra were obtained on a Perkin Elmer LS50 luminescence spectrometer, with the thin layer cell held at a 45° angle to the incident light. Excitation was chosen as the wavelength at which least change in absorption intensity occurred in the absorption spectroelectrochemistry (i.e. the isosbestic point if one existed) for the particular complex. Spectroelectrochemistry was only carried out at anodic potentials therefore no degassing of samples was carried out.

2.6 Analytical and semi-preparative HPLC.

Analytical cation exchange HPLC experiments were carried out using a Waters HPLC system, consisting of a model 6000A HPLC pump fitted with a 20 μl injection loop, a Waters 990 photodiode array detector connected to a NEC APC III computer, and a μ-partisil SCX radical PAK cartridge mounted in a radial compression Z module.

The mobile phase used for routine work was 80:20 CH_3CN:H_2O containing 0.08M $LiClO_4$. For photolysis experiments, better separation of fractions was required and the retention time was increased using 80:20 CH_3CN:H_2O containing 0.06M $LiClO_4$. The flow rate for routine work was 2.5 cm^3min^{-1} and 2.0 cm^3min^{-1} for photochemical experiments.

Semi-preparative HPLC was carried out on an a model 353 Applied Chromatography Service pump (model RR066) and ACS detector (model 353 / UV/vis) fitted with a 1 ml injection loop and a Magnum-9 Partisil cation exchange column (10 mm x 25 cm). The mobile phase employed was 80:20 CH_3CN:H_2O containing 0.1M KNO_3 for mononuclear complexes and 0.15M KNO_3 for dinuclear complexes. The flow rate ranged between 2 and 3 cm^3min^{-1}.

2.7 Resonance Raman spectroscopy.

Time resolved resonance Raman was carried out in Queens University Belfast under the supervision of Prof. J. J. McGarvey. The measurements were carried out using a Q-switched Nd/YAG laser (Quanta-ray GCR2, pulse width 5-9 ns, depending on output wavelength) using harmonic generating crystals for the excited state spectra, excited at 355 nm. Ground state spectra were carried out employing a Spectra Physics Argon ion laser, at 364 nm. Measurements were carried out using water as solvent, with minimum acetone to dissolve the complexes. The samples were degassed by maintaining a constant stream of nitrogen bubbling through the sample throughout the experiment.

2.8 Photochemical experiments.

Photochemistry was carried out by dissolving the sample in the chosen solvent system, the sample was irradiated in a 1 cm quartz cell using a halogen lamp, employing filters to cut out radiation below 300 nm. The photolyses were carried out in either acetonitrile or dichloromethane (both HPLC grade) in the presence of chloride anions (0.005M benzyltriethylammonium chloride). The complexes were deprotonated by addition of ethylenediamine, and protonated by addition of triflouroacetic acid. The photolysis were followed as a function of time by both absorption spectroscopy using a Shimadzu UV-240 spectrophotometer, and analytical HPLC (see (vi)).

2.9 Molecular modelling.

Basic modelling of complexes and ligands was carried out using Hyperchem software. Molecular mechanics optimisation of ligand and complex structures was carried out employing the Hyperchem Polak-Ribiere algorithm. Modelling and computational chemistry of Bpt and the Bpt-hydroquinone co.-crystal was carried out in Queens University Belfast under the supervision of Prof. K.R. Seddon using Apple Macintosh molecular modelling package.

2.10 Mass spectroscopy.

Mass spectra of some ligands were carried out at DCU by Dr P. Kenny, while the remainder were carried out by the Mass spectrometry service at Queens University, Belfast, using EI ionisation method.

2.11 Elemental Analyses.

Elemental analyses were carried out by the Microanalytical laboratories at University College Dublin.

2.12 References.

[1] J. N. Demas; G. A. Crosby; *J. Phys. Chem.* **1971**, 75, 8, 991.

[2] K. Nakamura; *Bull. Chem. Soc. Japn.*,**1982**, 55, 2697.

[3] C. W. Hand; H.L. Blewitt; Acid-BaseChemistry, 1986, Macmillan, N.Y..

[4] J.F. Ireland, P.A.H. Wyatt, *Adv. Phys. Org. Chem.*, 12, 131, 1976.

Chapter 3

N,N coordinated complexes: The influence of hydroxy-substituted aryl groups on the photophysical and photochemical properties of mononuclear Ru(II) complexes containing pyridyl-1,2,4-triazole ligands; electron and proton transfer reactions.

3.1 Introduction.

In section 1.3.2 the importance of the charge separated state in the photosynthetic cycle was described, and indeed the question of photoinduced electron transfer has been applied to ruthenium polypyridyl complexes. For the most part these investigations have involved bimolecular quenching of the excited state of $[Ru(bpy)_3]^{2+}$ with considerably less research conducted into intramolecular electron transfers.

In this chapter the synthesis and characterisation of a number of ligands containing substituted pyridyltriazoles and their mononuclear Ru(II) complexes is described. The structures of the complexes are elucidated by NMR and comparison with other similar complexes of known structure. Detailed investigations of the redox, acid-base and photophysical properties of these complexes are also described. The purpose in creating these complexes was to observe the influence of the redox active groups, hydroquinone, quinone and phenol on the excited state properties of Ru(II) and the resulting electron and proton transfers are described and discussed. Figure 3.1 displays the ligands discussed in the text.

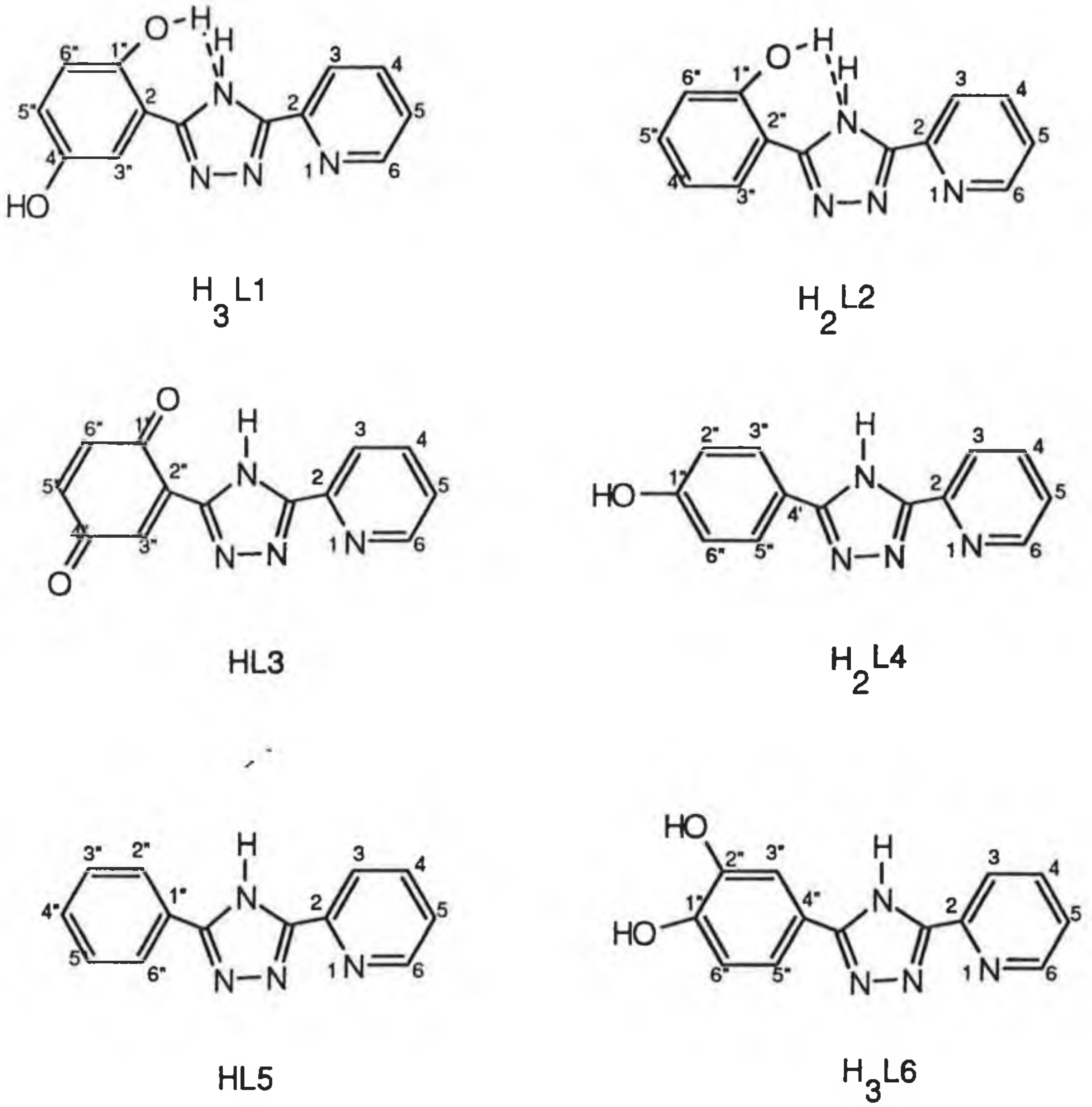

Figure 3.1: Structures of ligands discussed in this chapter.

3.1.1 Pyridyltriazole ligands.

The bulk of investigation into tuning of the Ru(II) polypyridyl excited state has involved substitution of class a ligands (strong π-acceptors, weak σ-donors), such as the biquinolines (see section 1.5). The first report of Ru(II) complexes containing 1,2,4-triazole was by Vos and coworkers, in 1983 [1]. In this account two 1,2,4-triazole were bound in a monodentate fashion to Ru(II) bipyridyl. It was noted that the triazole possessed only weak π-acceptor properties by comparison with bipyridyl, which increased on protonation of the ligand. This work lead to the creation of a number of 3-(pyridin-2-yl)-1,2,4-triazole bidentate ligands, investigation into the ruthenium complexes of which, lead to the elucidation of the characteristics which make them unique as ligands [1-4]. Triazoles are class b ligands, strong σ-donors and weak π-acceptors, they contain two different coordination sites, N'^1 and N'^4, which have been shown to have quite different σ-donor properties [2]. Triazole possesses an acid-base chemistry which may be utilized to control the properties of the complex [2], since protonation reduces the σ-donor ability of the ligand, this has marked effects on the ground and excited state properties of the complex. Pyridyltriazole complexes in the deprotonated state are in general photostable, whereas when protonated, as a result of their decreased σ-donating ability, they exhibit a marked photochemical reactivity. This pH dependent photoreactivity was demonstrated for a series of simple pyridyltriazole complexes employing temperature dependent luminescence lifetime data and photolyses studies [3]. It was revealed that photolysis in the absence of anions, for example, in Ru(II) complex of 3-(pyridin-2-yl)-1,2,4-triazole (figure 3.2) resulted in photoisomerisation (from coordination at N'^1 to N'^4) and substitution of pyridyltriazole in the presence of anions.

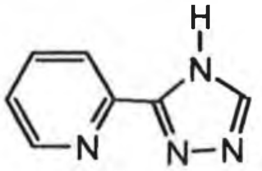

Figure 3.2. 3-(pyridin-2-yl)-1,2,4-triazole.

Triazoles have also been combined with π-acceptors, to produce a unique ligand, pyrazyltriazole which possess both class a and class b ligand properties. Investigations of these complexes revealed that the emitting state could be switched between the bipyridyl and pyrazyltriazole moieties simply by altering the state of protonation of the triazole [4].

Finally, as a result of the availability of two coordination sites (N1' and N4') on triazolate ligands, they have become important as bridging species in polymetallic complexes. It has been found that the negative charge on the bridging triazole in such complexes facilitates communication between the two metal centres. One of the most extensively investigated complexes of this type is that containing bis(pyridyl)triazole [5-7]. This complex, of which there are two geometric isomers, exhibits strong interaction between the two metal centres in the mixed valence state. Intervalence transitions are observed for this complex in the near IR region. For these systems the extent of electronic delocalisation is quite high and is deemed most likely to be induced by enhanced hole transfer via the deprotonated triazolate bridge.

3.1.2 The Chemistry of Quinone and Hydroquinone.

Quinones and hydroquinones form an integral part of many of the biological redox chains, the most commonly noted being their role in electron transport chains in mitochondrial reactions and their function in both electron and proton transport in plant and bacterial photosynthesis as discussed in section 1.3. Quinonoid species, as a result of their redox properties have found frequent use as acceptors and donors in charge transfer complexes or as excited state quenching agents, free in solution. Use of these species has allowed detailed studies of quinone related electron and proton transfers on the basis of thermodynamics, structure and kinetics [8-10].

(i) The electrochemistry of quinones and hydroquinones

The simple quinhydrone redox couple is one of the most extensively studied electrochemical systems. Reference is made to this couple in most physical or electrochemical textbooks whereby the typical reversible couple is expressed as

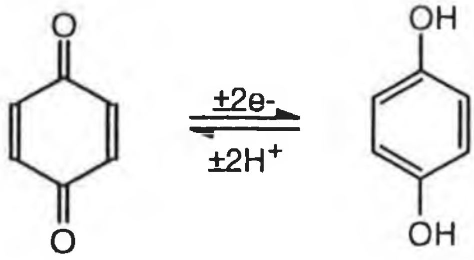

(3.1)

On closer examination however, the electrochemistry of this species, in terms of both mechanism and kinetics contains many non-textbook complexities. In particular, their detailed electrochemical reaction routes are complicated by the fact that electrons and protons are involved consecutively, leading to numerous possible pathways in the overall redox process.

The simplest pathway is that observed for the reduction of a simple quinone in non-protic solvent. In general two consecutive reversible waves are observed [11]. corresponding to the production of the following deprotonated species the intermediate of which is the anionic semiquinone radical.

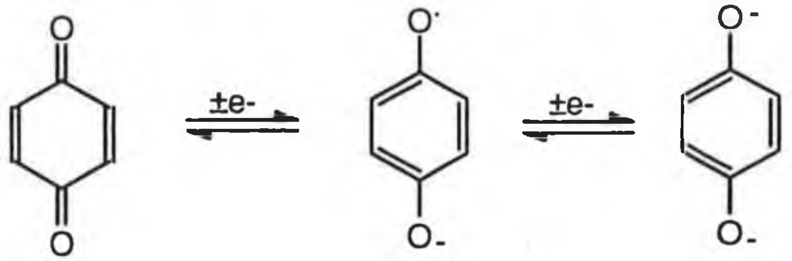

Q $Q^{\cdot -}$ Q^{2-} (3.2)

This straightforward polarographic behaviour, may be altered easily by perturbations in the diffusion layer concentrations of Q, $Q^{\cdot -}$ or Q^{2-}. Examples of such perturbations are acids or bases, ion-pairing, or complex formation equilibria, whose effects may simply shift the first or second reduction wave with respect to one another or its anodic couple, or may completely alter the process.

The electrochemistry of the quinone increases in complexity with increasing solvent proticity, and reversible waves are in general not observed. In fact the quinone redox process is inherently dependent on solvent pH, whereby potential shifts of as much as one volt for the reduction of a quinone may result by variation of the amount of and type of proton donor present in non-aqueous solvents [12].

In protonated media, the possible intermediates and products of quinone electrochemistry are manifold, and are expressed by means of a scheme of squares [13], (see figure 3.3).

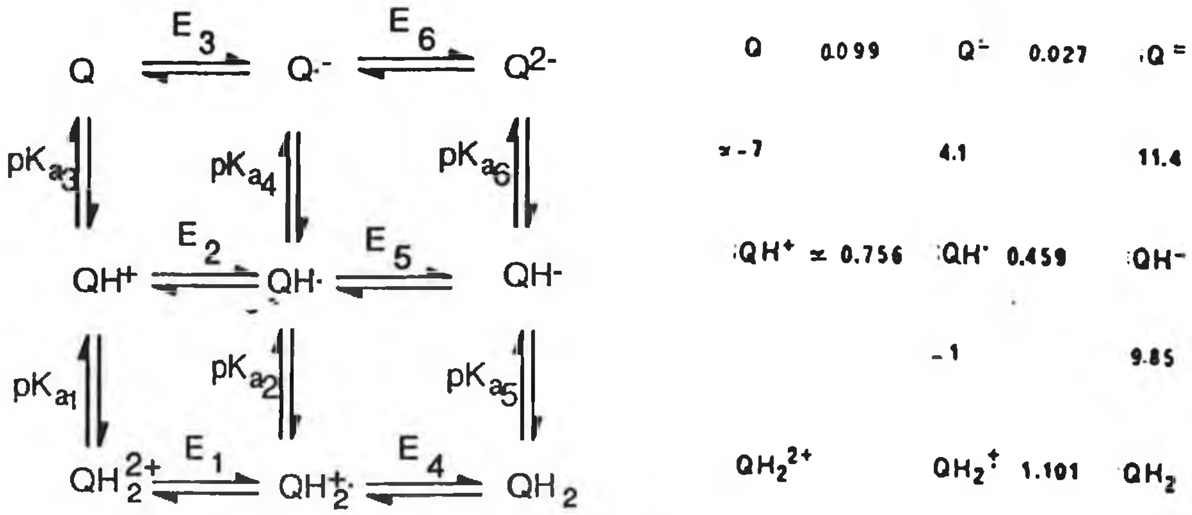

Figure 3.3: Electron and proton transfer scheme of squares for the quinone/hydroquinone redox couple [14-16].

In this scheme all electron exchanges are given by the horizontal arrows and all chemical changes are given on the vertical arrows. Electron transfers occur between structurally similar species whereas proton exchanges occur only between species of the same oxidation state, independently of electron transfer. From the scheme of squares six reaction routes are possible in the reduction of Q to H_2Q and for oxidation of H_2Q to Q. The reaction path taken depends on the acid-base equilibrium constants involved in the general scheme, and also on the kinetics of electron transfer and proton transfer.

For a given electrode potential several reaction pathways may occur simultaneously. Reaction pathways may be different in oxidation and reduction. Laviron, carried out exhaustive examination of this scheme of squares for quinones investigating the kinetics of proton and electron transfers as a function of pH. The results of his examination are shown on the right of figure 3.3, whereby some of the pK_as of the intermediates were determined [14 -16].

The oxidative pathways of hydroquinones are included in the scheme of squares and are applicable in non-aqueous solvents. In the presence of strong base, both protons are removed from simple hydroquinones and separate one electron waves are observed [17], from the oxidation of Q^{2-}. Use of non-hydroxylic base such as pyridine generates the QH^- species which is oxidised at 0.7V, more positive than the corresponding H_2Q oxidation. Oxidation of the fully protonated H_2Q, occurs via an irreversible two electron process which is strongly pH dependant. The role of protons in the electrochemistry of H_2Q was demonstrated firstly by Müller [18], who observed that the addition of the enzyme carbonic anhydrase (which catalyses proton transfer in carbonate buffer) to a solution of quinone in carbonate buffer, converted an irreversible Q/H_2Q couple into a reversible one. Secondly, Bessard and coworkers found that addition of 0.01M $HClO_4$ to a solution of tetramethoxybiphenylhydroquinone produced a 40% increase in linear sweep voltammetry current [19]. Both experiments suggest an increase in reversibility of the redox process on addition of protons, thus implicating them in the rate determining steps of the redox reaction of hydroquinone species. In fact Bessard suggested that oxidation preferentially occurs via a protonated QH_2^{2+} intermediate in the presence of protons.

The previous discussion referred only to the electrochemistry of quinones and hydroquinones in non-aqueous solvents. In aqueous solvents, the non-textbook complexities of these species increases as more intermediates in the scheme of squares become possible, simultaneously, over relatively small pH ranges. Since the electrochemistry treated in this report is limited to non-aqueous solvents, aqueous electrochemistry will not be discussed.

The redox properties of the quinonoid couple have made them attractive candidates as components in donor - acceptor systems, where these accessible redox properties have allowed them to become directly involved in electron transfer processes. One of the commonest uses of quinones in supramolecular photochemistry is in covalently linked porphyrin-quinone systems, in which these moieties are considered simple analogues of the chlorophyll-acceptor system [9, 10]. The quinone /hydroquinone redox process produces the intermediate radical, the semiquinone, which may be anionic or cationic depending on its state of protonation. It is this intermediate of electron transfer, which can be remarkably stable, which makes such systems useful, since it opens up avenues of investigation such as ESR spectroscopy [20, 21]. The involvement of quinones in metal complexes has not been so fast to develop, but in terms of Ruthenium diimine complexes most likely evolved from bimolecular studies of rates of oxidative and reductive quenching of $[Ru(bpy)_3]^{2+*}$ by quinone and hydroquinone [21, 22-24].

3.1.3 Electron transfer reactions involving the Ru(II) polypyridyl complexes.

The long-lived excited state of $[Ru(bpy)_3]^{2+}$ permits it to undergo excited state reaction. As discussed in section 1.4, in the excited state this complex becomes a stronger reductant and oxidant. Since quenching by electron transfer is essentially a redox reaction, photoredox processes are particularly efficient in $[Ru(bpy)_3]^{2+}$. To date most of the investigations into photoinduced electron transfers of $[Ru(bpy)_3]^{2+}$ have been bimolecular. These studies most commonly employing paraquat quenchers [25-28] as a result of their potential as relay molecules in the water reduction process [29] and aromatic amines [30-32].

Quinones and hydroquinones have also been investigated, although to a lesser extent. Early work carried out by Darwent and coworkers explored the electron transfer reactions of both quinones, hydroquinones and methylviologen with $[Ru(bpy)_3]^{2+}$ in aqueous media [33]. The quenching rates for hydroquinones were observed to be considerably slower than those of quinones and methylviologen which possessed similar rates, but the back electron transfer rates for both hydroquinone and methylviologen were slower. This was associated with the increased positive charge on these species which caused fast diffusion apart of the products as a result of repulsive forces. Intermediate semiquinone formation was observed by difference absorption spectroscopy. Vlcek and Boletta [22] carried out quenching experiments with quinones in aprotic media and results compared well, with increased rates for benzoquinone by comparison with aqueous media.

In 1987, von Zelewsky and coworkers followed the quenching reactions of $[Ru(bpy)_3]^{2+}$ by hydroquinones and quinones as a function of pH by ESR spectroscopy [21, 23]. Comparison was made between observed electron transfer rates and theoretical values extrapolated from Marcus theory. One of the most interesting aspects of this report [21] was that at high pH (>8) and low pH (<3) semiquinone radicals appear to form spontaneously from their parent quinone/hydroquinone. This, in particular at low pHs, caused serious deviation between calculated and theoretical electron transfer rates, since semiquinones are very efficient quenching agents.

Intramolecular systems, involving covalently linked Ru(II) polypyridyl species and quencher, again, have predominantly involved paraquat species, where some very fast electron transfer devices have been produced. For example, ruthenium(II) trisbipyridine-diquat complexes were created by Elliot and coworkers as early as 1985 [34], where the influence of introducing substituents onto the bipyridyl units on electron transfers was studied. These complexes were for the most part found to be non-luminescent, as a result of their rapid forward electron transfer, and the existence of electron transfer was related to the excited state redox potentials of the chromophore. Absence of transient absorbance spectra indicated that back-electron transfer is also very rapid.

In 1988 Elliot, Kelley and coworkers reported intramolecular electron transfers in related complexes, in which the methylene chain linking the diquat to the methylbipyridine was of variable length (see figure 3.4) [35].

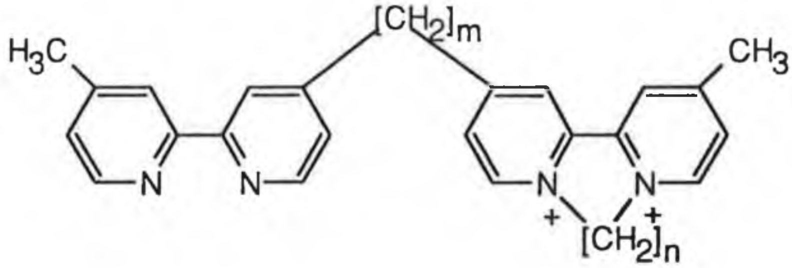

Figure 3.4. The methylbipyridine linked diaquat ligand L, in complexes $[Ru^{II}(L)_n(bpy)_{x-n}]$ *as studied by Kelley and coworkers [35].*

The lowest MLCT excited state is apparently localized on the least methylated bpy and rapid forward electron transfer (80-1700 ps) was observed to occur. From bleach recovery rates it was determined that reverse electron transfer is considerably faster than forward, less than 30 ps. The model employed to describe this process assumed that fast electron transfer occurs between the remote ligand and adjacent ligand producing an equilibrium MLCT population. The electron transfer between the remote and quencher ligand is presumed to be slower (i.e. rate determining). In 1987, this group produced a complex containing covalently linked donor (phenothiazine) and acceptor groups (diaquat) [36]. Analysis of the transient absorbance difference spectrum of this complex suggested that excitation produces a relatively long lived charge separated state (165 ns).

Schmehl and co-workers have also carried out investigations into ruthenium(II)diimine-diaquat complexes [37, 38]. This group reported on Ru(II)-viologen complexes in which the reverse electron transfer rates are weakly inverted, allowing the manipulation of relative forward and reverse electron transfer rates simply by altering solvent.

Although relatively common in porphyrin systems, reports of ruthenium(II)diimine complexes covalently linked to pendant hydroquinone or quinone quenchers are surprisingly rare, and covalently linked phenolic quenchers appear to be completely absent from the literature.

One of the few examples of such systems was reported by Schanze and Sauer, in which a Ru(II)polypyridyl complex was covalently linked to a p-benzoquinone via a peptide oligomer spacer [39].

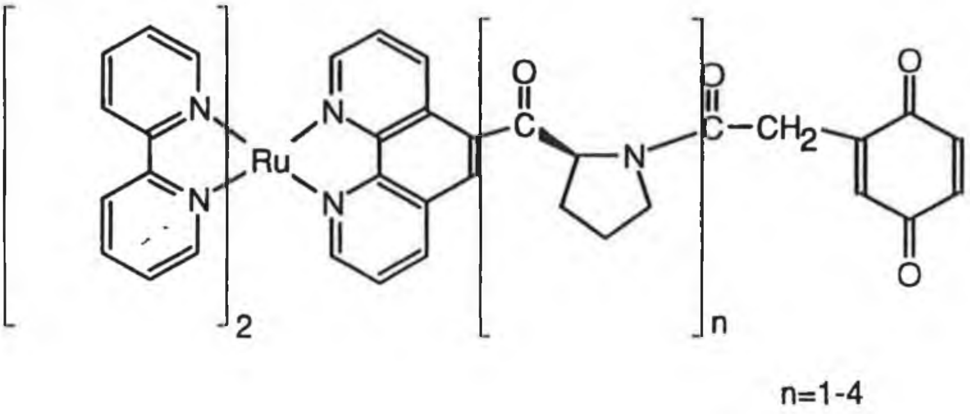

Figure 3.5. Example of a peptide-bridged quinone complex created by Schanze and Sauer [39]

Significant quenching of the excited ^{3}MLCT state was detected which was attributed to transfer from Ru*⟶Q electron transfer. This process was found to be strongly dependent on the number of peptide linkages between chromophore and quenchers. This work was hampered by multiexponential lifetime decays which would appear to be due in part to the presence of hydroquinone impurities, and also to the presence of peptide confomers.

In 1993, Colbran and coworkers reported on a $[Ru(bpy)_2(phen)]^{2+}$ complexes in which the phen is substituted with a hydroquinone or quinone moiety [40]. No luminescence quenching was observed in neutral acetonitrile for the complex containing the pendant hydroquinone. The group were unable to prepare a ligand or complex which contained a pendant quinone moiety, however, the complex which contained a coordinated quinone exhibited quenching. Lehn and coworkers recently reported on a ruthenium(II) polypyridyl complexes containing a bipyridyl group linked by a methylene to a hydroquinone (figure 3.6), [41].

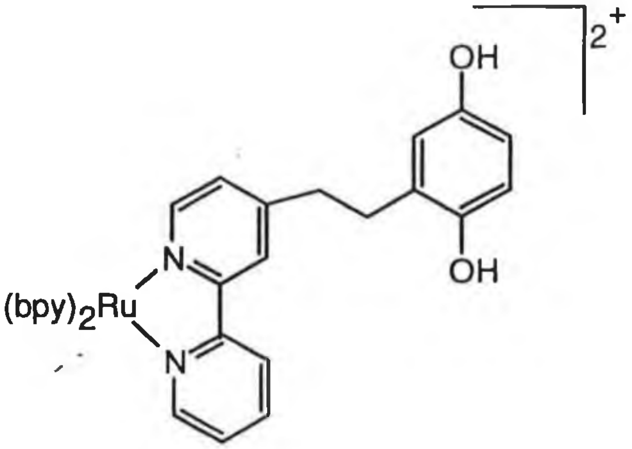

Figure 3.6. Lehns covalently linked hydroquinone-bpy Ru(II) complex [41].

Their study involved the oxidation of this complex to quinone, employing cerium (IV) ammonium nitrate (leaving 8% hydroquinone) or in-situ electrochemistry, which they reported, quenched the ^{3}MLCT state very efficiently. Neither the dimethoxy nor hydroquinone substituted complexes exhibited any significant quenching.

Overall, despite the small amount of literature on the subject, several points consistently emerge. Firstly, the hydroquinone moiety in a covalently linked donor acceptor metal complex is largely incapable of quenching. Secondly, in all reports to date, either great difficulty is encountered in creating the quinone moiety, (i.e. hydroquinone impurities remain after oxidation) or it could not be created at all. Finally, in all cases reported for the quinone/hydroquinone and for a large portion of diquat quenchers, the quenching agent is bound either on or in close proximity to the lumophoric site. The complexes described in this chapter are designed to break some of these moulds.

3.2 Synthetic procedure:

3.2.1 Preparation of ligands

H_3L1, 1.3-(2,5-dihydroxyphenyl)-5-pyridin-2-yl)-1,2,4-triazole.

2,5-dihydroxybenzoic acid (20g, 0.13M) was esterified by reflux in pure ethanol (150 cm^3) and conc. sulphuric acid (10 cm^3) over activated molecular sieve (type 3A) for 8 hours. The product was neutralised with saturated sodium hydrogen carbonate, filtered and then extracted into diethyl ether. The ether fractions were combined and dried over magnesium sulphate and the ether was removed under vacuum to yield the ester, 11g, 46.5%. The ester (8g, 0.044M) was dissolved in pure ethanol (25 cm^3) and hydrazine monohydrate (2.2g, 0.044M) was added dropwise. After 2 hours at RT the solution was cooled to 0^{o}C and then left at -20^{o}C overnight. The resulting tan coloured precipitate was washed with diethyl ether (25 cm^3).

Cyanopyridine (3.22g, 0.031M) was refluxed for 2 hours in pure methanol (100 cm^3) in the presence of sodium metal (0.76g, 0.033M). After this period the 2,5-dihydroxybenzoylhydrazide (5.2g, 0.031M) was added in pure ethanol (25 cm^3) to the reaction mixture. This was refluxed for a further two hours after which the solvents were removed under reduced pressure to produce a pale yellow solid which was washed with diethyl ether (25 cm^3).. After drying the solid it was refluxed in minimum ethylene glycol for 1 hour to cyclize the triazole. After cooling the solution, excess water was added to the solution to precipitate the product, which was then recrystallised from ethanol/water (2:1v/v) treated with 0.05g decolourising charcoal, producing 1.6g (20.3% yield, 10.2% overall) of product. Mp = 200-204^{o}C. M/e = 254, (calc. 254).

^{1}H NMR (DMSO-d$_6$,ppm) = d, 8.16, (d, 1H, pyridyl H^3); 7.99, (t, 1H, pyridyl H^4); 7.49, (t, 1H, pyridyl, H^5); 8.79, (d, 1H, pyridyl H^6); 674-6.79, (m, 2H, dihydroxyphenyl H$^{5''}$ and H$^{6''}$); 7.57, (s, 1H, dihroxyphenyl H$^{3''}$), 12.1 (s,broadened OH), 15.0, (s, broadened triazole NH).

OAc_2L1, Acetylation of H_3L1.

The ligand H_3L1 (2.0g, 7.87x10^{-3}M) was dissolved in pyridine (25 cm^3) with one drop of sulphuric acid as a catalyst [42]. A slight excess of acetic anhydride (2.45g, 2.4x10^{-3}M) was added and the solution was refluxed for 45 minutes. The reaction mixture was allowed to cool and then poured onto ice (150 cm^3). This mixture was left at 4°C overnight and a white crystalline product (1.63g, 61%) was obtained. Mp = 168-172°C, m/e = 339 (calc. 339)

^1H NMR, (DMSO-d_6 , ppm):, 8.19, (d, 1H, pyridyl H^3); 7.96,(t, 1H, pyridyl H^4); 7.6, (t, 1H, pyridyl H^5); 8.71, (d, 1H, pyridyl H^6); 7.0-7.2, (m, 2H phenyl $H^{5''}$ and $H^{6''}$); 7.8, (s, 1H, phenyl $H^{3''}$); 2.26(s, 3H acetate H); 2.75, (s, 3H, acetate H).

H_2L2, Synthesis of 3-(2-phenol)-5-(pyridin-2-yl)-1,2,4-triazole.

This ligand was prepared via a modified literature method [43]. 60g (0.4M) of methyl salicylate was combined with a slight excess of hydrazine hydrate in ethanol (20 cm^3). The mixture was left stirring at room temperature for 3 hours and then left under refrigeration overnight. The white crystalline product was collected by filtration. This product was then refluxed with equimolar methyl-2-picolinimidate for two hours in ethanol (50 cm^3). The reaction mixture was concentrated to 20 cm^3 and allowed to cool, the resulting yellowish sold was collected by filtration and dried. Cyclisation took place by refluxing the product in ethylene glycol for 30 minutes. Yield 52g, 55%, Mp 220-221°C (Lit 221-222°C) [43].

1H-NMR, (DMSO-d_6, ppm): 8.10, (d, 1H, H^3); 7.90, (t, 1H, H^4); 7.25, (t, 1H, H^5); 8.64, (d, 1H, H^6); 11.10, (s, OH); 15.0, (s, NH); 7.98, (m, 1H, $H^{3''}$); 7.0, (m, 1H, $H^{4''}$); 7.51, (t, 1H, $H^{5''}$); 6.95, (m, 1H, $H^{6''}$).

HL3, Synthesis of 3-(2,5-benzoquinone)-5-(pyridin-2-yl)-1,2,4-triazole.

3-(2-phenol)-5-(pyridin-2-yl)-1,2,4-triazole (H_2L2) (0.711g, 3 x 10^{-3}M) was dissolved in dichloromethane and this was heated to reflux under an argon atmosphere. A slurry of benzeneseleninic acid (0.832g, 4.4 x 10-3M) in dichloromethane (10 cm^3)was then prepared and this was added dropwise to the refluxing phenol over a 20 minute period. The mixture was then refluxed for a further 6 hours by which time the solution had turned a deep red colour. After reaction the solution volume was reduced to 10 cm^3 and this was then left at -20^oC overnight. A deep red solid was produced which was purified by chromatography on alumina with chloroform-hexane-methanol (5:4:1 v/v), yielding 0.61g, 81%, quinone product. Mp = 98-101^oC.

^1H NMR, (DMSO-d_6, ppm): 8.1, (d, 1H, pyridyl H^3), 7.92, (t, 1H, pyridyl H^4), 7.5, (t, 1H, pyridyl H^5), 8.61, (d, 1H, pyridyl H^6), 6.55-6.72, (m, 2H, quinone "H^5 and "H^6), 5.65, (s, 1H, quinone "H^3). Carbonyl groups were verified from ^{13}C nmr where two resonances at 181.8 and 182.9 ppm corresponding to C=O were observed and IR where a C=O strectching vibration was observed at 1661 cm^{-1}.

H_2L4, Synthesis of 3-(4-phenol)-5-(pyridin-2-yl)-1,2,4- triazole.

Methyl-2-picolinimidate was prepared by refluxing cyanopyridine (31g, 0.3M) in methanol with sodium metal (2g, 0.086M) for 2 hours. Following this reaction, 4-hydroxybenzoichydrazide (40g, 0.263M) dissolved in methanol was added to the reaction mixture which was then refluxed for a further hour. A tan solid was formed on cooling which was collected by filtration. This solid was washed with water (25 cm^3) and diethyl ether (25 cm^3) and allowed to dry. The product was cyclised by refluxing the dry solid in minimum ethylene glycol for 1 hour. The product was collected by adding water to the mixture and leaving at 4^oC for two hours. The yield was 30g (50%), mp >250^oC.

H^1NMR (DMSO-d6, ppm): 8.28, (d, 1H, pyridyl H^3), 8.00, (t, 1H, pyridyl H^4), 7.54, (t, 1H, pyridyl H^5), 8.76, (d, 1H, pyridyl H^6), 7.04, (d, 2H, phenol "H^3 and "H^2), 8.09, (d, 2H, "H^5 and "H^6).

HL5, Synthesis of 3-(phenyl)-5-(pyridin-2-yl)-1,2,4-triazole.

2-cyanopyridine (22g, 0.21M) was dissolved in ethanol (60 cm^3). Hydrazine hydrate (7.5g, 0.3M) was added and the mixture was stirred for 12 hours to produce 2-picolylamhydrazone as white needles. The 2-picolamhydrazone (27.2g, 0.2M) and triethylamine (30g, 0.3M) were dissolved in THF (25 cm^3). Benzoylchloride (0.2M) was dissolved in THF and this was added dropwise to the reaction mixture to produce a tan solid which was collected by filtration and washed with water (25 cm^3) and diethyl ether (25 cm^3). The solid was cyclised by reflux in minimum ethylene glycol for 30 minutes. The product was collected by addition of water to the solution to precipitate out a grey solid, which was recrystallised in hot ethanol/water with decolorising charcoal (0.05g) to produce white needles (21.3g, 46%). Mp = 188-191^{o}C, m/e = 220.

1H NMR, (DMSO-d_6, ppm): 8.34,(d, 1H, pyridyl H^3), 8.25, (t, 1H, pyridyl H^4), 8.15, (t, 1H, pyridyl H^5), 8.75, (d, 1H, pyridyl H^6), 7.55-7.70, (m, 5H, benzene).

H_3L6, Synthesis of 3-(3,4-dihydroxyphenyl)-5-pyridin-2-yl)-1,2,4-triazole.

3,4-dimethoxybenzoylchloride (2.005g, 0.01M) was dissolved in THF (10 cm^3). A solution of 2-picolylamhydrazone (see above) (1.36g, 0.01M), in THF (30 cm^3) with triethylamine (1.5g, 0.015M). The former solution was added dropwise to the latter at 0^{o}C with vigorous stirring. The exothermic reaction produced an off-white crystalline product. The mixture was quickly heated to boiling for a brief period and the solution reduced in volume to 25 cm^3. An equivolume of H_2O was added and the mixture left overnight at 4^{o}C. The resulting white precipitate was collected by filtration, washed with water (50 cm^3) and allowed to dry. Once dry the compound was cyclised by reflux for 40 minutes in minimum ethylene glycol. After this period, when the solution had been allowed to cool, crushed ice was added to the mixture, and the resulting tan solid was collected by filtration, washed with water and diethyl ether. Yield 1.48g, 52.6%. Mp = 186-188°C.

1H NMR, (DMSO-d_6, ppm): 8.12,(d, 1H, pyridyl H^3) 7.95, (t, 1H, pyridyl H^4), 7.63, (t, 1H, pyridyl H^5), 8.68, (d, 1H, pyridyl H^6), 7.45, (s, 1H, $H^{2''}$), 7.6, (d, 1H, $H^{6''}$), 7.05, (d, 1H, $H^{5''}$), 3.62, (s, 6H, O-methyl).

The methylated ligand (1.0g, 0.004M) was then dissolved in dichloromethane (anal. grade) (20 cm^3). This was stirred under N_2 on a cold plate (at -50°C) for 20 minutes for the reagents temperature to equilibrate. BBr_3 (2 M in dichloromethane) (20 cm^3) was then added dropwise to the solution over a 20 minute period. The reagents were then removed from the cold palate and allowed to heat to room temperature overnight. The mixture was then poured into a sodium chloride saturated solution of crushed ice, and the ligand crashed out to produce 1g of H_3L6. Yield 0.9g, 89%. Mp 262-266°C.

1H NMR, (DMSO-d_6, ppm): 8.18,(d, 1H, pyridyl H^3) 7.98, (t, 1H, pyridyl H^4), 7.52, (t, 1H, pyridyl H^5), 8.74, (d, 1H, pyridyl H^6), 6.58-6.78 (m, 3H, catechol).

3.2.1 Synthesis of complexes.

$[Ru(bpy)_2(HL1)]PF_6.2H_2O$.

The acetylated ligand (0.4g, 1.3 x10^{-3}M) was dissolved in ethanol/water (70 cm^3 1:1 v/v) which was heated to reflux. $Ru(bpy)_2Cl_2.2H_2O$ (0.65g, 1.25 x 10^{-3}M) was added slowly and the reaction mixture refluxed for 5 hours. After this period the solution was concentrated under vacuum to 20 cm^3 and a few drops of concentrated NH_4PF_6 solution was added to form the PF_6 salt. This product was collected by filtration and recrystallised from acetone/water (1:1 v/v). The $[Ru(bpy)_2(OAc_2L1)]PF_6$ was dissolved in methanol/water (30 cm^3, 2:1, v/v) and saturated sodium carbonate solution was added (20 cm^3) to deacetylate the complex. The solution was stirred for 1 hour at 30 °C and then neutralised with conc. HCl, the solution was filtered and the solvent removed under vacuum. The complex was then recrystallised in acetone/water (1:1 v/v), to produce 0.741g, (70%) $[Ru(bpy)_2(H_2L1)]PF_6$.

Analyses calculated for $[RuC_{33}H_{29}N_8O_4PF_6]$. C, 46.76; H, 3.45; N, 13.22%.

Found C, 46.69; H, 3.23; N, 13.31%.

Direct reaction with the hydroquinone ligand was also initially used to produce $[Ru(bpy)_2(H_2L1)]PF_6.2H_2O$. However, as a result of bpt produced as a side product of the H_3L1 synthesis, (see appendix 1) other impurities were often inadvertently generated, and the product required semi-prep HPLC.

$[Ru(bpy)_2(H_2L2)](PF_6).2H_20$.

HL2 (0.30g, 1.27 mmol) was dissolved in ethanol/water (1:1 v/v) 50 cm^3. $Ru(bpy)_2Cl_2.2H_2O$ (0.658g, 1.27 mmol) was added to this and the mixture was refluxed for 5 hours. After reaction the mixture was filtered, and the volume reduced under pressure to 10 cm^3. A few drops of concentrated NH_4PF_6 was added to this solution until precipitation ceased, and the bright orange solid was collected under vacuum. The complex was recrystallised from acetone/water 1:1 v/v and a drop of 1M NaOH. Yield = 0.7g, 69%, (C.H.N in reference [44]

$[Ru(bpy)_2(L3)]PF_6.2H_2O$

Two different methods were employed for this synthesis

(a) Synthesis employing HL3;

HL3 (0.252g, 1 x10^{-3}M) was dissolved in ethanol/water (40 cm^3, 1:1, v/v) and this was heated, $Ru(bpy)_2Cl_2.2H_2O$ (0.494g, 9.5 x 10^{-4}M) was then added slowly. The mixture was refluxed for 5 hours. The product was isolated as the PF_6 salt, as described above and purified using semi-preparative HPLC yielding 0.38g, 47%.

(b) $[Ru(bpy)_2(H_2L1)]PF_6.2H_2O$ (0.2g, 2.5 x 10^{-4}M) was dissolved in dichloromethane (20 cm^3) and this was refluxed. A slurry of Benzeneseleninic acid (0.66g, 3.5 x 10^{-4} M) was made up in dichloromethane (10 cm^3) and this was added slowly to the refluxing solution over a 20 minute period. The mixture was then left refluxing for a further 2 hours. The course of the reaction was followed by HPLC and after 2 hours the complex had been completely oxidised. The solvent was removed under vacuum and the solid collected was washed with copious amounts of water followed by diethyl ether. The complex was then recrystallised twice from diffusion of diethyl ether into acetone, to yield 0.19g, (94%) quinone complex.

Analyses for $[RuC_{34}H_{30}N_9O_4PF_6.]$:calculated: C, 47.7 ; H, 3.40; N, 14.3%.

Found: C, 47.71; H, 3.19; N, 13.92%.

$[Ru(bpy)_2(HL4)](PF_6)_2$

This complex was synthesised as described for $[Ru(bpy)_2(HL2)]PF_6$, except recrystallisation from acetone/water, (1/1, v/v) was carried out in the presence of 1 drop of 0.1M sulphuric acid. Yield 0.64g, = 62%.

Analysed for $[RuC_{33}H_{25}N_8OP_2F6]$:calculated: C,42.09 ; H, 2.80; N, 11.90%.

Found: C, 42.88; H, 3.24; N, 11.92%.

$[Ru(bpy)_2(HL5)](PF_6)_2$

HL5 (0.3g, 1.35 mmol) was dissolved in ethanol/water (40 cm^3 1:1 v/v) and this was heated. To this $Ru(bpy)_2Cl_2.2H_2O$ (0.67g, 1.3 mmol)was added slowly. This mixture was refluxed for 5 hours. The solvent evaporated to 10 cm^3 of water and the orange complex was precipitated as the PF_6 salt. The complex was recrystallised from acetone/water (1:1 v/v) in the presence of one drop of triflouroacetic acid to yield 0.8g, (64%).

Analysed for $[RuC_{33}H_{26}N_8P_2F_{12}]$; calculated C,42.8; H, 2.81; N, 12.1%.

Found C, 42.9; H, 3.2; N, 12.29%.

$[Ru(bpy)_2(L6)]PF_6.2H_2O$

This complex was prepared in two ways;

(a) The methylated ligand was reacted with $Ru(bpy)_2Cl_2.2H_2O$ in the usual manner and deprotected in the manner described for the ligand.

(b) The deprotected H_3L6 ligand was complexed directly in the manner described above. The drawback in this method is that three products form the required mononuclear N,N coordinated complex, an O,O coordinated complex, particularly when the reaction is carried out in the presence of base, (see appendix II) and some dimer. Therefore semi-preparative HPLC was required for purification of product.

Analyses calculated for $[RuC_{33}H_{29}N_8O_4PF_6]$. C, 46.76; H, 3.45; N, 13.22 %.

Found C, 46.59; H, 3.33; N, 12.89 %.

3.3 Results and discussion

3.3.1 Synthetic procedures.

The synthetic procedures employed for the ligands were modifications of methods previously described [45-47]. The oxidation of the phenol by benzeneseleninic acid (BSA) to produce the quinone ligand HL3 is based largely on the work of Barton and coworkers [48, 49]. This group demonstrated the oxidation of substituted phenols by benzeneseleninic acid in dichloromethane yielded p-quinones in good yield. This oxidation was first attempted on 3-(2-phenol)-5-(pyridin-2-yl)-1,2,4-triazole. This resulted in formation of the p-quinone in high yield (>80%), the o-quinone was not formed as a by-product. This oxidation was also attempted on the 3-(4-phenol)-5-(pyridin-2-yl)-1,2,4-triazole ligand with no success. This may be attributed to the fact that p-quinone could not be formed in this reaction and that the other alternative, o-quinone formation may be inhibited by deactivation at this site which is meta to the pyridyltriazole substituent. But since in the 3-(2-phenol)-5-(pyridin-2-yl)-1,2,4-triazole, o-quinone formation involves substitution at a position also meta to the pyridyltriazole this may not be the case. But whatever the reason, o-quinone formation (which has been observed in lesser fractions by Barton et al in their reactions 48, 49]) does not occur for either of these phenols, it is possible that a change in reaction conditions such as using bezeneseleninic anhydride instead of the acid, or reaction in other solvents might encourage o-quinone formation.

The second synthesis for $[Ru(bpy)_2(L2)]PF_6$ involved direct oxidation of the hydroquinone $[Ru(bpy)_2(L1)]PF_6$. This is the first time BSA was employed to oxidise a hydroquinone in a metal complex. The result was complete oxidation of the hydroquinone to form a stable quinone moiety. This oxidation was monitored on HPLC until completion, no side products were observed and 100% oxidation occurred. We had previously attempted this oxidation with other oxidising agents such as cerium(IV)sulphate and 2,3-dichloro-4,5-dicyano-1,4-benzoquinone the result in these instances was either incomplete oxidation of the hydroquinone or oxidation of the entire complex inclusive of the metal. Similar problems in the direct oxidation of hydroquinone in metal complexes have been reported [39, 40]. Oxidation of the pendent hydroquinone using BSA provides an ideal route for this synthesis, since the reaction is one-pot, the conditions are very mild, and the yields high. Attempts were also made to oxidise the o-phenol complex directly with BSA to form the quinone, this was unsuccessful, most likely as a result of the considerable steric hindrance in the complex. The ortho or para orientation of the product quinone is known to be dependent on the steric hindrance of the substituents on the phenol [49]. This is the case because the mechanism of reaction of the acid involves electrophillic substitution on the phenol to form a phenylselenylated intermediate followed by sigmatropic rearrangement, to form the quinone.

3.3.2 ^1H NMR spectroscopy and general structural characterisation.

The NMR data for the complexes under investigation are shown in table 3.1, and the COSY spectra for these complexes are displayed in appendix 1.

In each instance there are two coordination possibilities for these complexes. The metal may bind via $N^{1'}$ or $N^{4'}$ of the triazole moiety. By employing 2-D-correlation NMR and complexes in which the bipyridyl moieties are deuterated (see chapter 6) a complete assignment could be made.

Utilising the hydroquinone complex $[Ru(bpy)_2(H_2L1)]PF_6$ as an example (see figure 3.7), the most significant shift observed in all these complexes by comparison with their free ligand NMR is the that of the pyridine H^6 proton. An upfield shift of 1.2 ppm is observed in $[Ru(bpy)_2(H_2L1)]PF_6$, this is behaviour typical of coordinated pyridines [50-52], as a result of diamagnetic anisotropic interaction of the H^6 proton with the adjacent bipyridyl ring.

This shift eliminates any possibility that the hydroquinone moiety may be involved in coordination.

Table 3.1. ^{1}H-NMR data for coordinated ligands L1-L6 in d_3-acetonitrile.

	Chemical shifts /ppm vs Me_4Si							
Complex	**H^3**	**H^4**	**H^5**	**H^6**	**$H^{3''}$**	**$H^{4''}$**	**$H^{5''}$**	**$H^{6''}$**
1*	8.20 (d)	8.0 (t)	7.21 (t)	7.70 (d)	7.64 (d)	---	6.89 (m)	6.80 (d)
2*	8.24 (d)	8.04 (t)	7.32 (t)	7.78 (d)	7.98 (d)	6.78(m)	7.15 (m)	6.84 (m)
3*	8.28 (d)	8.04 (t)	7.35 (t)	7.80 (d)	7.65 (s)	----	7.2 (m)	7.3 (m)
4*	8.24 (d)	8.04 (t)	7.38 (t)	7.70 (d)	6.83 (d)	-----	6.98 (m)	6.88(m)
5*	8.30 (d)	8.03 (t)	7.23 (t)	7.62 (d)	phenyl	protons	7.38-	7.48 (m)
6*	8.33 (d)	8.05(t)	7.35(t)	7.77 (d)	7.25(s)	-----	7.42 (d)	6.95(d)

*1 = $[Ru(bpy)_2(H_2L1)]PF_6$, 2 = $[Ru(bpy)_2(HL2)]PF_6$, 3 = $[Ru(bpy)_2(L3)]PF_6$, 4 = $[Ru(bpy)_2(HL4)]PF_6$, 5 = $[Ru(bpy)_2(L5)]$ 6 = $[Ru(bpy)_2(H_2L6)]PF_6$.. Hydroxyl protons were observed at roughly 11.4 ppm for 1, 2 and 6.

Bipyridyl resonances could not be assigned to individual rings but were observed to occur in the following regions;

H^3	H^4	H^5	H^6
8.3-8.8	7.6-8.2	7.4-7.7	7.9-8.15.

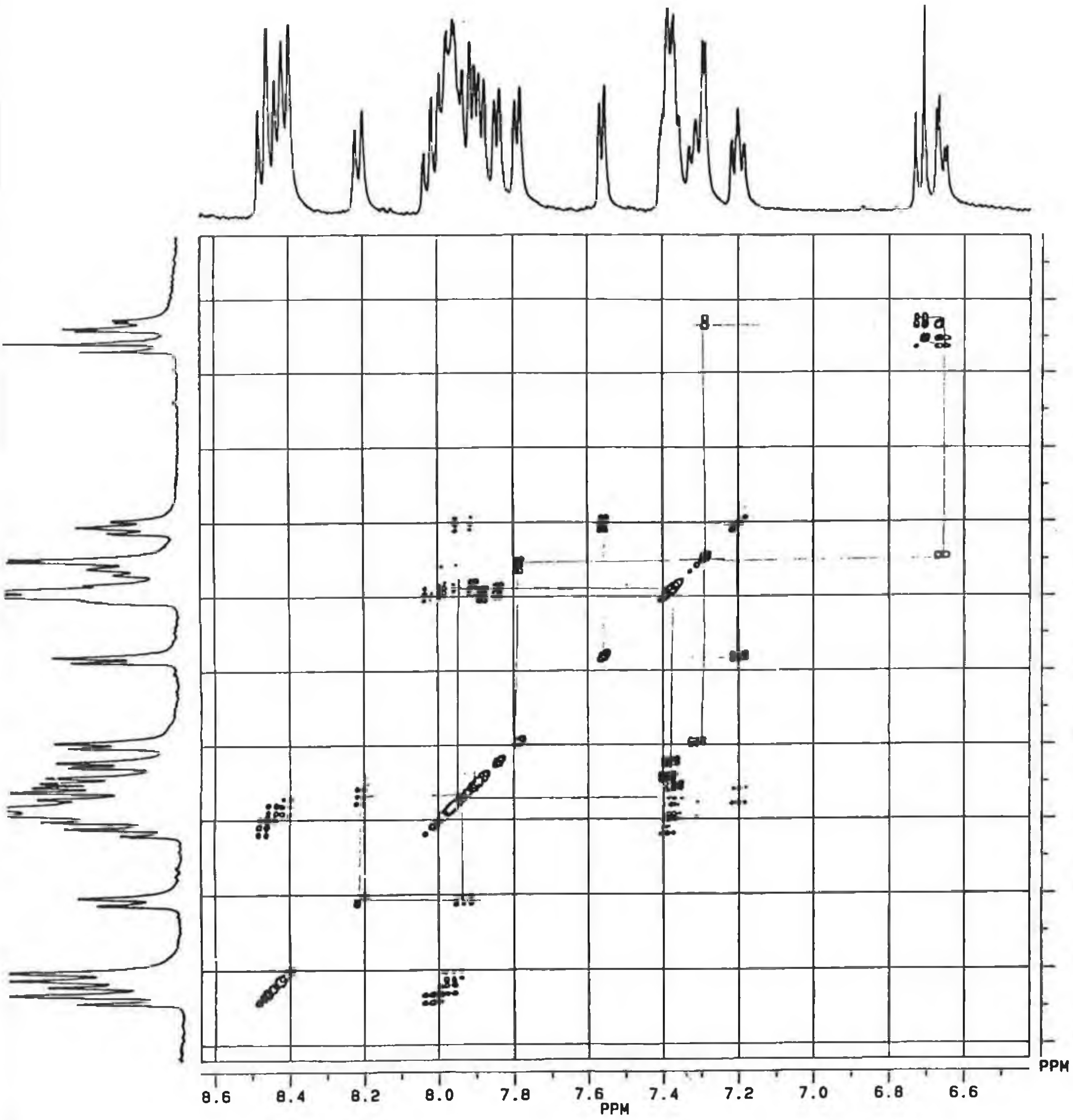

Figure 3.7. ^1H and COSY nmr spectrum of $[Ru(bpy)_2(H_2L1)]PF_6$ in acetonitrile-d_3.

In order to ascertain whether the metal is bound via $N^{1'}$ or $N^{4'}$ of the triazole ring comparison of the influence of coordination on NMR of the hydroquinone ring is made with the o-phenol complex $[Ru(bpy)_2(HL2)]PF_6$ [44]. X-ray crystallography of the o-phenol complex has revealed that this complex is $N^{1'}$ coordinated. In $[Ru(bpy)_2(HL2)]PF_6$ the $H^{5''}$ proton experiences the largest upfield shift (0.41 ppm) for the phenol moiety. Similarly, for $[Ru(bpy)_2(H_2L1)]PF_6$ the most significant shift for the hydroquinone moiety is $H^{5''}$ (0.32 ppm). This suggests that the complex is $N^{1'}$ bound. If $N^{4'}$ bound one would expect larger chemical shifts for the hydroquinone moiety by comparison with the free ligand as a result of the considerable steric hindrance between the hydroquinone and the adjacent bpy group. This point is illustrated well by a complex in which the pendent species is a methyl group which, although considerably smaller, experiences a shift of 0.5 ppm when coordinated via $N^{4'}$ [53]. Therefore, the complex is deemed to be bound via the pyridyl N^1 and $N^{1'}$ of the triazole of H_3L1.

Similar arguments may be applied to the other complexes discussed here, as may be seen from the data in table 3.1, the nmrs for all these species are comparable. It would appear therefore that in the circumstances, where the pyridyl triazole ligand contains a pendent aryl group the $N^{4'}$ coordination mode does not transpire. This is most likely a result of the steric hindrance potentially occurring in such circumstances. This is illustrated by computational values for the geometry optimised structures of $[Ru(bpy)_2(H_2L1)]PF_6$ (figure 3.8) modelled using Hyperchem. The energy of the equilibrated $N^{4'}$ coordinated complex of the hydroquinone is found to be 74 $Kcalmol^{-1}$ whereas that of the $N^{1'}$ linked complex is lower at 60 $Kcalmol^{-1}$. Since these values are based on simple Newtonian mechanics, they can only be viewed as rough approximations. However, comparison of computationally optimised structures with those of real crystal structures were carried out and although bond lengths were found on average to be longer in modelled structures, bond angles were found to be almost identical to those of genuine crystal structure of $[Ru(bpy)_2(HL2)]PF_6$.

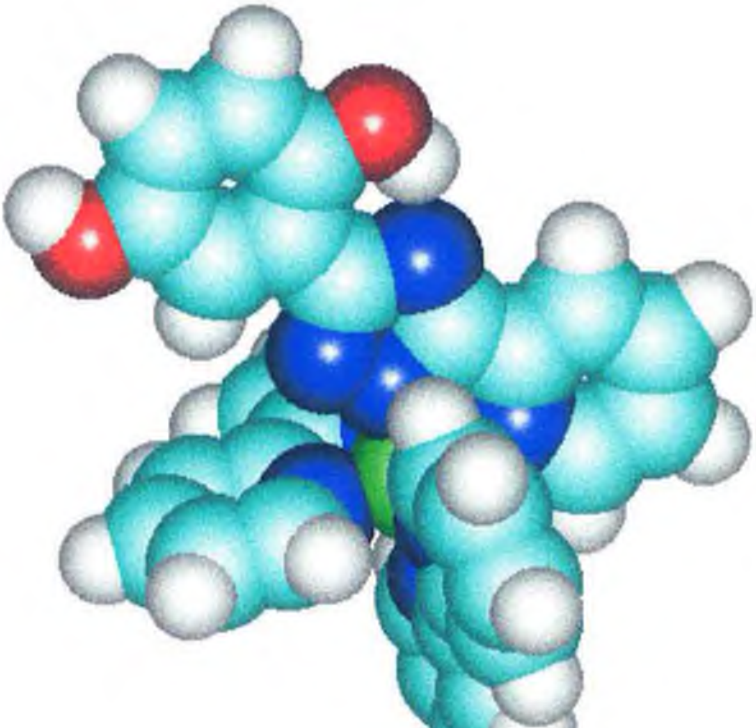

Figure 3.8. Computationally modelled structures for $N^{1'}$ *coordinated* $[Ru(bpy)_2(H_2L1)]^+$ *where pale blue = carbon, dark blue = nitrogen, red = oxygen, green = ruthenium and white = hydrogen.*

The absence of N'^4 coordination has also been noted in mononuclear bpt complexes, where the pendent group is a similarly bulky pyridine [54].

The quinone complex $[Ru(bpy)_2(L5)]PF_6$ is verified as such from both ^{13}C and IR spectroscopy. The ^{13}C spectra reveals two resonances at 181.83 ppm and 182.93 ppm , and in the IR an intense peak is observed at 1646 cm^{-1} corresponding to a C=O stretching vibration there is also no evidence in the ^{1}Hnmr for the presence of OH. This carbonyl peak is absent in the IR spectra of both the hydroquinone and phenyl complexes.

3.3.3 Electronic and Redox properties.

3.3.2.1 Electronic properties:

The absorbance and emission data for the complexes discussed are presented in table 3.2. Figure 3.9 shows the absorption spectra of the model phenyl complex $[Ru(bpy)_2(L5)]^+$ which is typical of these complexes. The compounds discussed all exhibit intense absorption in the visible region around 470 nm, for the deprotonated species. These bands are attributed to $d\pi$-π^* metal to ligand charge transfer transitions (MLCT), and are typical of complexes of this type [55].

Table 3.2. Absorption and Emission data.

Complex	Absorbance	Emission		Lifetimes		ϕem
	λ_{max} (nm)	(nm)		(ns)		
	(log ε)	RT	77K	RT*	77K	
$[Ru(bpy)_2(H_2L1)]^+$	475 (3.99)	672	614	160	3564	1.4×10^{-3}
pH > 10	475	672	614	90	1830	2.5×10^{-4}
$[Ru(bpy)_2(H_3L1)]^{2+}$	430 (4.36)	623	577	-----[B]	4364	2.9×10^{-4}
$[Ru(bpy)_2(HL2)]^+$	463 (4.02)	665	623	220	1689	1.4×10^{-3}
pH > 10	475	672	623	140		2.44×10^{-4}
$[Ru(bpy)_2(H_2L2)]^{2+}$	435 (4.12)	616	585	----[B]	4278	4.40×10^{-4}
$[Ru(bpy)_2(L3)]^+$	470 (4.00)	667	627	190	5094	8.6×10^{-4}
pH > 10	470	667	627	120		2.4×10^{-4}
$[Ru(bpy)_2(HL3)]^{2+}$	440 (4.11)	638	585	----[B]	3878	-----
$[Ru(bpy)_2(HL4)]^+$	467 (3.99)	672	623	140	3849	1.36×10^{-3}
pH > 10	467	672	623	101	1689	2.44×10^{-4}
$[Ru(bpy)_2(H_2L4)]^{2+}$	436 (4.06)	626	585	----[B]	4278	4.4×10^{-4}
$[Ru(bpy)_2(L5)]^+$	482 (3.93)	690	615	225	2613	2.20×10^{-3}
$[Ru(bpy)_2(HL5)]^{2+}$	440 (4.01)	658	589	----[B]	3073	-------
$[Ru(bpy)_2(H_2L6)]^+$	495 (4.01)	662	611	183	3414	1.5×10^{-3}
pH > 10	495	662	611	110	1883	1.50×10^{-4}
$[Ru(bpy)_2(H_3L6)]^{2+}$	439 (4.07)	647	578	----[B]	5084	2.3×10^{-4}

* RT measurements were carried out in acetonitrile degassed by purging with argon. At 77K solvent employed was methanol/ethanol 4:1 v/v.

[B] The values for complexes in which the triazole was protonated are outside the range of the instrumentation (i.e. < 20 ns).

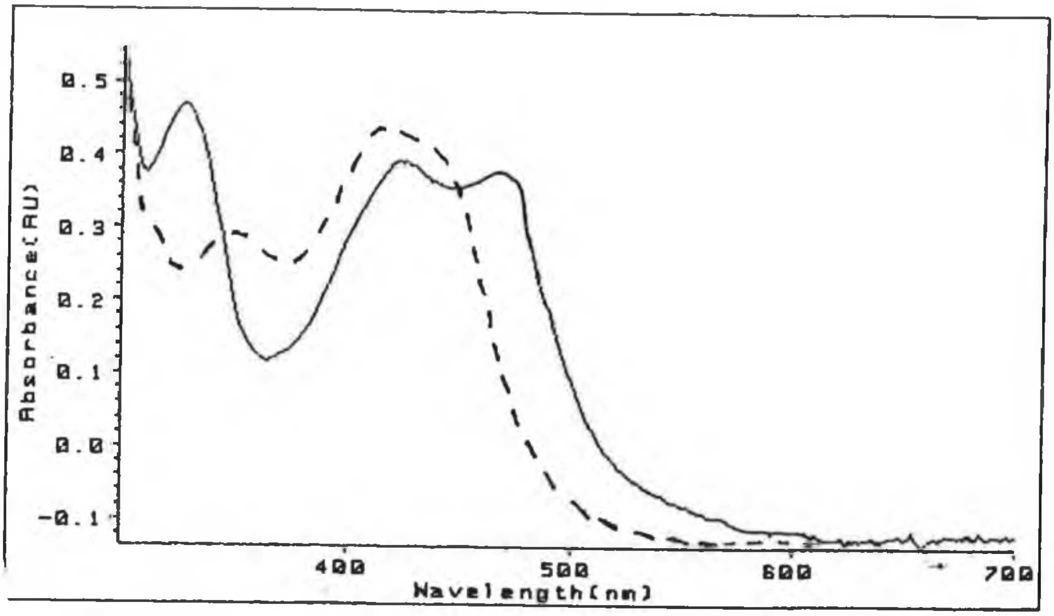

Figure 3.9. Absorption spectra of [Ru(bpy)$_2$(H$_2$L1)]PF$_6$ in acetonitrile at room temperature, (a) at neutral pH (b) in acidified media (1 drop of perchloric acid).

The absorbances are red-shifted with respect to $[Ru(bpy)_3]^{2+}$ as a result of the strong σ-donation of the deprotonated triazole moiety. On protonation of the triazole ring the λ_{max} is blue shifted to approximately 430 nm. The Ru t_{2g} level is stabilised by increased π-acceptance by the ligand and the t_2g-MLCT gap is increased resulting in the perceived blue-shifted absorbance.

All the complexes described exhibit room temperature emissions in acetonitrile at neutral pH associated with decay from the ^{3}MLCT state (figure 3.10). Again, as with the absorbance spectra, the emission λ_{max} is blue shifted by protonation of the triazole ring, and for the same reasons. This blue shift is associated with a marked decrease in emission intensity, again, this is a result of the lower σ-donation of the ligand. The ligand field splitting (Δ_o) is decreased with lower σ-donation, resulting in thermal population of the e_g* (^{3}MC) state, and faster radiationless decay.

At low temperature in an alcohol glass the emission λ_{max} is further blue shifted, in both protonated and deprotonated species. This is associated with a phenomena termed "rigidchromism" by Wrigton and coworkers who were one of the first to report on it [56].

splitting (Δ_o) is decreased with lower σ-donation, resulting in thermal population of the e_g* (^{3}MC) state, and faster radiationless decay.

At low temperature in an alcohol glass the emission λ_{max} is further blue shifted, in both protonated and deprotonated species. This is associated with a phenomena termed "rigidchromism" by Wrigton and coworkers who were one of the first to report on it [56].

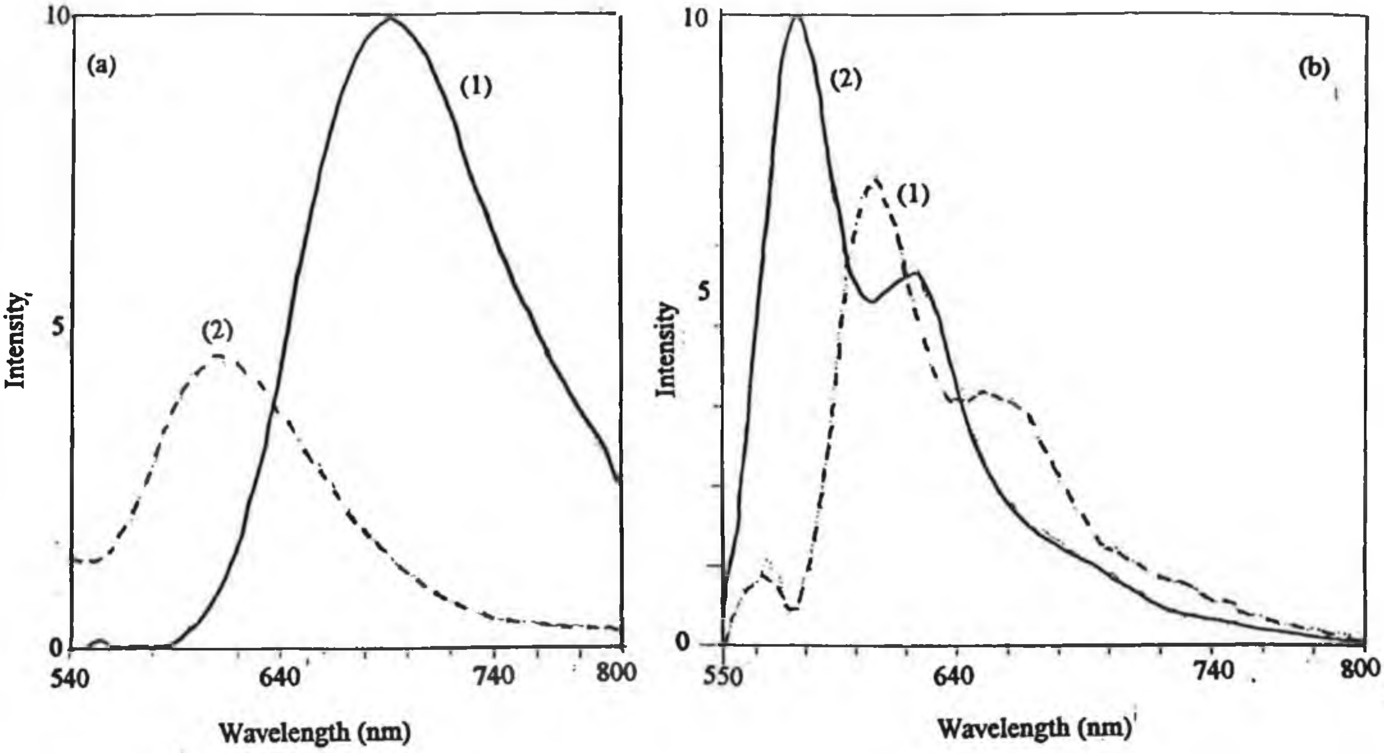

Figure 3.10 Emission spectra of [Ru(bpy)$_2$(H$_2$L1)]PF$_6$, (a) at room temperature in acetonitrile, (1) in neutral (2) in acidified media. (b) At 77K in MeOH/EtOH 4:1, (1) in neutral media, (2) in acidified media.

In the alcoholic glasses formed at 77K the solvent dipoles are "frozen" in averaged orientations appropriate to the ground state electronic configuration of the complex. In fluid solution the dipole orientation times are (usually) short on the scale of the lifetime of complex excited state. Whereas in frozen matrix solvent dipoles reorient very slowly with respect to the excited state, and may not reach equilibrium with the electronic distribution of the polar excited state, $[Ru(III)(L)(bpy)(bpy^{\cdot -})]^{n+}$, within its lifetime. The result is an increase in the energy of the transition as manifested by the blue shift observed in the emission.

A second important influence of low temperature on emission spectra is the increase in intensity and lifetime of emission observed. This is associated with two factors, the first is solvent dependent. At low temperatures the complex and its surrounds are rigid, making it less susceptible to vibronic coupling to low frequency, high amplitude Ru-N vibrations, which contributes to k_{nr}. Solvent interactions which may contribute to k_{nr}, are also reduced considerably in the frozen matrix, as is oxygen quenching since diffusion of O_2 to the excited sites is restricted. The second factor is related to the ^{3}MLCT-^{3}MC transition. Since this transition is thermally activated, at 77K there will be insufficient thermal energy to populate ^{3}MC, and as a result intensity and lifetimes are observed to increase.

Complexes in which the triazole is protonated exhibit radiative lifetimes at cryogenic temperature which are considerably increased with respect to the deprotonated complexes. This apparent anomaly is a result of the energy-gap law [57]. As described, protonation leads to stabilisation of the t_{2g} level and hence an increase in the t_{2g}-^{3}MLCT gap. According to the energy gap law the smaller the energy gap, the faster the rate of decay between the two states. This implies that in the absence of sufficient thermal energy to populate the ^{3}MC state, the lifetime of the protonated complex is longer than that of the deprotonated complex. The influence of basic solution on the photophysical properties is discussed in section 3.3.4.

3.3.3.2 Resonance Raman studies and the nature of the excited state.

Time resolved resonance Raman studies were carried out on $[Ru(bpy)_2(H_2L1)]^+$ in acetone at room temperature, in order to ascertain the nature of the excited state of these complexes. The ground state spectra was carried out by irradiation at 364 nm and the ground and transient excited state spectra at 355 nm of $[Ru(bpy)_2(H_2L1)]^+$ these spectra are shown in figure 3.11. By comparison of the rRaman spectra of $[Ru(bpy)_3]^{2+}$ [58] the most important enhanced vibrations could be assigned. $[Ru(bpy)_2(H_2L1)]^+$ exhibits straight-forward Raman spectra, with bipyridyl vibrations observed in the ground state at 1567, 1493, 1477, 1173, and 1035 cm^{-1}. A number of unassigned bands remain which may be due to vibrations of the pyridyltriazole or hydroquinone moieties. The excited state spectra is less complicated, and clearly reflects the fact that the excited state of this species is bipyridyl based. The enhanced vibrational bands at 1584.5, 1501.7 and in particular at 1288.3 cm-1 are the typical symmetric bpy^- stretching modes [58]. Some low intensity ground state bpy features remain, that these exist concurrently with the bpy^- features is evidence of the localised nature of the excited state. Some remaining features are unaccounted for, such as those at 1107.5 and 1020 cm-1, and these may be associated with the hydroquinone moiety.

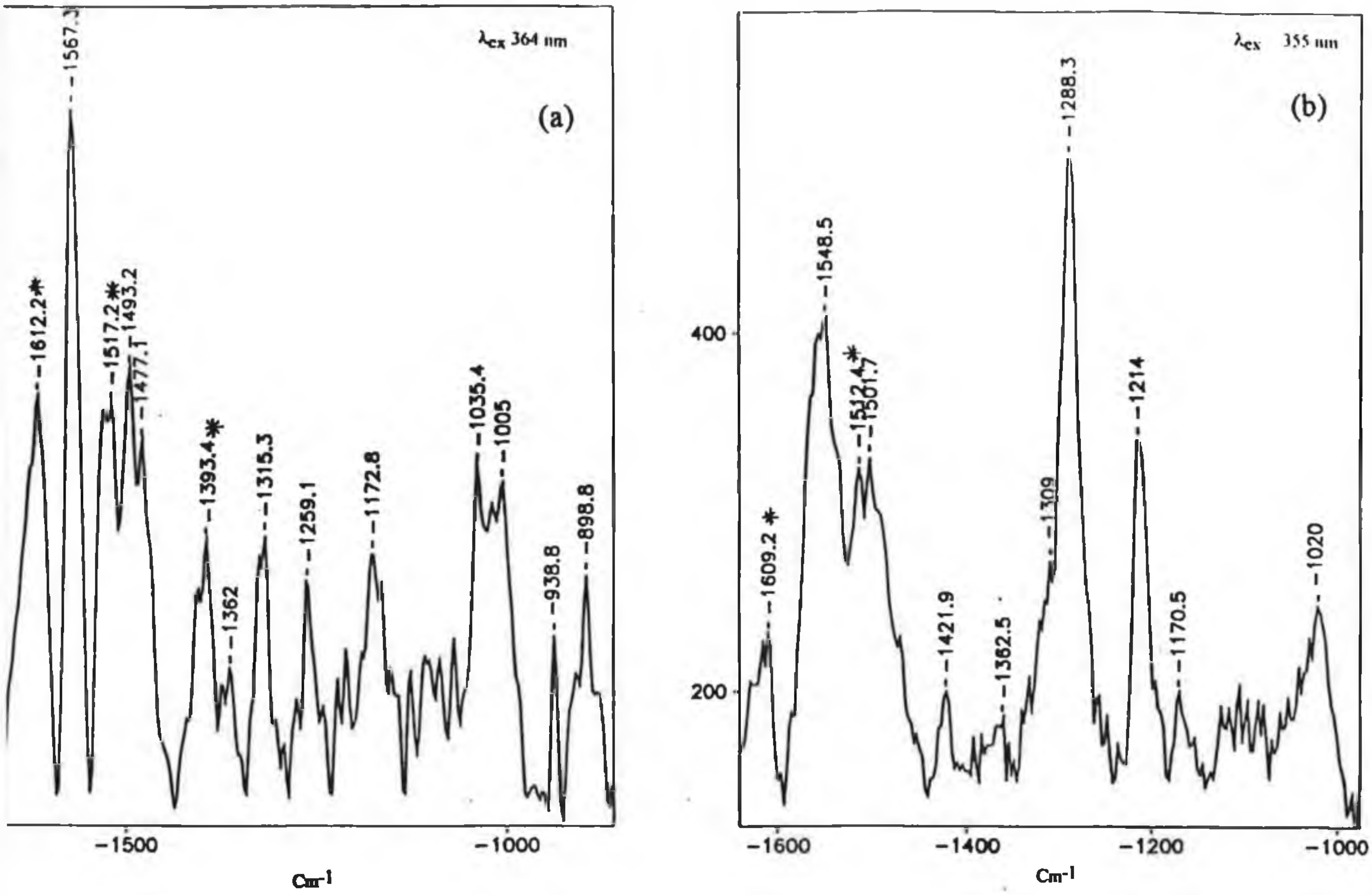

Figure 3.11. Resonance Raman spectra of $[Ru(bpy)_2(H_2L1)]^+$ carried out in degassed acetone, (a) Ground state spectra, (b) transient resonance Raman of the excited state.

3.3.3.3 Redox properties.

The redox potentials of the ligands discussed are presented in table 3.3.

Table 3.3. Redox properties of free ligands in neutral acetonitrile.

Ligand	**Redox potential (V vs SCE)**	**ΔE**
H_2L1 (neutral)	0.79	0.68
H_3L1 (acidic)	1.14	0.74
pH_2Q*	0.51, 1.14[A]	B
oH2Q*	0.64[A]	B
HL3	-1.0, -1.52	irreversible
H_3L6	0.91	0.86
H_3L6	1.12	0.87

* H_2Q = unsubstituted hydroquinone (p = para, o = ortho). [A] reference [79], [B] ΔE unspecified.

The ligand H_2L1 and H_2L6 exhibit two electron, quasi-reversible oxidations at 0.79V for H_2L1 and 0.91V for H_2L6 in dry acetonitrile, see figure 3.12. Attempts were made to separate the two individual one electron oxidations but these were unsuccessful. Addition of perchloric acid causes a decrease in reversibility but an increase in current for both ligands. This effect is anomalous in comparison with the experiments of Bessard and coworkers [19] who found that both reversibility and linear sweep voltammetric current increased. The increase in current, is most likely a function of the influence of proton transfer in the redox process. Whereas, release of the proton is likely to be the rate determining step in the redox process. That the reversibility does not increase is more complex. It is possible that proton transfer from the hydroxyl to the adjacent triazole catalyses the oxidation reaction and the protonation of this moiety prevents this occurring.

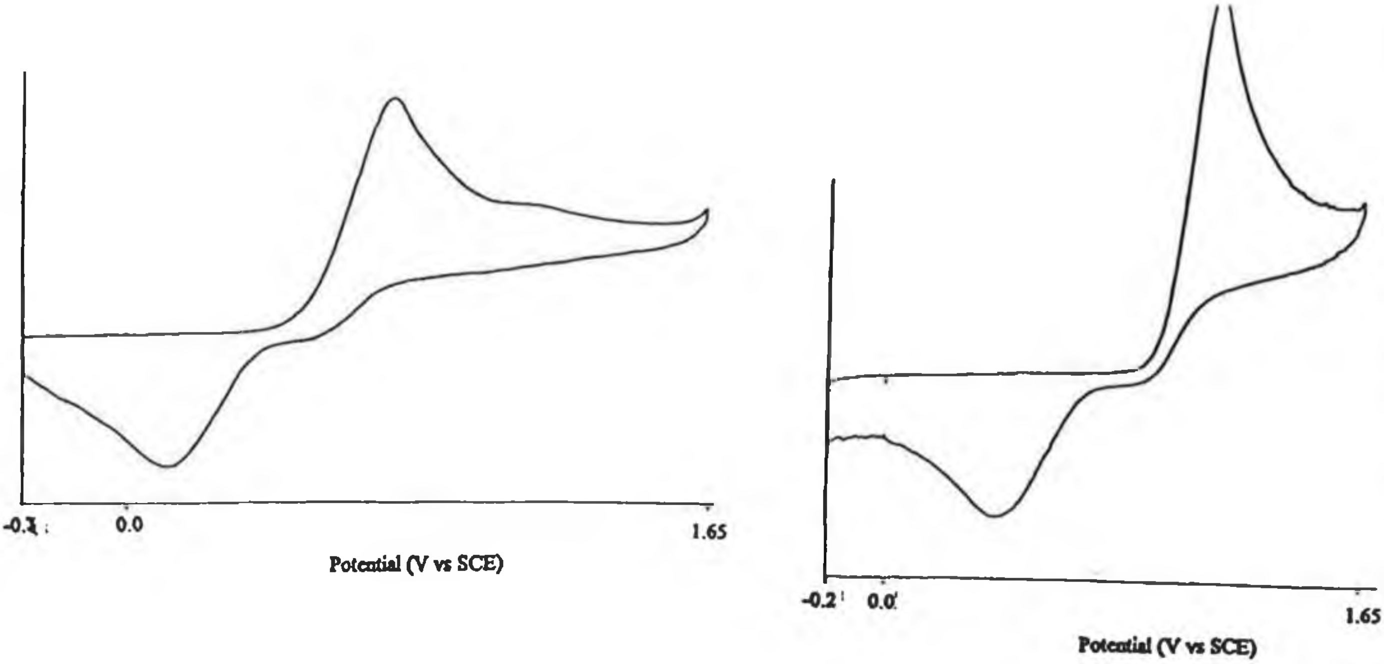

Figure 3.12 Ligand electrochemistry, H_3L1 in (i) neutral acetonitrile, (ii) acidic acetonitrile.

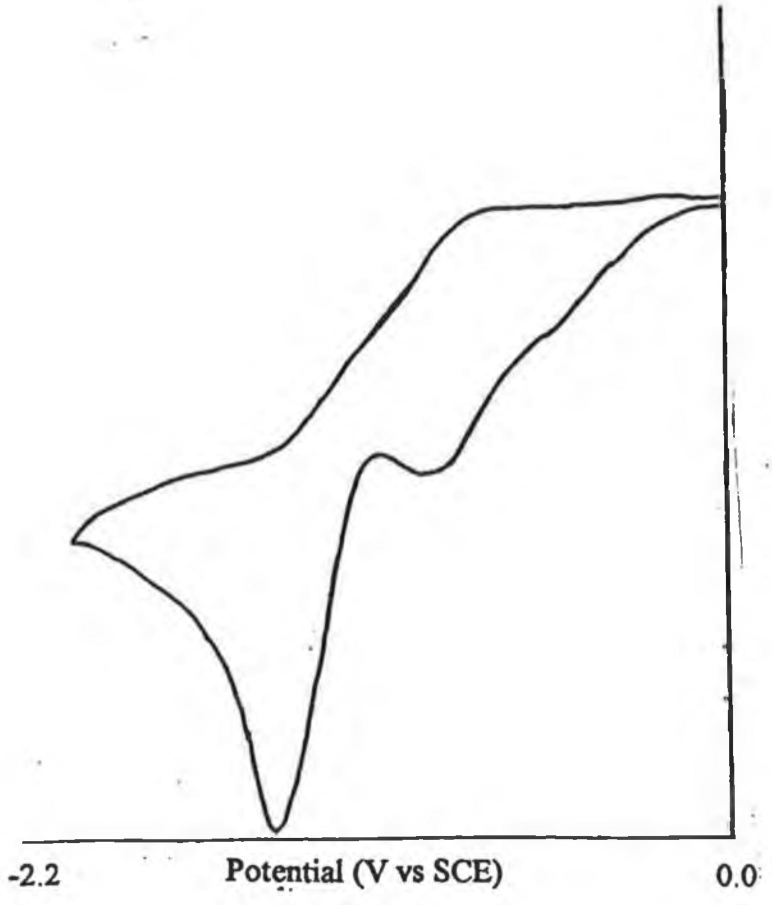

Figure 3.13 Ligand electrochemistry, HL3 in neutral acetonitrile.

This would cause the proton to be released into solution, which in this instance is acetonitrile, a bad proton acceptor. These proton transfer reactions will be dealt with in detail in section 3.3.3. For both hydroquinone species the observed oxidation potentials are anodically shifted with respect to the unsubstituted analogues, p and o-benzoquinone. This gives some measure of the influence of the pyridyltriazole moiety on the hydroquinone, which would appear to be electron withdrawing. Attempts were made to investigate the oxidation potential of the ligands in basic media, however, at the high concentrations of base required to deprotonate the hydroquinones the background current was so large it interfered with the measurements.

The quinone ligand HL3, exhibits a completely irreversible electrochemistry (see figure 3.13). Unlike H_3L1, the two individual one electron redox steps are separated. The origin of the irreversibility of these waves is difficult to pinpoint, since ordinarily irreversibility of quinone reductions occurs only in aqueous or protic solvents, whereas this behaviour is essentially independent of solvent, although the reduction potentials do vary with solvent. Such irreversibility suggests that a reaction is occurring on a time scale competitive with the redox process, i.e. the reduction product forms a new species as soon as it is formed. Since the hydroquinone ligand is stable and few pathways for reaction present themselves as being probable, it seems likely that the quinone adsorbs onto the surface of the carbon electrode.

The phenol ligands exhibited no electrochemistry within the potential window investigated, and no reductions were observed for any of the ligands with the exception of quinone. As they are all weak π-acceptors it is expected that their reductions are at very negative potentials. It is expected that deprotonation of the phenols will result in a cathodic shift in oxidation potential, prehaps bringing them into an accessible potential window however, for reasons described above this was not possible.

The redox potentials for the complexes are displayed in table 3.4. The excited state redox potentials are obtained from equation (3.3) and (3.4).

$$Ru^{3+} / Ru^{2+\bullet} = E\left(Ru^{3+} / Ru^{2+}\right) - E^{o-o} \qquad (3.3)$$

$$Ru^{2+} / Ru^{+\bullet} = E\left(Ru^{2+} / Ru^{+}\right) + E^{o-o} \qquad (3.4)$$

Figure 3.14 shows the CV for $[Ru(bpy)_2(H_2L5)]^+$, in order to illustrate the electrochemistry of these complexes. The complexes in which the triazole is deprotonated exhibit oxidation potentials lower than that of $[Ru(bpy)_3]^{2+}$. This is expected for complexes containing class b ligands, as a result of the increased electron density at the metal centre. Protonation increases the oxidation potentials for the complexes to around 1.3V, which is actually higher than that observed for $[Ru(bpy)_3]^{2+}$ under the same conditions. This serves to illustrate the influence the negative charge on the triazole exerts on the complex. The anodic shift is due to the decrease of electron density at the metal centre as the σ-donor ability of the triazole is diminished. The increase in overall charge on the complex also bears an influence.

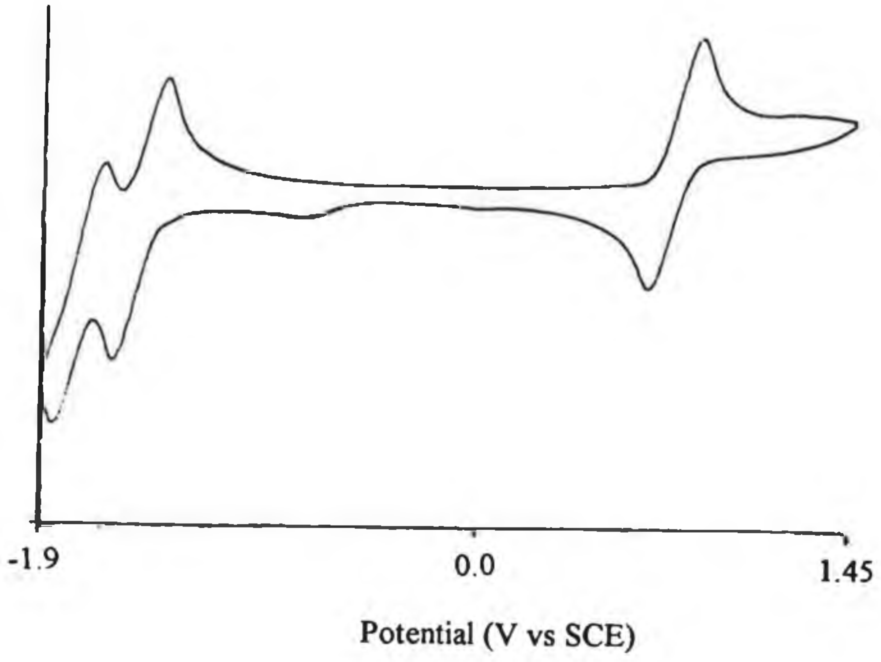

Figure 3.14 Cyclic voltammogram of $[Ru(bpy)_2(H_2L5)]^+$ in neutral acetonitrile.

Table 3.4. Electrochemical data for Ru(II) complexes in Volts vs SCE^{A}–.

Complex	Ru(II)/Ru(III)	E_{redox} (ligand)	E_{red} (bpy based)	Ru^{2+}/Ru^{3+*}	Ru^{2+}/Ru^{+*}
$[Ru(bpy)_2(H_2L1)]^+$	0.91	0.71, 1.07	-1.50, -1.76	-1.11	0.519
$[Ru(bpy)_2(H_3L1)]^{2+}$	1.31	1.10	*	-0.85	*
$[Ru(bpy)_2(HL2)]^+$	0.87		-1.46, -1.71	-1.13	0.330
$[Ru(bpy)_2(H_2L2)]^{2+}$	1.12		-1.35, -1.55	-1.02	0.790
$[Ru(bpy)_2(L3)]^+$	0.95	-1.31	-1.65, -1.92	-1.03	0.328
$[Ru(bpy)_2(HL3)]^{2+}$	1.35	*	*	-0.77	*
$[Ru(bpy)_2(HL4)]^+$	1.14	0.73, 1.58	-1.43, -1.70	-0.85	0.560
$[Ru(bpy)_2(H_2L4)]^{2+}$	1.31	*	*	-0.81	*
$[Ru(bpy)_2(L5)]^+$	0.96		-1.60, -1.88	-1.056	0.416
$[Ru(bpy)_2(HL5)]^{2+}$	1.30		-1.59, -1.82	-0.81	0.415
$[Ru(bpy)_2(H_2L6)]^+$	1.08		-1.51, -1.71		
$[Ru(bpy)_2(H_3L6)]^{2+}$	1.37	0.5, 0.88	*		
$[Ru(bpy)_2(3Mptr)]$+b	0.80		-1.48, -1.74		
$[Ru(bpy)_2(3Mptr)]$2+	1.20		-1.39, --1.61		
$[Ru(bpy)_2(N2'ptr)]$+b	0.83		-1.47, -1.72		
$[Ru(bpy)_2(N2'ptr)]$2+	1.14		-1.49, -1.73		
$[Ru(bpy)_3]^{2+}$	1.26		-1.35, -1.55, -1.80	-0.87	0.78

^{A} Measurements carried out in acetonitrile with TEAP as electrolyte. – Electrochemistry of deprotonated complexes was carried out in the presence of sufficient diethylamine or ammonium hydroxide to ensure a pH of 8-8.5. * Surface effects for electrochemistry carried out in the presence of acid prevented these measurements from being carried out. ^{b} Values taken from reference [43].

Cathodic potentials reveal two reductions for each complex, which are similar to those observed in $[Ru(bpy)_3]^{2+}$. These reductions are therefore thought to be bpy-based. As strong σ-donors the reduction potentials for the triazole ligands are presumed to be strongly cathodic. The homoleptic complex $[Ru(1M3Ptr)_3]^{2+}$ containing three methyl-substituted pyridyltriazole ligands (figure 3.15) displays a first reduction potential at -1.75V [59], which is cathodic compared to the complexes described here.

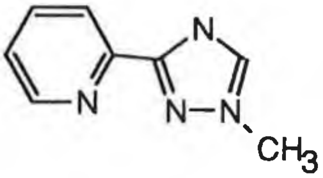

Figure 3.15, 1-methyl-3-(pyridin-2-yl)-1,2,4-triazole (1M3ptr).

Reduction potentials for protonated complexes were in most situations not obtained, as a result of surface effects which become prevalent at low pH. For those complexes for which measurements were possible the trend was towards an anodic shift. This is expected as a result of the reduced electron contributed to the bpys from the metal, which itself receives less electron density from the protonated triazole. In fact the reduction potentials for $[Ru(bpy)_2(HL2)]^+$ are identical to $[Ru(bpy)_3]^{2+}$.

It is apparent from table 3.4 that introduction of the various groups on the pendant aryl moiety possess some influence over the redox properties of the metal in these complexes, although this is small. The reduction potentials of the bipyridyl are also weakly affected by the nature of pendent group. The redox potentials for the analogous complexes $N1''$ which are coordinated to the simple pyridyltriazole, and the methylpyridyl ligand are also shown [43]. The redox potentials are all relatively similar among the aryl substituted complexes, suggesting that the interaction between the ruthenium and the pendent group and the bipyridyls is small in the ground state. There is significant difference between the metal-based redox potentials of the simple pyridyltriazole complexes and the L1--L6 complexes when they are protonated. Overall, the redox potentials of $[Ru(bpy)_2(Lx)]^{n+}$ are anodically shifted, suggesting that some of the negative charge of the triazole is accepted by the aryl moiety as well as the metal.

The true oxidation potential of the metal in $[Ru(bpy)_2(H_2L1)]^+$ cannot be determined since the hydroquinone moiety oxidation precedes the $Ru^{2+/3+}$ process. This means that what is observed is actually the oxidation of the metal in the quinone complex. As can be seen from table 3.4 the potentials of metal oxidation for both hydroquinone and quinone complexes are essentially identical. The electrochemistry of the hydroquinone and catechol complexes $[Ru(bpy)_2(H_2L1)]^+$ and $[Ru(bpy)_2(H_2L6)]^+$ will be discussed in more detail in section 3.3.3. The electrochemistry of $[Ru(bpy)_2(L3)]^+$ is marred by surface effects. The metal oxidation is irreversible as is the quinone reduction (see figure 3.16), which occurs at -1.3V.

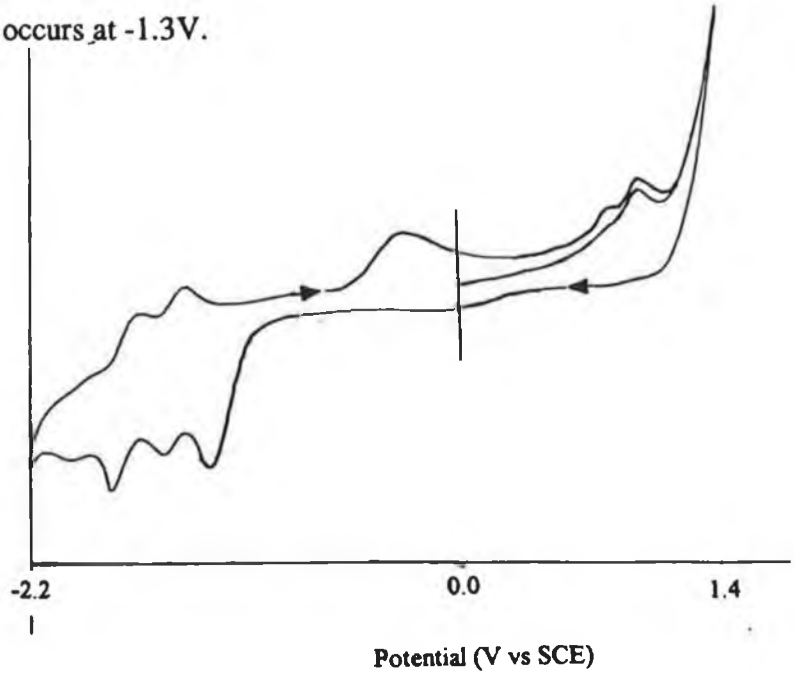

Figure 3.16. Cyclic voltammogram of $[Ru(bpy)_2(L3)]^+$ in acetonitrile at room temperature.

This is not surprising since the same influences were observed in the electrochemistry of the ligand. However, the values obtained for the irreversible metal oxidation in

$[Ru(bpy)_2(L3)]^+$ is presumed accurate since it was determined to be identical to that observed in $[Ru(bpy)_2(H_2L1)]^+$.

The redox properties of the p-phenol complex, $[Ru(bpy)_2(HL4)]^+$ show some anomalous tendencies. Namely, a very anodic oxidation in the deprotonated complex. As can be seen in figure 3.17, three oxidations are observed, the quasi-reversible process occurring at 1.14V is (from spectroelectrochemistry) associated with the metal based redox reaction. By comparison with the o-phenol complex, this is anodically shifted by 270m. Further inspection of the CV of this complex reveals two irreversible waves at 0.73 and 1.58V with areas of 22% and 78% of that of the metal based oxidation. These are assigned as oxidations of the O^- and OH respectively, as determined by the investigation of the complex in both acidified and strongly basic solution. As will be discussed, pH 8.5 (at which the experiment is conducted) approaches the pKa of the phenol in this complex. Therefore, both species will exist in solution at this pH. Both oxidations are completely irreversible and it would seem likely that this is because there is extensive polymerisation of the OH onto the carbon electrode surface. This is a fairly well known phenomena for redox active oxygen species [60]. Since at least 20% of the hydroxyls are deprotonated and hence are oxidised before the metal, they are polymerising at the electrode surface and the oxidation of the bulk solution for the most part is not observed. What is observed is the metal oxidation for the adsorbed species which may explain its unusual potential.

As was described in section 1.4, there is a strong correlation between the redox chemistry of Ru(II) polypyridyl complexes and their optical transition properties. Figure 3.17 shows the correlation of the redox properties of the complexes described above with their absorption and emission properties.

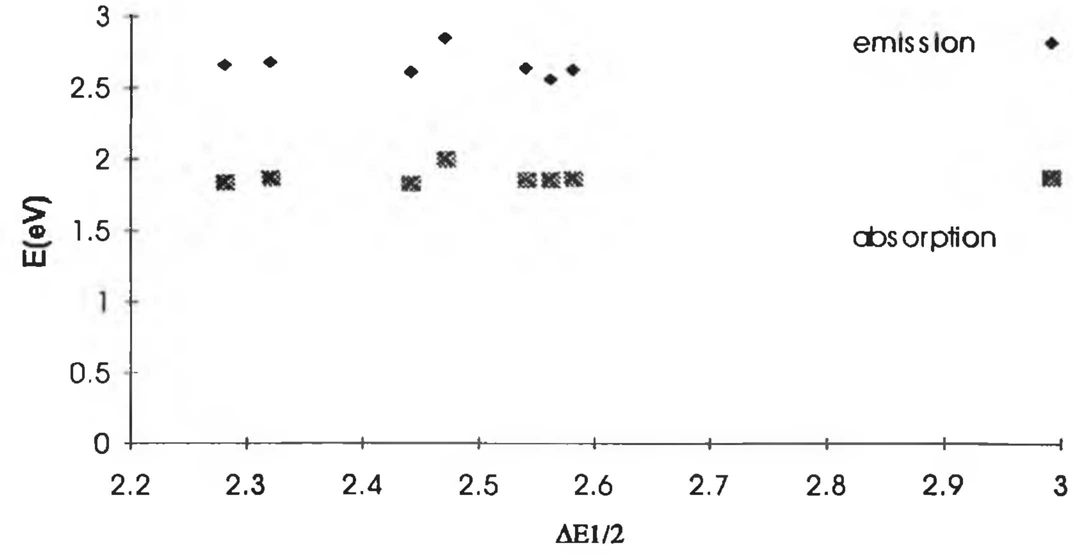

Figure 3.17. Redox dependence of optical electronic transitions, for complexes $[Ru(bpy)_2(Lx)]^{n+}$ *where x = 1-6.*

By plotting $\Delta E_{1/2}$ against the λ_{max} of absorption and emission (in eV) at room temperature, a roughly linear correlation is observed, indicating that the bipyridyl is directly involved in the CT. The following correlation may be made by applying the equation of the line to the data above;

$$E_{abs}(CT) = 0.81.\Delta E_{1/2} - 2.2. \qquad (3.4)$$

$$E_{em}(CT) = 0.012.\Delta E_{1/2} + 1.85. \qquad (3.5)$$

$\Delta E_{1/2}$ represents the difference between the first oxidation potential and first reduction potential of each complex. In each instance the first reduction potential was taken to mean the first bipyridyl reduction. That the correlation is linear implies that in each instance the excited state resides on the same ligand for each complex. This conclusion is based on the assumption that the same orbital participates in the excited state and first reduction potential. Since from resonance raman studies we have established that the excited state of $[Ru(bpy)_2(H_2L1)]^+$ is bipyridyl localised, it can be concluded from the correlation above that this is the case for all the complexes discussed here.

3.3.4 Acid-Base properties.

Considerable electronic redistribution occurs between protonation and deprotonation of pyridyltriazole complexes, which is reflected in the optical transition spectroscopy of the complexes. As described, protonation/deprotonation alters the σ-donor and π-acceptor properties of the ligand. In Ru-polypyridyl complexes the Ru-N link is mainly σ in nature, but is stabilised by backbonding between t_{2g} and π* of metal and ligand. Determination of the pK_a of a complex yields information about the extent of backbonding from the metal and the σ-donor and π-acceptor properties of the ligands. Moreover, determination of pK_a and pK_a^* offers a unique probe into the excited state chemistry of the species. For this reason, considerable investigation has been made into ground and excited state acid-base behaviour of a number of complexes [61-63]. For most ruthenium complexes the pK_a value of the ligand decreases on coordination , which is an electrostatic effect caused by the Ru(II) centre. Pyrazine provides the exception to the rule, [64]. This species becomes more basic on coordination to the $Ru(bpy)_2$ centre. This behaviour has been associated with strong π-back donation to the ligand.

Comparison of pK_a and pK_a^* for complexes usually reveals large differences. If in the excited state the pK_a of the complex is lower, i.e. more acidic, than the ground state, this implies that the source of the protonation site is a spectator ligand, not directly involved in the excited state. The triazoles are examples of such ligands [63, 65]. Alternatively, if the complex is more basic in the excited state, this implies that the site of protonation contains the LUMO. The bipyrazines represent such complexes [66].

(i) Ground state behaviour.

The acid-base properties of ligands and complexes are shown in table 3.5. In all situations the titrations are carried out in Britton Robinson buffer, except where otherwise stated. All titrations were reversible over the pH range 1 to 12.

Table 3 5. Acid-base* properties of complexes and ligands, measured in aqueous media.

Complex/ ligand	**Pyridyl** (pKa_1)	**Triazole** (pK_{a2})	**Hydroxyl** ($pK_{a3, 4}$).	**PK_a***
H_3L1	2.95	6.69	9.59, 11.73	
$[Ru(bpy)_2(H_2L1)]^+$		1.88	10.31, 11.73	0.00
H_2L2^B	3.22	6.0	11.60	
$[Ru(bpy)_2(HL2)]^{+B}$		3.73	11.20	2.70
HL3	2.6	6.41		
$[Ru(bpy)_2(L3)]^+$		3.86		2.25
H_2L4	2.83	9.0	10.68	
$[Ru(bpy)_2(HL4)]^+$		4.0	9.30	1.72
HL5	2.99	8.74		
$[Ru(bpy)_2(L5)]^+$		3.7		2.22
H_3L6	3.00	8.75	10.85, 12.26	
$[Ru(bpy)_2(H_2L6)]^+$		3.05		2.32

* All values quoted are ± 0.01. ^{B} Taken from reference [43].

From the structure of the free ligand H_3L1, there are 4 sites of acid-base behaviour predicted., and indeed 4 stepwise acid-base equilibria are observed, corresponding to the pyridine, the triazole, and the hydroquinone, i.e.

$$L^{3-} \xleftrightarrow{pKa4} HL^{2-} \xleftrightarrow{pKa3} H_2L^{-} \xleftrightarrow{pKa2} H_3L \xleftrightarrow{pKa1} H_4L^{+} \quad (3.5)$$

Q^{2-} QH^{-} QH_2 triazole H pyrH

The absorption titration spectra for these steps are shown in figure 3.18. Isobestic points are observed over some pH ranges although few are maintained cleanly for more than a few pH steps. This suggests that there are intermediates forming over the pH ranges employed.

The complex pH behaviour for H_3L1 and HL3 is most likely a function of the H_2Q/Q unit, which has very complex acid-base behaviour, which is further aggravated in aqueous solution. For example, it has been shown via ESR studies that semiquinone radicals form spontaneously in aqueous solutions above pH 8 [77]. However, employing the titration values, graphical analyses was carried out by plotting percentage change in absorbance vs pH. The pK_a was determined from the point of inflection of the curve. For H_3L1 titrations between pH 8 to 10 and 9.5 to 11.0 produced pK_a values of 9.6 and of 10.75 (± 0.1), which are assigned as pK_{a3} and pK_{a4} respectively. The next step observed was in the titration range 3.4-8.0, with pK_{a2} determined to be 6.7 (± 0.1), which is assigned as the triazole pK_a. Finally, for the titration range 1.2 to 3.5, the pK_{a1} assigned to the pyridine was 2.9 (± 0.1).

The pK_a titration of the quinone ligand, HL3 and catechol ligand H_3L6 are similar in that isobestic points are badly resolved. The influence of the quinone and hydroquinone moieties over this behaviour is demonstrated by the phenyl ligand HL5, (figure 3.19) This species exhibits a very clean spectral titration as is seen in figure a, with clear isobestic points at 253 and 283 nm. This ligand contains only two sites of acid-base equilibria, corresponding to pKa_1 and pKa_2. The phenol containing ligands also appear to be free of this complexities in their titrations.

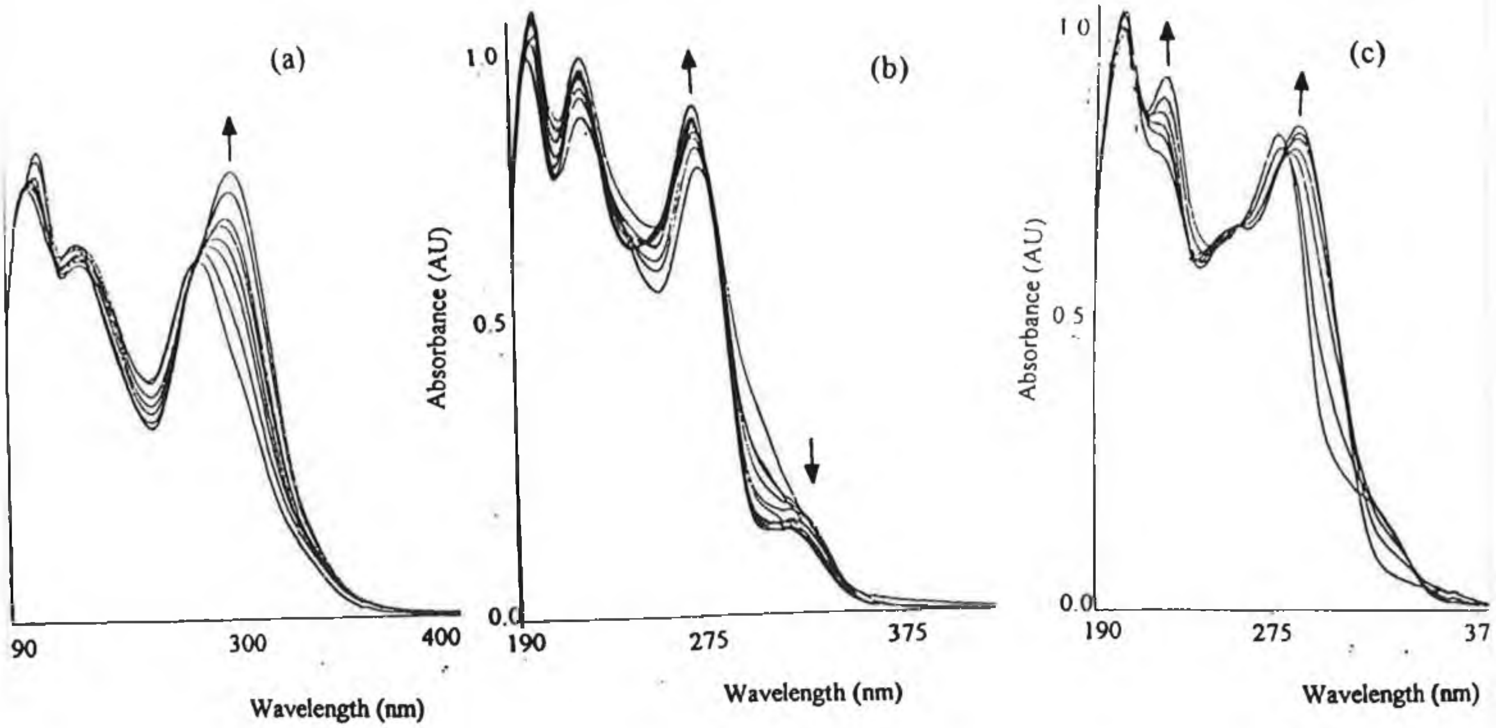

Figure 3.18. Absorbance as a function of pH for H_3L1 (a) pH 1.2-3.2, (b) pH 3.9-6.5, (c) pH 8-10.

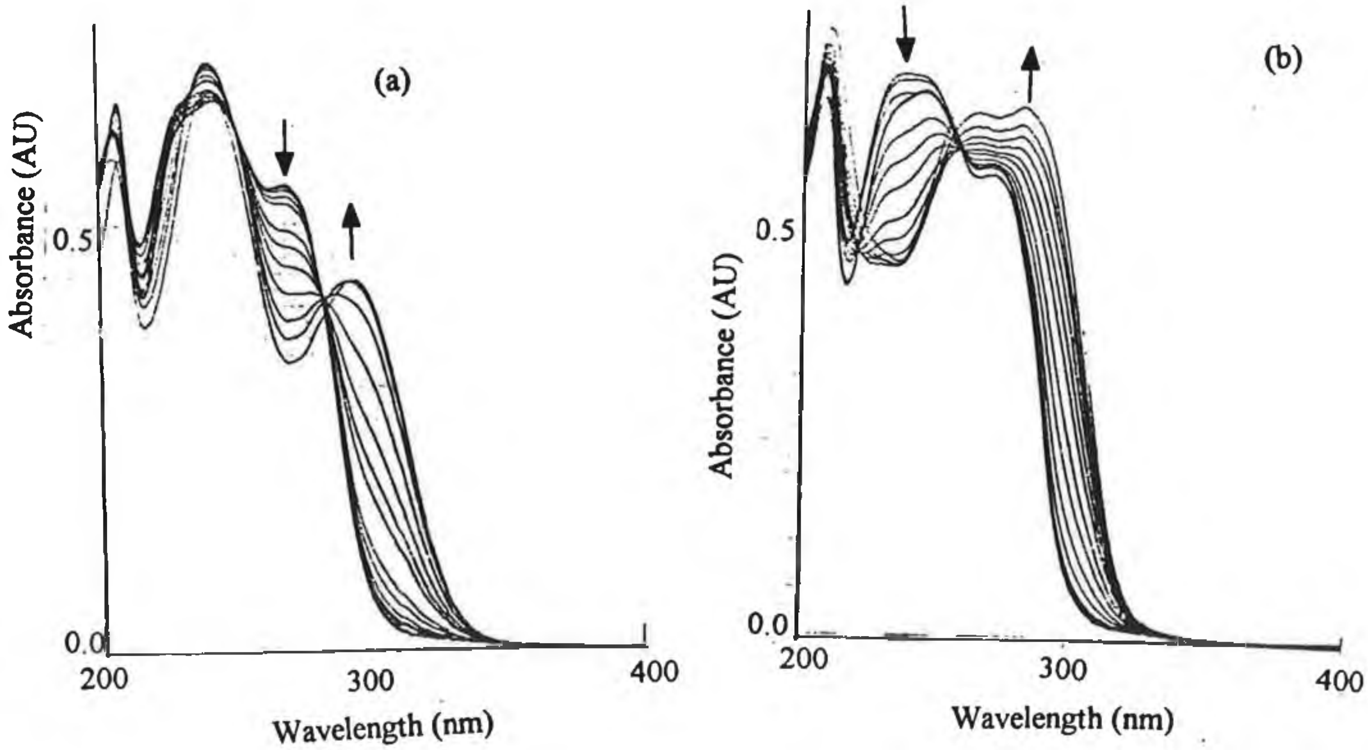

Figure 3.19. Absorbance as a function of pH for HL5, (a) pH 1.7-6.0, (b) pH 5.9-11.

The pKa_2 value for H_3L1 is considerably lower than that of the , H_2L4, HL5 and H_3L6, but is comparable to that of H_2L2 and HL3 It seems likely that the influence of the strongly electron withdrawing carbonyls on the pendant aryl in HL3 is responsible for the increased acidity of the triazole in this instance. Since in the deprotonated ligand the negative charge on the triazole will be stabilised by the electron poor quinone moiety.

The low basicity of the triazole in the hydroquinone and o-phenol ligands is likely to be a result of H-bridge formation between the hydroxyl ortho to the triazole and a triazole $N^{4''}$. Such a bridge would reduce the electron density on the triazole and hence basicity. The large difference in pK_{a2} values in particular, between H_2L2, H_2L4, H_3L1 and H_3L6 provide evidence for this intramolecular H-bridging. Since pK_{a2} values are more in line with those obtained for simple pyridyl triazole ligands, i.e. around 9. Models computed (using hyperchem) for both H_2L1 and H_2L2 ligands exhibit inter-atom distances between hydroxyl H and the adjacent N4' to be less than 1.9Å, which is consistent with the formation of a hydrogen bridge. Furthermore, the pK_{a3} (of the hydroxyls) of H_3L1 and H_3L6 are very different. Pk_{a3} at 9.59 for H_3L1 and 10.85 for H_3L6 are more than 1 pH unit apart, whereas their pKa4 values, although different are not so significantly distinct. The reason for this difference in pK_a3 is uncertain.

The pyridine pKa_1 value corresponds well with other similar complexes [65], and the fact that the pyridyl is protonated before the triazole has been associated with H bridge formation to the adjacent triazole. However, from modelling of the crystal structure of the free 3,5-bis(pyridin-2-yl)-1,2,4-triazole (bpt) (appendix 1) the N^1 to $N^{1'}$ distance exceeds 2.7Å, eliminating any possibility of bridge formation.

Finally, in the pH range 4.8-7.8 for ligands H_3L1 and H_3L6 (pH 4.8 to 9.0) a band of medium intensity appears centered around 322 nm, this band is similar to the charge transfer band at 330 nm in the spectra of $[Ru(bpy)_2(H_2L1)]^+$ and $[Ru(bpy)_2(H_2L6)]^+$

and also retains the same pH dependant character (see below). It seems most likely therefore, that since this transition persists in both catechol and hydroquinone ligands and their associated complexes, and does not occur in either the phenolic, phenyl or quinone ligands, that this is a $\pi-\pi^*$ transition based on the hydroquinone ring.

The pK_a values for the complexes are also tabulated in table 3.5. As expected the coordinated ligand is more acidic than the free ligand, this is usual for weak π-acceptors like the triazoles. The pK_{a4} value for $[Ru(bpy)_2(H_2L1)]^+$ is not resolved but pK_{a3} has been determined as 10.31 (±0.2), which suggests that coordination has little influence on the electronic distribution of H_2Q. For $[Ru(bpy)_2(H_2L1)]^+$ the triazole, however, shows dramatic increase in acidity on coordination, pK_{a3} is 1.98, which is remarkably low. It is possible that formation of a hydrogen bridge, in a similar fashion as described for H_3L1 the free ligand is at work here. Since on the basis of comparison of pK_{a2} of both the other complexes described and other similar complexes [65] such an increase in acidity is unlikely to be solely due to coordination effects.

The validity of the persistence of this bridge in $[Ru(bpy)_2(H_2L1)]^+$ is enhanced by examining the crystal structure of the phenol analogue $[Ru(bpy)_2(HL2)]^+$ [44]. Where bridging is clearly observed between the hydroxyl and adjacent triazole nitrogen. Computational modelling also predicts that bridging will exist in both $[Ru(bpy)_2(H_2L1)]^+$ and $[Ru(bpy)_2(HL2)]^+$ figure 3.8 shows a computational space filled model of $[Ru(bpy)_2(H_2L1)]^+$ where the intramolecular H-bond is clearly seen. Interestingly, the pK_a of $[Ru(bpy)_2(HL2)]^+$ is not irregularly low despite the fact that the bridge is seen in its crystal structure. This may be attributed to the fact that in the hydroquinone as a result of the bulk of the two hydroxyls, free rotation of the moiety is not possible and the complex is left at normal temperatures in its lowest energy bridged configuration. In $[Ru(bpy)_2(HL2)]^+$ since only one OH is present, the bulk of the aryl group is reduced and some rotation may be possible, particularly in aqueous solution where intermolecular bridging is possible with the surrounding solvent.

The pH titrations of the quinone, hydroquinone and catechol complexes exhibit the same absence of well resolved isobestic points as their respective ligands. This is exhibited by the titration shown for [Ru(bpy)$_2$(H$_2$L1)]$^+$ in figure 3.20. Again, this is attributed to the presence of the quinone and hydroquinone moieties as a result of the pH dependent solvated semiquinone intermediates they are capable of forming in aqueous solution. This complexity is not observed in either the phenol or phenyl containing complexes demonstrated by the pH titration of [Ru(bpy)$_2$(L5)]$^+$ shown in figure 3.21. The pK$_a$ values of the remaining complexes are unsurprising and correspond well with those of similar complexes [65, 67].

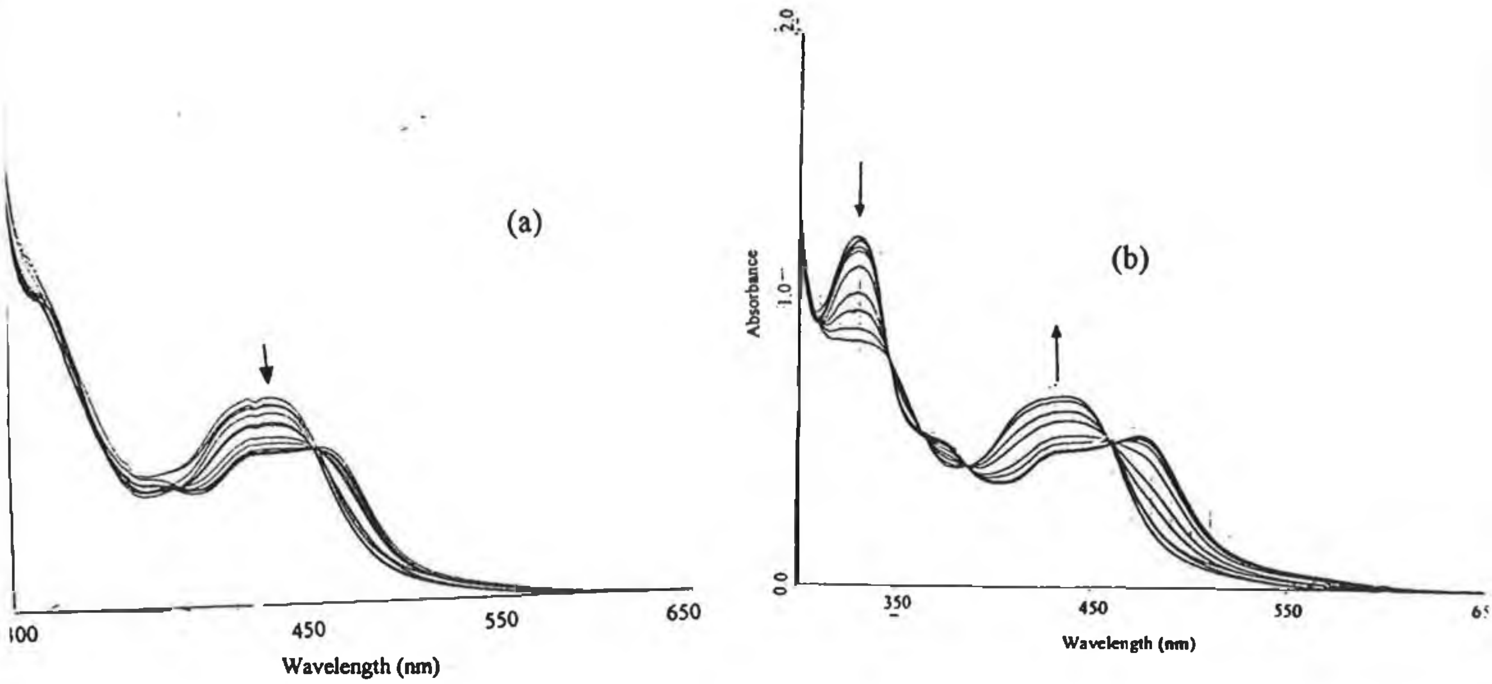

Figure 3.20 PH dependent absorbance of [Ru(bpy)$_2$(H$_2$L1)]$^+$ in the range pH 1-7 (a) in Britton-Robinson buffer, (b) in acetonitrile.

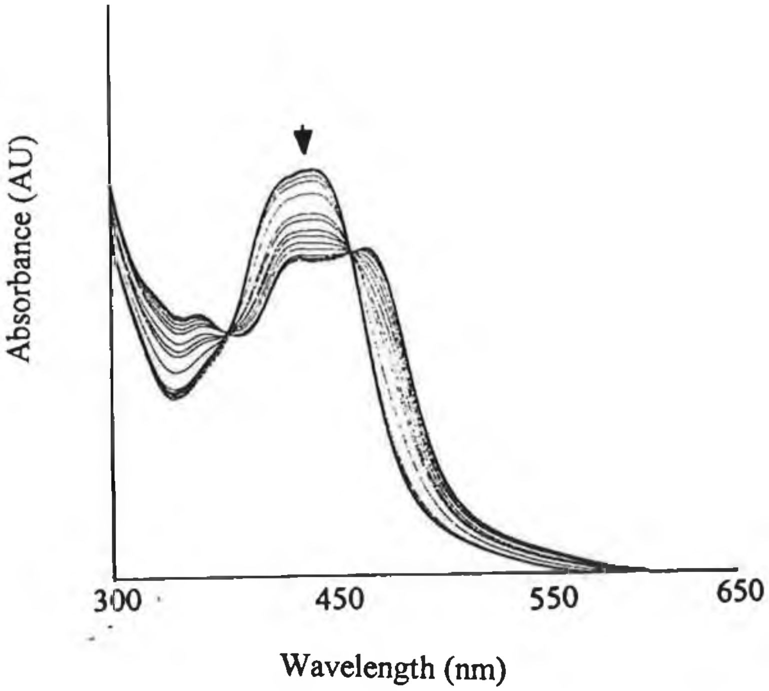

Figure 3.21. PH dependent absorbance of [Ru(bpy)$_2$(L5)]$^+$ in the range pH 1-6.

In order to assess the influence of the aqueous nature of the buffer on the titration and on the pKa$_2$ of these complexes, a number of titrations were carried out in acetonitrile. Figure 3.20 (b) shows the spectra of [Ru(bpy)$_2$(H$_2$L1)]$^+$ as a function of pH to represent such a titration. This diagram reflects very clearly the influence of aqueous media on the acid-base chemistry of [Ru(bpy)$_2$(H$_2$L1)]$^+$. The titration is very clean with four well defined isobestic points at 346 nm, 364 nm, 386 nm and 458 nm. The pK$_a$ of the triazole in this instance is determined to be 2.57 (±0.05). This value, as was the case in aqueous solution, is remarkably low, having increased by less than one pH unit of the aqueous value. Davila and coworkers carried out numerous experiments on acid-base titrations in acetonitrile [70] and found a dramatic increase in pK$_a$ values in acetonitrile with respect to pK$_a$ values from aqueous media. This increase is associated with the inability of acetonitrile to solvate the proton as efficiently as water. Davila and coworkers [70] observed differences in pK_a values of $Ru(bpy)_2CN_2$ in water where they recorded it as 4.2 and in acetonitrile where $pK_a = 6.7$, i.e. a difference of greater than 2 pH units. Comparison of the pK_a values for the triazole of $[Ru(bpy)_2(L5)]^+$ in aqueous media and acetonitrile verifies this behaviour. The pK_{a2} in aqueous media is 3.7, whereas in acetonitrile pK_{a2} is 7.4 (±0.1). This decrease of nearly 4 pH units is in considerable contrast to that of $[Ru(bpy)_2(H_2L1)]^+$. It would seem logical to assume that the root of this difference lies in the hydroquinone moiety, since two hydroxyls is all that separates the two complexes. It may be that the presence of intramolecular H-bridging in acetonitrile is the source of this anomaly. This could be a result of the stronger bridging experienced by the $N^{4'}$ and OH in acetonitrile, the triazole "feels" as though it is partially protonated. As a result, this nitrogen is more acidic than similar complexes which do not experience the influence of intramolecular H-bonding of this nature.

(ii) Excited state behaviour.

One of the first and most important contributions to excited state acid-base equilibria was published by Forster [65]. Whose thermodynamic treatment, based on the enthalpic changes following protonation/deprotonation in the exited state of an organic species lead to the Forster cycle. equation (3.6). Whereby the excited state pK_a* of a species may be calculated from it s ground state properties.

$$pK_a^* = pK_a + \left(\frac{0.625}{T}\right)(\nu_{B-} - \nu_{HB}) \quad (3.6)$$

Where υ_{B^-} and υ_{HB} are the $E_{0\text{-}0}$ values (in cm^{-1}) of the deprotonated and deprotonated complexes respectively. These values are taken from the λ_{max} of the emission spectra at 77K, therefore T is 77K.

The most important difficulty in dealing with the Forster cycle as a means of determining pK_a* is the accurate ascertainment of $E_{0\text{-}0}$ for ν_{B^-} and ν_{HB} since small errors in these values produce distended errors in pK_a* [68]. A second approach exists for measuring the pK_a* in these complexes based on a kinetic model evolved by Ireland and Wyatt [69], based on the following scheme 3.1.

$$\begin{tikzcd}
{[Ru^{III}(L)_2(HL')]^{3+*}} \arrow[r, leftrightarrow, "k_{H*}", "k_{-H*}"'] \arrow[d, shift left] \arrow[d, leftarrow, shift right] & {[Ru^{II}(L)_2(HL'^-)]^{2+*}} \arrow[d, shift left] \arrow[d, leftarrow, shift right] \\
{[Ru^{II}(L)_2(HL'^+)]^{3+}} \arrow[r, leftrightarrow, "kH", "k_{-H}"'] & {[Ru^{II}(L)_2(L')]^{2+}}
\end{tikzcd}$$

Scheme 3.1

Where pKa* may be measured from the emission lifetimes of the protonated (τ_{HB})and deprotonated (τ_{B-}) complexes and the point of inflection of the emission titration curve, pH_i. According to equation (3.7).

$$pK_a^* = pH_i + \log\left(\frac{\tau_{HB}}{\tau_{B-}}\right) \quad (3.7)$$

Unfortunately, although the Ireland Wyatt equation would be the preferred method to use, since it involves direct measurement of the excited state pK_a via pH_i and does not rely so heavily on accuracy of the E_{0-0} value, it was not possible to use it here. This is due to the fact that on protonation, most of the complexes described possess lifetimes outside the range of the equipment employed. As a result, the Forster cycle must suffice for the values reported here. The excited state pK_a* values are shown in table 3.5. The general trend is that pKa* values are more acidic than ground state values. This observation has important consequences since following the logic described in the introduction to this section, this means that the triazole is a spectator ligand and does not become directly involved in the excited state. This means that the ^{3}MLCT is indeed a bpy based state, this conclusion corroborates conclusions from the electrochemical and resonance Raman spectroscopy discussed in sections 3.3.3.2 and 3.3.3.3.

3.3.5 Electrochemically induced proton transfer.

The importance of proton transfers in the biological energy producing process is well known [71]. In section 1.3 the importance of these reactions in photosynthesis was described. In the photosynthetic system the continuous replenishment of the reaction centre requires the rereduction of the oxidised special pair $Bchl_2$ and replacement of the reduced hydroquinone species by quinone present in the membrane lipids [72]. These redox processes occur transmembranaly, in order to establish and maintain a transmembrane electric field. They occur concomitantly with transmembranal proton transfers as part of an overall protonmotive machinery. The protonation upon reduction of the quinone produces a stable differential in the electrochemical potential of protons across the reaction centre membrane. In fact two protons are transferred through chains of proton exchanging amino-acid residues from the cytoplasmic side of the membrane to the doubly reduced quinone. As a result, protons are consumed on the reaction centre side of the membrane and the electric charge separation produced by the photochemical reaction is maintained along the membrane surface. The resulting hydroquinone is then released from the reaction centre and eventually reoxidised, completing the transmembranal proton translocation cycle.

Despite the obvious importance of proton transfer processes in photosynthetic systems, there are relatively few documented cases of electrochemically induced proton transfer in areas of study of abiotic models. Relevant examples come mostly form work carried out by Meyer and coworkers, [73] who demonstrated that the oxidation of OH in $[Ru(bpy)_2(py)OH]^{2+}$ to produce the oxo species is coupled with proton transfer. This process was found to be slow and possess an unusually large kinetic isotope effect in D_2O, which was associated with a homogeneous proton transfer reaction as opposed to a simple outer sphere electron transfer. In 1985 this group carried out a detailed study on the dimeric $[(bpy)_2(OH_2)RuORu(OH_2)(bpy)_2]^{4+}$ in which oxidation at a glassy carbon electrode produced a proton coupled electron transfer which was dependent on pH [74] . Also in that year , Meyer and coworkers reported on the redox processes for a number of $Ru(bpy)_2$ complexes at an anodised glassy carbon surface [75]. They found that the anodised electrode surface activated proton coupled electron transfers in these complexes, and in fact selectively catalysed the wave characteristics in catechol. The most recent and possibly relevant contribution from this group discusses the proton coupled redox reaction of various substituted hydroquinones and $[Ru(bpy)_2(py)OH]^{2+}$ and $[Ru(bpy)_2(py)O]^{2+}$ [76]. These processes show kinetic isotope effects, and hydrogen-bridge formation as a precursor to the concerted proton and electron transfer is suggested. Other examples of such proton coupled electron transfer processes exist [77, 78], but the common feature of all these reports is that the proton is obtained from an external source, usually the solvent. To our knowledge there have been no reports on systems where the source and destination of the protons are elucidated and known not to be the solvent, and certainly none in which the proton is transferring intramolecularly.

3.3.5.1 Electrochemical evidence.

The cyclic voltammogram of the [Ru(bpy)$_2$(H$_2$L1)]PF$_6$ complex in acetonitrile at neutral pH exhibits 5 oxidation waves[1] (see figure 3.22).

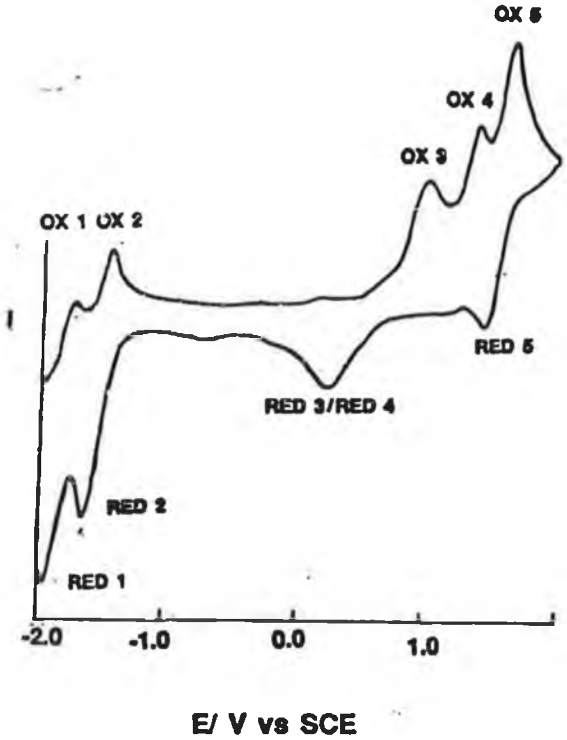

Figure 3.22. Cyclic voltammogram of [Ru(bpy)$_2$(H$_2$L1)]$^+$ in neutral acetonitrile at room temperature (potential vs SCE).

---

[1] The resolution of these individual waves required pretreatment of the electrode. This meant anodisation of the glassy carbon electrode by placing it in 1M H$_2$SO$_4$ at a potential of 1.8V for 1 minute. Without pretreatment the hydroquinone oxidation appears as one wave at around 1V [75].

Ox1 and ox2 and their reductions are assigned as the two 1 electron reactions of the bipyridine ligands (see section 3.3.1.2). The oxidations ox3 and ox4 are attributed to the two one electron oxidations of the hydroquinone moiety. The one electron status of each of these processes was verified using coulometery. Coulometric measurements carried out after exhaustive oxidation of the complex revealed that the associated reduction wave red 3/4 is a two electron process, and therefore is presumably the 2 electron reduction of the quinone moiety.

The reversible couple ox5/red5 at E_{ox} of 1.31V is assigned as the metal based redox waves, on the basis of comparison with other similar complexes and spectroelectrochemistry which will be discussed below. The redox potential of the metal is, however, anomalous in that it is anodicaly shifted by comparison with other triazole complexes, for example, the model complex for these species $[Ru(bpy)_2(L5)]PF_6$ exhibits a Ru(II)-Ru(III) couple at 0.8V. The redox potential observed does however correspond well to those observed for complexes containing the protonated triazole moiety. For $[Ru(bpy)_2(HL5)](PF_6)_2$ the oxidation potential of the metal is 1.3V under the same conditions is essentially identical to that of the hydroquinone complex. Furthermore, the metal oxidation potential for $[Ru(bpy)_2(L3)](PF_6)$ is 0.95V and as was discussed this should be identical to that of $[Ru(bpy)_2(H_2L1)]PF_6$. On protonation of $[Ru(bpy)_2(L3)](PF_6)$ however the potentials are almost identical.

In order to investigate further the state of protonation of the triazole in $[Ru(bpy)_2(H_2L1)]PF_6$, the electrochemistry of the complex was investigated at different pHs[2] in acetonitrile. At pH 1, no change was observed in the potential of the metal oxidation from that in neutral media. At this pH, as discussed, the triazole is protonated. This result, therefore, would imply that the complex contains a protonated triazole. At pH 1 there is a significant change in the electrochemistry of the hydroquinone moiety. The

---

[2] Control of pH was carried out by addition of known concentrations of acetonitrile or ammonium hydroxide, the former is known to dissociate completely in MeCN [70] and measurements suggest that the latter also undergoes considerable dissociation in this solvent.

hydroquinone oxidation is no longer resolved and a single two electron wave is observed, which has shifted anodicaly to 1.17V. This result is contrary to expectations since reversibility and charge current are expected to increase for hydroquinones in acidic media [27] as a result of the role played by the proton in the rate determining steps of hydroquinone electrochemistry. This apparently anomalous behaviour has two possible sources. Firstly, since the triazole is protonated, any bridging between the hydroquinone OH and N of the triazole is rendered impossible. This reduces the electron density on the oxygen since the proton is bound exclusively to it. Secondly, the triazole is no longer negatively charged and depending on the amount of delocalisation between the rings this may in turn produce a reduction in electron density on the HQ hydroxyl. Finally, it is known [78] that proton transfer is usually the rate determining step in hydroquinone electrochemistry. The intramolecular bridge between the triazole and hydroxyl may facilitate this process perhaps by reducing the free energy of the transfer since the triazole N is a far better proton acceptor than acetonitrile. In protonated media, transfer to the triazole is prevented and the proton either remains on the OH to produce the radical cation OH^+ or is released into the solvent.

Comparison of the electrochemical data obtained for $[Ru(bpy)_2(H_2L1)]^+$ in neutral and acidic acetonitrile suggests that the triazole is protonated in these media. From pK_a measurements this is unexpected since in acetonitrile the pK_a of $[Ru(bpy)_2(H_2L1)]PF_6$ is 2.6. At a pH of 9.5 differential pulse polarography reveals two oxidations one at 0.65V tentatively assigned as the $HQ^- \text{-->} HQ\cdot$ reaction, and one at 0.91V assigned as the Ru(II)/Ru(III) oxidation for the complex in which the triazole is deprotonated.

3.3.5.2 Spectroelectrochemical evidence.

Spectroelectrochemistry of $[Ru(bpy)_2(H_2L1)]^+$ in neutral acetonitrile confirmed that the complex is deprotonated at 0V, where the λ_{max} was observed to be 475 nm corresponding to that of the deprotonated complex. Upon scanning the applied potentials between 0 and 0.9V (see fig 3.23) λ_{max} experiences a gradual blue shift until the λ_{max} is maintained at 430 nm and complete protonation has occurred.

Complete protonation has in fact occurred before the commencement of the second hydroquinone oxidation. This suggests that the proton responsible for the protonation of the triazole is associated with the oxidation of the first hydroxyl moiety on the hydroquinone.

Isobestic points are not maintained in the spectroelectrochemistry of the oxidation process (fig. 3.23(a)). It is likely that semiquinone intermediates are responsible, since the λ_{max} of such radicals have been shown to occur around 430 nm [79, 80]. For the reduction process (fig. 3.23(b)) the reaction appears to be much cleaner with isobestic points maintained at 410 and 450 nm. Often in quinone/hydroquinone electrochemistry the prevalent reaction sequence for oxidation differs to that of reduction. This behaviour illustrates this point well. It is likely that on reduction the intermediate semiquinone is rapidly protonated and disproportionated, since release of the second proton from oxidation will have increased solvent acidity. This is discussed below.

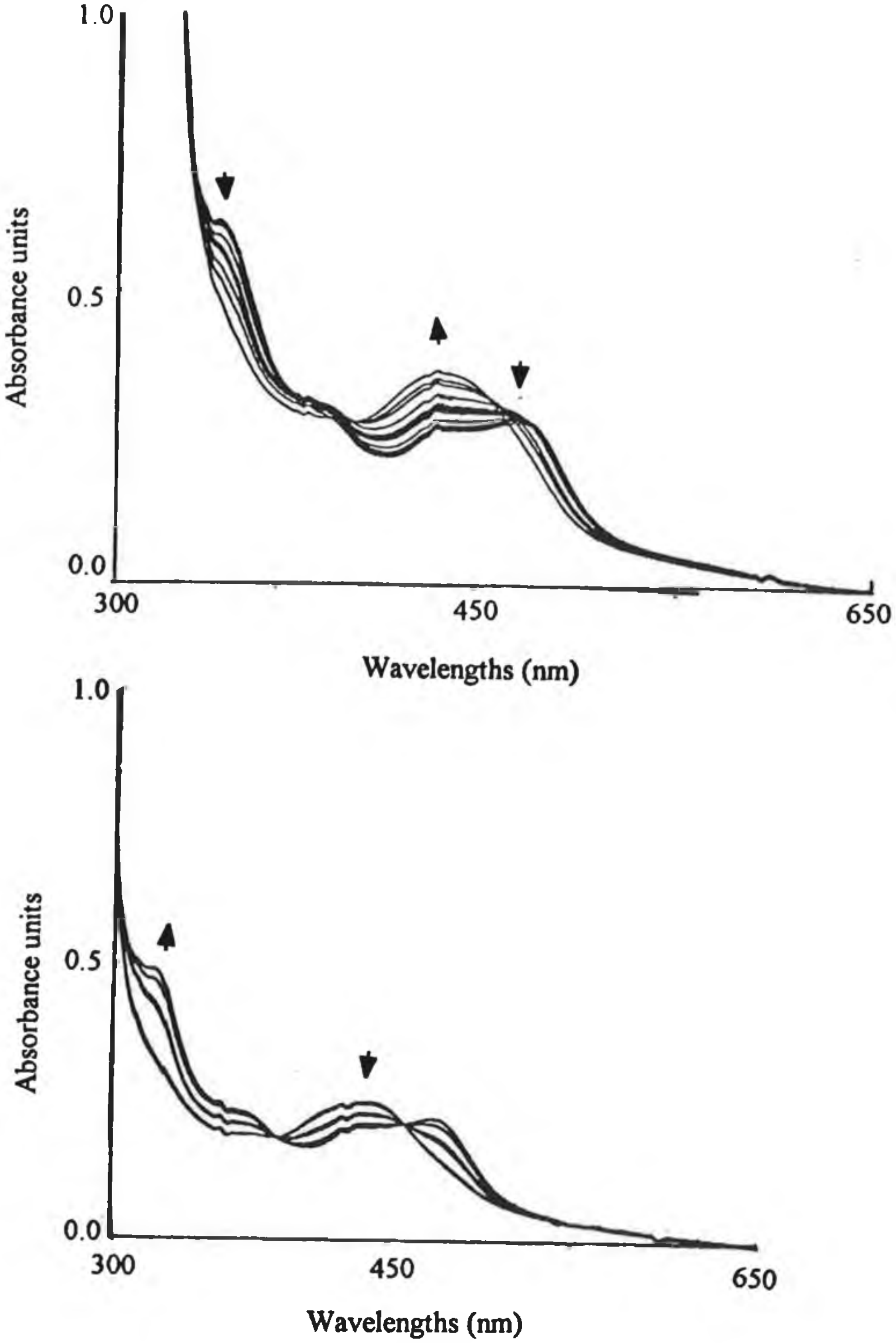

Figure 3.23. Spectroelectrochemistry of $[Ru(bpy)_2(H_2L1)]^+$ in neutral acetonitrile, potential range 0 to 0.9V in 0.1V increments, (a) forward scan (0-0.9V) (b) reverse scan (0.9-0V).

For $[Ru(bpy)_2(H_2L1)]PF_6$ the proton transfer is independent of pH in acetonitrile solution within the range 5-8. It is also observed in dichloromethane, but occurs only to a small extent in water, protonation also takes place in methanol but is not concluded in this solvent until oxidation of the second hydroxyl commences. For the analogous complex $[Ru(bpy)_2(H_2L6)]^+$, containing a catechol moiety as opposed to p-hydroquinone protonation was also observed in acetonitrile, on oxidation. However, in this instance the protonation did not reach completion within the first hydroxyl oxidation. In the phenolic complexes $[Ru(bpy)_2(HL4)]PF_6$ and $[Ru(bpy)_2(HL2)]PF_6$ hydroxyl oxidation occurs after the metal oxidation and therefore proton transfer is difficult to monitor. However, preliminary experiments suggest that proton transfer occurs in $[Ru(bpy)_2(HL2)]PF_6$ but to a much lesser extent in $[Ru(bpy)_2(HL4)]PF_6$. The difference between the proton transfers observed fpr the catechol and hydroquinone complex is illustrated in figure 3.24.

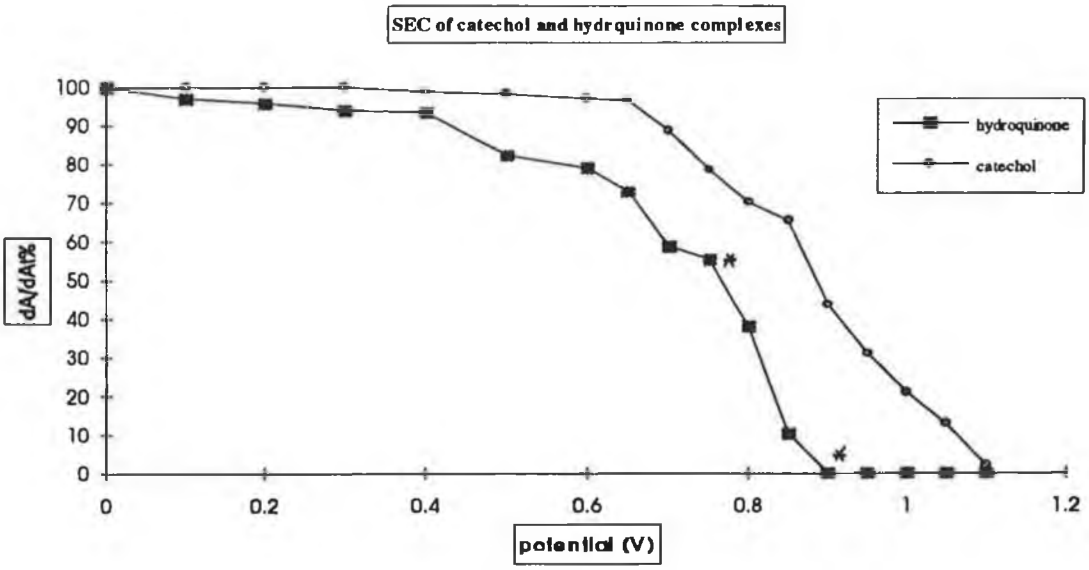

Figure 3.24. Comparison of protonation as a function of potential for $[Ru(bpy)_2(H_2L1)]^+$ and $[Ru(bpy)_2(H_2L6)]^+$ from spectroelectrochemistry in neutral acetonitrile.

The change in absorbance as a function of potential are plotted, the first and second hydroquinone based oxidations are also marked* on the graph. It can be seen that the oxidation for the catechol complexes actually occurs at lower potential than that of $[Ru(bpy)_2(H_2L1)]PF_6$. This implies that there is a different process operating between the p-hydroquinone and the phenol and catechol containing complexes In fact comparison of the CVs of $[Ru(bpy)_2(H_2L1)]^+$ and $[Ru(bpy)_2(H_2L6)]^+$ in neutral acetonitrile show that metal oxidation waves for $[Ru(bpy)_2(H_2L6)]^+$ when the triazole is both protonated and deprotonated appear, whereas there is no appearence of a metal oxidation for a deprotonated complex in $[Ru(bpy)_2(H_2L1)]^+$ even though the former possesses a considerably higher pK_a (pK_a = 2.6 for $[Ru(bpy)_2(H_2L1)]^+$ and 4.5 for $[Ru(bpy)_2(H_2L6)]^+$ in acetonitrile).

It has been shown that in the solid state in the analogous o-phenolic complex $[Ru(bpy)_2(HL2)]^+$ a strong H-bridge exists between the hydroxyl of the phenol and the adjacent N on the triazole where the N-O distance is 2.62Å [44]. From the acid-base properties of this complex there is reason to believe that this interaction exists in $[Ru(bpy)_2(H_2L1)]PF_6$ and in fact persists in solution.

This suggests that the proton in the H_3L1 complex may be transferring intramolecularly in non-H-bonding solvents such as dichloromethane and acetonitrile. Since the process is pH independent in the range studied, the protonation of the triazole is unlikely to be simply a manifestation of increased acidity of the solution as a result of the release of protons from the oxidised hydroxyl. This is because protonation is complete in $[Ru(bpy)_2(H_2L1)]PF_6$ before the start of the second hydroxyl oxidation. Whereas in the catechol complex protonation reaches completion only after the second hydroxyl oxidation despite the fact that the pK_a of the catechol complex is higher by more than 2 pH units than the hydroquinone complex in acetonitrile. Furthermore, since the pK_a of the triazole in $[Ru(bpy)_2(H_2L1)]PF_6$ in acetonitrile is approximately 2.6 and the concentration of the complex for spectroelectrochemistry ranges between 2×10^{-4} and 2×10^{-3} M a change in proton concentration to 2.5×10^{-3} M (i.e. pH 2.6) is clearly unlikely during the first hydroxyl oxidation.

From the observations described a tentative mechanism is devised (see scheme 3.2).

The first hydroquinone based oxidation is accompanied by a proton transfer, if the o-OH is bridged to the triazole, this bridged O will possess more negative character and hence be the first group oxidised. This will produce the intermediate semiquinone radical **II**. Oxidation of the second hydroxyl will produce the quinone species **III** at 1.01V. Since the triazole is already protonated at this stage the destination of this second proton is not known, but is presumed to be released into the solvent. Further scanning to 1.3V leads to the oxidation of the Ru(II) to Ru(III) to produce **IV** as manifested by the disappearance of the MLCT band in spectroelectrochemical measurements.

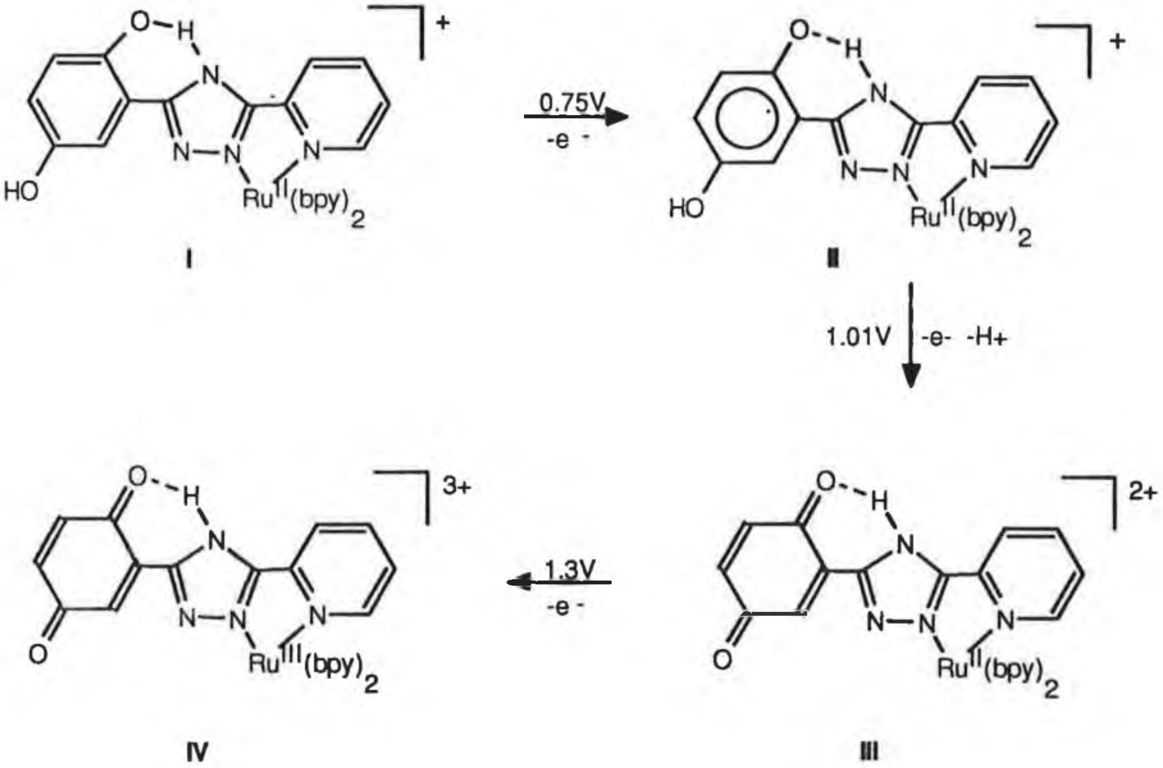

Scheme 3.2.

Rereduction results in the grow-in of the MLCT band and the gradual build up of the band at 330 nm associated with the hydroquinone. From the C.V. (figure 3.23), the rereduction of the quinone to hydroquinone appears to occur in one step, and from the very clean SEC it would appear that intermediates do not occur. Two possibilities for the reduction process present themselves here. Since the solution will be moderately acidic after oxidation of the hydroquinone, protonation of the quinone may occur, or the proton may not have been released after hydroquinone oxidation at all.

$$Q \xleftrightarrow{\pm H^{+}} QH^{+} \xrightarrow{+e^{+}} QH^{\bullet}$$

leading rapidly to either electrochemical reduction

a) $$QH^{\bullet} \xleftrightarrow{\pm e^{-}} QH^{-} \xleftrightarrow{\pm H^{+}} QH_2$$

or chemical dismutation

b)

$$\begin{aligned} &QH^{\bullet} \leftrightarrow Q^{\bullet -} + H^{+} \\ &QH^{\bullet} + Q^{\bullet -} \leftrightarrow Q + QH^{-} \\ &QH^{-} + H^{+} \leftrightarrow QH_2 \end{aligned}$$

Since the reductive wave represents two electrons, it is likely that a) is the dominant process.

A particularly interesting aspect of the electrochemically coupled proton transfer encountered in these complexes is their potential as molecular electrochemical switches. Protonation of the triazole of Ru(II) pyridyltriazole complexes as described, results in a massive decrease in both lifetime and intensity of emission.

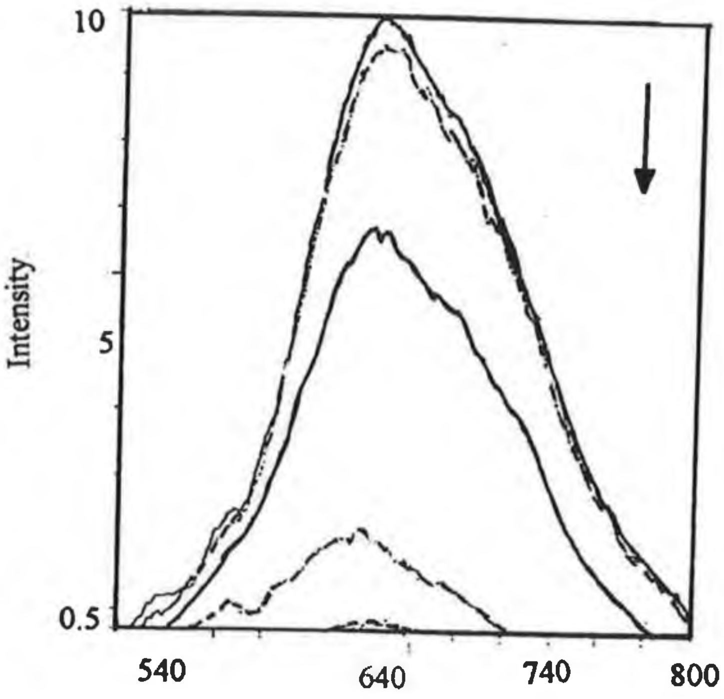

Figure 3.25 Emission spectroelectrochemistry of $[Ru(bpy)_2(H_2L1)]^+$ *in acetonitrile at pH 8.0. At potentials 0, 0.3, 0.6, 0.7 and 0.8 V (vs SCE).*

The emission spectroelectrochemistry for $[Ru(bpy)_2(H_2L1)]^+$ shown in figure 3.25 illustrates this well, along with the potential versus emission intensity plot, (figure 3.26).

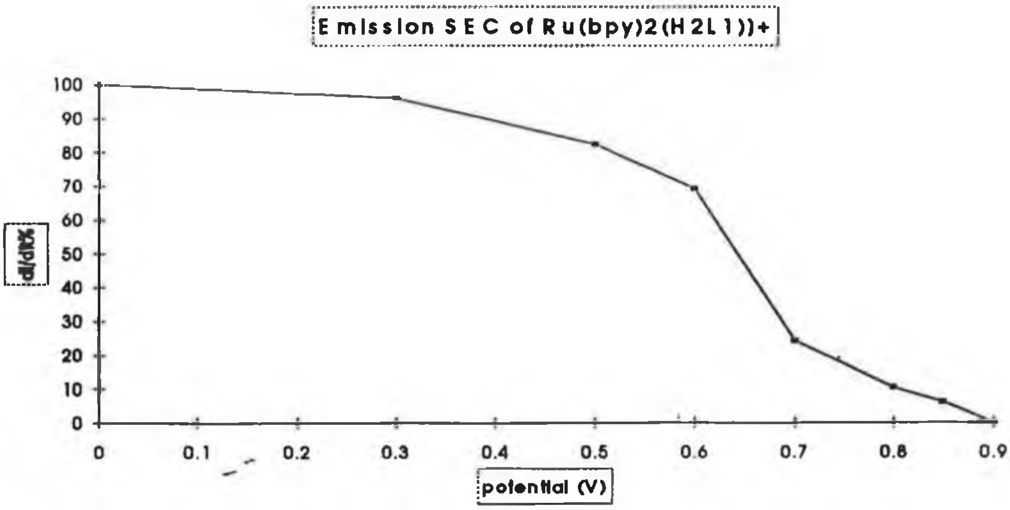

Figure 3.26, Potential vs change in Emission intensity for $[Ru(bpy)_2(H_2L1)]^+$.

The typical blue shift and dramatic decrease in emission intensity are observed with the electrochemical protonation of the triazole moiety, and an associated drop in emission intensity occurs. In lifetime measurements followed as a function of potential the same behaviour is observed is observed however, the lifetimes observed after protonation of the complex are generally too short to be measured accurately by nanosecond instrumentation (i.e. < 20 ns). Because of the associated protonation of the triazole on oxidation of the hydroquinone, the individual influences of the semiquinone and quinone species on the emission of the complex cannot be examined. However, emission SEC was carried out at pH >9.5 to observe the influence of oxidation in the absence of proton transfer. The result is not terribly satisfactory since at high pHs the oxidation of the QH^- or Q^{2-} species is examined and the initial emission intensities for these complexes is low as a result of quenching, as discussed in the following section.

3.3.6 Photoinduced electron transfers.

Phenols, hydroquinones and in particular quinones are noted for their ability to quench the excited state of $[Ru(bpy)_3]^{2+}$ and related complexes [22, 24, 81, 82]. This quenching is related to the redox activity of these species allowing them to function as electron donors in the case of phenols and hydroquinones and as acceptors in the case of quinones. Most studies of such electron transfers have been of bimolecular processes, the aim in creating these complexes is to observe whether quenching of the excited ^{3}MLCT state is achieved when the quenching species is bound via a negative triazolate bridge to the luminophore. And if it does occur whether it is an inter or intramolecular process.

To ascertain the feasibility of electron transfer occurring in these systems the redox properties of the quenchers must be determined in their neutral and anionic states (or raidcal in the case of quinone). The Weller [34] equation (3.8) may be employed to obtain an estimate for the free energy of electron transfer in a donor - acceptor system. This equation was devised for use as an estimate of ΔG in bimolecular reactions.

$$\Delta G\ (\mathrm{kCal\ /\ Mol}) = 23.06\ [E(D^{+\cdot} / D) - E(A / A^{+\cdot}) - e^2 / \varepsilon d_{dssip}] - E^*_D \quad (3.8)$$

Where E are redox potentials for donor and acceptor groups, $e2/\varepsilon d_{SSIP}$ is the solvent coulombic contribution ε is the solvent dielectric constant, and d_{SSIP} is the distance between the ions. This entire term is neglected when the solvent has a large dielectric constant, and this is reduced to equation (3.9) which is employed in this report for unimolecular systems.

$$\Delta G(\mathrm{eV}) = \left[E(D^{+\cdot} / D) - E(A / A^{+\cdot})\right] - E^*_{DorA} \quad (3.9)$$

3.3.6.1 Bimolecular quenching between ligands and $[Ru(bpy)_3]Cl_2$.

The ability of the ligands employed to quench bimolecularly was initially investigated. This was achieved by assessing their ability to quench the excited state of $Ru(bpy)_3^{2+}$ in aerated aqueous solution at constant pH and ionic strength. The quenching reactions were analysed employing the Stern-Volmer relation [83] (3.8).

$$\frac{I_f^o}{I_f} \text{ or } \frac{\tau^o}{\tau} = 1 + K_{sv}[Q] \text{ (3.9), where } K_{sv} = \frac{k_q}{k_f}$$

I_f is the fluorescence intensity, [Q] is the concentration of quenching species, k_f is the radiative rate constant of $[Ru(bpy)_3]^{2+}$, obtained from the recipricol lifetime of $[Ru(bpy)_3]^{2+}$ under the same condition but in the absence of quencher.

The electron transfer rates in the bimolecular quenching experiments (k_q) involving the free ligands and $[Ru(bpy)_3]^{2+}$ are shown in table 3.6 along with their Stern-Volmer constants. All Stern-Volmer plots were linear over the concentration range 4 $\times 10^{-5}$ to 2 $\times 10^{-3}$ M, with correlation coefficients greater than 0.996. This adherence to the Stern-Volmer relation (when the relation τ^0/τ was employed) indicated the absence of any static quenching.

Table 3.6: Rates of quenching of the excited state of $[Ru(bpy)_3]Cl_2$ by ligands.*

Compound	**K_{sv}**	**k_q ($dm^3mol^{-1}s^{-1}$)**
L1	1957	5.16×10^9
L2	342.2	9.03×10^9
L3	1335	3.52×10^9
L4	1369.6	3.61×10^9

* Carried out in buffered solution at pH 12 at constant ionic strength. Error for K_{sv} and k_q is estimated to be 2%.

The ΔG estimated from equation (3.9) are as follows for L1 (H_2Q) in neutral solution ΔG = 0.01 eV; anionic $HL1^-$ HQ^- ΔG = -0.298 eV; quinone L3 Q in neutral solution ΔG = -0.13 eV; semiquinone $L3^{\cdot 2-}$ $Q^{\cdot -}$ as acceptor ΔG = -0.388 eV and as donor species ΔG = -0.699 eV. The values derived for the ligands in the radical and anionic states are taken from reference [84] when they were not measured directly via electrochemistry.

In aqueous media at pH 6.5 quenching was only observed for the quinone ligand, and this was too slow to be fit adequately by a Stern-Volmer plot. This is due to the large negative reduction potential of this ligand, which produces a weakly negative ΔG for this process. Simple p-benzoquinone is known to oxidatively quench the excited state of $[Ru(bpy)_3]^{2+}$ efficiently (kq = 3.7 $\times 10^9 dm^3 mol^{-1} s^{-1}$) [33] at this pH. In buffered solution at pH 12 considerable quenching was detected for all ligands with the exception of $L5^-$. The rates of electron transfer observed correlate well with other reported p-benzoquinone quenching of $[Ru(bpy)_3]^{2+}$ in aqueous media [33], and phenols in basic media [82] with transfer rates between 3 $\times 10^{-9}$ and 9 $\times 10^{-9}$ s^{-1}. At neutral pH no quenching is observed for H_3L1, whereas Darwent and co-workers reported K_q for HQ quenching of $[Ru(bpy)_3]^{2+}$ in neutral aqueous solution as 5 x 10^{-7} $dm^3 mol^{-1} s^{-1}$. At pH 12 the rate of quenching of L1 far exceeds this value, and correlates well with observations of rate constants of reduction of Fe^{3+} by HQ^- [84].

At pH 12 the pH is beyond the pKas of the hydroxyls, and in the case of the quinone at a pH where spontaneous creation of semi-quinone has been observed [21, 90]. Two interesting results are obtained. The quenching rate observed for hydroquinone containing ligand H_3L1 surpasses that of the quinone HL2 at high pHs, whereas at neutral pHs there is effectively no quenching observed for either, this is unusual since simple benzoquinone is usually reported to be a strong quenching agent. At pH 12 both the triazole and hydroquinone are expected to be deprotonated, and since the quenching is reductive the 2^- charge on the ligand should facilitate this process. The quinone however oxidatively quenches, itself becoming reduced in the process. It is conceivable that the negative triazole on the quinone, increases the electron density on the quinone making it more difficult to oxidise. This 1^- charge will therefore also the reduce the efficiency of this electron transfer. Since from the ΔG values quoted above the implication is that quinone quenching from the radical should be more exothermic than the HQ^- electron transfer, it must be presumed that the considerations described above play a dominant role in the efficiency of electron transfer for the quinone.

For reductive phenolate quenching, there is a considerable difference in quenching rates observed between the 2 and 4-hydroxy ligands H_2L2 and H_2L4. The lower quenching rate observed for the 2-hydroxy ligand is most likely due to the steric hindrance to the phenolate caused by the proximity of the pyridyltriazole group, making formation of an intermediate collision-complex difficult. Bulky groups in close proximity to the quenching sites have been reported to reduce the efficiency of electron transfer in di-tert.butylquinones [22].

3.3.6.2 Intramolecular electron transfer involving complexes.

From the preceding studies, it was established that the ligand species are capable of pH dependent quenching of the excited state of $[Ru(bpy)_3]^{2+}$. Therefore, the complexes these ligands produced were investigated in order to determine if quenching could occur intramolecularly across a triazole bridge. Since the negative triazole species has been shown previously to facilitate hole and energy transfer in dinuclear complexes [85].

Comparison of the absorbance spectra of the substituted complexes with that of the phenyl complex reveals no new features which would indicate that introduction of O or OH groupings perturb the electronic levels of the complex at any pH. The strong absorbance observed in $[Ru(bpy)_2(H_2L1)]^+$ at 330 nm is also observed in the ligand and would appear to be a $\pi-\pi^*$ transition. Consequently, the chromophore and donor/acceptor site are not electronically coupled in the ground state.

From equation 3.10, a comparison may be made between the quantum yields of emission of the complexes ϕ and the model complex ϕ_0 in order to determine the efficiency of electron transfer.

$$\eta_{et} = \phi_o - \phi \qquad (3.10)$$

Rates of intramolecular electron transfer (k_{et}) are determined from the reciprocals of the lifetimes of the sample τ and model complexes τ_0 according to equation (3.11), where conditions are identical for each species.

$$k_{et} = \frac{1}{\tau} - \frac{1}{\tau_o} \qquad (3.11).$$

The phenyl complex $[Ru(bpy)_2(L5)]^+$, which shows no quenching at any pH is employed as the model compound.

The electron transfer rates in various media are shown in table 3.7 along with the efficiency of electron transfer in acetonitrile. Although an accurate assessment of pH cannot be made in organic media such as dichloromethane a value of pH is given. In such media a concentration of base was added which would in aqueous media produce the quoted pH. The aim in addition of this base was deprotonation of the OH sites. This was determined to be achieved by spectroscopic means, making accurate assessment of the pH of solution unnecessary.

Table 3.7 Electron transfer data for complexes.

Complex	**Solvent**	**pH**	k_{el}	η**el**
$[Ru(bpy)_2(H_2L1)]^+$	MeCN	neutral	none	
$[Ru(bpy)_2(L1)]^-$	MeCN	>12	6.35×10^6	2.0×10^{-3}
$[Ru(bpy)_2(H_2L1)]^+$	H_2O	neutral	2.95×10^6	
$[Ru(bpy)_2(L1)]^-$	H_2O	>12	1.46×10^7	
$[Ru(bpy)_2(H_2L1)]^+$	Alcohol	neutral	2.12×10^6	
$[Ru(bpy)_2(L1)]^-$	Alcohol	>12	$5.20\ 10^6$	
$[Ru(bpy)_2(H_2L1)]^+$	DCM	neutral	none	
$[Ru(bpy)_2(L1)]^-$	DCM	2% DEA*	1.62×10^6	
$[Ru(bpy)_2(L3)]^+$	MeCN	neutral	none	
$[Ru(bpy)_2(L3)]^{\cdot}$	MeCN	>12	3.38×10^6	2.0×10^{-3}
$[Ru(bpy)_2(L3)]^+$	H_2O	neutral	7.93×10^5	
$[Ru(bpy)_2(L3)]^{\cdot}$	H_2O	>12	2.10×10^6	
$[Ru(bpy)_2(L3)]^+$	alcohols	neutral	1.8×10^5	
$[Ru(bpy)_2(L3)]^{\cdot}$	alcohols	>12	1.53×10^6	
$[Ru(bpy)_2(L3)]^+$	DCM	neutral	none	
$[Ru(bpy)_2(L3)]^{\cdot}$	DCM	2% DEA*	none	
$[Ru(bpy)_2(HL4)]+$	MeCN	neutral	none	
$[Ru(bpy)_2(L4)]$	MeCN	>12	2.70×10^6	2.01×10^{-3}
$[Ru(bpy)_2(HL4)]^+$	H_2O	neutral	6.97×10^6	
$[Ru(bpy)_2(L4)]$	H_2O	>12	1.46×10^7	
$[Ru(bpy)_2(HL4)]^+$	alcohols	neutral	6.97×10^6	
$[Ru(bpy)_2(L4)]$	alcohols	>12	3.33×10^7	
$[Ru(bpy)_2(HL4)]^+$	DCM	neutral	none	
$[Ru(bpy)_2(L4)]$	DCM	2% DEA*	none	
$[Ru(bpy)_2(H_2L6)]^+$	MeCN	neutral	none	
$[Ru(bpy)_2(L6)]^-$	MeCN	>12	3.7×10^{-6}	1.9×10^{-3}

* As described, in a non-polar solvent such as dichloromethane the term pH becomes meaningless. Therefore in this instance 5% diethylamine was added, which from absorption spectra was more than sufficient to deprotonate the hydroxyls in the hydroquinone and phenols.

It is apparent that in acetonitrile no quenching is occurring at neutral pH for $[Ru(bpy)_2(H_2L1)]^+$. The absence of quenching in this complex is not surprising at this pH based on the fact that it was not observed at all in the ligand. This result also complies with the endoergonic ΔG_{el} value predicted for electron transfer in $[Ru(bpy)_2(H_2L1)]^+$ which is estimated to be 0.32 eV in acetonitrile, suggesting that significant quenching should not be occurring. The ΔG_{el} value estimated for $[Ru(bpy)_2(L3)]^+$ is 0.20 eV in acetonitrile at neutral pH. This predicts that the transfer will be mildly endoergonic, which is consistent with the lack of electron transfer observed. This is again, an unusual situation for quinones which are in general more conducive to electron transfers than hydroquinones [21], and is associated with the uncommonly cationic reduction potential of the quinone in this complex.

At high pH a considerable decrease in quantum yield is observed for all complexes with the exception of $[Ru(bpy)_2(L5)]^+$, suggesting that as was the case with the free ligands electron transfer does occur. The electron transfer rates displayed in table 3.7 are 100 times slower than those observed in the bimolecular ligand processes. This is most likely a result of the distance forced between the chromophore and quencher via the triazolate spacer in the complex. This also suggests that the quenching observed in the complexes is intramolecular. These electron transfers are also slow relative to other similar reports of intramolecular transfers, this is associated with the fact that the excited state is remote from the quenching ligand, and most other reports have involved binding of quencher to the bipyridyl [37, 38].

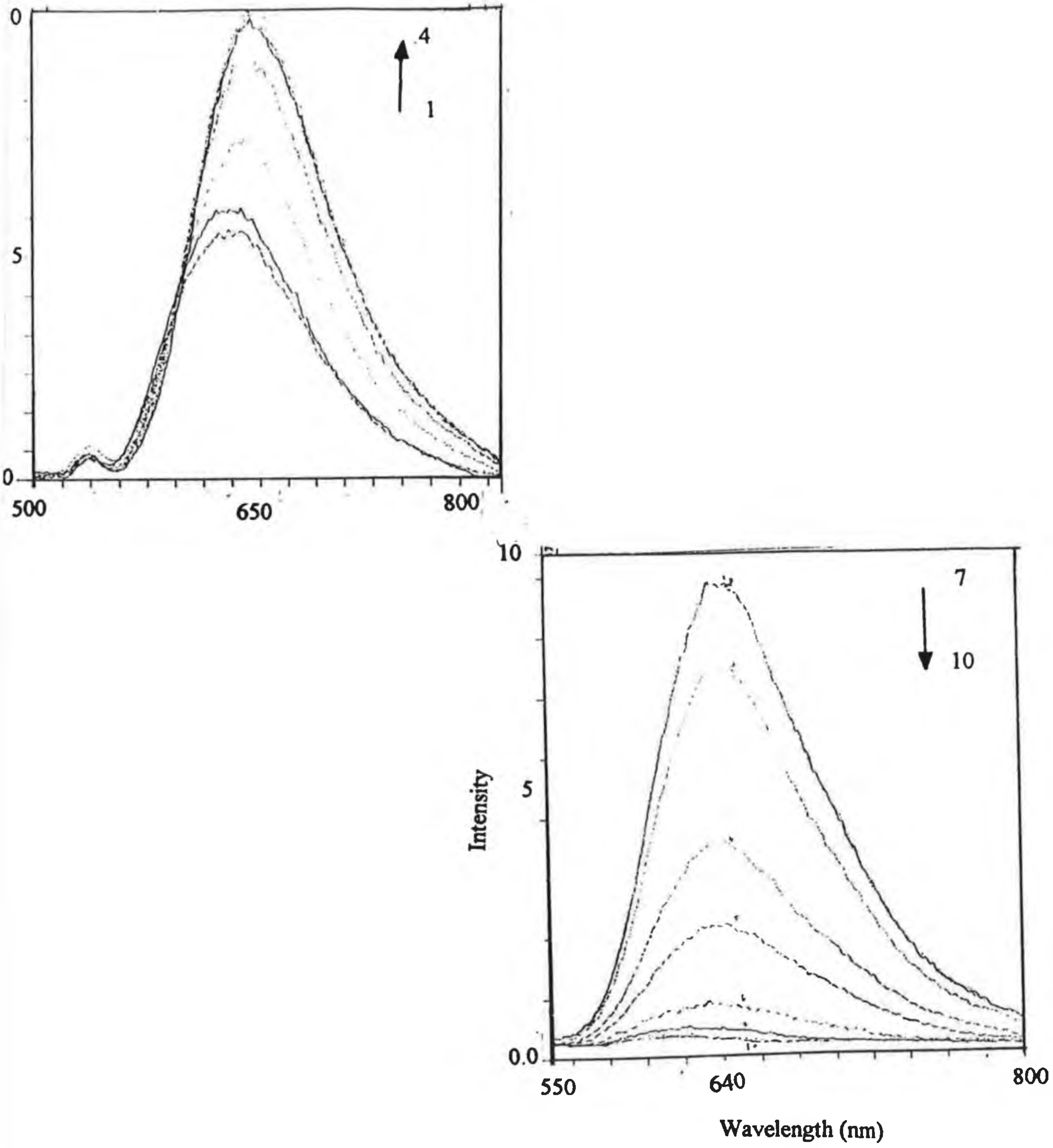

Figure 3.27. PH dependent emission of $[Ru(bpy)_2(H_2L3)]^+$ *in aqueous Britton Robinson buffer.*

It is unlikely that this quenching is an energy transfer process from the perspective of energetics for the phenolic and hydroquinone complexes. Since the triplet energy of the Ru(II)bpy is approximately 1.9 eV and the excited state energy of the hydroquinone is 3.8 eV and the phenols is 4.13 eV, the difference is too great to support energy transfer. For the neutral quinone the energy difference is just as large, even at high pH, if the species responsible for quenching is the semiquinone, which possesses a longer wavelength absorbance the energy difference would be too large to support energy transfer. Furthermore, the strong solvent dependence exhibited by the process, which is described below, also refutes energy transfer, since such a process does not generate polarised intermediates it would be expected to posses minimal solvent dependence.

The pH dependant emission titration is shown for $[Ru(bpy)_2(L3)]^+$ in figure 3.27, along with the titration curves. This same predictable pH dependent emission behaviour over a wide pH range is observed in both the phenol and hydroquinone complexes. A difference exists however in the behaviour of titration curve for quinone (figure 3.27), whereby hydroquinone and phenol complexes reach a plateau in their titration curves around neutral pHs (pH 5-8), and quinone shows pH activity over the whole pH range. This is likely to be a result of the fact that the quenching species created in the phenols and hydroquinone are different to that of the quinone. The strong pH dependence observed for the phenol and hydroquinone complexes is thought to be associated with quenching by the anionic hydroxyls produced at high pH. Previous reports of bimolecular quenching involving phenolates have been made [81, 82], and for hydroquinone it is thought that in the photosynthetic cycle it is the anionic HQ^- that dominates the reductive functions [84]. In fact preliminary experiments show that under conditions of constant ionic strength, addition of Li^+ or Ca^{2+} to solutions of $[Ru(bpy)_2(L1)]^-$ and $[Ru(bpy)_2(L3)]^+$ causes an increase in emission intensity which stabilises at equimolar concentrations of complex and salt. It would seem likely therefore, that these metals are coordinating to the anionic oxygens and preventing electron transfer (it was for this reason that the bases used, for quenching studies did not contain alkali metals, such as NaOH).

For the electron transfer in $[Ru(bpy)_2(L1)]^-$ at high pH, mediated by the QH^- ion the ΔG_{el} is estimated to be -0.10 eV, as a result of the cathodic shift of the hydroquinone oxidation in the presence of base. This predicted change from endoergonicity to exoergonicity correlates well with the observed electron transfers in basic solution.

For the quinone, the pH dependence may be a little more complicated, it was reported by von Zelewesky and coworkers [21] that quinones form semiquinones at high pHs. It is possible that the faster quenching at high pHs for the quinone complex is either caused by or catalysed by semiquinone. The semiquinone intermediate may act as either an electron donor or acceptor. The ΔG_{el} value for $Q^{\cdot -}$ as a donor is -0.37 eV and as an acceptor is -0.38 eV. It is obvious, therefore, that the semiquinone is equally efficient as a donor or acceptor species in these circumstances. However, since the quinone moiety is remote from the bpy- species and directly connected to the $Ru^{(III)}$ in the excited state, it is most likely that it will behave as a donor, this is discussed in more detail in the mechanism. The influence of base on this complex is demonstrated in figure 3.28 where addition of diethylamine to a solution of $[Ru(bpy)_2(L3)]^+$ in acetonitrile causes significant broadening of the MLCT band 470 nm, this is most likely associated with semiquinone formation which absorbs in this region.

These quenching processes are entirely independent of complex concentration over the range 1 $x10^{-5}$M to 1 $x10^{-3}$M, implying that it is occurring intramolecularly. The discrepancy observed between quenching rates of the phenolic ligands is not observed for the complexes which show almost identical electron transfer rates in acetonitrile also suggesting that the electron transfer is intramolecular when coordinated.

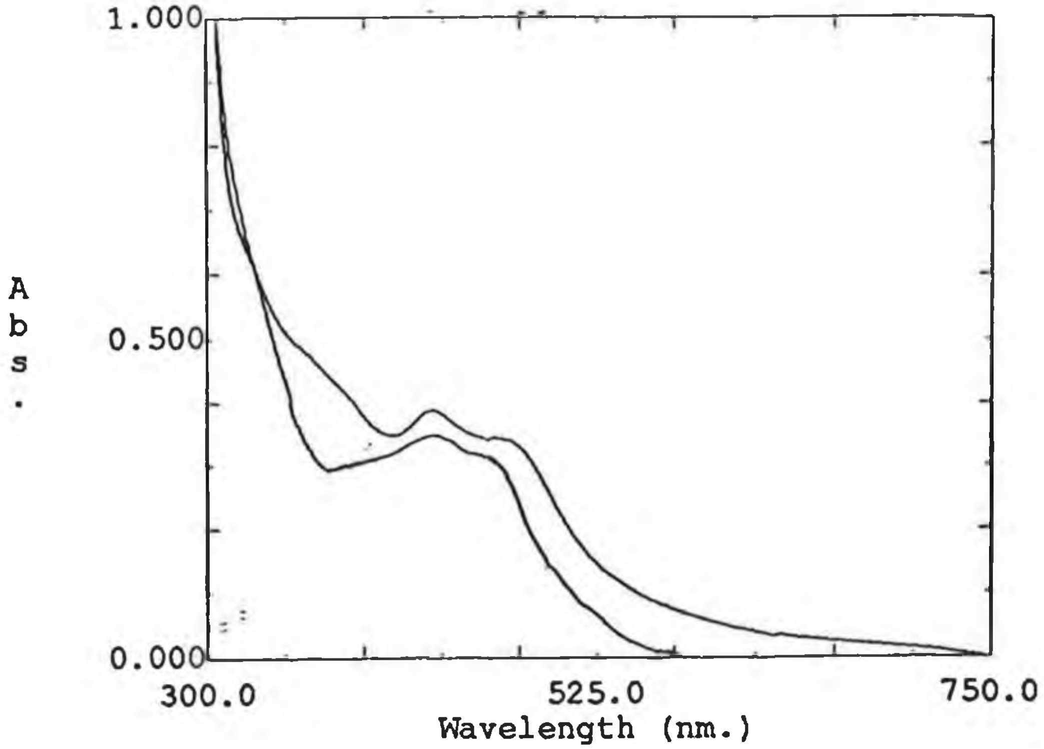

Figure 3.28, Absorption spectra of $[Ru(bpy)_2(H_2L'3)]^+$ *(a) in presence and (b) absence of base in acetonitrile.*

3.3.6.2.1 Solvent effects:

The solvent governs two parameters that are capable of radically altering the electron transfer rates. Firstly the exogonicity of the reaction may be altered by the presence or absence of electrostatic stabilisation through solvation of the final charge separated product of electron transfer. Secondly, the rate of electron transfer and solvent characteristics are intrinsically linked by equation (3.12) [86]:

$$k_{et} = \upsilon_{et} \exp -[(\lambda + \Delta G^{o})^{2}/4\lambda)/k_{b}T] \qquad (3.12)$$

where ΔG^{o} is the Gibbs free energy of reaction, υ_{et} is the vibrational frequency, k_b is the Boltzmann constant and the reorganisational energy $\lambda = \lambda_i + \lambda_o$, where λ_i relates to structural changes in the molecule, and

$$\lambda_o = B\left[\frac{1}{\varepsilon_{op}} - \frac{1}{\varepsilon_{s}}\right] \qquad (3.13)$$

relates to changes in the surrounding solvent. B relates to the molecular dimensions and ε_{op} is the square of the solvent refractive index and ε_s is the solvent dielectric constant. Finally solvent dynamics may contribute to the υ_{et} term in (3.12).

The electron transfers observed exhibit a strong solvent dependence. The rates of electron transfers appear to decrease in the following solvent dependent order:

water > ethanol/methanol > acetonitrile > dichloromethane

i.e. electron transfers increase with increasing solvent polarity. Relatively rapid electron transfers are observed in aqueous solvents when both basic and neutral, whereas in most instances transfer appears to be absent in dichloromethane. Water supports the fastest electron transfers in these systems, this would imply that as described above, electrostatic stabilisation of the electron transfer product is the most important factor, dominating over the influence of the λ_0 term.

3.3.6.2.2 Temperature dependence of electron transfer:

The electron transfer processes observed for these complexes at high pH persist at low temperature. This is immediately apparent by comparing the emission lifetime of the complexes in alcoholic glass at 77K in the presence and absence of base (table 3.2), a decrease of greater than 50 % is observed for $[Ru(bpy)_2(H_2L1)]PF_6$ on addition of 5% diethylamine. The fact that this decrease is not caused by quenching due to interaction between complex and base is verified by comparison of lifetimes for $[Ru(bpy)_2(L5)]PF_6$ in the presence and absence of base, where no decrease is observed.

That electron transfer proceeds in glass and at low temperature implies that the process does not require significant conformational or vibrational change in order to approach a transition. This is particularly interesting since although charge separation is achieved at near unity quantum yields at cryogenic temperatures in photosynthesis, most model systems [87, 88] exhibit none or at least significantly reduced electron transfer in rigid glass media. The reason for this may be that in rigid media because solvent dipoles are slow to reorient around and hence stabilise the charge separated state. In addition, as mentioned, the lack of electron transfer in frozen media may be due to the inability of the donor-acceptor to reach an appropriate conformation from which electron transfer may occur. An example of such a situation was described by Meyer and co-workers, where the transfer of an electron from Re to the viologen (MQ^+) species for $[(4,4\ COOEt\text{-}bpy)ReI(CO)3(MQ^+)]^{2+}$ required conversion of MQ^+ from twisted to planar [89]. In glass matrix, no electron transfer was observed because this conformational change was no longer possible.

It would appear therefore that rapid equilibrium of solvent dipoles is not required for these systems. Since these complexes are essentially very rigid it is not surprising that significant conformational changes are not required prior to electron transfer. The occurrence of electron transfer in solid media also rules out the possibility of through solvent electron transport as the pathway for the transfer, since the large dipole changes incurred by such a process would be difficult in rigid media.

The temperature dependence of electron transfer processes may be employed to determine the free enthalpy and entropy changes for the reaction from equation (3.14), the Eyring equation.

$$\ln\left(\frac{k_{el}}{T}\right) = \ln\left(\kappa \frac{k_B}{h}\right) - \frac{\Delta H^{\neq}_{el}}{RT} + \frac{\Delta S^{\neq}_{el}}{R} \qquad (3.14)$$

Where ΔH_{el} and ΔS_{el} are the activation enthalpy and entropy of forward electron transfer respectively. κ is the electronic transmission coefficient of electron transfer (presumed to be unity, i.e. adiabatic). Therefore, by plotting $\ln(k_{el}/T)$ vs 1000/T ΔH_{el} may be determined from the slope of the line and by plotting $T.\ln(k_{el}/T)$ vs T ΔS_{el} may be determined from the slope. Table 3.8 displays the electron transfer rates (k_{et}) at different temperatures for the various complexes.

It is apparent that the electron transfer rates for $[Ru(bpy)_2(H_2L1)]PF_6$ is largely temperature independent with the exception of the 77K value for which the electron transfer although present is slower. This is likely due to the slow solvent reorganisation in the glassy phase. The quinone complex shows somewhat stronger temperature dependence, again with the largest difference showing in the glass phase.The reason for the lack of substantial temperature dependence for these ETs may be related to the fact that these processes are rather slow, competing with the radiative processes.

Table 3.8 Temperature dependent electron transfer in alcoholic media.

Electron transfers rates* for complexes: (s^{-1}).

T(K)	$[Ru(bpy)_2(L1)]^+$	$[Ru(bpy)_2(L2)]^+$	$[Ru(bpy)_2(L3)]^+$	$[Ru(bpy)_2(L4)]^+$
77	5.46 x 10^5	3.40 x10^5	1.20 x 10^5	3.07 x 10^{-5}
150	7.89 x 10^5	1.03 x10^6	1.10 x 10^6	1.03 x10^{-6}
180	8.19 x 10^5	1.35 x106	1.65 x 10^6	1.35 x10^{-6}
230	6.59 x 10^5	1.35 x10^6	1.74 x 10^6	2.73 x 10^{-6}
273	2.75 x 10^6	4.4 x 10^6	2.32 x 10^6	5.52 x 10^{-6}
293	5.20 x 10^6		3.89 x10^6	3.33 x10^{-7}

* Values based on equation (3.9), where τ_0 = lifetime at the appropriate temperature for $[Ru(bpy)_2(H_2L1)]^+$, except at 77K where value for the unknown complex in neutral solution is used.

This means that the solvent has more time to reorient as the electron (relatively) slowly traverses the molecule. This will be discussed in further detail in the following section. Application of these values to the Eyring equation (3.14) was not very satisfactory as a result of the small differences between the k_{et} values at different temperatures.

3.3.6.2.3 Transient Absorption spectroscopy.

The transient absorption spectra of $[Ru(bpy)_2(L1)]^+$ and $[Ru(bpy)_2(L3)]^+$, are shown in figure 3.29 and 3.30 respectively over timebases of 2 and 5 μs in acetonitrile. $[Ru(bpy)_2(L5)]^+$ exhibits a transient absorption spectrum consistent with those previously described for other ruthenium polypyridyl complexes [89]. Essentially, bleaching of the ^{3}MLCT was observed within 0.2 μs with no transients observed to grow in over any time period examined. Since this complex contains no quenching moieties this is exactly what was expected. The hydroquinone and quinone complexes behaved similarly on a short time scale, i.e. transient absorbances spectra at 200 ns revealed depletion of the ground state MLCT band. However when studied over longer timebases, a transient is observed to grow-in after approximately 1 μs, which decays over roughly a 9 μs period, (see figure 3.29). The transient absorption spectra for these two complexes are different, with absorbances at 400-440 nm growing in over 5 μs for $[Ru(bpy)_2(L1)]^-$, and a transient absorbance at 460 nm is produced on a 1 μs timebase for $[Ru(bpy)_2(L3)]^+$ which decays to produce a band at 420 nm on a 5 μs timebase. The absorptions observed for $[Ru(bpy)_2(L1)]$ around 400-440 nm are associated with the formation of the semiquinone radical , since the Q^{2-} should reductively quench to produce the $Q^{\cdot -}$ radical anion. The absorption spectra of the simple p-benzoquinone radical was reported from flash photolyses studies to absorb at 430 nm [90]. The absorbance at 550 nm is likely to be associated with bpy^- formation, this is derived from the reduction spectroelectrochemistry carried out on this complex which shows red shifting of λ_{max} on reduction of the first bipyridyl (see figure 3.31.). This absorbance disappears with the semiquinone absorbance. The semiquinone absorbance is strongest at the 5 μs timebase, making its formation very slow, the electron transfer rate for this complex under these conditions was found to be 6.35×10^6 s^{-1}, since the rate of radiative decay of $[Ru(bpy)_2(L1)]$ in neutral solution is roughly 5.56×10^6 s^{-1} the electron transfer is a slow process and is competitive with the radiative decay of the complex. The long evolution of the semiquinone implies that the electron transfer, although slow, results in a stable charge separated species. The stability of the charge separated species may be a function of the complexity of the reverse electron transfer pathway (see next section) and the fact that the semiquinone intermediate is known to be stabilised in basic media [21].

The electron transfer in $[Ru(bpy)_2(L3)]^+$ is most likely associated with the semiquinone species, this is derived from the fact that the oxidative transfer of the neutral quinone is exoergonic, and that the quinone in basic solution is known to spontaneously form semiquinone [21].

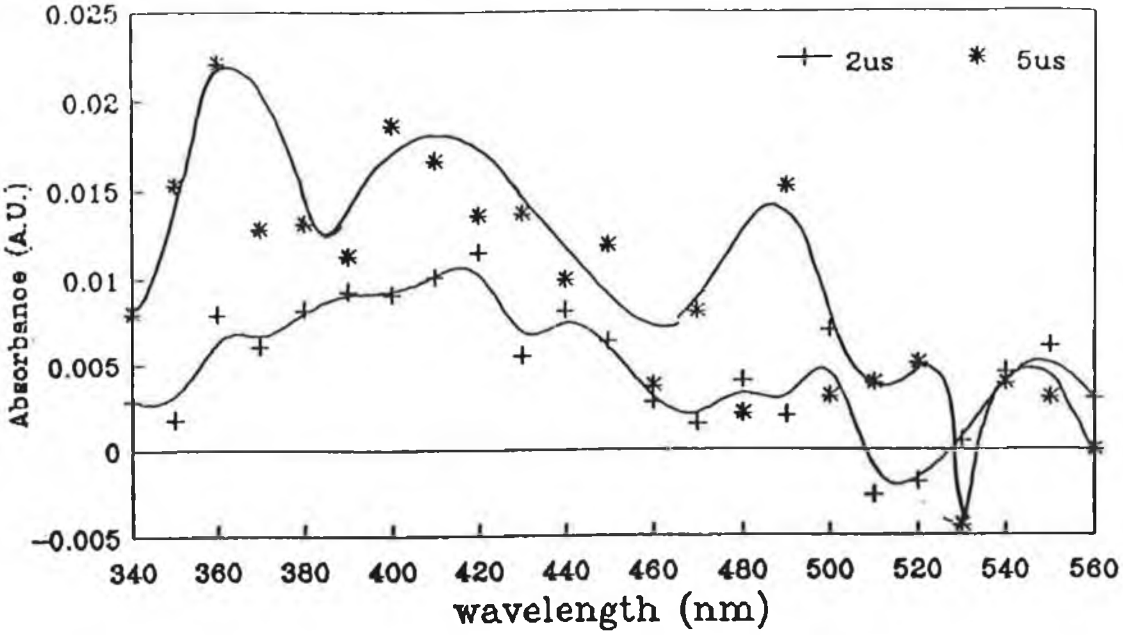

Figure 3.29 Transient absorbtion spectra of [Ru(bpy)$_2$(L1)]$^-$ at 2 and 5 μs delays in degassed acetonitrile.

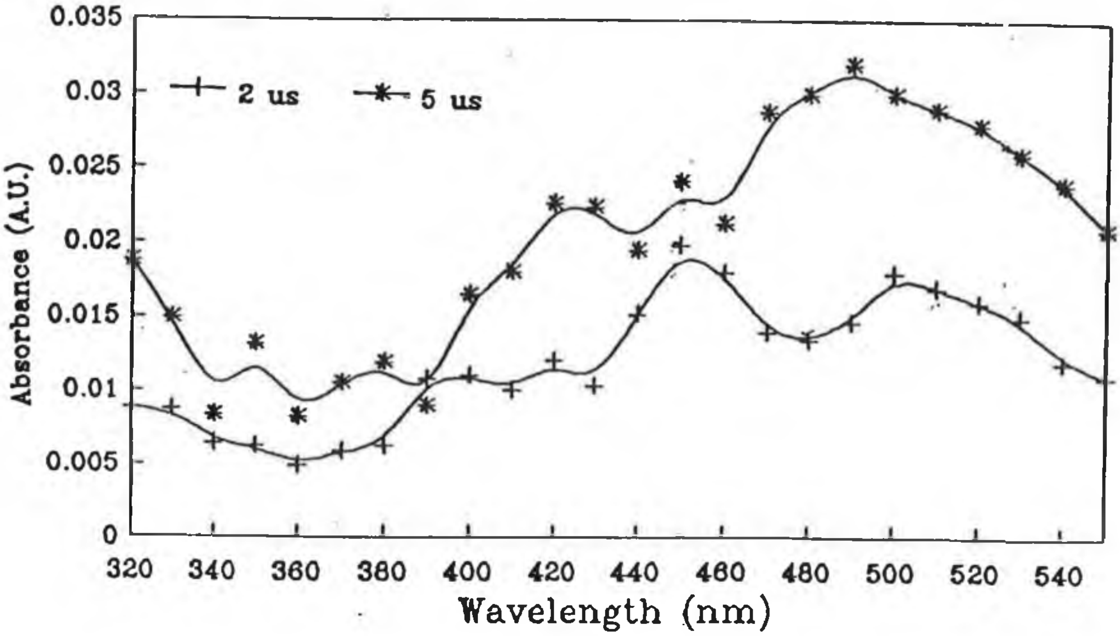

Figure 3.30 Transient absorbtion spectra of [Ru(bpy)$_2$(L1)]$^-$ at 2 and 5 μs delays in degassed acetonitrile.

Addition of base to a solution of the quinone complex caused a marked increase in extinction coefficient of the λ_{max}. This would seem to validate the fact that the semiquinone is forming since, its strong absorbance would be expected to overlap with the MLCT transition in the absorption band. The semiquinone anion radical, although stable in basic media, may also undergo disproportionation reactions according to :

$$2Q^{\cdot -} \underset{K_{-d}}{\overset{K_d}{\rightleftharpoons}} Q + Q^{2-}$$

Thereby making it likely that a number of species may be present simultaneously in basic solution for this complex, with both Q^{2-} and $Q^{\cdot -}$ capable of quenching the excited state of the complex. On the basis that the electron transfer from $[Ru(bpy)_2(L3)]^+$ is based on the semiquinone, the quinone would be the expected product. From the UV-vis spectra of the free ligand HL3 the λ_{max} of the quinone would be expected to be roughly 443 nm. and indeed a strong absorbance is observed in the transient absorbance spectra of $[Ru(bpy)_2(L3)]^+$ at 440 nm as is observed in figure 3.30. Although absent at shorter timebases, i.e. below 1 μs, this absorbance persists (although some decrease in intensity is observed) over 10 μs. This may be associated with the fact that the resulting quinone, is not a radical intermediate and hence may persist as a stable species in solution. A second transient absorbance is also present for $[Ru(bpy)_2(L3)]^+$ at 500 nm, this is most likely due to the $Q^{\cdot -}$ species as seen in the transient absorbance spectra of $[Ru(bpy)_2(L1)]^+$. Since, as was described disproportionation of the semiquinone leads to some Q^{2-} formation and thus some of the electron transfers observed may involve this species.

The electron transfers of both $[Ru(bpy)_2(L1)]^-$ and $[Ru(bpy)_2(L3)]^+$ both exhibit strong dependence on the presence of oxygen, since in both instances no transients are observed in aerated solution. This adds plausibility to the argument that both complexes are quenched by similar processes. Since oxygen will act as an interfering agent by oxidising reactants or intermediates

For example, in the presence of oxygen the Q·⁻ species produced in the electron transfer of $[Ru(bpy)_2(L1)]^+$ will be rapidly oxidised to form quinone. The same argument does not hold for the semiquinone quenching of $[Ru(bpy)_2(L3)]^+$ since the fully oxidised quinone is the product. It is possible that in this instance oxygen interferes by competing with the excited $Ru(bpy)_2$ centre for oxidation of the semiquinone. It is expected that oxygen will compete very efficiently for quenching of the excited $Ru(bpy)_2$ centre for both complexes since the quenching rate for oxygen is in the order of $2.4\ x10^{-9}\ s^{-1}$ [97], considerably faster than the electron transfer rate observed for these compounds.

Transient absorption spectra of the phenol complexes did not reveal significant transients. This may be related to the fact that any radical intermediates from quenching by O^- may not absorb in the visible region examined, since the advantage of quinone/hydroquinone is their highly coloured intermediates.

3.3.6.2.4 Mechanism of electron transfer.

On the basis of the estimated free energies of electron transfers, consideration of distance between donor/acceptor sites and the transient absorption data, it is likely that both electron transfers originate from donor species. The Q^{2-} ion for $[Ru(bpy)_2(H_2L1)]^+$, and the $Q\cdot^-$ for $[Ru(bpy)_2(L3)]^+$ and O^- phenolates for $[Ru(bpy)_2(HL2)]^+$ and $[Ru(bpy)_2(HL4)]^+$.

That the $Q\cdot^-$ radical anion species is responsible for the electron transfer in the quinone complex at high pH is derived from the fact that no quenching is observed at neutral pH, implying that an electronic change must occur between neutral and basic pH to make electron transfer feasible. Also on the basis of ΔG calculations electron transfer processes for the neutral quinone species will be mildly endoergonic, whereas ΔG for the semiquinone species as a donor or acceptor is exoergonic.

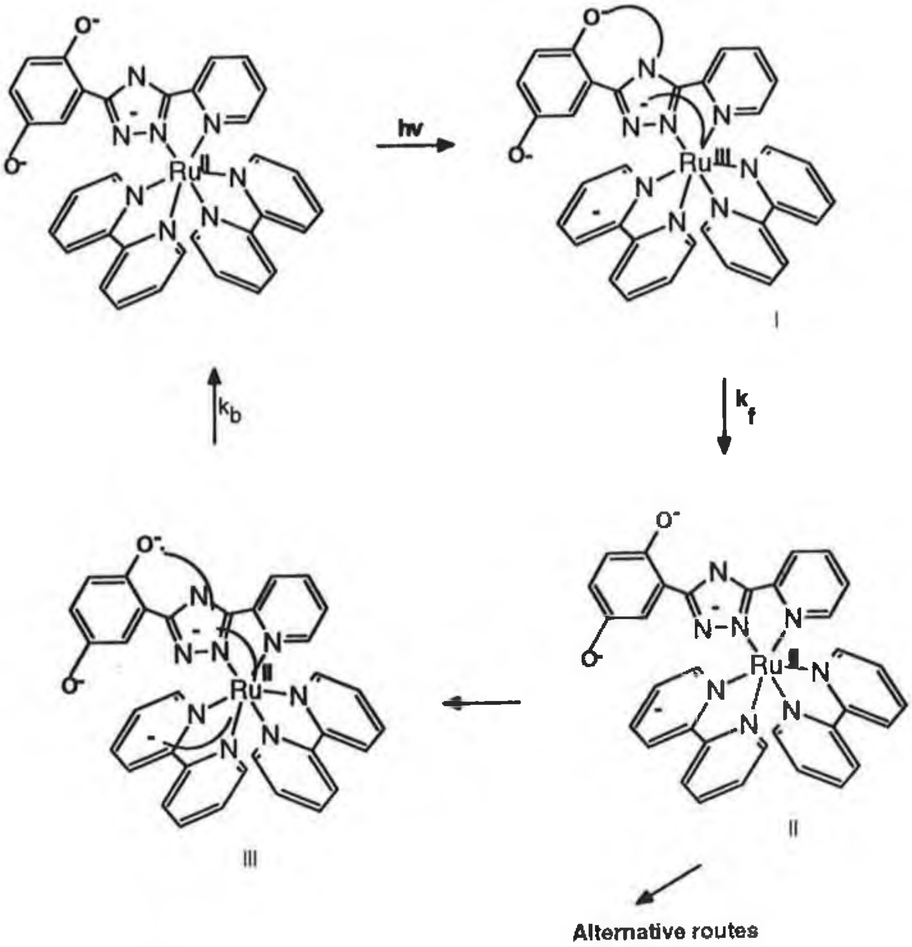

Scheme 3.4. Suggested mechanism of electron transfer.

Finally, it has been conclusively established that at high pH many quinones tend to spontaneously form $Q\cdot^-$ anion radicals [21, 90, 91]. These species are relatively stable at these pHs, it has been proposed as a result of the resonance stabilisation of the radical between the two oxygens [91].

That all electron transfer processes appear to be reductive in nature implies that they share a common pathway. Scheme 3.4 has been tentatively proposed as the mechanism for these transfers.

Light absorption leads to the creation of an excited state with localisation of the excited state electron on a bipyridyl ring, leading to I. Verification of the nature of the excited state was established from transient resonance raman studies on the hydroquinone complex (see section 3.3.5.). Since the excited state electron is localised on part of the complex remote from the quenching species the electron transfer process is slow. For example, in acetonitrile for $[Ru(bpy)_2(L1)]^-$ k_{el} = 6.35 x10^{-6} s^{-1}, implying competition occurs between radiative and electron transfer processes. The electron transfer is thought to occur via hole transfer between the excited state Ru(III) and the quinolate O^- across the triazolate bridge leading to the intermediate II, [Ru (II)(bpy)(bpy-)(L1·)]. As described, this process is relatively slow and the semiquinone intermediate is observed to grow-in approximately 800 ns after initial laser pulse in laser flash photolysis studies. The intermediate II from these studies would appear to last for 5 to 10 μs indicating the formation of charge separated state which is relatively stable. The decay of the semiquinone intermediate may occur via charge recombination leading to rereduction to the hydroquinone. The mechanisms for electron transfers in the phenolate and the quinone complexes is thought to occur in a similar manner, since all appear to react via reductive quenching. The difference in the transients produced for $[Ru(bpy)_2(L3)]^+$ and $[Ru(bpy)_2(L1)]^-$ is likely to be due to the fact quinone is formed from the electron transfer in the former, in its semiquinone state, and semiquinone from the electron transfer involving the deprotonated hydroquinone for the latter. Absence of transient absorbances phenolates is as described, most likely due to the fact that such species would absorb in the U.V..

3.3.7 Temperature dependent studies of ruthenium polypyridyl arylpyridyltriazole complexes.

The data obtained from the temperature dependent studies are shown in table 3.9. The measurements were carried out in ethanol/methanol 4:1 v/v in the temperature range 150-300K, lower temperatures were not examined to avoid the complications of the glass-phase transition.

Table 3.9. Temperature dependent data.

Complex	**E_a (cm^{-1})**	**A (s^{-1})**	**k_r (s^{-1})**	**k_{nr} (s^{-1})**	**k_0 (s^{-1})**
$[Ru(bpy)_2(H_2L1]^+$	113	6.69×10^7	8.8×10^3	3.17×10^7	3.17×10^7
$[Ru(bpy)_2(H^3L1]2+$	2928	4.47×10^{13}	1.5×10^4	4.01×10^6	4.02×10^6
$[Ru(bpy)_2(L3)]^+$	556	8.74×10^8	5.7×10^3	3.82×10^6	3.83×10^6
$[Ru(bpy)_2(HL3)]^{2+}$	812	6.38×10^{10}	-----^{Z}	-----^{Z}	7.61×10^5
$[Ru(bpy)_2(HL4)]^+$	67	2.43×10^8	1×10^4	5.82×10^6	1.06×10^7
$[Ru(bpy)_2(H_2L4)]^{2+}$	2059	8.0×10^{16}	------^{Z}	------^{Z}	9.82×10^6
$[Ru(bpy)_2(L5)]^+$	362	3.59×10^7	1×10^4	6.46×10^5	1.55×10^6
$[Ru(bpy)_2(HL5)]^{2+}$	2170	1.16×10^{12}	-----^{Z}	-----^{Z}	6.56×10^5
$[Ru(bpy)_2(H_2L6)]^+$	366	1.92×10^8	7.9×10^4	2.1×10^5	2.21×10^6
$[Ru(bpy)_2(H_3L6)]^{2+}$	1669	7.0×10^{14}	------^{Z}	------^{Z}	1.1×10^7

$^Z k_r$ and k_{nr} values are unavailable for these compounds since the room temperature τ values are not measured.

The data obtained were analysed employing assuming Arrhenius behaviour, using iterative techniques, by applying the data (in the region of strongest temperature dependence from 220 to 300 K) to equation (3.15) [92].

$$\frac{1}{\tau_{obs}} = k_o + A\exp(-E_a / RT) \quad (3.15)$$

Where $k_o = k_{nr} + k_r$ i.e. the sum of the radiative and non-radiative decay rates, A is the frequency factor, associated with the frequency at which activated surface crossing occurs, and E_a is the activation energy for surface crossing. The radiative rate constant is obtained from (3.16)

$$k_r = \phi_{em} / \tau \qquad (3.16)$$

Where ϕ_{em} is the luminescent quantum yield and τ the lifetime both measured at room temperature. K_r is generally accepted to be a temperature independent term above 77K and hence room temperature measurements suffice [93]. At 77K since no interfering states may be thermally populated the k_{nr} may be presumed to be solely due to deactivation from the ^{3}MLCT levels. Hence the temperature independent non-radiative rate constant k_r may be determined from (3.17)

$$k_{nr} = \frac{1}{\tau_{77K}} - k_r \qquad (3.17)$$

Where τ_{77K} is the luminescent lifetime at 77K.

An increase in temperature dependent behaviour for the protonated complexes is manifested by the steep rise in the ln($1/\tau$) vs 1000/T plot at higher temperature figure 3.33. Similar behaviour has been observed in studies of $[Ru(bpy)_3]^{2+}$ [94] this is associated with the stabilisation of the ground t_2g state with respect to the MLCT levels and hence reduction of the t_2g-eg* energy gap.

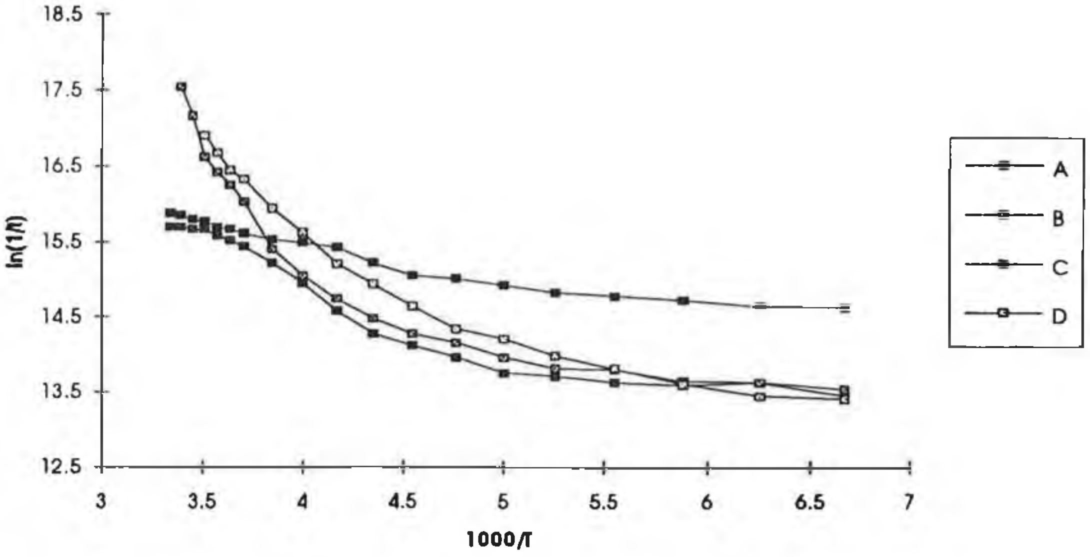

Figure 3.33 Temperature dependent luminsescent plot of A, ***[Ru(bpy)$_2$(H$_2$L1)]$^+$***, *B, [Ru(bpy)$_2$(H$_3$L1)]$^{2+}$, C, [Ru(bpy)$_2$(L3)]$^+$, and D, [Ru(bpy)$_2$(HL3)]$^{2+}$ in ethanol/methanol (4:1, v/v).*

Activation parameters for Ru(II) polypyridyl complexes usually fall into one of two categories: (i) Small activation energy (<800 cm^{-1}) and low prefactors (<10^{9}s^{-1}).

(ii) Large activation energies (>2000 cm^{-1}) and large prefactors (>10^{12} s^{-1}).

Complexes exhibiting the former behaviour are typically unreactive towards ligand loss photochemistry. The low prefactor suggesting population of a state which is only weakly coupled to ^{3}MLCT, this state was proposed by Kober and Meyer to be MLCT which is mainly singlet in character [95]. Complexes exhibiting the latter behaviour are generally photoreactive, the activated process they undergo is attributed to population of ^{3}MC state. This process is viewed as an electron transfer in a strongly coupled system, therefore the prefactor is expected to be large (10^{12} - 10^{14} s-1) [94]. In the protonated complexes this fourth ^{1}MLCT plays no role since its influence is concealed by the surface crossing to ^{3}MC.

For the protonated complexes, the high frequency factor A' (> 10^{13}) and large E_a for $[Ru(bpy)_2(H_3L1)]^{2+}$, $[Ru(bpy)_2(HL4)]^{2+}$ $[Ru(bpy)_2(H_3L6)]^{2+}$ and suggest that thermally activated surface crossing between ^{3}MLCT and ^{3}MC states is occurring, i.e. Ru(dπ) → Ru(e_g*). For the $[Ru(bpy)_2(HL3)]^{2+}$ and $[Ru(bpy)_2(HL5)]^{2+}$ complexes in particular, the prefactors are not as high ranging between 10^{10} and 10^{12}. This implies that the ^{3}MLCT and ^{3}MC states are in thermal equilibrium, this is particularly the case in the quinone complex where both the prefactor and activation energy corresponding to the gap between the two equilibrated states are relatively low for a protonated complex. The increased accessibility of the ^{3}MC state on protonation of these complexes is due to the stabilisation of the ground state of the complex on elimination of the negative charge on the triazole which increases the π-acceptor ability and decreases the σ-donation of the ligand. The cumulative effect of these changes is a decrease in the Ru(dπ)-Ru(e_g*) energy gap, making the photoactive ^{3}MC state thermally accessible at room temperature.

The fact that quinone and hydroquinone complexes exhibit different temperature behaviour may be attributed to the net deficit of electron density on the quinone ring by comparison with the hydroquinone which contains the electron donating OH groups. This may influence the ligand as a whole if there is sufficient delocalisation of charge between the three rings. The effect is that the ^{3}MLCT and ^{3}MC gap may be smaller in the quinone resulting in equilibrium between states. The differences between the temperature dependent data for $[Ru(bpy)_2(H_2L1)]^+$ and $[Ru(bpy)_2(H_2L6)]^+$ and their protonated analogues are rather surprising, however, the class of behaviour remains the same in each case. For the phenyl complex the behaviour is intermediate. The phenyl increases the electron density on the ligand without the influence of the ring activating hydroxyl groups. The deprotonated complexes possess both small activation barriers and small prefactors. This is associated with the increased ligand field strength for the deprotonated compounds as a result of the strong σ-donation of the negative triazole ligand which destabilises the metal t_{2g} level and increases the ^{3}MLCT -^{3}MC energy gap. The result is thermal inaccessibility of the ^{3}MC state and hence photostability is expected to be a feature of these compounds. The pre-factor and activation barrier for this class of compounds as mentioned, has been proposed to be due to the population of a fourth MLCT state which is largely singlet in character and hence only weakly coupled to the ^{3}MLCT [95].

Analyses of both the redox and photophysical behaviour of these species leads to estimates of the relative energies of the states for these complexes. Estimates of these states comes from a combination redox and luminescence values. The relative ground state energies are obtained from the Ru$^{(II)/(III)}$ and the ^{3}MLCT energy may estimated from room temperature luminescence maxima. ^{3}MC levels cannot be estimated directly, but may be approximated from activation parameters obtained from the temperature dependent lifetime studies of the protonated complexes employing equation 3.18.

$$E_{(t_{2g}-e_g*)} = E_{em} + E_{a(^3MLCT-^3MC)} \qquad (3.18)$$

The t_{2g}-$e_{g}*$ gap is expected to be considerably larger for the deprotonated complexes as a result of the stronger σ-donation of the deprotonated triazole. The exact value for this gap cannot be determined, therefore a minimum ^{3}MLCT-^{3}MC gap is estimated for the deprotonated species by assuming that the energy gap is the same for both protonated and deprotonated species. The values obtained for the energy levels in this manner are expressed for the complexes discussed here in figure 3.36.

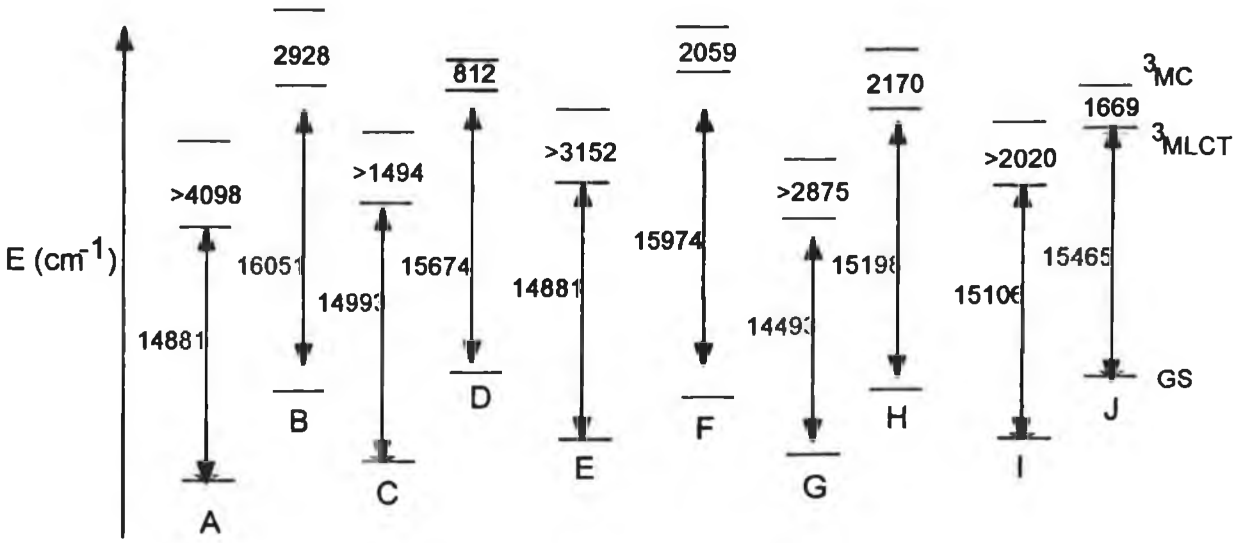

Figure 3.36. Relative energy levels for complexes where A = [Ru(bpy)$_2$(H$_2$L1)]$^+$, B = [Ru(bpy)$_2$(H$_3$L1)]$^{2+}$, C = [Ru(bpy)$_2$(L3)]$^+$, D = [Ru(bpy)$_2$(HL3)]$^{2+}$, E = [Ru(bpy)$_2$(HL4)]$^+$, F = [Ru(bpy)$_2$(H$_2$L4)]$^{2+}$, G = [Ru(bpy)$_2$(L5)]$^+$, H = [Ru(bpy)$_2$(HL5)]$^{2+}$, I = [Ru(bpy)$_2$(H$_2$L6)]$^+$, J = [Ru(bpy)$_2$(H$_3$L6)]$^{2+}$.

3.3.8 Photochemistry.

The discussion on temperature dependence is assessed by the examination of susceptibility of the protonated complexes to photochemical reaction. In the absence of acid, or in the presence of base, no reaction is perceived to occur over a 5 hour photolysis, for any of the complexes discussed. This result correlates well with the temperature dependence, which suggests that the complexes should be photostable when deprotonated.

Employing the model compound [Ru(bpy)$_2$(HL5)](PF$_6$)$_2$ as an example, the photolysis of this compound in acetonitrile in the presence of Cl$^-$ (5 mmol) and TFA was monitored by UV-vis spectroscopy and HPLC. Spectroscopic results show no maintenance of isobestic points, indicative of the formation of intermediates. From HPLC it was determined that over 8 hours of photolysis the initial compound breaks down into 4 products. Free ligand, compound and starting material. The assignments of these products were made by comparison with known or similar compounds [96]. Complete disappearance of the starting material required up to 8 hours continuous photolysis. The major product was species 4 which is thought to be the bisacetonitrile material $[Ru(bpy)_2(MeCN)_2]^{2+}$ from the λ_{max} of 425 nm. The $[Ru(bpy)_2(H_2L1)]PF_6$ at the same concentration showed similar behaviour but was photolysed completely in 6 hours. The quinone complex required up to 12 hours to reach complete photolyses.

These results endorse those of the temperature dependence. The hydroquinone and catechol complexes exhibits a high prefactor at 5 x10^{13} s^{-1} and 7.0 x10^{14} respectively, indicating that relaxation of the ^{3}MC state is rapid relative to back transfer (^{3}MC to ^{3}MLCT), and hence photochemistry from the ^{3}MC state should be relatively efficient. For the quinone and phenyl containing complexes where the ^{3}MC and ^{3}MLCT states appear to be in equilibrium the rate of decomposition from ^{3}MC is slower. This is because relaxation from ^{3}MC and back electron transfer to the ^{3}MLCT state are in competition.

3.4 Conclusion.

A series of aryl-substituted pyridyltriazole ligands were synthesised and their subsequent complexes prepared. The aryl moieties were phenols hydroquinone and quinone and the phenyl was prepared as the model compound. Preparation of the quinone substituted complex employed a novel synthesis involving oxidation of the hydroquinone using benzeneseleninic acid. This method produced $[Ru(bpy)_2(L3)]PF_6$ with no trace of the starting hydroquinone, thus eliminating a problem which has plagued other workers in oxidation of hydroquinone in related complexes.

The OH containing complexes exhibit electrochemically induced proton transfers, whereby on oxidation of an hydroxyl the proton produced is accepted by the deprotonated triazole. In the case of $[Ru(bpy)_2(H_2L1)]PF_6$ there is strong evidence to suggest that this transfer is occurring intramolecularily across a H bridge between the ortho hydroxyl and adjacent triazole nitrogen.

Electron transfer via intermolecular quenching between $[Ru(bpy)_3]^{2+}$ and the free ligands is not observed to any significant degree in neutral solution, nor is intramolecular transfer in the complexes at this pH. However, at high pH the free ligands (except HL5) are observed to quench the excited state of $[Ru(bpy)_3]^{2+}$ very efficiently, with rates of transfer approaching the diffusion controlled limit. In the complexes (with the exception of the phenyl complex) intramolecular electron (or hole) transfer is observed basic pH. This quenching in the OH containing complexes is associated with the anionic O^- species produced at high pH. These moieties possess lower oxidation potentials than their protonated counterparts making the free energies of electron transfer exoergonic in both inter and intramolecular reactions. For the quinone, the increased pH is thought to produce the semiquinone radical, and since reductive quenching is exoergonic and the more likely process for this species $[Ru(bpy)_2(L3)]PF_6$ is though to quench in a similar manner to it's hydroxyl counterparts.

The electron transfers involving the complexes show strong solvent dependence, suggesting the formation of a strongly polar charge separated species, since faster electron rates are observed in more polar solvents. There is a very weak temperature dependence and electron transfers continue to occur at cryogenic temperatures, suggesting that large conformational change is not necessary for electron transfer to occur. That electron transfer can occur in glass may be associated with the fact that the electron transfer is slow thus allowing time for the dipoles to reorient in the glass to stabilise the charge separated state. This is novel for such complexes since many reports of donor-acceptor complexes state that electron transfer ceases at these temperatures. Thus these complexes, in particular that of the hydroquinone $[Ru(bpy)_2(H_2L1)]PF_6$, may be thought of a simple abiotic models of the photosynthetic system since (1) it is capable of electrochemically induced proton transfers, where the donor and acceptor is intramolecularly linked via a hydrogen bridge. In photosynthesis, the redox processes of the quinone acceptors is coupled to proton transfers which are thought to proceed across H-bridged protein residues. (2) Electron transfers occur between the HQ^- and $Q\cdot^-$ (and O^- for the phenol complexes) species and the Ru(II) centre leading to a charge separated state. In the photosynthetic system the reoxidation of the hydroquinone is mediated by reduction of cytochrome c. This has been proposed to occur via the deprotonated QH^- or Q^-. (3) Finally, electron transfers in these complexes proceed at cryogenic temperatures, similarly the photosynthetic electron transfer cycle proceeds at such temperatures.

Therefore, the complexes discussed, on a considerably simpler level, mimic some of the unit functions of the photosynthetic system, and therefore may provide some insight into some of the mechanistic problems remaining for photosynthesis.

References:

[1] J. G. Vos; J. G. Haasnoot; G. Vos, *Inorg. Chim. Acta*, 162, 155 1983.

[2] B. E. Buchanan, J. G. Vos, M. Kaneko, W. J. M. van der Putten, J. M. Kelly, R. Hage, R. A. G. de Graaff, R. Prins, J. G. Haasnoot, J. Reedijk, *J Chem Soc., Dalton Trans.*, 2425, 1990.

[3] R. Wang, J. G. Vos, R. Schmehl, R. Hage, *J. Am. Chem. Soc.*, 114, 1964, 1992.

[4] R. Hage, J. G. Haasnoot, J. Reedijk, R. Wang, J. G. Vos, *J Chem Soc., Dalton Trans.*,

[5] H. P. Hughes, D. Martin, S. Bell, J. J. McGarvey, J. G. Vos, *Inorg. Chem.*,

[6] R. Hage, J. G. Haasnoot, H. A. Nieuwenhuis, J. Reedijk, D. de Ridder, J. G. Vos, *J. Am. Chem. Soc.*,112, 9245, 1990.

[7] L. De Cola, F. Barigelletti, V. Balzani, R. Hage, J. G. Haasnoot, J. Reedijk, J. G. Vos, *Chem. Phys. Lett.*, 178, 491, 1991.

[8] R.B. Salmonson, A. Abelleiron, I. M. J. Clarke, *Inorg. Chem.* 23, 4, 385, 1984.

[9] Y. Aoyama, M. Asakawa, Y. Matsui, H. Ogoshi, *J. Am. Chem. Soc.*, 113, 6233, 1991.

[10] G. L. Gaines, M. P. O'Niel, W. A. Svec, M. P. Niemczyk, W. Wasielewski, *J. Am. Chem. Soc.*, 113, 719, 1991.

[11] S. Wawzonek, R. Berkey, B. Laha, *J. Electrochem. Soc.*, 117, 186, 1970.

[12] O. Muller, *J. Am. Chem. Soc.*, 62, 2434, 1940.

[13] J. Jacq, *Electrochim. Acta*, 12, 1345, 1967.

[14] E. Laviron, *J. Electroanal. Chem.*, 169, 29, 1984.

[15] E. Laviron, *J. Electroanal. Chem.*, 164, 213, 1984.

[16] E. Laviron, *J. Electroanal. Chem.*, 208, 373, 1986.

[17] B. R. Eggins, J. Q. Chambers, *J. Electrochem. Soc.*, 117, 186, 1970.

[18] O. H. Muller, *Proc. 2nd Intern. Pol. Congr.*, 1, 251, 1959.

[19] J. Bessard, G. Cauquis, D. Serve, *Tetrahed. Lett.*, 3103, 1970.

[20] L. Pasimeni, M. Brustolon, C. Corvaja, *J. Mag. Res.*, 21, 259, 1976.

[21] D. Plancheral, J. G. Vos, A. von Zelewsky, *J. Photochem.*, 36, 267, 1987.

[22] A. Vleck, F. Bolletta, *Inorg. Chim. Acta*, 76, L227, 1983.

[23] D Plancheral, A. von Zelewsky, *Helv. Chim. Acta*, 65, 6, 1929, 1982.

[24] H. B. Kim, N. Kitamura, Y. Kawanishi, S. Tazuke, *J. Phys. Chem.*, 93, 5757, 1989.

[25] G. Jones II, V. Malba, *J. Org. Chem.* 50, 5776, 1985.

[26] P. M. Ennis, J. M. Kelly, C. M. O'Connell, *J Chem Soc., Dalton Trans.*, 2485, 1986.

[27] H. Rau, R. Frank, G. Creiner, *J. Phys. Chem.*, 90, 2476, 1986.

[28] F. M. el Torki, R. H Schmehl, W. F. Reed, *J. Chem. Soc. Faraday Trans. 1*, 85, 349, 1989.

[29] I. Willner, W. E. Ford, J. W. Otvos, M. Calvin, *Nature*, 280, 823, 1979.

[30] D. Sandrini, M. Maestri, P. Belser A. von Zelewsky, V. Balzani, *J. Phys. Chem.*, 89, 3675, 1985.

[31] H. A. Garrera; H. E. Gsponer, N. A. Garcia, J. J. Cosa, C. M. Previtali, *J. Photochem.* 33, 257, 1986.

[32] N. Kitamura, H. B Kim, S. Okano, S. Tazuuke, *J. Phys. Chem.*, 93, 5750, 1989.

[33] J. R. Darwent, K. Kalyanasundaram, *J. Chem. Soc. Faraday Trans. 2*, 77, 373, 1989.

[34] C. M. Elliot, R. A. Freitag, D. D. Blaney, *J. Am. Chem. Soc.*, 107, 4647, 1985.

[35] L. F. Cooley, C. E. L. Headford, C. M. Elliot, D. F. Kelley, *J. Am. Chem. Soc.*, 110, 6673, 1988.

[36] E. Danielson, C. M. Elliot, J. W. Merkert, T. J. Meyer, *J. Am. Chem. Soc.*, 109, 2519, 1987.

[37] E. H. Yonemoto, R. L. Riley, Y. I. Kim, S. J. Atherton, R. H. Schmehl, T. E. Mallouk, *J. Am. Chem. Soc.*, 114, 8081, 1992.

[38] C. K. Ryu, R. Wang, R. H. Schmehl, S. Ferrere, M. Ludwikow, J. W. Merkert, C. E. L. Headford, C. M. Elliot, *J. Am. Chem. Soc.*, 114, 430, 1992.

[39] K. S. Schanze, K. Sauer, *J. Am. Chem. Soc.*, 110, 1180, 1988.

[40] R. A. Berthon, S. B. Colbran, G. M. Moran, *Inorg. Chim. Acta*, 204, 3, 1993.

[41] V. Goulle, A. Harriman, J. M. Lehn, *J. Chem. Soc., Chem. Comm.* 1034, 1993.

[42] Vogels textbook of Organic chemistry 5th Edition 1990.

[43] R. Hage, Ph.D Thesis, Leiden University, The Netherlands, 1991.

[44] R. Hage, J. G. Haasnoot, J. Reedijk, R. Wang, E. Ryan, J. G. Vos, A. L. Spek, A. J. M. Duisenberg, *Inorg. Chim. Acta*, 174, 77, 1990.

[45] M. Uda, G. Hisazumi, K. Sato, S. Kubota, *Chem. Pharm. Bull.*, 24, 3103, 1976.

[46] S. Kubota, M. Uda, T. Nakagawa, *J. Heterocyc. Chem.*, 12, 855, 1975.

[47] E.J. Browne, J.B. Polya, *J. Chem. Soc. (C)*, 824, 1968.

[48] D.H.R Barton, A.G. Brewster, S.V. Ley, C.M. Read, C.M.N.J. Rosenfeld, *J. Chem. Soc., Perkin 1*, 1473, 1981.

[49] D.H.R Barton, J.-P. Finet, M. Thomas, *Tetrahedron*, 44, 6397, 1988.

[50] E. Constable, J. Lewis, *Inorg. Chim. Acta*, 70, 251, 1983.

[51] P. Belser, A von Zelewsky, *Helv. Chim. Acta*, 57, 239, 1971.

[52] R. Hage, R. Prins, J. G. Haasnoot, J. Reedijk, J. G. Vos, *J. Chem. Soc., Dalton Trans.*, 1389, 1987.

[53] D.J.R. Fennema, J. G. Haasnoot, R. Hage, J. Reedijk, J. G. Vos, *Inorg. Chim. Acta*, 171, 223, 1990.

[54] R. Hage, A.J.H. Dijkhuis J. G. Haasnoot, R. Prins, J. Reedijk, B.E. Buchanan, J. G. Vos, *Inorg. Chem.* 27, 2185, 1988.

[55] A. Juris, V. Balzani, F. Barigelletti, S. Campagna, P. Belser, A. von Zelewsky, *Coord. Chem. Rev.*., 84, 85, 1988.

[56] M. Wrighton, D.L. Morse, *J. Am. Chem. Soc.*, 96, 996, 1974.

[57] T. J. Meyer, *Prog. Inorg. Chem.* S.J. Lippard (Ed.) 30, 389, 1983.

[58] P.G. Bradley, N. Kress, B.A. Hornberger, R.F. Dallinger, W.H. Woodroff *J. Am. Chem. Soc.*, 103, 7441, 1981.

[59] R. Hage, J.G. Haasnoot, J. Reedijk, J.G. Vos, *Inorg. Chim. Acta*, 118, 73, 1986.

[60] A.J.Bard, L.R. Faulkner, *Electrochemical methods*, Wiley, N.Y., 1980.

[61] P.J. Giordano, C.R Rock, M.S. Wrighton, L.V. Interrante, R.F.X Williams, *J. Am. Chem. Soc.*, 99, 9, 3187, 1977.

[62] R.J. Crutchley, N. Kress, A.B.P. Lever, *J. Am. Chem. Soc.*, 105, 1170, 1983.

[63] C. Long, J.G. Vos, *Inorg. Chim. Acta*, 125, 131, 1984.

[64] P.Ford, D.F.P.Rudd, R. Gaunder, H. Taube, *J. Am. Chem. Soc.*, 90, 1187, 1968.

[65] B. E. Buchanan, J. G. Vos, M. Kaneko, W. J. M. van der Putten, J. M. Kelly, R. Hage, R. A. G. de Graaff, R. Prins, J. G. Haasnoot, J. Reedijk, *J Chem Soc., Dalton Trans.*, 2425, 1990.

[66] S.D. Ernst, W. Kaim, *Inorg. Chem.*, 28, 1520, 1989.

[67] R. Wang, J.G. Vos, R.H. Schmehl, R. Hage, *J. Am. Chem. Soc.*, 114, 1964, 1992.

[68] J.G. Vos, *Polyhedron*, 11, 18, 2285, 1992.

[69] J.F. Ireland, P.A.H. Wyatt, *Ad. Phys. Org. Chem.*, 12, 131, 1976.

[70] J. Davilla, A. Bignozzi, F.Scandola, *J. Phys. Chem.*, 93, 1373, 1989.

[71] P. Mitchell, *J. Theor. Biol.*, 62, 327, 1976.

[72] R.K Clayton, Photosynthesis; Physical mechanisms and Chemical patterns, Cambridge University Press, Cambridge, 1980.

[73] R.A. Binstead, B.A. Moyer, G.J. Sanvels, T.J. Meyer, *J. Am. Chem. Soc.*, 103, 2897, 1981.

[74] J.A. Gilbert, D.S. Eggleston, W.R. Murphy Jnr., D.A. Geselowitz, S.W. Gersten, D.J. Hodgson, T.J. Meyer, *J. Am. Chem. Soc.*, 107, 1845, 1985.

[75] G.E. Cabaniss, A.E. Diamantis, W.R. Murphy Jnr., R.W. Linton, T.J. Meyer, *J. Am. Chem. Soc.*, 107, 1845, 1985.

[76] R.A. Binstead, M.E. McGuire, A. Douletoglou, W.K. Seok, L.E. Roecker, T.J. Meyer, *J. Am. Chem. Soc.*, 114, 173, 1992.

[77] H.H. Thorp J.E. Surneski, G.W. Brudvig, R.H. Crabtree, *J. Am. Chem. Soc.*, 111, 9249, 1989.

[78] H.H. Thorp, G.W. Brudvig, E.F. Bowden, *J. Electroanal. Chem.*, 290, 93, 1990.

[79] The Chemistry of Quinoid Compounds, Ed. S. Patai.

[80] G.E. Adams, B.D. Micheal, *Trans. Faraday Soc.*, 61, 49, 1965.

[81] S. Rajagopal, G.A. Gnanaraj, A. mathew, C. Sanivasan, *J. Photochem. Photobiol A: Chem.*, 69, 83, 1992.

[82] D.M. Vera, G.A. Arguello, G.A. Arguello, H.E. Gsponer, *J. Photochem. Photobiol A: Chem.*, 76, 13, 1993.

[83] K.R. Seddon, E. Seddon, The Chemistry of Ruthenium, Elsevier, Amsterdam, 1984.

[84] P.R. Rich, D.S. Bendall, *Biochim. Biophys. Acta*, 592, 506, 1980.

[85] R. Hage, J.G. Haasnoot, J. Reedijk, J.G. Vos, Chemtracts-*Inorg. Chem.* 4, 75, 1992.

[86] R.A. Marcus, *Ann. Rev. Phys. Chem.*, 15, 155, 1964.

[87] R.J. Harrison, B. Pearce, G.S. Beddard, J.A. Cowan, J. Sanders, *Chem. Phys.*, 116, 429, 1987.

[88] P. Chen, E. Danielson, T.J. Meyer, *J. Phys. Chem.*, 92, 3708, 1988.

[89] K. Miedler, P.K Das, *J. Am. Chem. Soc.*, 104, 7462, 1982.

[90] N.K. Bridge, G.Porter, *Proc. Roy. Soc. A*, 244, 259, 1958.

[91] L. Michaelis, *Chem. Rev.* 22, 437, 1938.

[92] J. van Houten, R.J. Watts, *J. Am. Chem. Soc.*, 98, 4853, 1976.

[93] J.V. Casper, T.J. Meyer, *Inorg. Chem.*, 22, 2444, 1983.

[94] S.R. Allsopp, A.Cox, T.J. Kemp, W.J. Reed, *J. Chem. Soc., Faraday Trans.*, 1, 74, 1275, 1978.

[95] E.M. Kober, T.J. Meyer, *Inorg. Chem.* 21, 3967, 1982.

[96] B.E. Buchanan, H. Hughes, J.H. van Diemen, R. Hage, J.G. Haasnoot, J. Reedijk, J.G. Vos, *J. Chem. Soc., Chem. Comm.*, 300, 1991.

[97] C.J. Timpson, C.C. Carter, J. Olmsted III, *J. Phys. Chem.*, 93, 4116, 1989.

Chapter 4.

O, N coordinated complexes: Mononuclear Ruthenium (II) complexes.

4.1 Introduction

One of the fundamental requirements of a solar sensitzer material is an ability to absorb light over a wide spectral range that is coincident with the solar spectrum. Figure 4.1 shows the spectral distribution of the solar radiation that reaches the earth when air mass (AE) is unity, i.e. on a clear day.

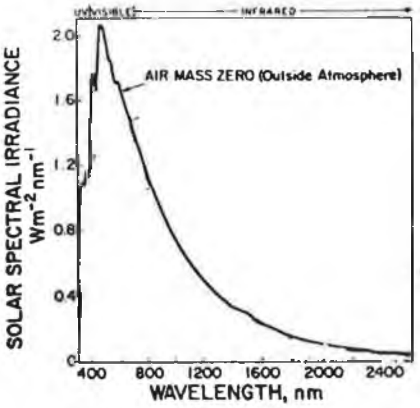

Figure 4.1. Solar spectral distribution outside the earth's atmosphere (air mass 0) and at normal incidence to the earth's surface, (air mass 1) [1].

Roughly half of the solar spectrum lies in the UV and visible region, with the remainder in the IR. In order to optimise the antenna capability of potential solar sensitizer material, it is necessary to optimise the absorption of light in the visible region, ensuring photochemical stability and suitable redox properties. Photochemical stability is important, and has been a problem blighting workers of long wavelength absorbers. Most complexes produced capable of intense, broad range, visible spectral absorbances such as the $[Ru(biq)_3]^{2+}$ [2, 3] or bipyrazine complexes [4, 5] are not photostable. This is because they contain strong π-acceptor ligands which are low in the spectrochemical series and hence do not induce strong ligand field splitting. Leading to both low lying ligand-π levels (hence, long wavelength absorbances) and unfortunately, low-lying, destructive, ^{3}MC states.

In this chapter the synthesis of some novel O,N coordinated Ru(II)bpy$_2$L(O,N) complexes and their associated ligands is described, along with the properties of both ligand and complex. The aim in creating these species was to create complexes capable of broad range visible absorbance, but which are also photostable. Since the metals are bound to electroactive ligands, particular emphasis is placed on the electrochemistry of these species and the influence of employing an oxygen coordination site instead of nitrogen.

4.1.1 Pyrazole ligands.

Pyrazole (figure 4.2), is a class b ligand i.e. the same classification as triazole. It is therefore, a strong σ-donor and weak π-acceptor species. As a ligand in ruthenium(II) complex chemistry it is not as well established as the triazoles or imidazole [6-8], which are structurally closely linked to pyrazole.

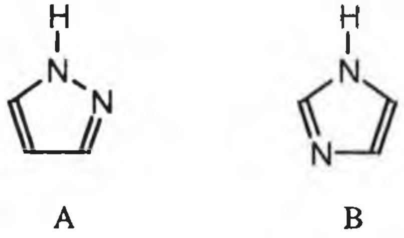

Figure 4.2. Pyrazole (A), and imidazole (B).

The first report of Ru(II) complexes containing pyrazole ligands was made Sullivan and co-workers in 1979 [9]. This group reported on the synthesis of both mono and dinuclear complexes shown in figure 3.3.

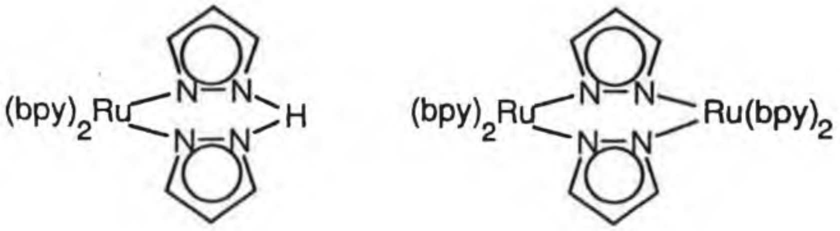

Figure 4.3. Mono and dinuclear Ru(II) pyrazole complexes created by Sullivan and co-workers *[9].*

The mononuclear complex exhibited acid-base properties, which altered the σ-donor properties of the ligand in much the same as in the analogous triazole complex described by Vos and co-workers [10], resulting in changes in the electronic and redox properties of the complex. Interestingly, the λ_{max} of the mononuclear complex was considerably red-shifted with respect to $[Ru(bpy)_3]^{2+}$, and exhibited a broad, intense absorbance at 581 nm. The dinuclear complex was unstable as a mixed valence species.

The bulk of investigation into the properties of pyrazole ligands has been carried out by Constable and co-workers. In 1983, Constable, Steel and co-workers reported on the coordination of Ru(II)(bpy)$_2$ to pyridylpyrazole [11]. This was followed by a report by Vos and co-workers, in 1987 [12], on a series of pyridyl-azol complexes , including a Ru(II)(bpy)$_2$ pyridylpyrazole complex. Although differences were perceived, the properties of the complexes containing the different azol substituents were found to be sufficiently similar to suggest that the excited states were localised on the same (bpy) ligand, and that the ligands all possessed relatively similar σ-donor properties. With one interesting exception, a difference was observed in the Ru(II)(bpy)$_2$ complexes containing 1-(pyridin-2-yl)-1H-1,2,4-triazole and 1-(pyridin-2-yl)pyrazole. Namely, the former is non-emissive, whereas the latter does. It was also found that in a plot of $\Delta E_{1/2}$ vs absorption energy, the triazole complex did not correlate with the other complexes, appearing as an outlier on the plot. This implied that the triazole ligand was directly involved in the excited state process, the absence of emission implying a d-d level was accessible at room temperature. The reason for this may be that in this particular triazole ligand, the triazole is bound to the pyridyl via a nitrogen, it cannot carry a negative charge and hence it is not as strong a σ-donor as the other triazole species, but is a stronger π-acceptor. That the analogous pyrazole complex does emit might imply that pyrazole is a stronger σ-donor, under these conditions, than triazole. Other reports of pyrazole ligands come from Constable [13] in 1990, in which related pyrazole containing ligands were systematically investigated. One of the most recent reports of pyrazole-containing complexes was made by Steel et al [14], where again the properties of pyridylpyrazole complexes are discussed.

The ligands described in the text are shown in figure 4.4 below.

H_2L2
3-(2-phenol)-5-(pyridin-2-yl)-1,2,4-triazole

H_2L7
1,4-Dihydroxy-2-pyrazol-1'-ylbenzene

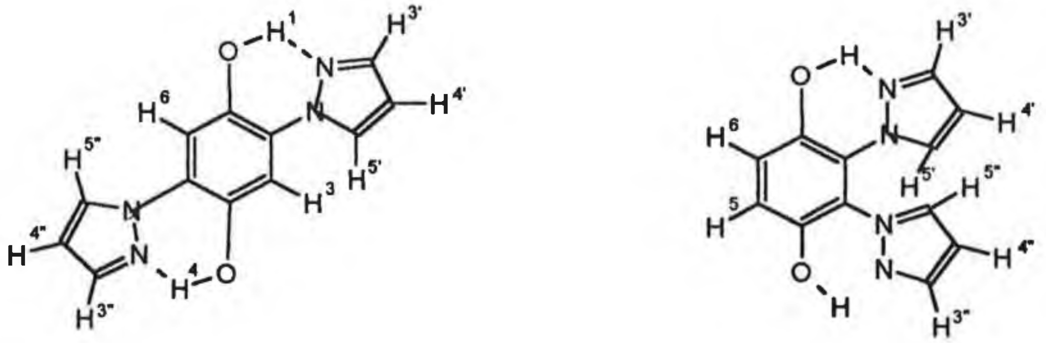

H_2L8
1,4-Dihydroxy-2,5-bis(pyrazol-1'-yl)benzene

H_2L9
1,4-Dihydroxy-2,3-bis(pyrazol-1'-yl)benzene

Figure 4.4. Structure of the ligands discussed in chapter 4.

4.1.2 Ru(bpy)$_2$ complexes containing oxygen donor ligands.

Although oxygen is recognised as a useful complexing site (Lewis base) in various molecules such as glyme, or acetylacetonate. Its exploitation has been rather limited in Ruthenium (II) coordination chemistry, where N,N coordinating ligands have been the mainstay of this field, although both possess strong σ-donor properties. The O coordination site is usually associated with either a hydroxyl or carbonylic groups, they are rather unique as donors in that they, like the metals they complex, possess their own electrochemistry.

Some of the earliest reports of O coordinated compounds was made by Merrell [15, 16], in which he coordinated Ru(II) and other d^6 transition metals to hydroxyl-containing dye molecules quinizarin and TSAB, these reports were mainly structural in nature. In 1983, Haga reported a series of $Ru(bpy)_2$ complexes containing benzimidazole ligands [17], this included the ligand shown in figure 4.5 below;

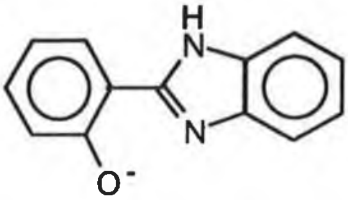

Figure 4.5. Benzimidazole-phenolate ligand described by Haga [17].

which is particularly relevant to the complexes discussed in this chapter. The complex possessed a λ_{max} of 530 nm, considerably blue shifted with respect to $[Ru(bpy)_3]^{2+}$, stron visible absorbances are a feature of such O^- coordinated complexes Also a low metal oxidation potential of 0.09 V. These properties are related to the strong σ-donor properties of the O^- ligand. No emission was observed for this complex at either room or cryogenic temperatures, again this seems to be a property common to such complexes in the literature.

Catalysis of alcohol oxidation or proton donation has proven an incentive for the synthesis of O,N or O,O coordinated complexes and $Ru(bpy)_2$ coordinated complexes have proven quite successful in this area [18-20]. These reports for the most part do not address any of the photophysical properties of the complexes investigated. A small number of dinuclear complexes based on o-substituted hydroquinones and anthraquinone ligands have been investigated [21-23], these will be discussed in more detail in chapter 5.

Significant work in the area O,O or O,N ligands in Ru(II) chemistry has mainly centered on complexes of the catechol [24-26], or ortho quinone, since the properties of catecholates as ligands has been known for some time in clinical chemistry as iron chelating agents [27]. O-quinones are weak σ–donors, this property strengthened in semiquinones and even more in quinols. The majority of complexes reported, for example, those of Lever and co-workers [25, 26], are coordinated to either the semiquinone or quinone species, as a result of the stabilisation effect the weaker σ–donor quinone species have on the low oxidation state of Ru.

The mode of bonding of complexes where the metal is bound directly to the quinonoid differ dramatically between o-quinone and p-quinone, in the former the metal binds directly through the two adjacent quinone oxygens, for example the complexes created by Lever and co-workers, [25, 26]. This group reported on the coordination of the entire redox range of 3,5-di-*tert*-butylcatechol to $Ru(bpy)_2$ yielding interesting electronic spectral transitions, and electrochemistry. For the p-quinone, as a result of the absence of a second adjacent coordination site to the oxygen, the metal will generally bond via the π electron density on the quinoid structure as in the case of π-duroquinone-iron-tricarbonyl [28]. There have been reports of p-quinones bonding via their oxygen atoms in the presence of other coordinating atoms at appropriate proximity for chelate formation. An example is the case of binuclear $Ru(bpy)_2$ complexes of 2,5-bis(diphenylphosphino)-p-semiquinone where the Ru is chelated by the O of the semiquinone and a phosphine substituent ortho to it [21]. Another example, also binuclear, is that of $Ru(bpy)_2$ O,O coordinated, via bridging 1,4,5,8-tetraoxonaphthalene [29]. A useful review of metal-quinonoid complex chemistry is given in [30]

Ward and co-workers have recently produced a number of very relevant papers on Ru(II) and other metal complexes O,N bound to non-quinoid ligands (for the most part phenolates) [31-35]. Of particular relevance, are the pyridine-phenol ligands and terpyridine-phenol ligands, see figure 4.6.

As was described by Haga [17], the oxidation potential for the O,N coordinated Ru(II)(bpy)$_2$ is unusually cathodic (0.03 V vs Fc/Fc$^+$) [33]. This, Ward attributed to the stabilisation of the Ru(III) state by the strong σ-donation of the anionic phenolate. In fact in series of ruthenium complexes RuL$_3$, in which all three ligands are O,N coordinated [34], the metal is in the (III) state and is easily oxidised to (IV) state as a result of this stabilisation.

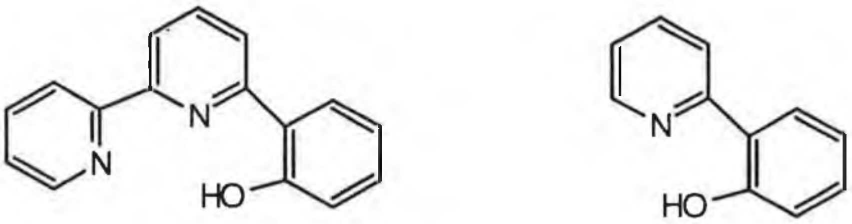

Figure 4.6; terpyridine phenol and pyridine phenol ligands [33].

The oxidation of the phenolate itself appears as an irreversible wave at 1.29V vs (Fc/Fc$^+$) in both Ru(bpy)$_2$L and RuL$_3$ complexes [33, 34].

For Ru(bpy)$_2$L complexes possess broad visible absorbances, red-shifted with respect to [Ru(bpy)$_3$]$^{2+}$. They do not luminesce, and again this is the feature which appears to unite all O,N coordinated complexes of this nature. No explaination is given for this behaviour but it is possible that the smaller field splitting of the O- ligand allows population of the ^{3}MC state.

4.2 Synthetic procedure.

4.2.1 Preparation of ligands.

3(2-phenol)-5-(pyridin-2-yl)-1,2,4-triazole, H_2L_2.

As described in the preceding chapter, this synthesis was carried out according to the method described by Hage [36], (see chapter 3).

1,4-dihydroxy-2-(pyrazol-1'-yl)benzene, (H_2L7), 1,4-dihydroxy-2,5-bis(pyrazol-1'yl)benzene (H_2L8), 1,4-dihydroxy-2,3-bis(pyrazol-1'yl)benzene (H_2L9).

Nucleophillic addition of pyrazole to benzoquinone was achieved by a method modified from that described by Catalan and co-workers [37]. Pyrazole (10g, 0.147 mol) was combined with benzoquinone (15.9g, 0.147 mol) in dry dioxane (100 cm^3). This mixture was refluxed for two hours under an argon atmosphere. Following this, the solvent volume was reduced under vacuum to 40 cm^3 and the solution was left at 4°C overnight. After this time white needle-like crystals had formed, which were collected by filtration. From thin layer chromatography (TLC), this solid was deemed pure. The TLC was carried out on silica gel (Merck Kiesegel 60 F_{254}) using chloroform-ethanol (95:5). The R_f value determined for the solid product was 0.67, corresponding to the reported value (0.61), [17] for 1,4 dihydroxy-2,5-bis(pyrazol-1'yl)benzene. Identity and purity were verified by ^{1}Hnmr after recrystallisation from chloroform/ethanol (60:40, v/v). The remaining products were collected from the filtrate, by evaporating the remaining solvent under vacuum. From TLC three products were obtained, including the remainder of H_2L8. These were separated, by column chromatography on silica gel, employing chloroform-ethanol (95:5) as eluent. The three products were not entirely pure after this process so the individual fractions were further purified by chromatography on silica gel, this time employing petroleum ether (60-40 b.r.)-ethyl acetate (60:40 v/v).

H_2L7 was recrystallized from chloroform to generate 2.2g (yield 8.5%) as pale yellow plates, M.P.178-180^{o}C (Lit. [37], 181^{o}C) Yield of H_2L8 was 3.5g (10%), M.p. 201-202 ^{o}C (Lit. [37] 206^{o}C). H_2L9 was recrystallized from water, yielding 1g of product (3%), M.p. 170-172 ^{o}C (Lit. [37], 177^{o}C).

4.2.2 Preparation of complexes.

$[Ru(bpy)_2(HL7)]PF_6.H_2O$.

1,4-dihydroxy-2-pyrazol-1-yl benzene, H_2L7 (0.1g, 0.57 mmol), was dissolved in ethanol/water (50 cm^3, 1/1, v/v), containing diethylamine (2% v/v) to deprotonate the ligand hydroxyls. This solution was heated to reflux under an argon atmosphere and $[Ru(bpy)_2Cl_2].2H_2O$ (0.275g, 0.53 mmol) was added slowly over roughly 30 minutes. The reaction remained at reflux for 3 hours by which time all the starting $[Ru(bpy)_2Cl_2]$ was observed from HPLC to have disappeared. The reaction mixture volume was then reduced to 10 cm^3 of water under vacuum. The pH of the reaction mixture was neutralised by addition of dilute H_2SO_4. An excess of concentrated aqueous NH_4PF_6 was added to the reaction mixture. A dark purple precipitate formed, which was collected by filtration and recrystallised from acetone/water (60/40 v/v), yielding 0.28g (67%) $[Ru(bpy)_2(HL7)]PF_6$. Purity was verified by HPLC.

Analyses calculated for: $[RuC_{31}H_{29}N_6O_3PF_6]$; C, 47.76; H, 3.75; N, 10.78%.

Found; C, 47.23; H, 3.50; N, 10.55%.

$[Ru(bpy)_2(HL8)]PF_6.2H_2O$.

This compound was prepared as for $[Ru(bpy)_2(HL7)]PF_6$, except after work-up of the reaction two products were obtained. The mononuclear isomer was isolated via semi-preparative HPLC chromatography described in section 2.6. Yield 60%.

Analyses calculated for:$[RuC_{32}H_{29}N_8O_4PF_6]$; C, 45.99; H, 3.50; N, 13.41%.

Found; C, 46.07; H, 3.34; N, 13.10%.

$[Ru(bpy)_2(HL9)]PF_6$.

This compound was prepared as for $[Ru(bpy)_2(HL8)]PF_6$, with the exception that no addition of NH_4PF_6 was required since on reduction of reaction volume the product fell out of solution, since it possessed no formal charge. Yield 59%.

Analyses calculated for $[RuC_{32}H_{24}N_9O_5K]$; C, 51.69; H, 3.2; N, 16.44%.

Found; C, 51.04; H, 3.61; N, 16.34%. Ir verified the occlusion of KNO_3 in the complex as a result of semi-prep. HPLC.

$[Ru(bpy)_2(o,n\text{-}HL2)]PF_6$.

This compound was prepared as described for $[Ru(bpy)_2(HL8)]PF_6$. Semi-preparative HPLC was required to remove the N,N coordinated complex (which was the main product 46%) and small amounts of dinuclear species. Yield 29%.

Analyses calculated for: $[RuC_{33}H_{33}N_8OPF_6]$; C, 49.25; H, 4.20; N, 12.21%.

Found; C, 49.65; H, 3.92; N, 11.50%. Presence of PF_6 counter ion was verified by IR.

4.3 Results and discussion

4.3.1 Pyrazole-hydroquinone ligand properties.

The pyrazolehydroquinone ligands described in this thesis merit significant study in their own right. This is a result of their unusual photostability, as described by Catalan and co-workers [37, 38]. This has been attributed to intramolecular proton transfer, which occurs from the singlet (but not the triplet state) in these compounds, leading to rapid deactivation of the quinoid form, but this mechanism was later disputed on the basis of theoretically calculated restrictions [38].

4.3.1.1 ^{1}H nmr and structural properties

These ligands have been demonstrated to show extensive intramolecular H-bonding between their hydroxyls and adjacent nitrogens [37, 38]. Table 4.1 shows the ^{1}Hnmr data for the ligands described (with the exception of H_2L2, which is described in chapter 3, in acetonitrile-d_3, with values obtained in chloroform-d displayed in parenthesis.

Table 4.1 ^{1}H NMR data for pyrazolehydroquinone ligands, in ppm vs TMS, in acetonitrile-d_3 {chloroform-d}. For atomic numbering see figure 4.4

proton	**H_2L7**	**H_2L8**	**H_2L9**
H^1	10.51 (s) {10.91 (s)}	10.97 (s) {11.10 (s)}	8.23 (s) {8.34 (s)}
H^4	6.78 (s) {4.81 (s)}	10.97 (s) {11.10 (s)}	8.23 (s) {8.34 (s)}
H^3	7.02 (d); $J_{3,5} = 2.9$ {6.92 (d); $J_{3,5} = 2.9$}	7.27 (s) {7.07 (s)}	------
H^5	6.68 (d); $J_{5,6} = 8.7$ {6.67 (d); $J_{5,6} = 8.8$	----------	6.96 (s) {7.04 (s)}
H^6	6.87 (d) {6.97 (d)}	7.27 (s) {7.07 (s)}	6.96 (s) {7.04 (s)}
$H^{3''}$, $H^{3'}$	7.77 (d); $J_{3',4'} = 2.0$ {7.73 (d); $J_{3',4'} = 2.0$}	7.78 (d); $J_{3',4'} = 2.0$ {7.67 (d); $J_{3',4'} = 2.0$}	7.66 (d); $J_{3',4'} = 2.0$ {7.82 (d); $J_{3',4'} = 2.0$}
$H^{4''}$, $H^{4'}$	6.55 (d); $J_{4',5'} = 2.5$ {6.5 (d); $J_{4',5'} = 2.5$}	6.57 (d); $J_{4',5'} = 2.5$ {6.46 (d); $J_{4',5'} = 2.5$	6.57 (d); $J_{4',5'} = 2.5$ {6.35 (d); $J_{4',5'} = 2.5$}
$H^{5''}$, $H^{5'}$	8.18 (d) {7.95 (d)}	8.24, (d) {7.91 (d)}	7.02 (d) {6.84 (d)}

Where applicable the shifts correspond almost exactly to those described in the literature [38]. ^{1}H nmr is a useful means of exploring the extensive H-bridging in these compounds. For example, ligands H_2L7 and H_2L8, possess phenolic proton resonances at low field suggesting H-bridging between the phenol and pyrazole $N^{2'}$ ($N^{2''}$). The shifts associated with these protons are solvent dependent, shifting to lower field in the less polar solvent (chloroform). This is associated with the strengthening of the intramolecular H-bonding in the compounds in the less polar medium. For compound H_2L9 the shift associated with the phenolic proton is at higher field, at 8.23 ppm than H_2L7 and H_2L8. This would imply that the H-bridging interaction is not occurring in this species, from crystallography of these molecules [38], H_2L7 has one H-bridge, H_2L8 two and H_2L9 is not bridged at all this complies exactly with the ^{1}Hnmr results described here. Absence of H-bridging in H_2L9 is due the conformation of this compound, the pyrazole groups are ortho to each other suggesting there will be considerable steric hindrance in the molecule. From geometry optimised molecular models of the hydroquinone-pyrazole ligands (figure 4.7), it is apparent that as a result of this steric hindrance this ligand is not planar as is the case with H_2L7 and H_2L9, and that both pyrazole rings are twisted out of plane. This accounts for the absence of H-bridging in this compound. In all cases dilution studies were carried out to establish that the H-bonding is intramolecular, in each instance no change in OH resonances was observed on dilution.

4.3.1.2 Absorption and emission properties.

The different conformations of these ligands are reflected in their electronic spectra. Table 4.2 shows the absorption and emission data of the ligands discussed.

The pyridyl triazole ligand H_2L2 exhibits intense absorptions and emissions which from solvent dependent studies are associated with $\pi-\pi^*$ transitions. Strong emissions are normal from such ligands. Interestingly the emission from this ligand is considerably weaker on deprotonation of the triazole, and are also considerably weaker than its para-phenolic analogue H_2L4. This may be the influence of the negative triazole on the charge distribution of the ligand. Alternatively, this may be due to the fact that when the triazole is deprotonated it $N^{2'}$ may be capable of accepting the proton transferred from the excited hydroxyl moiety. This excited state proton transfer has been reported for methyl salicylate by Weller and co-workers in 1955 [39] and has subsequently been proposed as a means of

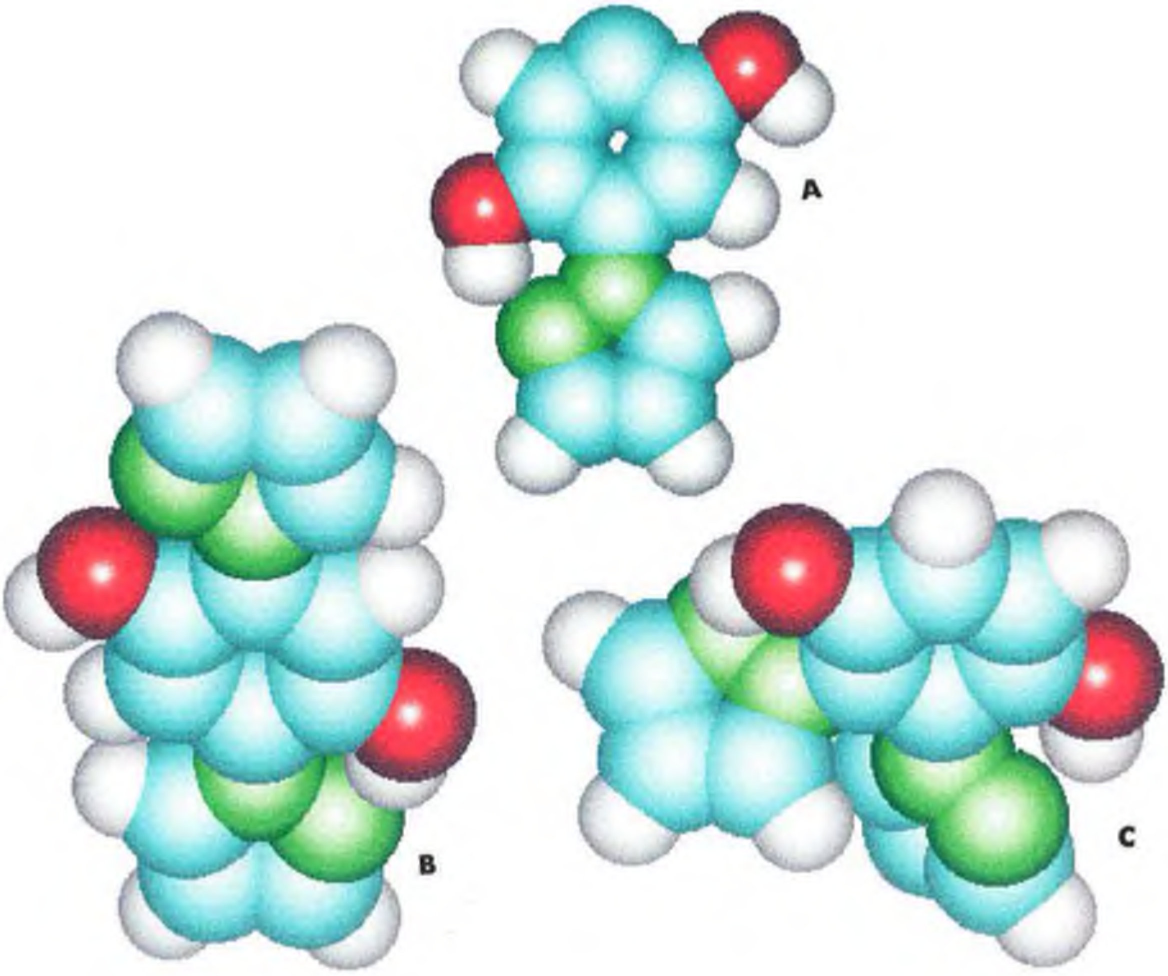

Figure 4.7 Computationally modelled structures of (a) H_2L7*, (b)* H_2L8 *and (c)* H_2L9*, where pale blue = carbon, white = hydrogen, red = oxygen, green = nitrogen.*

photostabilisation of such compounds via rapid excited state deactivation via the intermediate quinonoid structure [40]. It is interesting to note that methylsalicylate is in fact the precursor in the synthesis of this ligand [36].

Table 4.2. Ligand absorption and emission data

Compound	**Absorption λ_{max}*(nm), (log ε)**	**Emission λ_{max} (nm)**
H_2L2	285.2 (4.61)^A	430
H_2L7	315 (3.76)	361
H_2L8	313 (3.63)	368
H_2L9	335 (4.21)	383

* Measurements carried out in acetonitrile except where otherwise stated.

^{A} Carried out in ethanol.

Comparison of the absorption spectra of these compounds illustrates interesting differences. Figure 4.8 shows the overlaid absorption spectra for the three ligands, under equal conditions and concentrations. Compounds H_2L7 and H_2L9 show absorption properties which are almost identical, whereas H_2L8 is strongly red-shifted and approximately three times as intense as H_2L7 and H_2L9.

H_2L8 as described, is a highly symmetric and planar molecule whereas H_2L7 is asymmetric, and H_2L9 is non-planar. H_2L8 therefore possesses a π-electronic system which is extended uninterrupted across this planar molecule, most likely accounting for these differences. This spectral effect is in fact translated into the complex which is discussed below.

The emission spectra of these ligands are described in detail elsewhere [38].

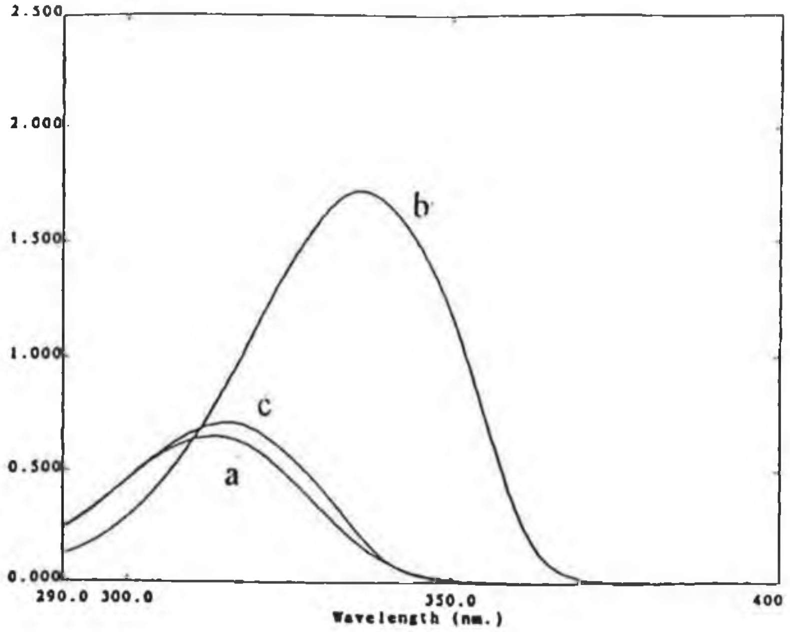

Figure 4.8 Absorbance spectra for ligands (a) H_2L7, (b) H_2L8 and (c) H_2L9 in acetonitrile (conc. =4 x10^{-4}M).

4.3.1.3 Electrochemistry.

The electrochemical data pertaining to the ligands discussed are shown in table 4.3.

Table 4.3. Electrochemical properties of the ligands.

Ligand	**Hydroquinone oxidation potentials, (V, vs SCE)**					
	neutral*	**ΔE**	**Acidic pH**	**ΔE**	**Basic pH**	**ΔE**
H_2L7	0.79 ($1e^-$), 1.02 ($1e^-$)	0.66, 0.71	1.30 ($2e^-$)	0.82	0.46($2e^-$)	0.82
H_2L8	0.89 ($2e^-$)	0.67	1.02 ($2e^-$)	0.66	0.31 ($2e^-$)	0.3
H_2L9	0.98 ($1e^-$), 1.19 ($1e^-$)	0.77, irrev.	1.36 (2e-)	0.94	0.25 ($2e^-$)	0.53

* In all cases the electrochemistry was quasi-reversible except where otherwise stated, and all values are given relative to saturated calomel electrode (SCE).

Interestingly, the addition of acid causes a positive shift in oxidation potential for example, for H_2L8 a shift of 0.87V is observed in acidic solvent. This is particularly the case for

H_2L7 and H_2L9 whose first oxidation potentials are anodically shifted by 0.6 and 0.56 V respectively. It is particularly noteworthy that H_2L8 is anodicaly shifted to a much lesser degree in acidified media, in line with the second oxidation potentials of H_2L7 and H_2L9. Differences between H_2L7, H_2L9 and H_2L8 are observed in basic media, where a considerable increase in reversibility is observed for H_2L8 by comparison with the remaining two ligands, H_2L7, in particular remains very irreversible at this pH. This suggests that despite their structural similarities, their electrochemistry proceeds via different routes. It is expected, that since H_2L8 is H-bridged, that proton transfer may occur between the oxidised hydroquinone and pyrazoles in a similar fashion to the proton transfer described in chapter 3. This proton transfer catalyses the electrochemistry of the ligand, and that of the first oxidation of H_2L7 (also expected to be H-bridged), allowing these to proceed at lower potentials. Since the initial step in oxidation of H_2L8 is proton catalysed it is not influenced by addition of acid.

Figure 4.8 shows the electrochemistry of H_2L7 in neutral, basic and acidic media. The trend described above for H_2L7 is apparent in neutral and acidic conditions. Interestingly, addition of base causes a considerable cathodic shift in oxidation potential for H_2L7 (and H_2L8 and H_2L9), and shifts the reduction cathodically also. The addition of base is accompanied by a colour change for these ligands whereby the solution turns yellow or orange from colourless. This is a result of the increased electron density on the ligand as a result of the negative charges on the oxygens on deprotonation. An increase in reversibility is also apparent in base, this is likely due to the effect of protons on the oxidation, whereby their release (or transfer) may form a rate-determining step in the hydroquinone electrochemistry . In their absence this "slow" step is eliminated and the electrochemistry becomes more reversible.

For H_2L7 and H_2L9, the electrochemistry in neutral solution reveals two overlapping ($1e^-$) oxidation waves, probably a result of the asymmetry at the two OH sites in these molecules. For H_2L9, although this molecule appears symmetric, asymmetry is induced by the steric hindrance incited out of plane twisting of the pyrazoles with respect to one another. In H_2L8 on the other hand the 2e$^-$ redox waves are symmetric and show no evidence for overlap, as expected for this symmetric molecule.

4.3.2 Complex properties; NMR and structural characterisation.

The ^{1}H-COSY nmr spectra for the complexes discussed are shown in figure 4.9(a)-(d), with their computational models in figure 4.10(a)-(d). The associated data for the coordinated ligands are shown in table 4.4.

The assignments were made by comparison with free ligand shifts and coupling constants, and the ^{1}Hnmr of some deuterated analogues of the complexes (see Chapter 6). In each instance a complete assignment of all peaks could be made. However, although all bipyridyl resonances could be identified they could not be assigned to particular bpy rings. What is becomes apparent on examination of the ^{1}H nmr of $[Ru(bpy)_2(o,nHL2)]^+$, is that the most downfield resonance of the HL2 pyridyl ring, at 8.38 ppm, (from its small j-value, and its long and short range coupling) corresponds to a pyridine H^6. In instances where pyridine is coordinated H^6 experiences a strong upfield shift [41, 42], as a result of the manner in which the H^6 protons lie within the shielding cone of the adjacent bipyridine rings. The structural analyses of the complexes described in chapter 3 demonstrate this. The pyridine ring is deemed free therefore, and comparison of the remainder of its resonances with the free ligand (H_2L2) show that there is little change between them. H^3 and H^6 exhibit upfield and downfield shifts respectively in the region of 0.2 ppm. The upfield shift in H^3 would suggest that the triazole is bound via N4', since if this is the case diamagnetic anisotropic interaction with an overlying bipyridyl ring is expected. This may be associated with the fact that the second coordinating site the O$^-$ is extended from the aryl ring and forces a distance between the two coordinating sites. In other words the $N^{2'}$

Table 4.4. ^{1}HNMR data for O,N coordinated complexes in acetonitrile-d_3.

Complex	**hydroquinone (phenol) (ppm)**					**pyrazole (pyridine) (ppm)**					
	H^3 ($H^{3''}$)	**H^4 ($H^{4''}$)**	**H^5 ($H^{5''}$)**	**H^6 ($H^{6''}$)**	**OH^4**	**$H^{3'}$ (H^3)**	**$H^{4'}$ (H^4)**	**$H^{5'}$ (H^5)**	**H^6**	**$H^{3''}$**	**$H^{4''}$**
$[Ru(bpy)_2(H_2L2)]$*	7.01	8.25	6.46	6.36	10.4	8.32	7.75	7.18	8.38		
$\Delta\delta^A$	-0.97	1.25	-1.04	-0.59		0.22	-0.15	0.07	-0.26		
$[Ru(bpy)_2(H_2L7)]^+$	6.67	------	6.16	5.97	6.32	6.36	6.30	8.10		----	-----
$\Delta\delta$	-0.35		-0.52	-0.90	-0.36	-1.41	-0.25	-0.08			
$[Ru(bpy)_2(H_2L8)]^+$	7.00	------	-----	6.37	10.38	6.44	6.37	8.24		7.71	6.46
$\Delta\delta$	-0.27			-0.90	-0.59	-1.34	-0.20	0.00		-0.07	-0.11
$[Ru(bpy)_2(H_2L9)]^+$	-----	-------	6.39	6.08	7.01	6.39	5.98	6.89		7.68	6.45
$\Delta\delta$			-0.37	-0.88	-1.22	-1.27	-0.59	-0.13		-0.02	-0.12

* Two singlets (1H) are observed for this complex, at 6.58 and 7.04 ppm which show weak (possibly long-range) coupling.

^{A} differences between resonances for complexes and the free ligands.

is too close to the oxygen to create the most stable configuration. The phenol moiety shows

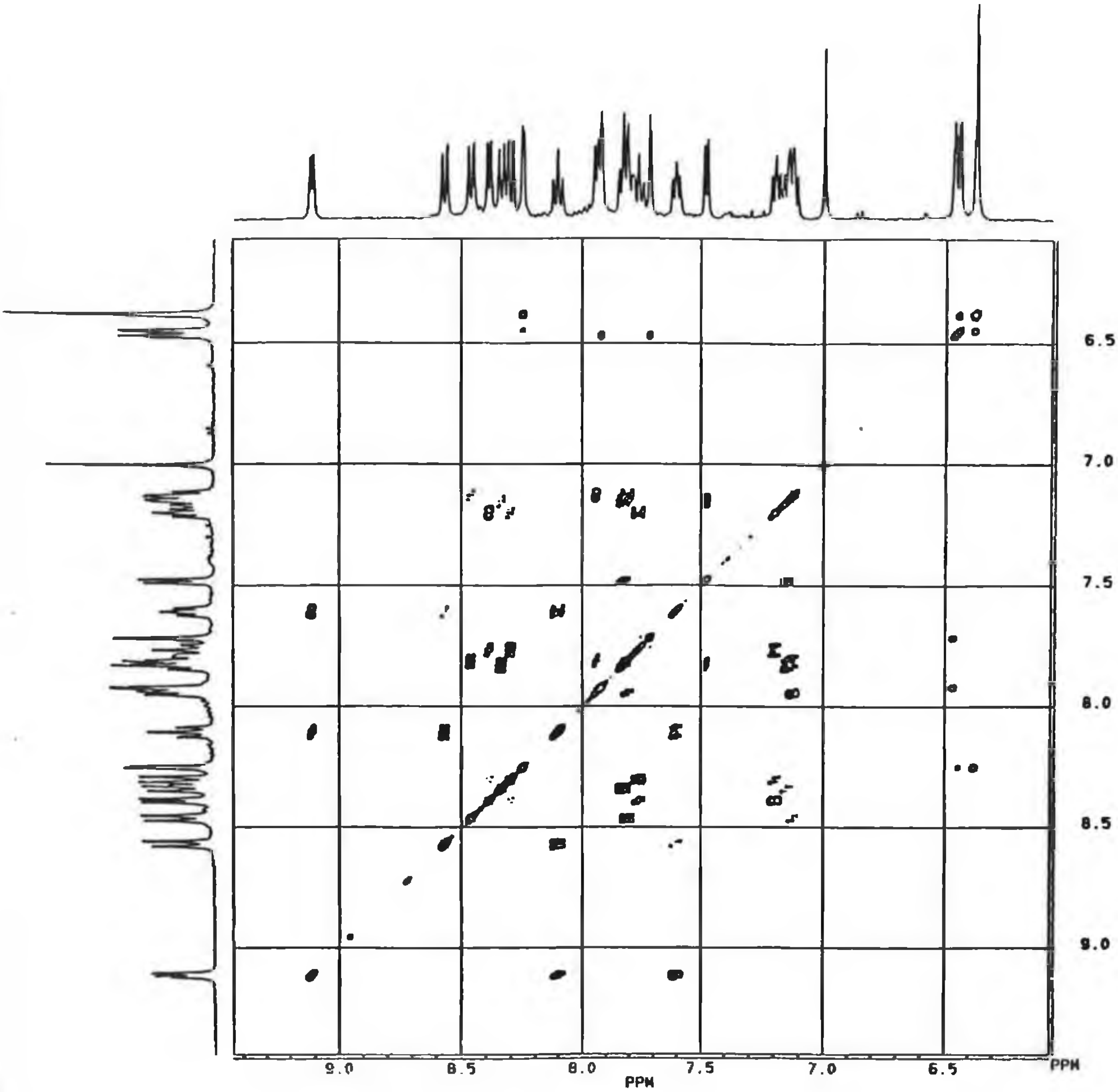

Figure 4.9(a). ^1H and COSY NMR spectrum of [Ru(bpy)$_2$(o,nHL2)]$^+$, in acetonitrile-d$_3$.

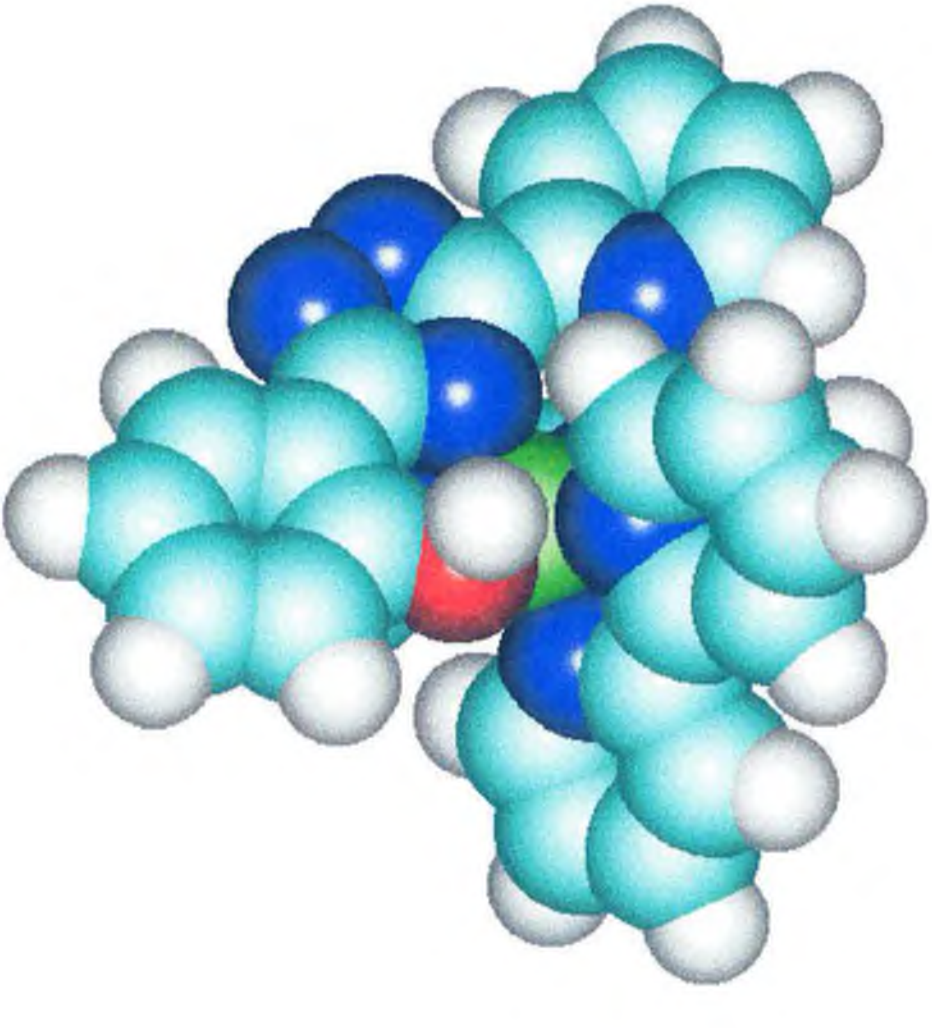

Figure 4.10 (a). Computational model of $[Ru(bpy)_2(o,nHL2)]^+$*, where pale blue = carbon, dark blue = nitrogen, white = hydrogen, red = oxygen, green =ruthenium.*

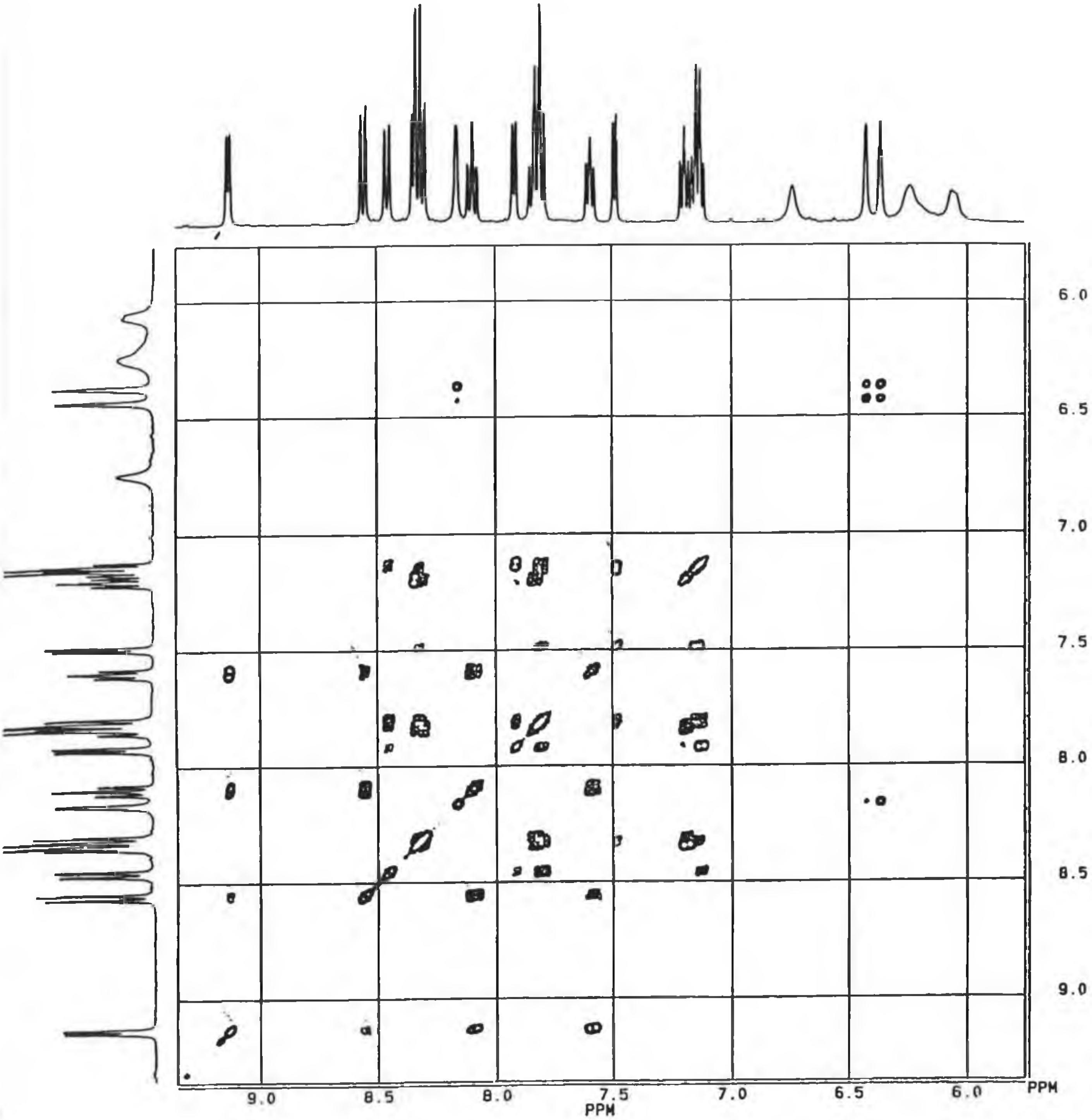

Figure 4.9 (b). ^1H *and COSY NMR spectrum of* $[Ru(bpy)_2(HL7)]^+$*, in acetonitrile-*d_3.

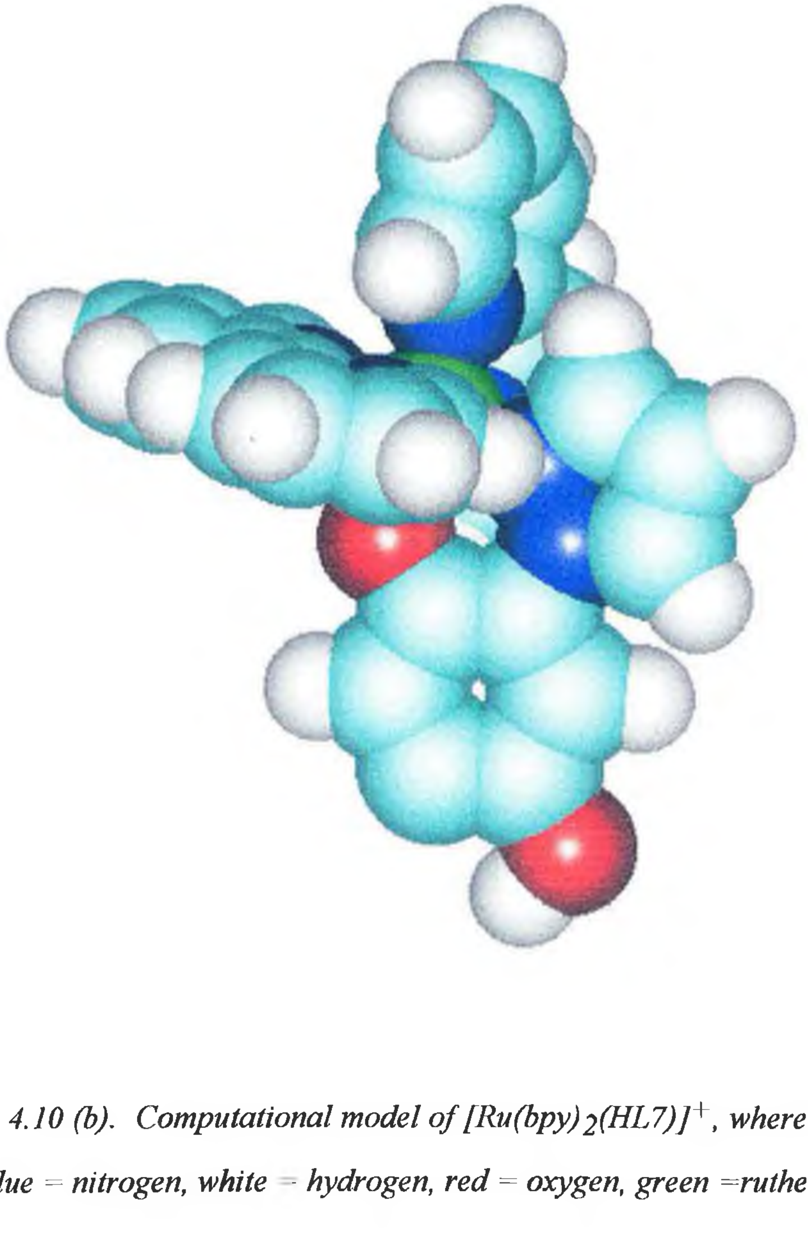

Figure 4.10 (b). Computational model of [Ru(bpy)$_2$(HL7)]$^+$, where pale blue = carbon, dark blue = nitrogen, white = hydrogen, red = oxygen, green =ruthenium.

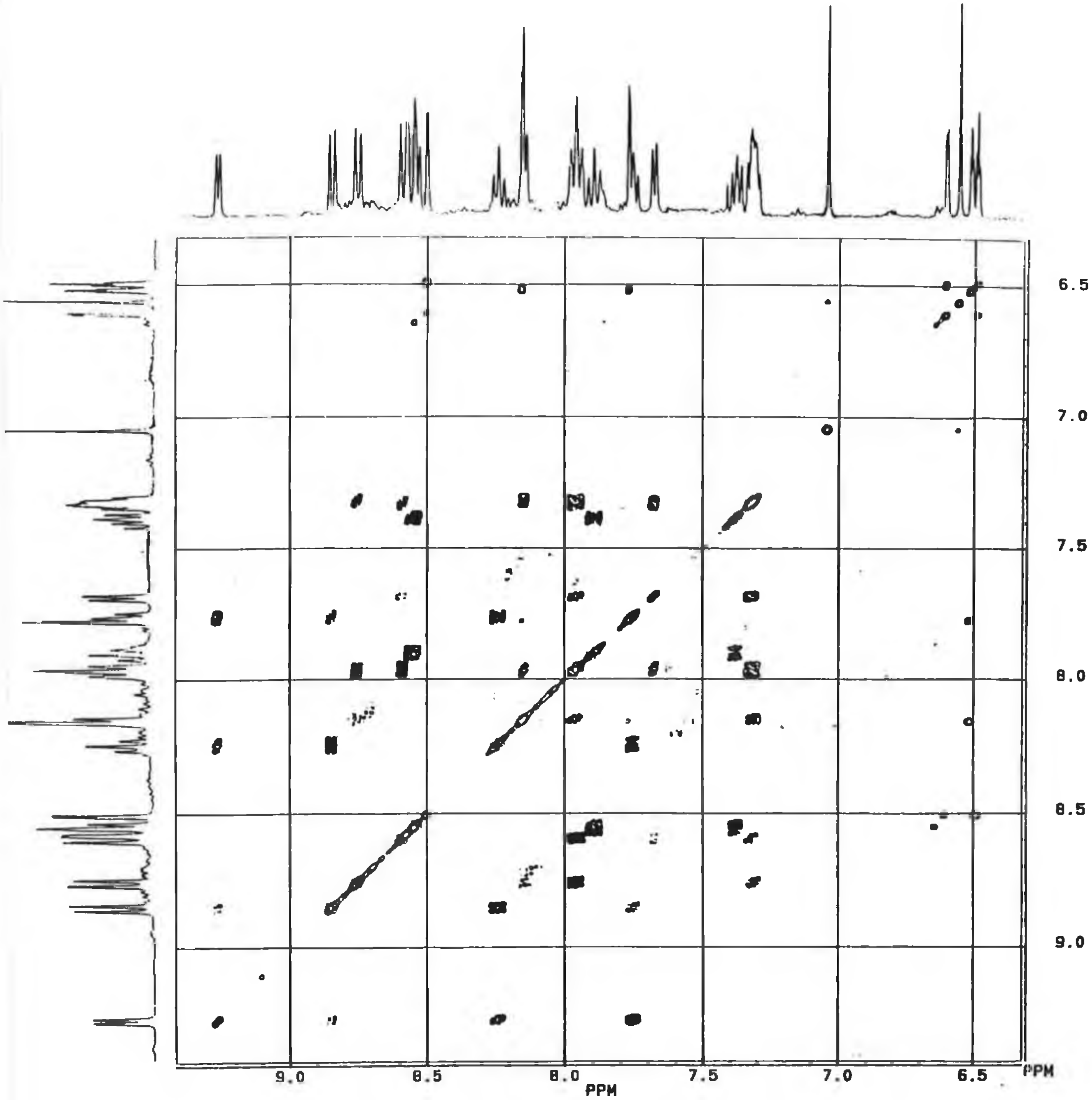

Figure 4.9 (c). ^1H and COSY NMR spectrum of $[Ru(bpy)_2(HL8)]^+$, in acetonitrile-d_3.

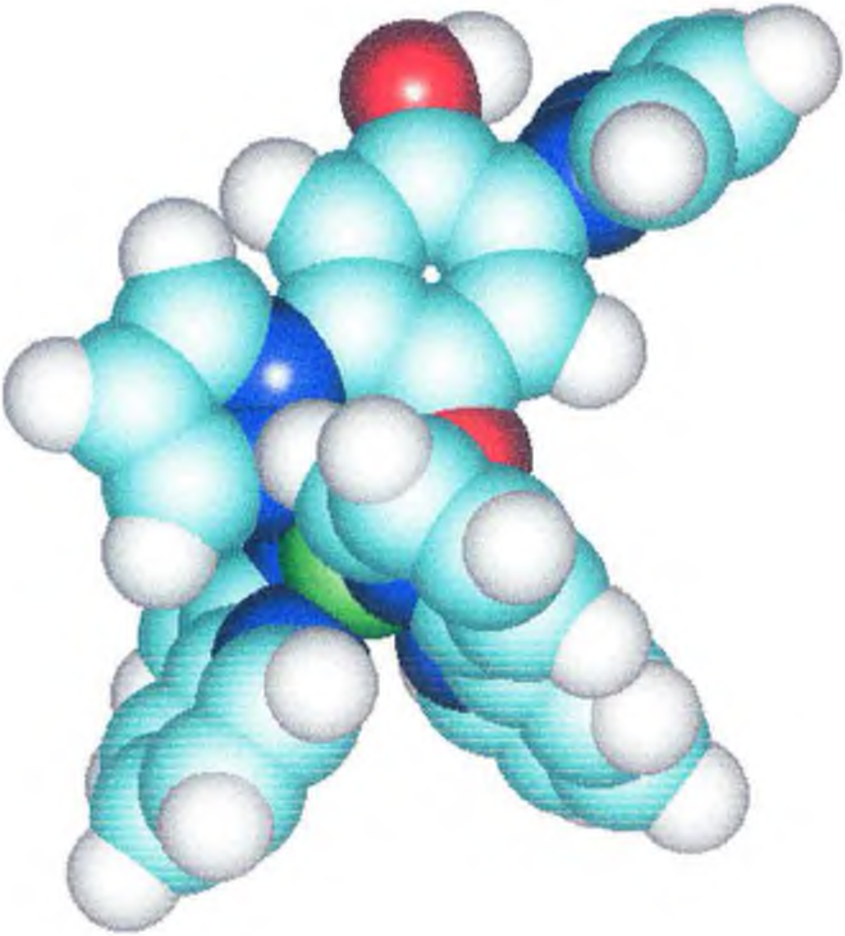

Figure 4.10 (c). Computational model of $[Ru(bpy)_2(HL8)]^+$*, where pale blue = carbon, dark blue = nitrogen, white = hydrogen, red = oxygen, green =ruthenium.*

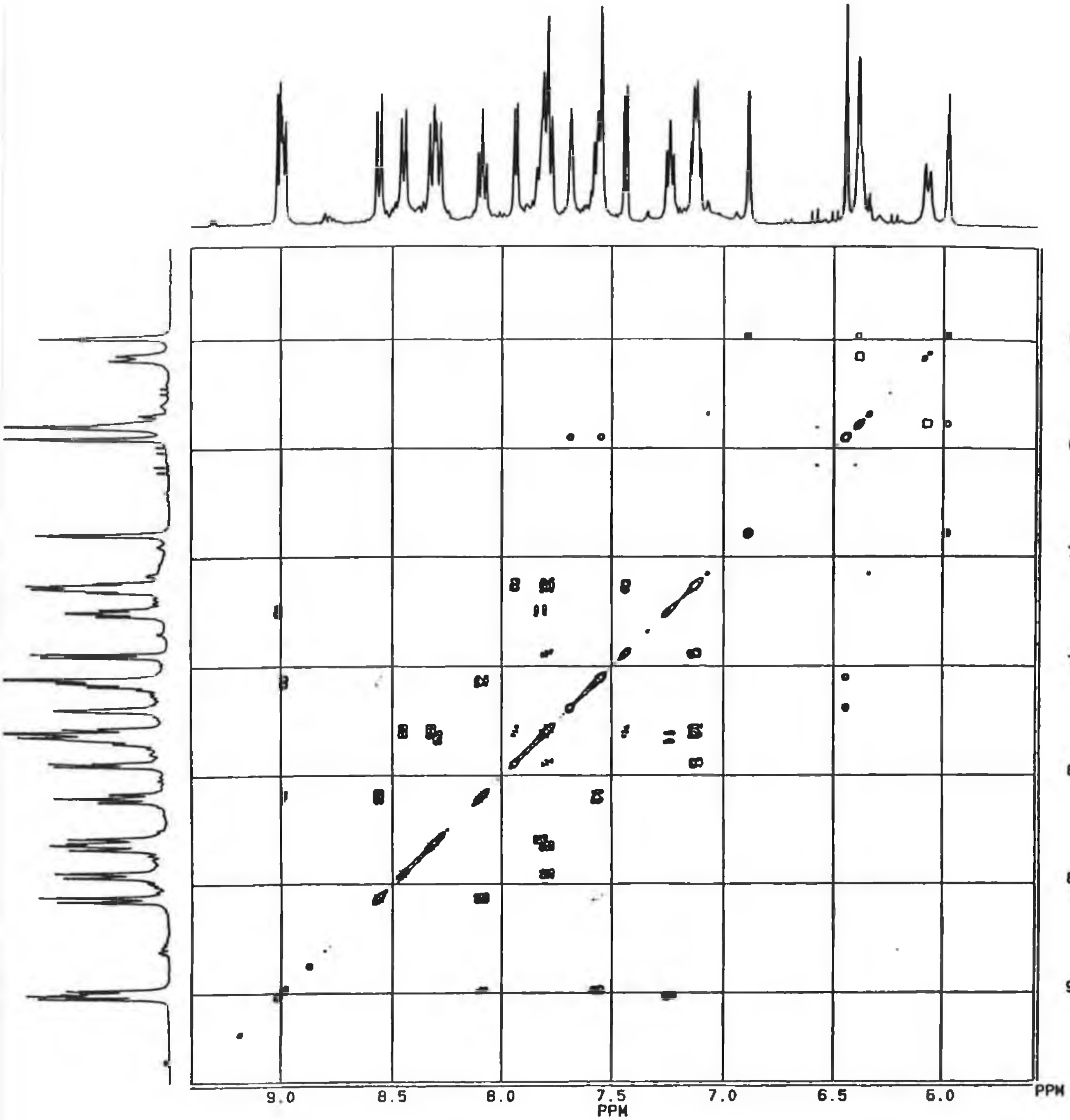

Figure 4.9 (d). ^1H and COSY NMR spectrum of [Ru(bpy)$_2$(HL9)]$^+$, in acetonitrile-d$_3$.

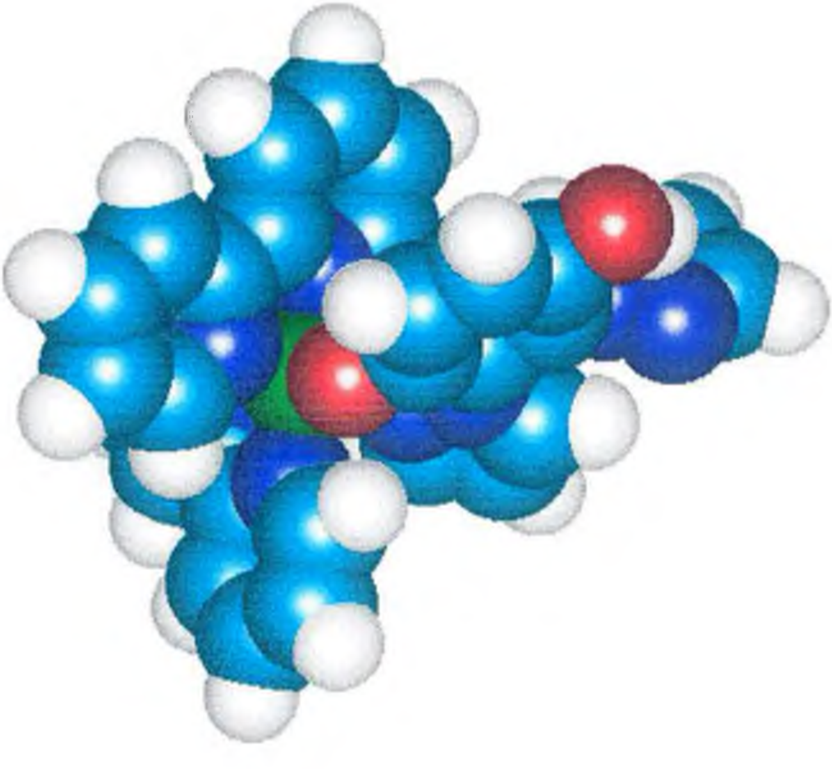

Computational model of $[Ru(bpy)_2(HL9)]^+$, where pale blue = carbon, dark blue = nitrogen, white = hydrogen, red = oxygen, green = ruthenium.

strong shifts, consistent with its coordination. One set of bipyridyl resonances is considerably downfield of the other pyridyls, this effect is observed in all complexes discussed. One of the, most significant points about the structure of $[Ru(bpy)_2(HL2)]^+$is the fact that the coordinated phenol is protonated. As will be discussed, protonation of the phenolate in the case of the hydroquinone-pyrazole complexes results in decomposition. Evidence for protonation of the phenol is derived from the fact that; (a) the C.H.N and IR analyses both show that $[Ru(bpy)_2(HL2)]^+$ carries a monopositive charge, associated with a hexaflourophosphate counter-ion; (b) the ^{1}Hnmr clearly shows a singlet (integrated for 1H) at 10.4 ppm, the shift for the OH in the free ligand is at 11.10, consistant with a H-bonded hydrogen, in this instance the downfield shift of the OH is associated with the electron drain on the phenol as a result of coordination; (c) finally, as will be discussed a reversible PK_a step associated with the phenol is observed. To our knowledge, there is only one other report of a similarily protonated O coordinated site [20], since the reduction in electron density at the coordination site, on protonation would be expected to make the complex unstable. The reason the protonation of the phenol is permissible may be associated with the negative charge on the triazole, which as a result of its strong σ-donation stabilises the complex.

For the interpretation of the pyrazole-hydroquinone complexes, $[Ru(bpy)_2(HL8)]^+$ will be described as an example, since the deuterated analogue was prepared and a complete assignment was possible. The ^{1}H-nmr COSY spectra for this complex is shown in figure 9c. Figure 10(c) shows a computational model of this complex, which proved invaluable in the assignment of the various protons. Two singlets are observed in this nmr, corresponding to the hydroquinone moiety, they exhibit weak, long-range coupling. Both singlets exhibit upfield shifts, the first, H^3, a moderate -0.27 ppm, and the second, H^6, a significant -0.9 ppm, this large upfield shift is due to diamagnetic anisotropic interaction with a bipyridyl ring, this orientation is clearly shown in figure 10c. This proton is weakly coupled to the doublet and singlet corresponding to H3' and H4' of the coordinating pyrazole. Both these protons experience upfield shifts with respect to their free ligands, in particular $H^{3'}$ which shifts an unprecedented -1.34 ppm. The reason for this shift is explained by examination of figure 10c, whereby the $H^{3'}$ proton can be observed lying above an adjacent bipyridyl ring. The induced ring current of the bipyridyl results in diamagnetic anisotropy of the $H^{3'}$ proton causing a strong upfield shift.

The remaining uncoordinated pyrazole experiences relatively weak upfield shifts, remaining for the most part essentially unchanged from the free ligand. Similar arguments may be applied to the assignments of $[Ru(bpy)_2(HL7)]^+$ and$[Ru(bpy)_2(HL9)]^+$, however, some differences do present themselves. For $[Ru(bpy)_2(HL7)]^+$ the resonances corresponding to the hydroquinone, in particular, and to a lesser extent the pyrazole are broadened and fine structure is difficult to see. The temperature at which the spectra were collected was varied to no avail, the broadening was observed in fact to increase with increasing temperature, thus ruling out the possibility that what is observed is the influence of restricted rotation. As will be described under normal conditions in acetonitrile (in the absence of acid) this complex exhibits no luminescence. It was therefore concluded that what was being observed was the influence of a paramagnetic species. This may be from one of two sources, the presence of Ru^{3+}, or of semiquinone. Absorbance spectra of $[Ru(bpy)_2(HL7)]^+$ show no evidence for the presence of Ru^{3+} (i.e. LMCT etc.), and if the broadening were due to the presence of oxidised metal the bipyridyl resonances would be expected to be broadened also. Since the synthesis of these species is carried out under strongly basic conditions which are known to support the creation of semiquinone radicals from hydroquinone/quinone [43], it seems most likely that semiquinone is present. Addition of a small amount of acid (pH 4-5) improved the situation somewhat, whereby the fine structure (doublet and triplet of $H^{3'}$ and $H^{4'}$) could be observed.

$[Ru(bpy)_2(HL8)]^+$ and $[Ru(bpy)_2(HL9)]^+$ exhibit shifts in the resonances of the $H^{5''}$ of the uncoordinated pyrazole in opposing directions. In both instances the largest shift for this uncoordinated ring with respect to the uncoordinated ligand occurs for $H^{5''}$. In

$[Ru(bpy)_2(HL8)]^+$ this proton is shifted upfield whereas for $[Ru(bpy)_2(HL9)]^+$ H5" is shifted downfield. The reason for this is unclear but may have something to do with the orientation of the uncoordinated pyrazole. In $[Ru(bpy)_2(HL9)]^+$ the ring lies ortho to the coordinated pyrazole and lies out of plane and in close proximity to the coordinated pyrazole. This fact is reflected in the upfield shift of H5' in $[Ru(bpy)_2(HL9)]^+$ whereas no change is observed for this proton in $[Ru(bpy)_2(H_2L8)]^+$.

4.3.3. Electronic and photophysical properties.

The electronic and photophysical properties of the complexes discussed are tabulated in table 4.5.

Table 4.5 Electronic and photophysical properties.

Complex	**Absorbance**	**Emission**	**(nm)**	**Lifetimes (ns)**		**ϕem^A**
	λ_{max} (nm) (log ε)	**RT**	**77K**	**RT**	**77K**	
$[Ru(bpy)_2(o,nHL2)]^+$	492 (3.92)	679	617	351	4532	5×10^{-7}
$[Ru(bpy)_2(o,nH_2L2)]^{2+}$	462 (4.04)	625	586	NA	4300	7.1×10^{-8}
$[Ru(bpy)_2(HL7)]^+$	493 (3.92)	680	625	465	5800	NA
$[Ru(bpy)_2(HL8)]^+$	485 (3.76)	680	605	503	3100	1.84×10^{-4}
$[Ru(bpy)_2(HL9)]^+$	501 (3.63)	695	645	NA	1710	1.0×10^{-5}

^{A} For room temperature aerated solutions.

NA, value not available.

The absorbance spectrum of $[Ru(bpy)_2(o,nHL2)]^+$ is shown in figure 11(a), with the absorbances of the hydroquinone complexes at equal concentration shown in figure 11(b). Although the λ_{max} recorded for these complexes is red-shifted with respect to $[Ru(bpy)_3]Cl_2$ [44] and other complexes containing strong σ-donor ligands [10, 45, 46],

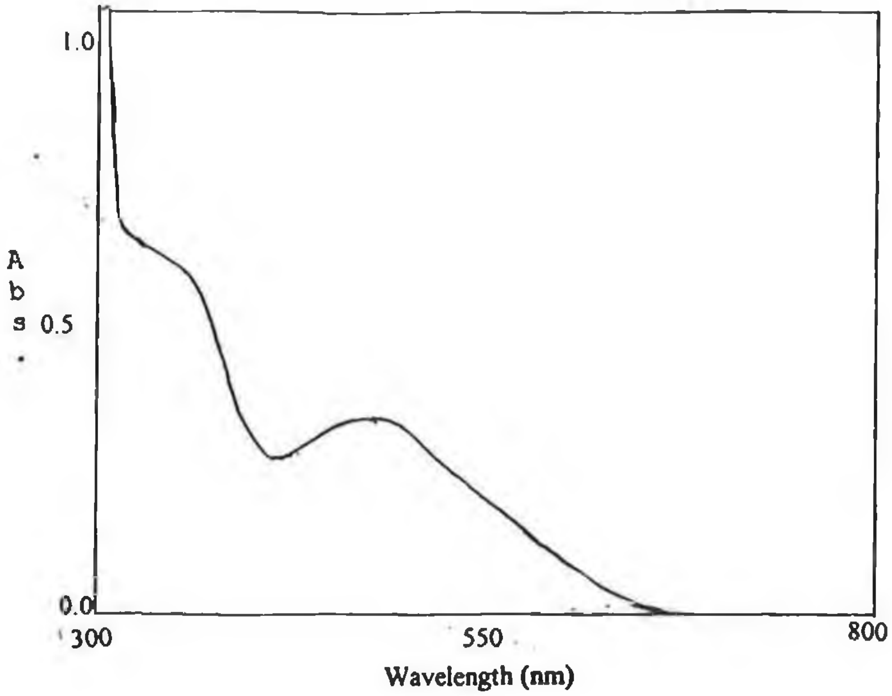

Figure 11 (a). Absorbance spectra of [Ru(bpy)$_2$(o,nHL2)]$^+$ in acetonitrile.

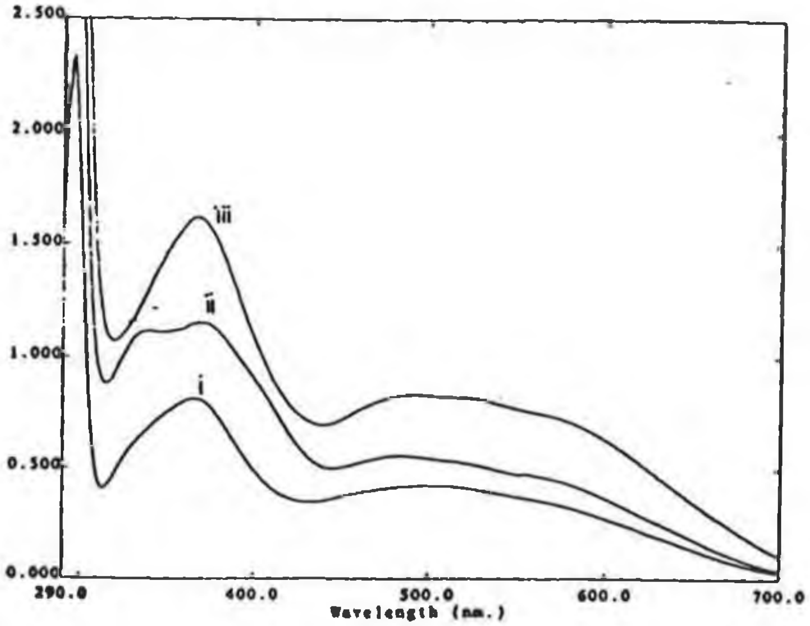

Figure 11 (a). Absorbance spectra of (i) [Ru(bpy)$_2$(HL7)]$^+$ (ii) [Ru(bpy)$_2$(HL8)]$^+$ and (iii) [Ru(bpy)$_2$(HL9)]$^+$ in acetonitrile.

the values shown in the table do not represent the true extent of the visible absorbance range of these compounds, since the visible absorbance is very broad, and tails to approximately 700 nm. In each case these are intense shoulders on the main absorbances. All complexes exhibit intense absorbances at wavelengths < 300 nm. These are assigned as π–π^* ligand based transitions, on the basis of their intensities and by comparison with other Ru(II) polypyridyl complexes [44]. The rather intense absorbances around 330-350 nm in each complex are associated with π-π^* transitions in hydroquinone hydroxyls, similar absorbances are observed in the hydroquinones described in chapter 3, this is discussed further in section 4.3.4. The visible absorption is assigned as a MLCT transition, since the most facile reduction occurs on a bipyridyl [17, 33], it is presumed that the transition is Ru(t_{2g}) to bpy (π^*). The phenolate is very unlikely to possess the LUMO since it possesses a high electron density. The large red-shift in absorbance with respect to $[Ru(bpy)_3]^{2+}$ is associated with the reduced ligand field splitting capability of the O^- by comparison with bpy, despite its strong σ-donor capability. The result of this smaller Δ_o is higher Ru(t_{2g}) energy levels and as a result the Ru(t_{2g}) to bpy (π^*) levels are closer. One of the obvious implications of this smaller Ru(t_{2g})-Ru(e_g) is the problem of thermal accessibility of anti-bonding d-d levels, this will be discussed in detail below.

An intense shoulder tailing to the red from approximately 530 nm is observed in the spectra of all the complexes discussed here. Lever et al have reported on similar transitions in their $Ru(bpy)_2$-catecholate complexes, which they attribute to (catecholate)π-π^*(bpy) transitions [47, 48]. In their O,N coordinated catecholate complexes, which provide the best comparison, λ_{max} is accompanied by a long wavelength shoulder at 667 nm [48]. The absorbances associated with (catecholate)π-π^*(bpy) transitions in Lever's complexes are at longer wavelength than described here. The assignment of these absorbances in the complexes described here is discussed further in chapter 5.

Table 4.5 reveals that the complexes discussed are in fact emissive. These emissions, although of low intensity, reflected in their low emission quantum yields, are surprisingly long-lived. The possibility that these emissions are due to impurity in the sample may be discounted from HPLC analyses. If the emissions were due to impurity the only impurities possible could be either unreacted ligand or $Ru(bpy)_2Cl_2$. The former is only weakly emissive and at wavelength ranges much higher in energy than noted for the complexes. The latter does not emit at all. For $[Ru(bpy)_2(o,nHL2)]^+$ the possibility exists for impurity from the formation of N,N coordinated complex, which does emit (see chapter 3). However, this complex possesses an emission lifetime which decays according to single exponential kinetics, which is nearly 200 ns longer than the N,N coordinated analogue. It would therefore appear that these emissions are real, making these compounds unique as O,N coordinated Ru(II) complexes. To our knowledge, no other similarly coordinated complex emits. The emissions in these complexes originate from a bpy based ^{3}MLCT state. It must be pointed out that the very low quantum yield are slightly misleading since they apply to aerated compounds, it has been noted that the emission of these species is strongly quenched in the presence of O_2, as is normal in complexes of long lifetime. The emission for $[Ru(bpy)_2(HL7)]^+$ is particularly weak, this is associated with the fact that the heteroligand in this complex is likely to be a semiquinone.

At 77K the emissions are blue-shifted as a result of the phenomena described rigidochromism, discussed in Chapter 3. The lifetimes at 77K are several microseconds long, these lifetimes are unprecedented, since for comparable O,N coordinated complexes no emission was observed even at low temperatures. Figure 4.12 shows the emission spectra of $[Ru(bpy)_2(O,NHL2)]^+$ and $[Ru(bpy)_2(HL8)]^+$ at 77K. Vibrational fine structure is evident at these temperatures in the form of a rather intense shoulder at roughly 660 nm.

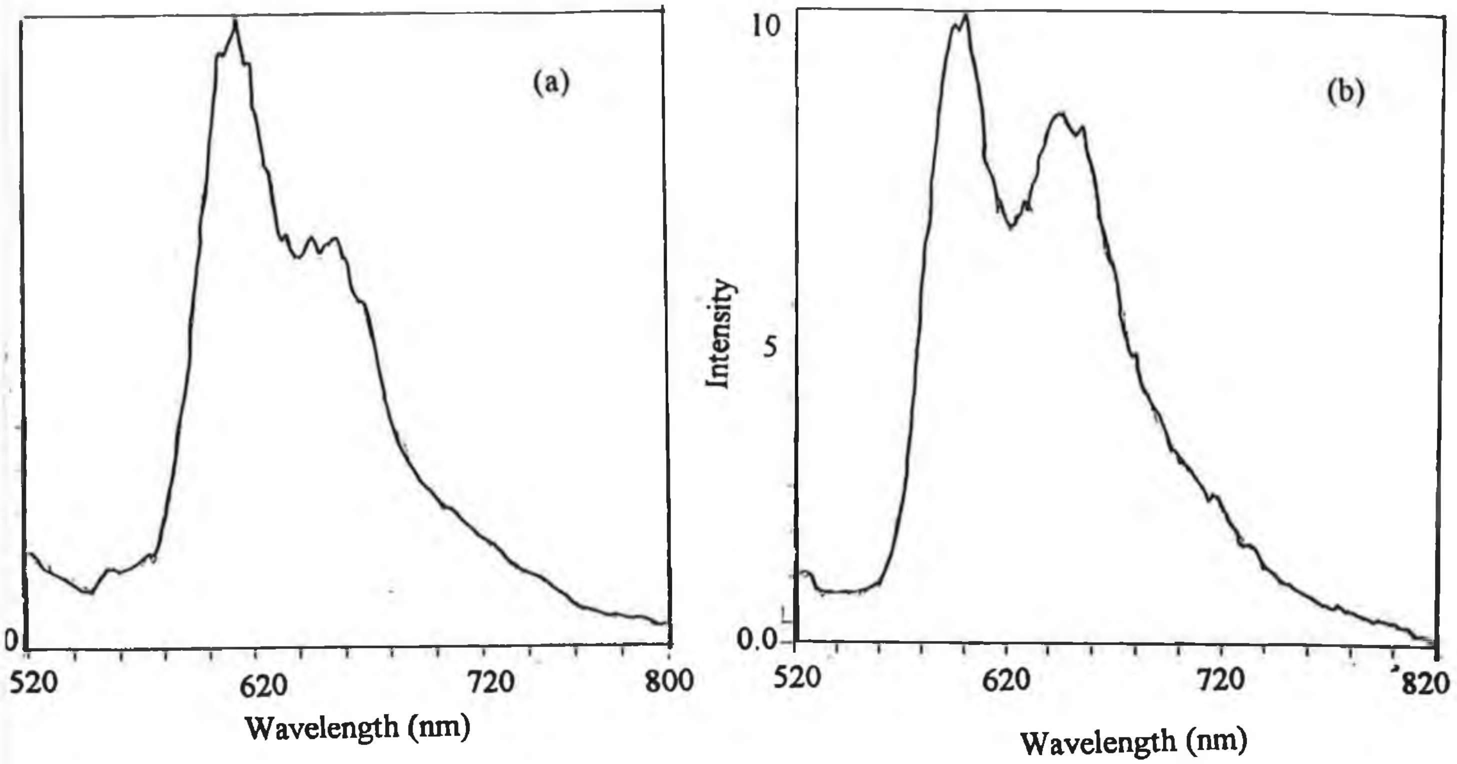

Figure 4.12. Low temperature emission spectra of (a) $[Ru(bpy)_2(O,NHL2)]^+$ and (b) $[Ru(bpy)_2(HL8)]^+$

4.3.4 Acid-base properties.

For the complexes $[Ru(bpy)_2(HL7)]^+$, $[Ru(bpy)_2(HL8)]^+$ and $[Ru(bpy)_2(HL9)]^+$ one step is predicted associated with the protonation/deprotonation of the uncoordinated hydroxyl. The corresponding ligands of these complexes (H_2L7-9) are capable of two steps associated with protonation/deprotonation of both hydroxyl moieties, whereas H_2L2 is capable of three steps as described in chapter 3. Table 4.6 show the acid-base properties of the ligands and complexes discussed here.

For $[Ru(bpy)_2(o,nHL2)]^+$ two protonation steps are anticipated (4.1).

$$[Ru(bpy)_2(H_2L2)]^{2+} \underset{}{\overset{PK_a1}{\rightleftharpoons}} [Ru(bpy)_2(HL2)]^{+} \overset{PK_a2}{\rightleftharpoons} [Ru(bpy)_2(L2)] \quad (4.1)$$

Where pK_a1 represents the protonation/deprotonation of the triazole and pK_a2 represents the protonation/deprotonation of the phenol. Protonation of the triazole is associated with a blue shift in λ_{max} from 493 nm to 465 nm, associated with the stabilisation of the metal t_{2g} level with respect to the ligand π^* levels. The pK_a of $[Ru(bpy)_2(o,nHL2)]^+$ was straight-forward to obtain, the spectra (figure 4.13) were clean and isobestic points were maintained between pH 1 and 4.5 at 333 nm and 484 nm, and between pH 6 and 12 at 338 nm.

The pK_a of the triazole, decreases on coordination, for N,N coordinated complexes, this is also the case for other N,N coordinated triazoles [49]. The pK_a more acidic than the analogous N,N complex. This may be associated with the fact that the coordinated hydroxyl is, as discussed, (surprisingly) protonated at this pH, and is therefore donating less electron density to the metal than a coordinated pyridyl moiety. The extent of electronic donation by the triazole is, therefore, increased to compensate for this deficit, and it becomes more acidic. It is very interesting to note that the phenol is protonated in this complex at neutral pHs this fact is corroborated by ^{1}Hnmr, IR and elemental analyses. As is discussed below, hydroxyl protonation leads to decomposition in the hydroquinone-pyrazole complexes. The stability of this complex on phenolate protonation is associated with the negative charge on the triazole, which is absent in the pyrazoles. Protonation of the pyridyl in $[Ru(bpy)_2(o,nH_2L2)]^{2+}$ should in theory be possible, however, no step was observed relating to this process was observed over the pH range examined.

The pK_a of both the complexes and ligands of the pyrazole-hydroquinone species were considerably more difficult. Isobestic points were rarely maintained and in the case of the ligands, changes occurring at high pHs were often irreversible. Figure 4.14 (a) and (b) shows the titration spectra for the pK_a of H_2L7 in the region pH 7-10, and

[Ru(bpy)$_2$(HL7)]$^+$ in 7 to 10, isobestic points are tentatively maintained in this titration range at 294 nm for the former and 293 nm for the latter. The isobestic points are not maintained during one pKa measurement and dramatic changes may occur over one pH unit.

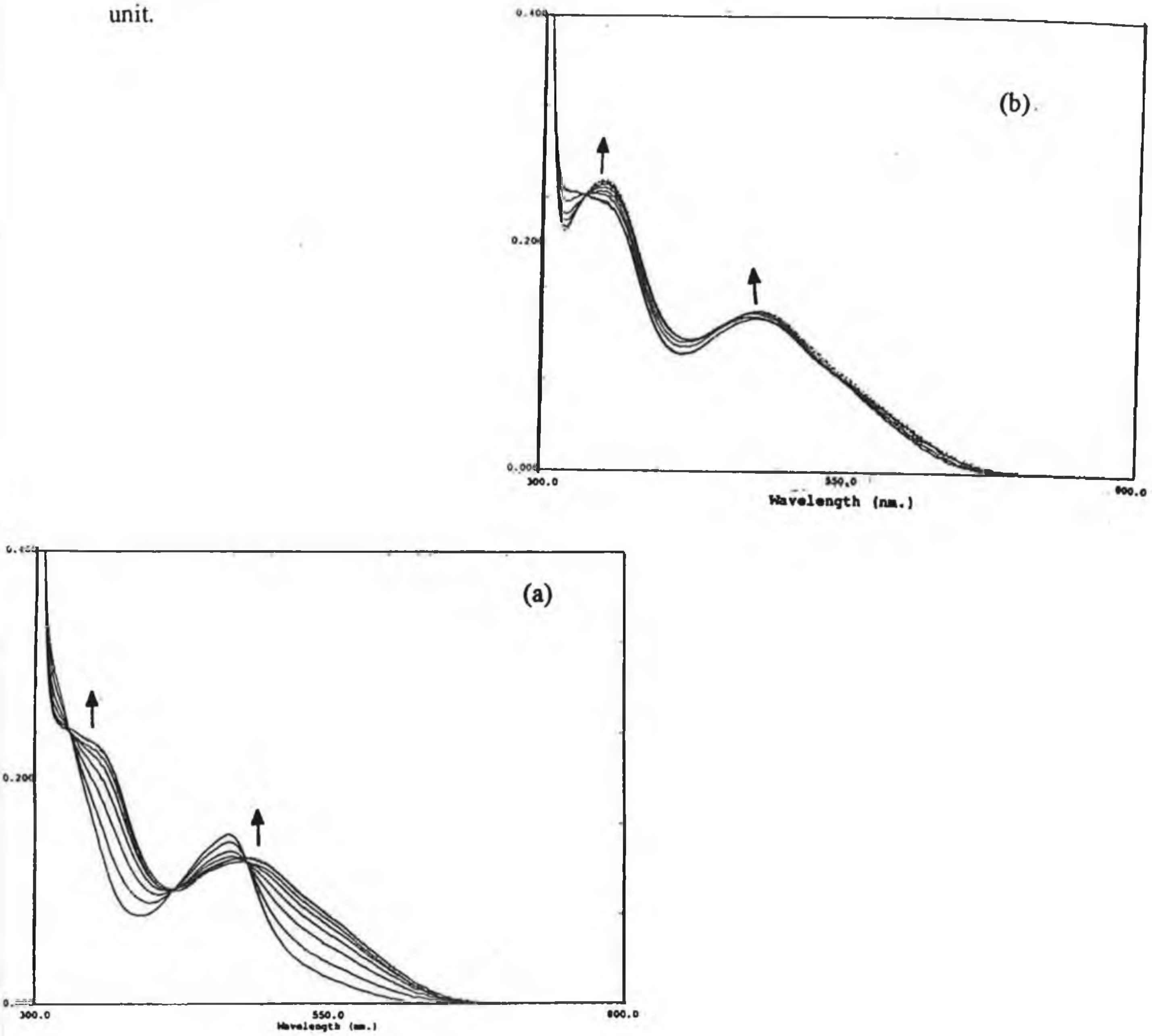

Figure 4. 13 pH dependent spectra of [Ru(bpy)$_2$(o,nHL2)]$^+$ (a) pH 1-5, (b) pH 6-12.

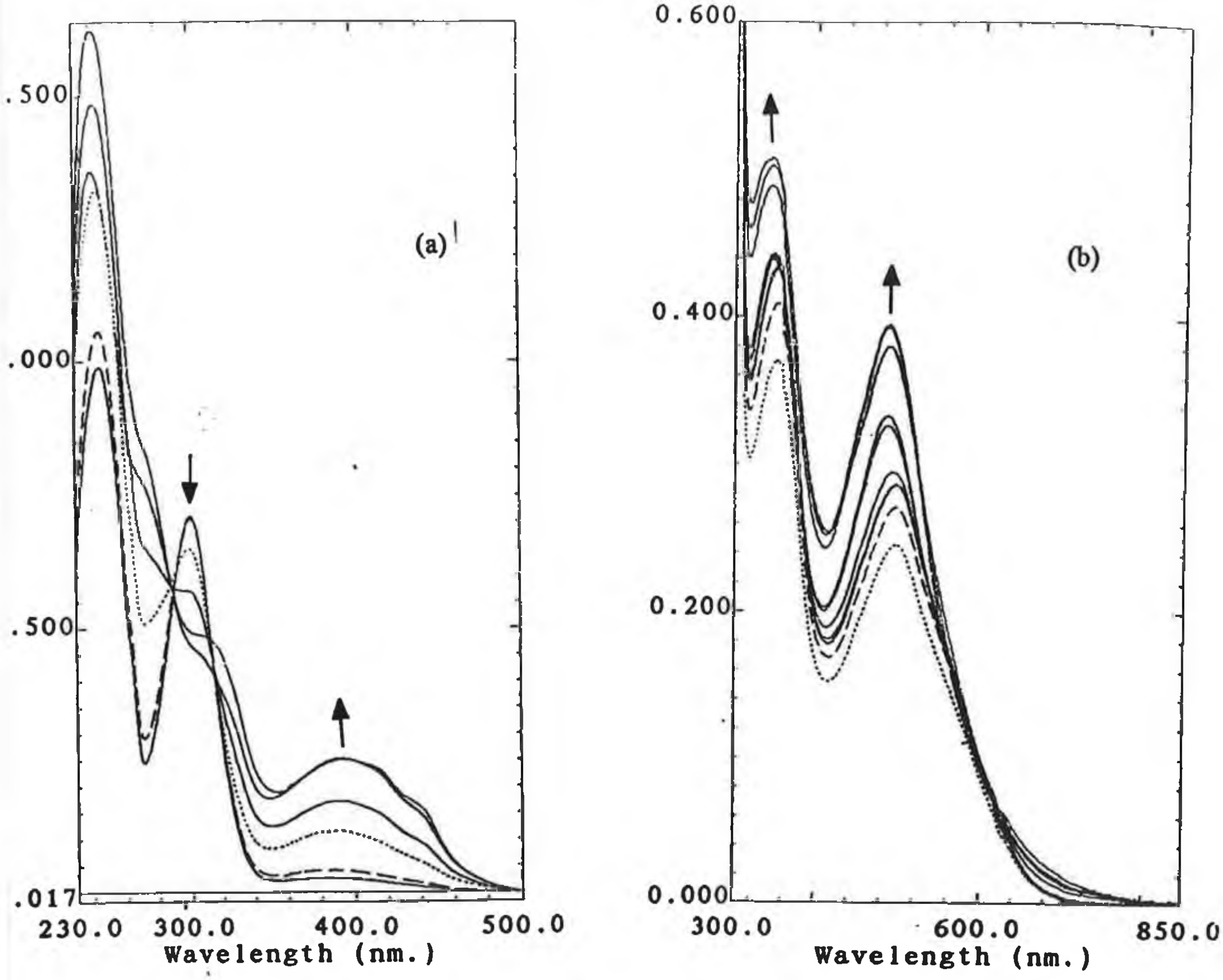

Figure 4. 14. pH dependent spectra absorbance spectra of (a) H2L7 in the pH range, and (b) $[Ru(bpy)_2(HL7)]^+$ pH 6-12.

Table 4.6. Ground state pKa values of mononuclear O,N coordinated complexes.

Compound	**pK_a (1)^A**	**pK_a(2)^A**	**PK_a (3)**
H_2L2*	3.22 (pyridyl)	6.00 (triazole)	11.60 (OH)
$[Ru(bpy)_2(o,nHL2)]^+$	2.31	9.08	-------
H_2L7	3.4 (OH^1)	8.85 (OH^2)	-------
$[Ru(bpy)_2(HL7)]^+$	-----	11.20	-------
H_2L8	8.20 (OH^1)	10.60 (OH^2)	-------
$[Ru(bpy)_2(HL8)]^+$	-----	10.10	-------
H_2L9	5.35	8.84	-------
$[Ru(bpy)_2(HL9)]^+$	------	11.01	-------

* Values from reference [36].

^{A} The values for the H_2L2 based compounds are ± 0.05 pKa unit. For the pyrazole-hydroquinone compounds the values are ± 0.2.

At high pHs for H_2L7 and H_2L9, strong absorbances appear centered around 420 nm leading to a change in colour in solution from colourless at acidic or nearly neutral pHs to dark yellow at high pHs. The shift in absorbance is not observed at such long wavelength for H_2L8. Deprotonation of the hydroxyl to produce its associated anion in conjugated species such as these would be expected to cause a red shift in absorbance as a result of delocalisation of the excess charge around the molecule. However, the constant shifting of absorbances and absence of any clear isobestic points over larger pH ranges (within the same pK_a step), suggests unstable intermediates are forming.

In Chapter 3, during measurement of the pK_a of hydroquinone and quinone ligands and complexes, the same problem was encountered. The spontaneous production of radical in basic (and acidic) solutions has been described [43, 50], and this formation of transient intermediate is aggravated in aqueous solution. Semiquinone in itself is not entirely responsible for the lack of clean reaction in these systems, it is the fact that this species can, in particular in aqueous solution where protons are readily available, undergo further reaction such as disproportionation to produce several stable and unstable species in solution simultaneously.

Attainment of clean spectra in the pK_a measurement of the complexes is equally difficult, and most likely for the same reason. In the complexes where one of the hydroxyls is coordinated, there is only one pK_a corresponding to (de)protonation of the free hydroxyl. With the exception of $[Ru(bpy)_2(o,nHL2)]^+$, all the complexes discussed here are unstable in acid. The change in spectra observed is a strong red shift to approximately 437 nm. This is accompanied by a visible change in the complex colour from deep purple to a orange/yellow colour. The complex appears to break down permanently on addition of acid. This is probably associated with protonation of the coordinated oxygen. The reduction in electron density on the oxygen reduces its capacity to bond and makes the Ru(II)-O bond unstable, possibly decomposing the complex completely Similar instability towards acid was reported for ruthenium O,N bound complexes based on flavin ligands [53]. This was not observed to occur in $[Ru(bpy)_2(o,nHL2)]^+$, where the pH could be safely reduced to 1.8. This is associated with increased σ-donor capacity of the deprotonated triazole ligand which stabilises the Ru(II)-OH bond.

Overall, the change associated with the de(protonation) of the free hydroxyl on the pyrazole-hydroquinone complexes is small. This is not surprising, since this site does not participate in coordination and any changes associated with this process should occur in the absorbances associated with this moiety. On this basis the absorbances around 330-350 nm in these complexes are indisputably associated with the hydroxyl moieties, and on the basis of their wavelengths and intensities are possibly π-π* transitions, associated with deprotonation of the hydroxyl.

The pKa values observed for the complexes are considerably more basic than the parent ligands. This would imply greater electron density in the case of the coordinated species, possibly a result of the increased charge on the compound as a result of the anionic coordinated O site, and perhaps also due to back-bonding between the metal and the ligand. For the ligands H_2L7 and H_2L9, the pK_a (1) is remarkably low for a hydroxyl species, whereas pK_a for H_2L8 is more usual. As was described in section 4.3.1.2, H_2L8 is a molecule planar which maintains strong bridging between its hydroxyls and adjacent pyrazoles. On the other hand H_2L7 possesses only one pyrazole and therefore only one H-bridge is possible, this species has a pK_a (1) of only 3.34, which is remarkably low. H_2L9, as a result of steric effects, has its pyrazole bent out of plane, disrupting the H-bridging. The reason for the anomalous pK_a values must therefore lie in these differences. It seems likely however, that the sites in which the proton may bridge is the more basic since this site contains more electron density, unless the site is somehow stabilised by a hydrogen on the pyrazole ring. Alternatively, the low pK_as for ligands may be associated with the formation of semiquinone, it is possible that the pK_a values obtained are those of the semiquinone species and not the hydroquinone. The pK_a vaulues quoted are very much in line with other quoted pH values for semiquinone [51].

Emission as a function of pH was examined for $[Ru(bpy)_2(o,nL2)]^+$, the results are shown in figure 4.15. In a manner reminiscent of the phenols and hydroquinones examined in Chapter 3, this complex exhibits pH dependent emission over a wide pH range. This is most likely associated with the (de)protonation of the triazole and phenol. Protonation of the triazole leads to a blue shift in λ_{max} of emission, from 680 to 625 nm, and a significant decrease in intensity, for reasons described in section 3.3.2.1. Deprotonation of the phenol also leads to a decrease in emission intensity, this was observed in the N,N coordinated phenol ligand (chapter 3). This was associated with quenching of the excited state by the anionic phenol, it would seem that since the O^- is directly bound to the Ru(III)*, electron transfer is likely, but it is probable that as a result of this proximity that charge recombination will be equally rapid. This process therefore warrants further investigation.

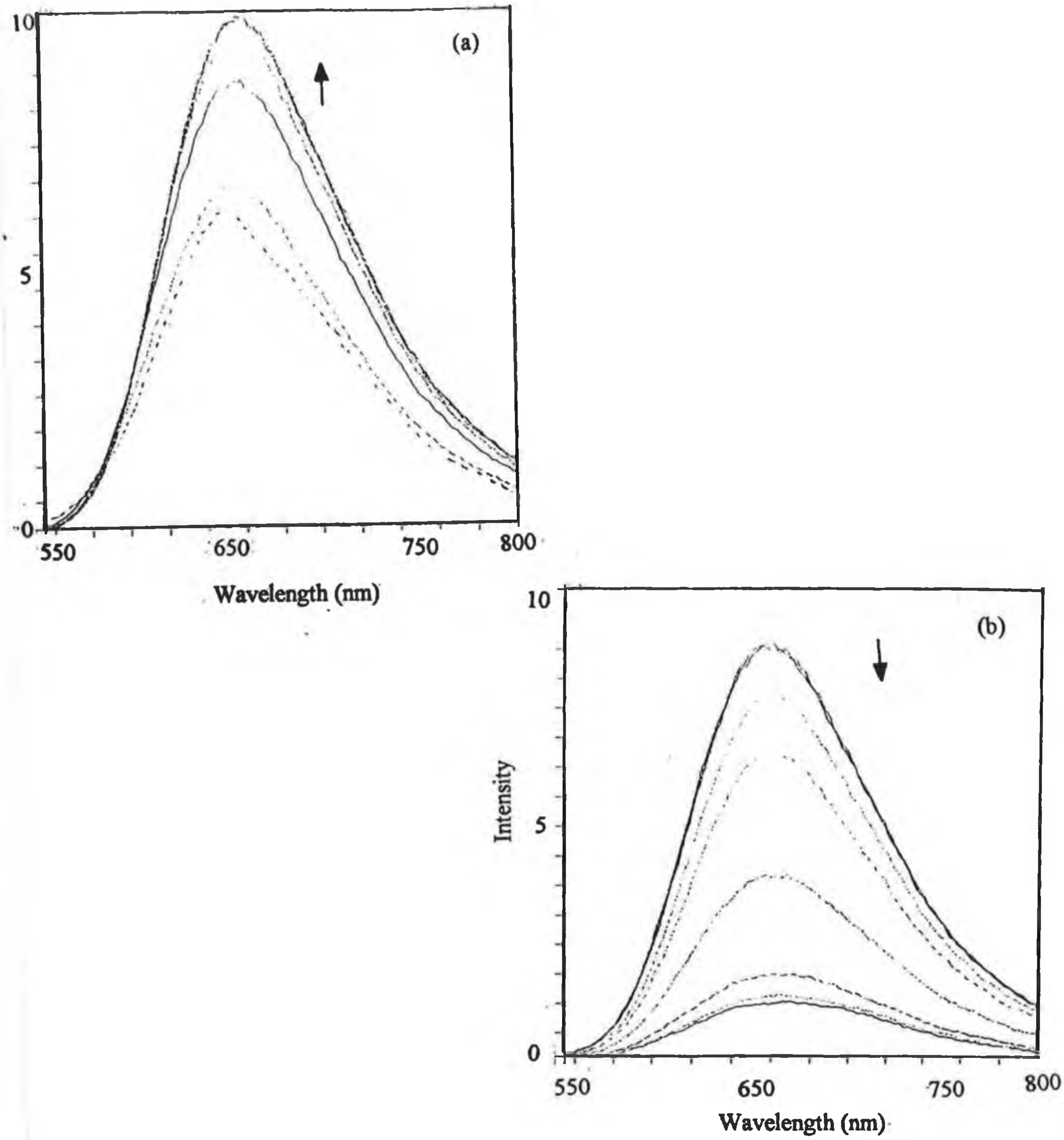

Figure 4.15. PH dependent emission spectra of [Ru(bpy)$_2$(o,nL2)]$^+$, in Britton-Robinson buffer at (a) pH 2 to 7, (b) pH 7 to 12.

4.3.5 Electrochemical properties.

The electrochemical properties of these complexes reveal very clearly the influence of O^- as a coordinating entity. As was described, oxygen is an interesting donor atom in these systems since it possesses it's own electrochemical properties. One of the problems encountered here, however, was the affinity of phenols for adsorption on glassy carbon during electrochemistry. Table 4.7 displays the electrochemical properties of the complexes discussed.

Electrochemistry is a useful tool in the evaluation of the σ-donor and π-acceptor ability of a ligand, for example, strong σ-donors tend to stabilise high oxidation states and π-acceptors stabilise low oxidation states. The most immediately apparent feature of these complexes is the strong negative shift in the oxidation potential with respect to $[Ru(bpy)3]^{2+}$. This implies that the ligands employed are stronger σ-donors than bpy. Furthermore, the oxidation potentials here are considerably cathodically shifted with respect to other N,N complexes such as the triazoles, which are traditionally known as strong σ-donor ligands. For example, for the N,N coordinated analogue of $[Ru(bpy)_2(o,nHL2)]^+$, the $Ru^{(II)/(III)}$ couple occurs at 0.86V [36] as opposed to 0.36V for $[Ru(bpy)_2(o,nHL2)]^+$, indicating that as a result of the stronger σ-donor capacity of O^- moiety the Ru(III) state is stabilised by 500 mV.

An irreversible oxidation is observed at approximately 1.3 V for all complexes examined, this is associated with the oxidation of the hydroxyl moiety, since repetitive scans produce polymerisation on the electrode surface. Presumably this is the coordinated oxygen centre species, since the same oxidation is observed in $[Ru(bpy)_2(o,nHL2)]^+$ and is also observed in similar complexes in which the only hydroxyl is coordinated [33]. The oxidation of the uncoordinated groups is not observed and are presumably outside the potential window examined.

Table 4.7 Electrochemical data for O,N coordinated complexes.

Compound	**Metal oxidation (V) Eox**	**Bipyridyl reduction (V)**	**OH redox (V)**	**Ru$^{(II)/(III)*}$**	**Ru$^{(II)/(I)*}$**
$[Ru(bpy)3]^{2+}$	1.26*	-1.35	-----	-0.87	0.78
$[Ru(bpy)_2(o,nHL2)]^+$	0.36	-1.57, -1.82	1.30 (irr.)	-1.64	0.439
$[Ru(bpy)_2(o,nHL2)]^{2+}$	0.80	------	1.30 (qrev.)	-0.85	-----
$[Ru(bpy)_2(HL7)]^+$	0.35	-1.62, -1.89	-1.03, 0.64, 1.30(irr)	-1.63	0.364
$[Ru(bpy)_2(HL8)]^+$	0.42	-1.52, -1.80	1.29 (irr.)	-1.63	0.469
$[Ru(bpy)_2(HL9)]^+$	0.44	-1.60, -1.89	1.30 (irr.)	-1.48	0.322

* From reference [44].

The assignment of the electrochemistry was verified by spectroelectrochemical measurements for $[Ru(bpy)_2(HL2)]^+$ and $[Ru(bpy)_2(HL8)]^+$. Figure 4.16 shows the cyclic voltammogram and SEC for $[Ru(bpy)_2(HL8)]^+$ at various potentials, by 0.5 V the MLCT band has collapsed significantly and an intense, broad band at 765 nm appears. This band is attributed to either the LMCT $O^-(\sigma)$-Ru(t_{2g}) transition, since oxygen is the strongest σ-donor here or possibly the π(bpy)-t_{2g}, neither possibility can be ruled out. Interestingly, there is no significant difference between the oxidation potential of $[Ru(bpy)_2(o,nHL2)]^+$ and the remaining complexes despite the fact that the phenol is thought to be protonated at neutral pH at which the electrochemistry is carried out. This is most likely due to the influence of the negative triazole which may compensate for the reduction in electron density as a result of protonation of the phenol, and the possibility that the phenol deprotonates on metal oxidation may also have some bearing. Addition of acid causes a marked anodic shift in the oxidation potential of the metal in $[Ru(bpy)_2(o,nHL2)]^+$ consistant with protonation of the triazole.

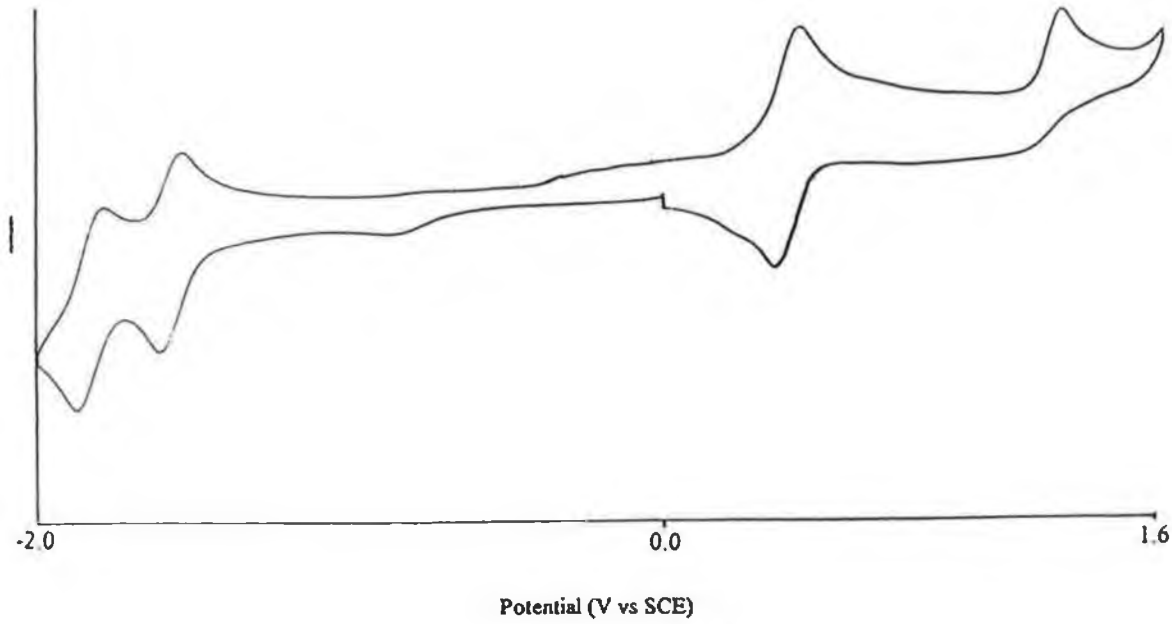

Figure 4.16(a) Cyclic Voltammogram of $[Ru(bpy)_2(HL8)]^+$ ***in neutral acetonitrile.***

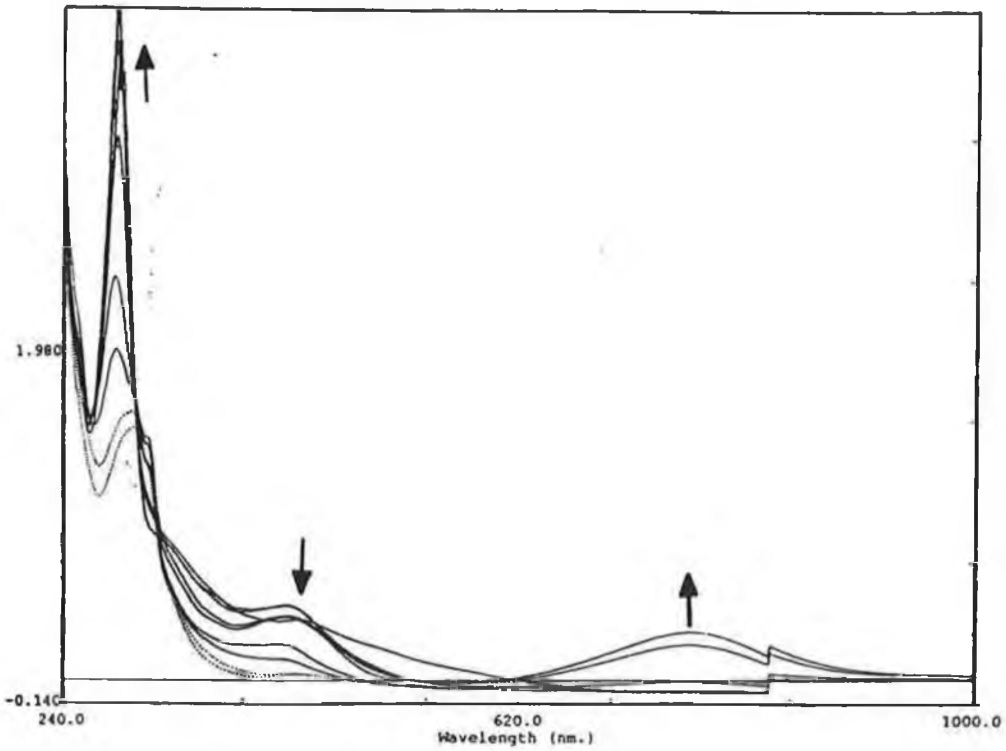

Figure 4.16(b) Spectroelectrochemistry of $[Ru(bpy)_2(HL8)]^+$ *in neutral acetonitrile at potentials, 0, 0.4, 0.5, 0.7 0.9, 1.2, 1.3 and 1.4V.*

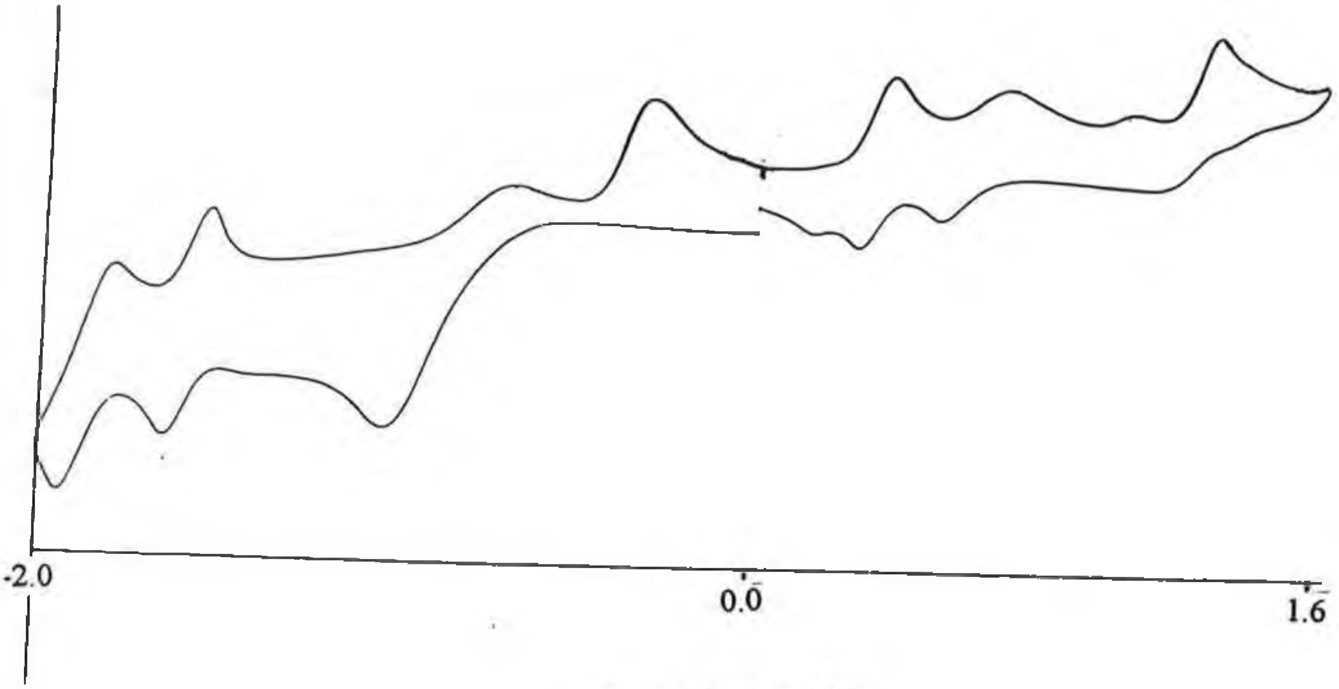

Figure 4.17 Cyclic Voltammogram of [Ru(bpy)$_2$(HL7)]$^+$ in neutral acetonitrile.

The CV of $[Ru(bpy)_2(HL7)]^+$ shown in figure 4.17, shows some interesting features, it possess two reversible oxidations, one at 0.35 V and one at 0.64 V (in an approximately 2:1 ratio). Since in general the OH oxidations are at best quasi-reversible, and both these waves reversible, it seems likely that they are both associated with metal oxidations. Two possibilities present themselves, firstly, that the first oxidation is $Ru^{(II)/(III)}$ and the second is $Ru^{(III)/(IV)}$. This is unlikely since the $Ru^{(III)/(IV)}$ couple is not observed in the other complexes discussed and the electronic distribution of the ligand H_2L7 is not sufficiently different to cathodically shift this oxidation potential to such an extent. Secondly, that the first oxidation is that of the $Ru^{(II)/(III)}$ couple coordinated to the normal anionic pyrazole hydroquinone anion, and the second is due to the $Ru^{(II)/(III)}$ couple in the complex coordinated to the semiquinone ligand. From ^{1}H-nmr (section 4.3.2) it was apparent semiquinone radical was present in $[Ru(bpy)_2(HL7)]^+$, the semiquinone will be less electron rich and a weaker σ-donor than the anionic ligand, hence the metal oxidation for this species would be expected to be anodically shifted. The most important evidence to substantiate the presence of a semiquinone in this complex comes from reduction electrochemistry of $[Ru(bpy)_2(HL7)]^+$. A quasi-reversible reduction is observed at -1.03 V, (see figure 4.17), with its associated reoxidation at -0.213 V. It is thought that this process is the reduction of the semiquinone radical, and since its reoxidation is at cathodic potential this implies that the semiquinone will be stable under zero potential conditions. Further substantiation should therefore come from E.S.R of this complex.

4.3.6 Temperature dependent studies.

All complexes discussed here are luminescent at both low temperature and at room temperature in fluid solution, it was therefore possible to explore the temperature dependence of the emitting process. The temperature dependent data are shown in table 4.8. The data was obtained as described in section 3.3.7.

Table 4.8. Activation parameters from temperature dependent luminescent lifetimes*.

Complex	**E_a (cm^{-1})**	**A(s^{-1})**	**k_0 (s^{-1})**
$[Ru(bpy)_2(o,nHL2)]^+$	639	$2.28\ x10^9$	$2.35\ x10^6$
$[Ru(bpy)_2(o,nHL2)]^{2+}$	798	$3.45\ x10^{10}$	$9.66\ x10^6$
$[Ru(bpy)_2(HL7)]^+$	646	$3.79\ x10^9$	$1.5\ x10^6$
$[Ru(bpy)_2(HL8)]^+$	235	$9.29\ x10^6$	$1.26\ x10^6$
$[Ru(bpy)_2(HL9)]^+$	720	$9.18\ x10^6$	$1.37\ x10^6$

* Overall error for these measurements is estimated to be 8% [52].

It is simplest to discuss the complexes in two groups, the $[Ru(bpy)_2(o,nHL2)]^+$ and its protonated analogue followed by the pyrazole-hydroquinone complexes. Figure 4.18 shows the temperature dependant lifetime curve of $[Ru(bpy)_2(o,nHL2)]^+$ in it's protonated and deprotonated state.

$[Ru(bpy)_2(o,nHL2)]^+$ shows a weak temperature dependent behaviour, which from examination of the curves in fig. 4.18 increases on protonation of the triazole. E_a for $[Ru(bpy)_2(o,nHL2)]^+$ is 639 cm^{-1} with a preexponential factor of 2.28 x10^{-9} s^{-1}. Indicating that this species falls into category (i) Small activation energy (<800 cm^{-1}) and low prefactors (<10^{9}s^{-1}). This complex is expected to be unreactive towards photosubstitution, since as was described in chapter 3 the E_a for such category (i) compounds represents activated population of a weakly coupled ^{1}MLCT state [53], not a ^{3}MC state.

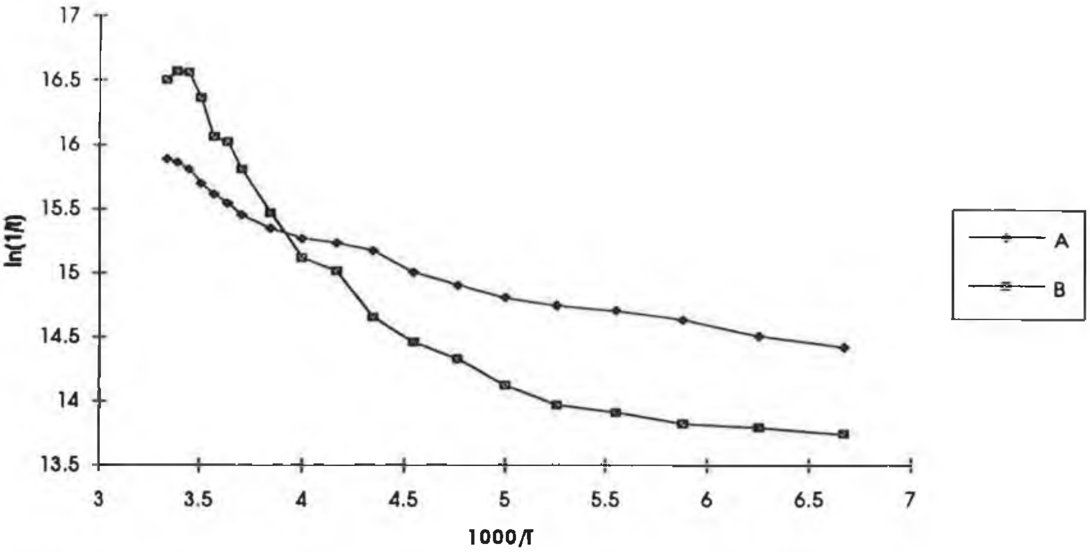

Figure 4.18, Temperature dependant lifetime plot of A = [Ru(bpy)$_2$(HL2)]$^+$, B =[Ru(bpy)$_2$(HL2)]$^{2+}$.

It is evident from figure 4.18 that the protonation analogue exhibits more temperature dependent behaviour, in particular in the higher temperature range. E_a was determined to be 798 cm^{-1} and A = 3.45 x10^{10} s^{-1}. This situation represents intermediate behaviour whereby the ^{3}MLCT and ^{3}MC states are possibly in equilibrium. The activation energy for ^{3}MC state at 800 cm^{-1} is however, unusually low, and would suggest class (i) behaviour, since such a small energy gap between ^{3}MLCT and ^{3}MC should lead to very rapid equilibrium between the two states, causing significant interference in decay from ^{3}MC. Comparison with the temperature dependent luminescent behaviour of similar N,N coordinated phenol complex [Ru(bpy)$_2$(HL4)]$^+$ reveals considerable differences. In the deprotonated state, the differences are not large, both complexes exhibit class (i) behaviour and are predicted to be photostable. However when protonated the behaviour diverges sharply, $[Ru(bpy)_2(HL4)]^+$ exhibits classical class (ii) behaviour i.e., large activation energies and large prefactors. E_a for this species is 2059 cm^{-1} and $A = 8 \times 10^{16}$ s^{-1}. This implies that although protonation of the triazole in both cases causes a change in behaviour, the behaviour is not so strongly modified in the O,N coordinated species.

The temperature dependent luminescent behaviour for the hydroquinone species is graphed in figure 4.19. To highlight the differences between the complexes, the plot for $[Ru(bpy)_2(HL8)]^+$ is shown twice as L8 which reflects the true results and as the unmarked

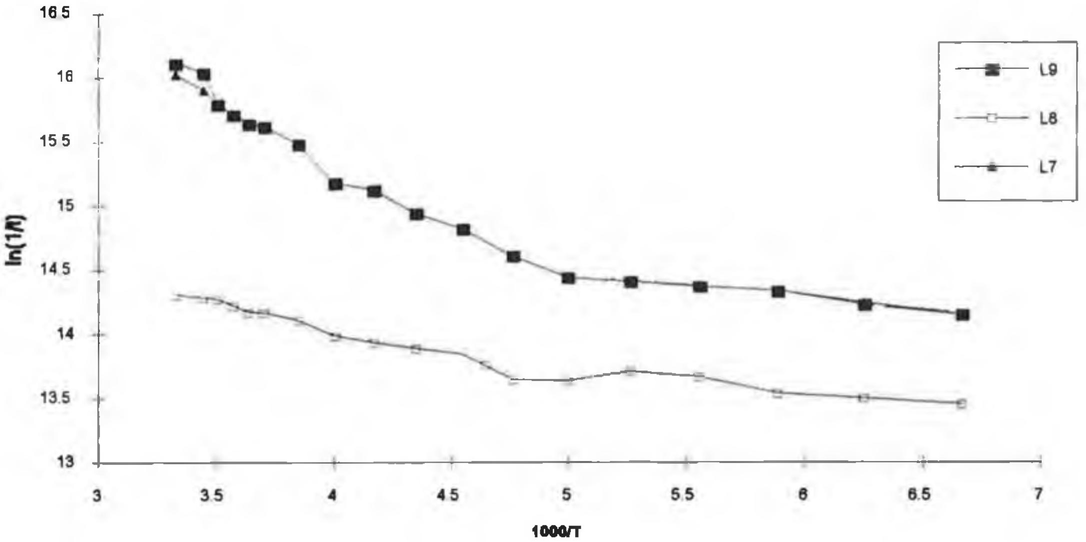

Figure 4.19 Luminescent lifetime temperature dependent plots of $[Ru(bpy)_2(HL7)]^+$ (L7), $[Ru(bpy)_2(HL8)]^+$ (L8), and $[Ru(bpy)_2(HL7)]^+$ (L9). The unmarked line in pale blue is the normalised line of L8.

(blue) line, where it is normalised to coincide with L7 and L9. From figure 4.19, it is apparent that $[Ru(bpy)_2(HL7)]^+$ and $[Ru(bpy)_2(HL9)]^+$ exhibit almost identical temperature dependent behaviour. This in itself is interesting, however, what is more curious is the considerable difference between these two complexes and $[Ru(bpy)_2(HL8)]^+$. Both $[Ru(bpy)_2(HL7)]^+$ and $[Ru(bpy)_2(HL9)]^+$ exhibit relatively strong temperature behaviour from approximately 200 K. $[Ru(bpy)_2(HL8)]^+$ on the other hand show little temperature dependent behaviour over the entire range investigated. The results of the temperature dependent data for $[Ru(bpy)_2(HL8)]^+$ reveal a complex which is strictly class (i). E_a at 235 cm^{-1}, and the small preexponential factor (9.29 $x10^6$ s^{-1}) indicate that this complex should be essentially photostable

It was not possible to create a chart of relative energy levels on the basis of the complexes described here, since unlike the pyridyltriazole complexes described in Chapter 3, with the possible exception of $[Ru(bpy)_2(HL2)]^+$ it was not possible to say for certain whether the E_a values related to the $E(t_{2g})$-$(e_g{}^*)$.

4.3.7 Photochemical stability.

In photochemical devices based on the Graetzel cell [55], the photostability of the potential sensitiser species has become less important. However, photostability remains a bonus, and may be important in other applications. The photostability of the some of the complexes discussed were investigated in order to verify some of the conclusions made from the temperature dependent data. The photostability of $[Ru(bpy)_2(o,nHL2)]^+$ was investigated in both acetonitrile and dichloromethane/Cl^-. For this complex photolyses over 6 hours revealed no appreciable decomposition in either media, and as the temperature dependent data suggested, this complex is deemed essentially photostable. For $[Ru(bpy)_2(o,nH_2L2)]^{2+}$, the same is true, little perceivable decomposition is observed over 6 hours continuous exposure to visible light (λ >300 nm) in either solvent.

The photochemical stability of these complexes is important since coordination via a strong σ-donor (but moderate ligand field splitter) like the phenolates, has allowed the formation of complexes with intense, broad visible absorbance spectra without loss of

The photochemical stability of these complexes is important since coordination via a strong σ-donor (but moderate ligand field splitter) like the phenolates, has allowed the formation of complexes with intense, broad visible absorbance spectra without loss of photochemical stability. Previous accounts of complexes with good visible spectral features have largely involved class a ligands (good π-acceptors and weak σ-donors), such as the biquinolines and bipyrazines [2, 3, 5]. In many cases as a result of strong M-L backbonding the t_{2g} level is strongly stabilised and the t_{2g}-e_g* gap is small making the ^{3}MC level easily accessible, hence photochemical reaction is regularly a feature of these species. In this instance although O^- is not a strong ligand field splitter, it cannot accept π-backbonded electron density. The result is good visible absorbance without the occurrence of photochemical instability. This was reflected in the absence any significant photochemistry in the complexes $[Ru(bpy)_2(HLx)]^+$, where x is 7, 8 or 9, over several hours photolyses in a variety of solvents.

4.4 Conclusions.

A series of novel Ru(II)bisbipyridyl complexes has been prepared in which the heteroligands, either hydroquinone-pyrazoles or phenol pyridyltriazole, were O,N coordinated to the metal centre. All complexes discussed exhibited intense broad range visible absorbance spectra in which the ^{1}MLCT transition showed little variation with ligand. Until now the main problem facing such O,N coordinated complexes has been lack of luminescence [17, 34], these complexes luminesce both at cryogenic and at room temperature. They exhibit unprecedented lifetimes > 300 ns at room temperature under argon atmosphere, and >3 μs at 77K.

On the basis of electrochemical studies the MLCT transitions responsible for their absorbance and luminescence are bpy based. $[Ru(bpy)_2(o,nHL2)]^+$ exhibits pH dependent luminescent spectra, whereby protonation of triazole and deprotonation of the phenol cause strong decreases in luminescent intensity, the pyrazole-hydroquinone complexes

4.5. References.

[1] C. Kutal, *J. Chem. Ed.*, 60, 10, 883, 1983.

[2] F. Barigelletti, A. Juris, V. Balzani, P. Belser, A. von Zelewsky, *Inorg. Chem.* 22, 3335, 1983.

[3] A. Juris, F. Barigelletti, V. Balzani, P. Belser, A. von Zelewsky, *Inorg. Chem.*, 24, 202, 1985.

[4] G.H. Allen, R.P White, D.P. Rillema, T.J. Meyer, *J. Am. Chem. Soc.*, 106, 2613, 1984.

[5] D.P. Rillema, G.H. Allen, T.J. Meyer, D. Conrad, *J. Am. Chem. Soc.*, 22, 1617, 1988.

[6] A.M. Bond, M. Haga, *Inorg. Chem.*, 25, 4507, 1986.

[7] T. Ohno, K. Nozaki, M. Haga, *Inorg. Chem.*, 31, 548, 1992.

[8] M. Haga, T. Ano, T. Ishizaki, K. Kano, K. Nozaki, T. Ohno, *J. Chem. Soc., Dalton Trans.*, 263, 1994.

[9] B.P. Sullivan, D.J. Salmon, T.J. Meyer, J. Peedin, *Inorg. Chem.*, 18, 3369, 1979.

[10] J.G. Vos, J.G. Haasnoot, G. Vos, *Inorg. Chim. Acta*, 21, 155, 1983.

[11] P.J. Steel, F. Lahousse, D. Lerner, C. Marzin, *Inorg. Chem.*, 22, 1488, 1983.

[12] R. Hage, R. Prins, J.G. Haasnoot, J. Reedijk, J.G. Vos, *J. Chem. Soc., Dalton Trans.*, 1389, 1987.

[13] P.J. Steel, E.C Constable, *J. Chem. Soc., Dalton Trans.*, 1389, 1990.

[14] A. J. Downard, G.E. Honey, P.J. Steel, *Inorg. Chem.* 30, 3783, 1991.

[15] P.H. Merrell, R.A. Osgood, *Inorg. Chim. Acta*, L33, 1975.

[16] P.H. Merrell, *Inorg. Chim. Acta*, 32, 99, 1979.

[17] M. Haga, *Inorg. Chim. Acta*, 75, 29, 1983.

[18] A.M. El Handawy, Polyhedron, 10, 21337, 1991.

[19] G. Juriga, M. Sattgast, M.E. McGuire, *Inorg. Chim. Acta*, 183, 39, 1991.

[20] M.J. Ridd, D.J. Gakowski, G.E. Sneddon, F.R. Keen, *J. Chem. Soc., Dalton Trans.*, 1949, 1992.

[21] S.Ernst, P. Hanel, J Jordanov, W. Kaim, V. Kasack, E. Roth, *J. Am. Chem. Soc.*, 111, 1733, 1989.

[22] G.G Sadler, N.R. Gordon, *Inorg. Chim. Acta*, 180, 271, 1991.

[23] C.A. Howard, M.D. Ward, Angew. Chem. Int., Ed. Eng., 31, 1028, 1992.

[24] R.B. Salmonsen, A. Abelleira, M.J. Clarke, *Inorg. Chem.*, 23, 385, 1984.

[25] M. Haga, E.S. Dodsworth, A.B.P. Lever, *Inorg. Chem.*, 25, 447, 1986.

[26] H. Masui, A.B.P. Lever, P.R. Auburn, *Inorg. Chem.*, 30, 2402, 1991.

[27] P.S. Dobbin, R.C. Hider, Chem. in Brit., 28, 6, 565, 1990.

[28] H.W. Sternberg, R. Markby, I. Wender, *J. Am. Chem. Soc.*, 80, 1009, 1958.

[29] A. Dei, D. Gatteschi, L. Pardi, *Inorg. Chem.*, 29,1442, 1990.

[30] C. Pierpont, R.M. Buchanan, *Coord. Chem. Rev..*, 38, 45, 1981.

[31] J.C. Jeffery, M.D. Ward, *J. Chem. Soc., Dalton Trans.*, 2119, 1992.

[32] J.C. Jeffery, E. Schatz, M.D. Ward, *J. Chem. Soc., Dalton Trans.*, 1921, 1992.

[33] B.M. Holligan, J.C. Jeffery, M.K. Norgett, E. Schatz, M.D. Ward, *J. Chem. Soc., Dalton Trans.*, 3345, 1992.

[34] D.A. Bardwell, D. Black, J.C. Jeffery, E. Schatz, M.D. Ward, *J. Chem. Soc., Dalton Trans.*, 2321, 1993.

[35] J.P. Maher, J.A. McCleverty, M.D. Ward, A. Mlodarczyk, *J. Chem. Soc., Dalton Trans.*, 143, 1994.

[36] R. Hage, J.G. Haasnoot, J. Reedijk, R. Wang, E.M. Ryan, J.G. Vos, A.L. Spek, A.J.M. Duisenberg, *Inorg. Chim. Acta*, 174, 77, 1990.

[37] J. Catalan, F. Fabero, M.S. Guijarro, R.M. Claramount, M.D. Santa Maria, M. de la Concepcion Foces-Foces, F.H. Cano, J. Elguero, R. Sastre, *J. Am. Chem. Soc.*, 112, 747, 1990.

[38] J. Catalan, F. Fabero, R.M. Claramount, M.D. Santa Maria, M. de la Concepcion Foces-Foces, F.H. Cano, M. Martinez-Ripoll, J. Elguero, R. Sastre, *J. Am. Chem. Soc.*, 114, 5093, 1992.

[39] A. Weller, Naturwissenshaften, 42, 175, 1955.

[40] T.Werner, *J. Phys. Chem.*, 83, 320, 1979.

[41] G.M. Bryant, J.E. Ferguson, Aust. J. Chem., 24, 441, 1971.

[42] P. Belser, A. von Zelewsky, Helv. Chim. Acta, 57, 239, 1971.

[43] D. Plancheral, J.G. Vos, A. von Zelewsky, J. Photochem., 36, 267, 1987.

[44] A. Juris, V. Balzani, F. Barigelletti, S. Campagna, P. Belser, A. von Zelewsky, *Coord. Chem. Rev.*., 93, 245, 1988.

[45] C. Long, J.G. Vos, *Inorg. Chim. Acta*, 125, 131, 1984.

[46] E.M. Ryan, R. Wang, J.G. Vos, *Inorg. Chim. Acta*, 208, 49, 1993.

[47] M. Haga, E.S. Dodsworth, A.B.P. Lever, *Inorg. Chem.*, 25, 447, 1986.

[48] H. Masui, A.B.P. Lever, P. Auburn, *Inorg. Chem.*, 30, 2402, 1991.

[49] B.E. Buchanan, J.G. Vos, M. Kaneko, W.J.M. Van der Putten, J.M. Kelly, R. Hage, R.A.G. de Graaff, R. Prins, J.G. Haasnoot, J. Reedijk, *J. Chem. Soc., Dalton Trans.*, 2425, 1990.

[50] N.K. Bridge, G. Porter, *Proc. Roy. Soc.*, A, 244, 259, 1957.

[51] The Chemistry of Quinoid Compounds, Part I, Ed., S. Patai, Wiley Interscience, N.Y., 1974.

[52] H. Hughes, Ph.D. Thesis, Dublin City University, 1993.

[53] E.M. Kober, T.J. Meyer, *Inorg. Chem.*, 21, 3967, 1982.

[54] M.J. Clarke, M.G. Dowling, *Inorg. Chem.*, 20, 3506, 1981.

[55] B. O'Regan, M. Gratzel, *Nature*, 353, 737, 1991.

Chapter 5.

O,N coordinated complexes: Dinuclear Ru(II) complexes.

5.1 Introduction.

5.1.1 Electronic properties of dinuclear mixed-valence complexes.

Since the observation of stable mixed valence polynuclear metal complexes by Taube *et al*, [1-3], figure 5.1, research into the area of polynuclear ruthenium and osmium complexes has escalated dramatically.

Figure 5.1. Creutz-Taube complex [1].

The creation of interacting metal centres provides a promising avenue to creation of viable intramolecular electronic devices [4].

Classical and semi-quantum dynamical approaches to electron transfer have been discussed briefly in chapter 1. Hush successfully [5, 6] applied electron transfer theory to the interpretation of electron transfer between mixed valence bimolecular complexes. For example, in the description a bimetallic Ru(II)-Ru(III) complex bridged via a non-insulating spacer, the optically induced transfer of a metal localised electron (or hole) from one metal to another may occur. Broad, long wavelength, solvent dependent absorbances are frequently observed in mixed valent ruthenium complexes [7-9].

The activation barrier to electron transfer, as described by Marcus [10] and Hush [5] is shown in equation (5.1).

$$\Delta G^* = \left(\lambda/4\right)\left(1 + \frac{\Delta G^o}{\lambda}\right)^2 \qquad (5.1)$$

Where ΔG^{0} is the standard free energy within the complex on electron transfer, and λ is the reorganisational parameter, (defined in section 1.6, equation 1.29 to 1.30). For a self-exchange reaction, or for a symmetric mixed valence ion, equation 5.1 is simplified to

$$\Delta G^{*} = \lambda/4 \qquad (5.2).$$

Furthermore, Hush has shown that for a symmetric mixed valence ion, the relationship between optical (vertical, see figure 5.2), E_{op}, and thermal (horizontal), E_{a}, electron transfer is (5.3),

$$E_{op} = 4E_{a} \qquad (5.3).$$

For asymmetric systems,

$$E_{op} = \Delta E + \lambda \qquad (5.4)$$

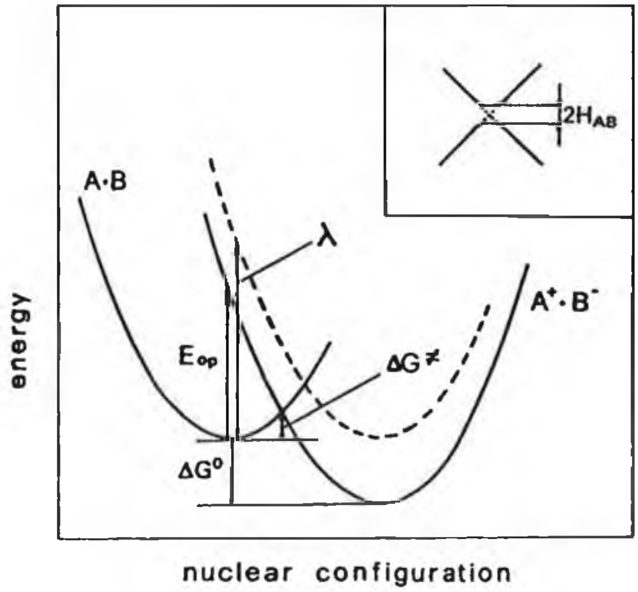

Figure 5.2 Energy profiles and kinetic parameters for intramolecular electron transfer [2].

Where E_{op} represents the energy gradient between the minima of the Ru(II)-Ru(III) and Ru(III)-Ru(II) curves (see figure 5.2) in the symmetric case $\Delta E = 0$.

The optical electron transfer band is expected to be Gaussian in shape, with a halfwidth directly related to the reorganisational energy [5, 6] according to (5.5)

$$\Delta\nu_{1/2}calc.(cm^{-1}) = [2310(E_{op} - \Delta E)]^{1/2} \quad (5.5)$$

Where $\Delta\upsilon_{1/2}$calc and E_{op} are the calculated bandwidth and energy of the intervalence band., and ΔE is the difference induced by the asymmetric environment of the molecule

Hush also correlated the intensity of the electron transfer band with the magnitude of the electronic coupling matrix element H_{AB} according to (5.6)and (5.7).

$$\varepsilon_{max} = \frac{2380d^2}{E_{op}\Delta\nu_{1/2}} H_{AB}^2 \quad (5.6)$$

therefore,

$$H_{AB} = \left[\frac{(4.2x10^{-4}.\varepsilon_{max}.\Delta\nu_{1/2}.E_{op}}{d^2}\right]^{1/2} \quad (5.7).$$

Where ε_{max} is the molar extinction coefficient for the intervalence band, d is the distance between the metal centre in angstrom, and $\Delta\upsilon_{1/2}$ the observed bandwidth at half height of the intervalence band.

Finally, the extent of delocalisation between the interacting centres α may be estimated from equation (5.8)

$$\alpha^2 = \frac{(4.2x10^{-4}).\varepsilon_{max}.\Delta\nu_{1/2}}{d^2.E_{op}} \quad (5.8).$$

The metal-metal interaction in bimetallic complexes can be categorised into three types according to the classifications of Robbin and Day [11]. This classification is reflected in the potential energy curves shown in figure 5.3(a)-(c).

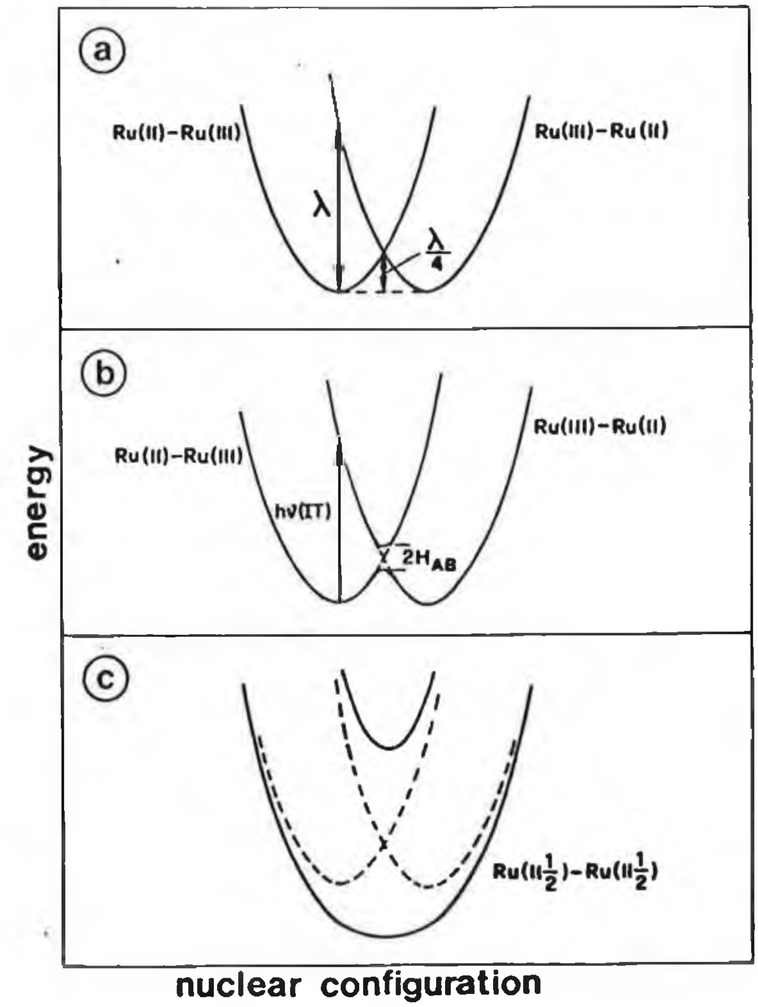

Figure 5.3. Potential energy curves of mixed valence compounds (a) with negligible, (b) weak and (c) strong electronic coupling [2].

Class I: Occurs if the inter-metal coupling (H_{AB}) is negligible compared with the reorganisational energy, for example in a complex where the bridging ligand is insulating. In class I behaviour negligible electron transfer is expected, and it is expected to be a highly activated process. The metal centres in this type of molecule act independently of one another, as isolated mononuclear complexes. In reality this type of behaviour is almost unheard of [12], possibly because few researchers are interested in making a molecule of this type.

Class II: This is the most common behaviour, and the one for which intervalence bands are observed [7-9, 13]. In this case the H_{AB} is no longer negligible but remains small, therefore the metal centres exhibit properties consistent with slightly perturbed states. These species may show new properties not observed in the isolated units, but remain essentially valence localised.

Class III: In this class the bridge supports strong coupling between the two metal centres. The limit to very large electronic coupling occurs when $H_{AB}=\lambda$, and the complexes first order curves show a single minimum at intermediate geometry (fig. 5.3(c)), corresponding to complete delocalisation of electron density which may be described as Ru(2.5)-Ru(2.5). Such species approach the line between what may be described as a supermolecule and a species which may be described as simply a large molecule [14].

Since the Hush treatment deals with both optical and thermal electron transfers, estimates may also be made of the rate of thermally induced electron transfers in these systems. Thermal electron transfer is a horizontal process. In figure 5.2 the thermal transfer occurs by passage of the electron along the lower surface passing over the activation barrier E_{th} (J). This is related to the energy of the intervalence transition according to equation (5.9);

$$E_{th} = \left[\frac{(E_{op})^2}{4(E_{op} - \Delta E)} \right] \text{-H}_{AB} \qquad (5.9)$$

Furthermore, the rate constant of thermally induced electron transfer k_{th} (s^{-1}), can be estimated from

$$k_{th} = \nu_n \exp(\frac{-E_{th}}{kT}) \qquad (5.10).$$

Where υ_n is the frequency factor (normally 5 x10^{12} s^{-1} [2]), T temperature, and k is the Boltzmann constant. Obviously, since E_{th} is exponentially related to the rate constant k_{th}, small errors in estimation of E_{th} are significantly magnified in k_{th}.

5.1.2 Dinuclear complexes containing negative bridges.

One of the problems facing the design of diruthenium (II) complexes is the creation of complexes capable of luminescence. Although not a necessary criterion for making a dinuclear electronic device, luminescence is a valuable probe for the investigation of electron and energy processes. The reason many bimolecular complexes do not luminesce [15,16] lies in the fact that for many bridging ligands the coordination of a second metal results in such a decrease of electron donation to both metals that the metal t_{2g} level is stabilised, in many cases making the ^{3}MC levels thermally accessible. The second problem associated with this phenomena is, of course, photoinstability.

Overall the aim in designing useful dinuclear metal complexes involves combining good π-orbital overlap across the bridging ligand in order to allow efficient communication between metal centres, (without creating delocalisation). Also a strong ligand field splitting ligand which will allow luminescence and prevent photoinstability. In general, strong π-acceptor bridge ligands will contribute better π-orbital continuity between metals, and a strong σ-donor bridge will create better photostability, luminescence (and also more accessible oxidation potentials). This means that a compromise must invariably be met between choosing class a or class b ligands as bridges in dinuclear complexes.

An interesting solution to this problem has been the use of triazolate bridges. They are unique in two respects, firstly, they carry a negative charge, and secondly, they are asymmetric, whereby N1' and N4 possess different σ-donation properties [17, 18]. With the quintessential of these ligands, bpt, see figure 5.4, dinuclear complexes have been prepared containing Ru [18, 19], and Ru-Os mixed metals [20, 21]. The Ruthenium-bpt dinuclear complex is found to be luminescent, but also photoactive. Most importantly, the triazolate bridge is found to support significant communication between the metal centres [19].

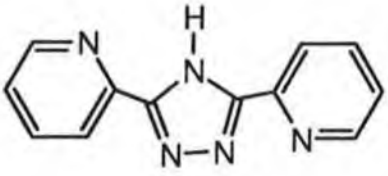

Figure 5.4. 3,5-bis(pyridin-2-yl)-1,2,4-triazole (bpt).

This strong metal-metal interaction across anionic bridges was also noted be Haga [8], and is thought to be associated with greater M(III)dπ-Lπ mixing induced by the negative bridge. This enhances the influence of oxidation of the first metal centre across the bridge to the unreduced metal. This also suggests that the influence of the bridge LUMOs is not overly important in such systems, and that intervalence transitions are predominantly hole transfers [22].

As described, luminescence provides an important probe of the excited state of a species and one of the major advantages of bpt as a bridging ligand is that the diruthenium complex is luminescent. This has allowed detailed investigation into the nature of the excited state of this species employing resonance Raman spectroscopy and temperature dependent luminescent studies. It was found for a series of mixed ligand bpy/phen complexes of bpt that the nature of the coordinating ligand determined the nature of the emitting state, and in the case of the bpy-phen compound that the excited state received contributions from both ligands. It was also noted that first metal oxidation in this complex is determined purely by the mode of coordination of the metal centres to the asymmetric bpt [23].

5.1.3 Binuclear complexes containing O,N donating ligands.

Reports of dimeric ruthenium containing O,N bound bridging ligands are rather uncommon. Although ruthenium and other transition metals such as nickel, copper and molybdenum have been bound in O coordinated binuclear complexes [24-26], these reports have for the most part been purely structural and synthetic in nature. Only a handful of reports deal with the photophysical or in particular the electrochemical properties of these complexes.

One of the earliest reports, relevant to this study, on O and N bound ruthenium binuclear complexes was made by Goldsby and Meyer in 1984 [27]. Where the two Ru centres, or mixed metal Os/Ru centres were bridged by bi and monodentate coordination though pyzc (see figure 5.5).

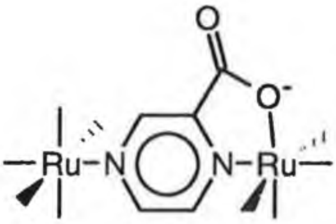

Figure 5.5. The dimeric structural unit based on 2-pyrazinecarboxylate (pyzc) [27].

The difference between the 1st and 2nd oxidation potentials for this complex is small ($\Delta E_{1/2}$ = 210 mV), and it was observed that the monodentate site is the first oxidised, although the order changes when Os is O,N coordinated. The mixed valence compounds for the Ru and mixed metal species were found to be relatively stable. Both dinuclear complexes of pyzc exhibited broad, low intensity absorbances around 1250 cm^{-1} attributed to intervalence (IT) transitions.

An O,O coordinated dinuclear ruthenium complex based on 1,4,5,8-tetraoxonaphthalene was reported by Pardi et al in 1990 [28]. The intervalence state of this complex was stable and interesting, since, as a result of the non-innocent behaviour of the bridging species, class III behaviour was exhibited. A significant contribution to this area has come from Kaim and co-workers [29,30], who have investigated a number of O,O and O,N coordinated ruthenium polypyridyl dimers, based on semiquinone ligands (see figure 5.6). Again, as a result of the electroactive nature of the bridging ligands investigated by Kaim a high degree of delocalisation was observed in these compounds.

Kaim's interpretation of the electrochemistry of these compounds was derived from analysis carried out by Lever and co-workers on their mononuclear quinone/semiquinone complexes [31-35].

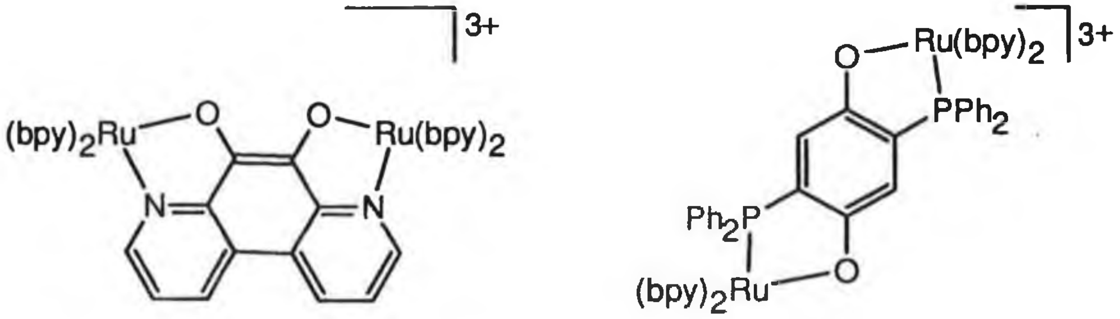

Figure 5.6. Dinuclear semiquinoid complexes reported by Kaim et al [30].

As a result of strong orbital mixing between the metals and quinone moieties definition of electrochemistry is difficult. In general in the complexes, there is no increase in redox steps compared with the free ligands and the observed processes the author associated with the ligand. The structure of the complexes at different oxidation potentials are then described as resonance forms between the metals in the 2+ and 3+ states and the ligands in the catechol, semiquinone and quinone state as a result of strong dπ-pπ mixing between the metal and quinoid ligands. This makes the assignment of spectra of the complexes at different potentials complicated, and in dinuclear complexes based on quinones, simple intervalence bands are not described [30], this interpretation is discussed in more detail in 5.3.3. What would seem to be the case for many of these species is that as result of ligand-metal orbital mixing a delocalised (class III) picture may apply [28, 30, 36]. Examples do exist however of ruthenium dinuclear complexes based on quinoid ligands which display class II behaviour [37, 38].

Examples of dimeric complexes containing O-donor ligands based on phenolates are particularly rare, some examples exist containing transition metals other than ruthenium [39, 40]. A recent example of a ruthenium dimer containing O,N donors came from Toma and co-workers [41]. Employing 3-hydroxypicolinate (figure 5.7), a ligand reminiscent of that described by Meyer et al, [27].

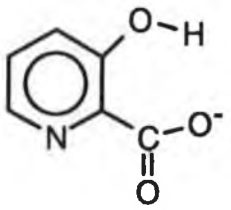

Figure 5.7. 3-hydroxypicolinate ion [42].

Both mono and dinuclear complexes bound O,O and O,N, to this ion were prepared, the latter of which showed Robin-Day class II behaviour.

This chapter reports on dinuclear complexes containing the Ruthenium(II)bisbipyridyl unit in which the coordinated ligands 3-(2-phenol)-5-(pyridin-2-yl)-1,2,4-triazole (H_2L2) and 2,5-bis(pyrazol-1-yl)-1,4-dihydroxybenzene (H_2L8) are coordinated via the oxygen and nitrogen donor sites. What is observed in each case is varying degrees of class II behaviour, which is particularly strong for the hydroquinone bridged species. A discussion of the metal-metal interaction is given in which to a large extent, the Kaim interpretation [30] is refuted.

5.2 Synthetic procedure.

5.2.1 Ligand synthesis.

The synthesis and structure of the ligands described in the text were described in chapter 3 and chapter 4.

5.2.2 complex synthesis.

$[(Ru(bpy)_2)_2(HL2)](PF_6)_3$

The N,N coordinated ligand $[Ru(bpy)_2(L2)]^+$ was synthesised first, as described in chapter 3. $[Ru(bpy)_2(L2)]^+$ (0.2g, 0.25 mmol) was then dissolved in ethanol/water (1:1, v/v) (50 cm^3) containing 0.05 M NaOH, and the solution was degassed using argon. $Ru(bpy)_2Cl_2.2H_2O$ (0.135g, 0.26 mmol) was then added to this solution and the reaction mixture heated under reflux. The reaction was monitored by HPLC, and after 5 hours was deemed to have reached completion, the starting complex $[Ru(bpy)_2(L2)]^+$ with an elution time of approximately 1.8 minutes had been replaced by the dinuclear product which took approximately 7 minutes to elute.

The reaction mixture was neutralized and reduced in volume under vacuum to approximately 10 cm^3. A concentrated aqueous solution of NH_4PF_6 was added dropwise to the product until precipitation was deemed to have ceased. The purple-brown product was then collected by filtration and washed with copious amounts of water followed by diethyl ether (30 cm^3). The product was then recrystallized from acetone/water (60:40, v/v). Yield 0.3g, 72%.

Anal. calc. for $[Ru_2C_{53}H_{46}N_{12}O_3P_3F_{18}.Na_2SO_4]$; C, 37.93; H, 2.76; N, 10.02 %. Anal. found C, 37.62; H, 2.46, N, 10.09 %. Verification of presence of Na_2SO_4, a remnant from neutralisation, was made by IR.

$[(Ru(bpy)_2)_2(L8)](PF_6)_2$

The mononuclear complex $[Ru(bpy)_2(L2)]^+$ was prepared as described in chapter 4. This (0.25g, 0.33 mmol) was then dissolved in ethanol/water (1:1, v/v) (50 cm^3) under an argon atmosphere in the presence of 0.05 M NaOH. To this solution $Ru(bpy)_2Cl_2.2H_2O$ (0.173g, 0.33 mmol) was added. The reacton mixture was refluxed under an argon atmosphere for 4 hours by which time the reaction, from HPLC was deemed complete. The reaction mixture was neutralized and the volume reduced under vacuum to approximately 10 cm^3. The deep purple product was precipitated out employing concentrated aqueous NH_4PF_6, filtered, washed and semipreparative HPLC was required to remove unreacted material. Yield 0.35g, 94%.

Anal. calc. for $[Ru_2C_{52}H_{40}N_{13}O_5P_2F_{12}.K]$; C, 42.80; H, 2.60; N, 12.4 %. Found, C, 43.12; H, 3.07; N, 12.35 %. Nitrate was deemed present from IR studies.

Preparation of mixed valence species.

The mixed valence complexes were prepared in one of two ways. Firstly, spectroelectrochemically, according to the procedure described in section 2.5, whereby the potential was held at an intermediate potential between the two metal oxidations. Secondly, the mixed valence complex was created chemically, by addition of a half equivalent of cerium(IV)sulphate to the complex in acetonitrile, followed by addition of diethyl ether followed by filtration to resolve the mixed valent complex. This method was inferior to the SEC method, since the intervalence state only lasted for an hour under these conditions, before complete oxidation occurred. This is a result of the unusually low oxidation potentials of the O,N coordinated dimers.

5.3 Results and discussion

5.3.1 ^{1}H nmr and structural characteristics.

Elucidation of the structure of $[(Ru(bpy)_2)_2(HL2)](PF_6)_3$ was not straight forward, for a number of reasons. Firstly, this complex is inherently asymmetric, therefore all 40 protons produce individual shifts in the nmr. Secondly, from the ^{1}Hnmr of the H_2L2 complex (figure 5.8), it seems likely that there are two geometric isomers present. This is further verified by the ^{1}Hnmr of the deuterated analogue, see chapter 6, where despite deuteration, the number of bpy singlets and the presence of two isomers makes the spectra complex. The isomers of $[(Ru(bpy)_2)_2(HL2)]^{3+}$ are not separated by HPLC, since the complex investigated here showed up as only one band on the HPLC trace. Nor do they appear to possess different photophysical or electrochemical properties, since lifetimes fit single exponential decays, and the electrochemistry of this complex show no extraneous waves. Such a situation has also been reported for the dinuclear complexes of bpt [42], and other dinuclear complexes [43-45] in which no differences in electronic or electrochemical properties between geometric isomers were perceived.

Fortunately, what may be ruled out is that what is observed here are coordination isomers, i.e. where in one case the O,N coordinated Ru is bound O, $N^{4'}$ and in the second O,$N^{1'}$. This is not the case, since the starting material is the N,$N^{1'}$ bound monomer which has been thoroughly structurally analysed [46], and the structure of the O,N bound monomer (chapter 4),where it is thought that the preferential binding mode is O,$N^{4'}$. Since the N,N bound complex $[Ru(bpy)_2(L2)]^+$ is stable when deprotonated, and the coordination modes of the N,N and O,N bound complexes are non interferant it is unlikely that the isomers are due to coordination differences. Furthermore, coordination isomer are known to possess different retention times on HPLC and also quite different physical properties [17].

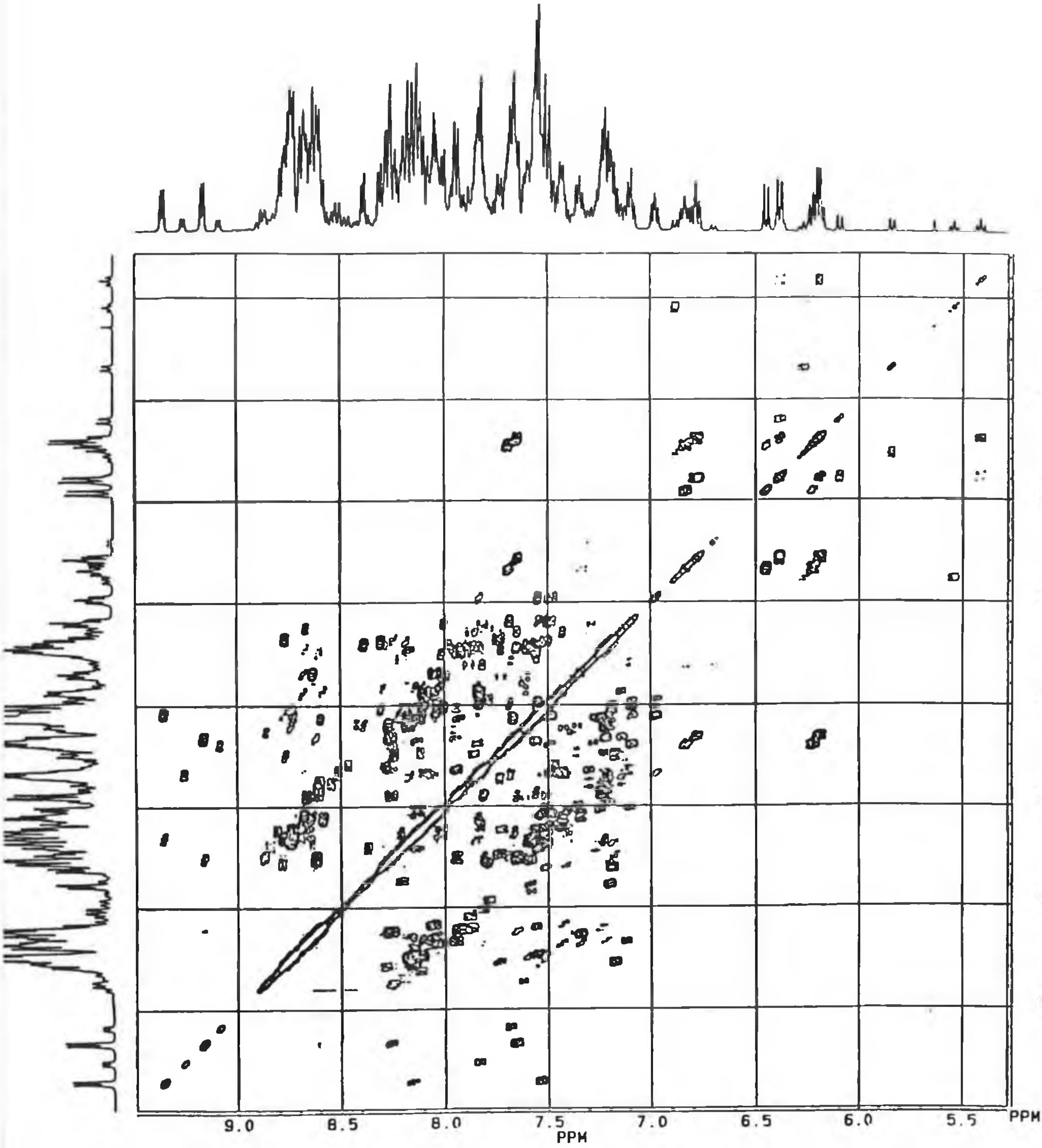

Figure 5.8 (a), ^{1}Hnmr and COSY spectra of $[(Ru(bpy)_2)_2(HL2)]^{3+}$ in acetonitrile-d_3.

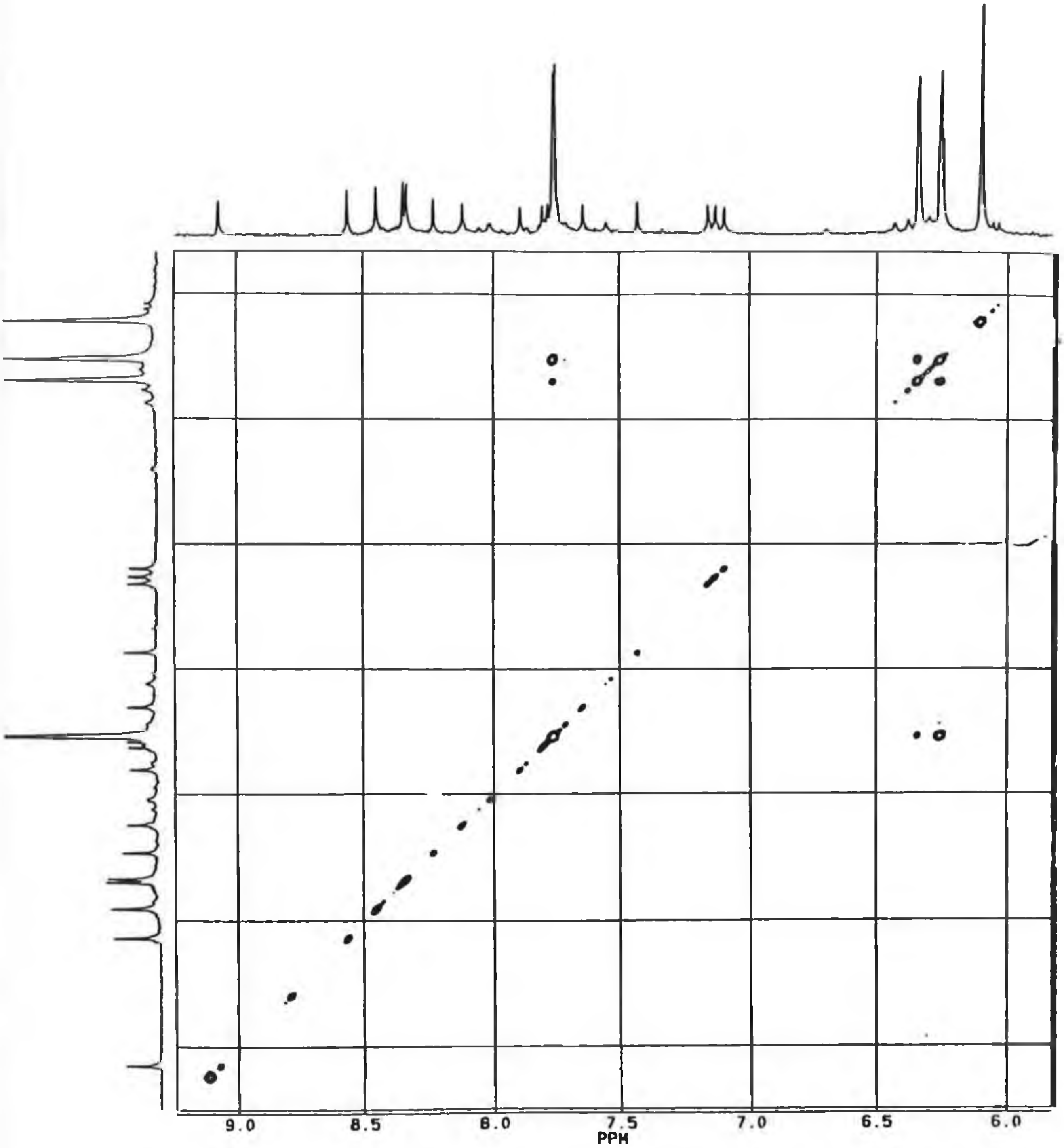

Figure 5.8 (b), ^{1}Hnmr and COSY spectra of [(Ru(d_8-bpy)$_2$)$_2$(L8)]$^{2+}$ in acetonitrile-d_3.

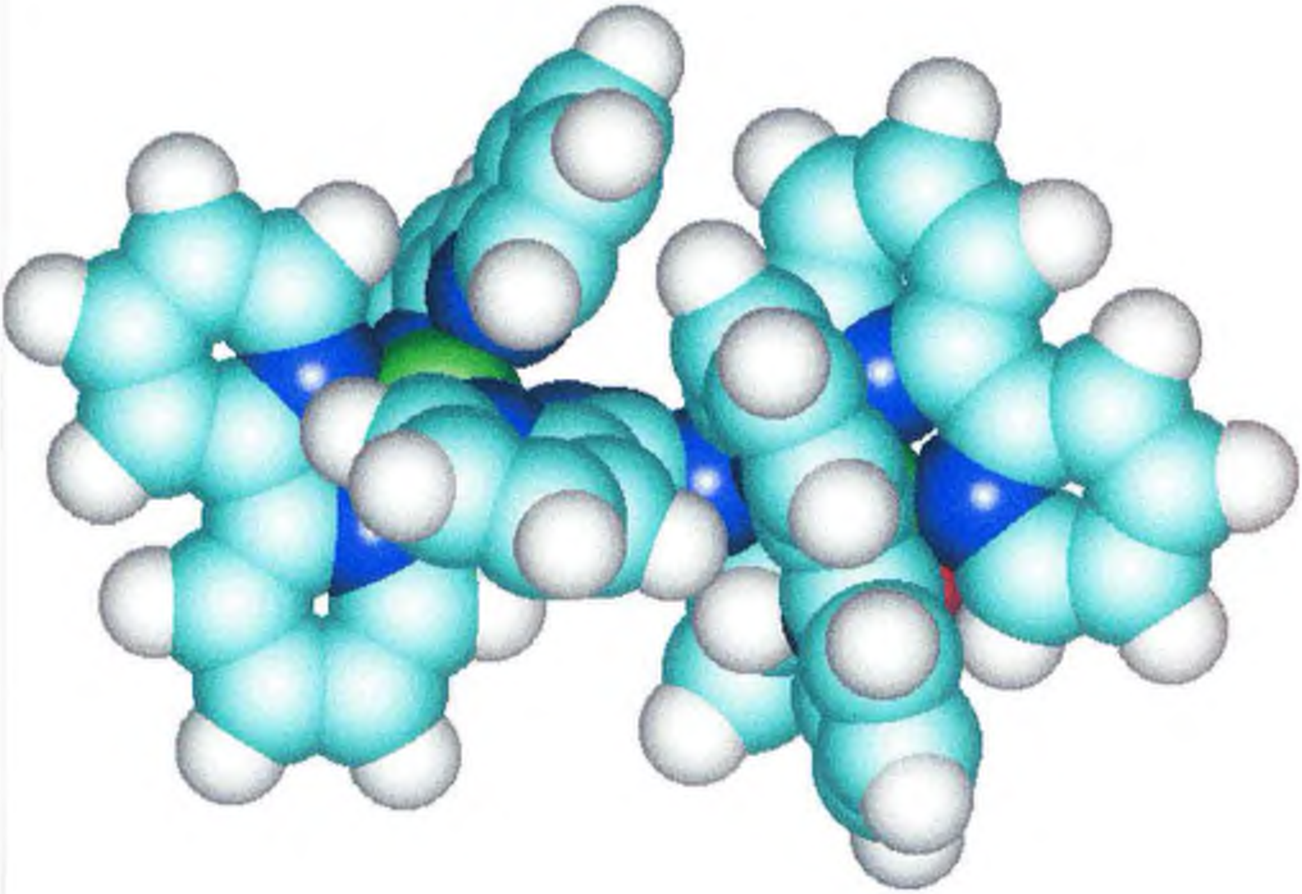

5.9(a) Computational model of [(Ru(bpy)$_2$)$_2$(HL2)]$^{3+}$ where pale blue = carbon, dark blue = nitrogen, red, = oxygen, white = hydrogen and green = ruthenium.

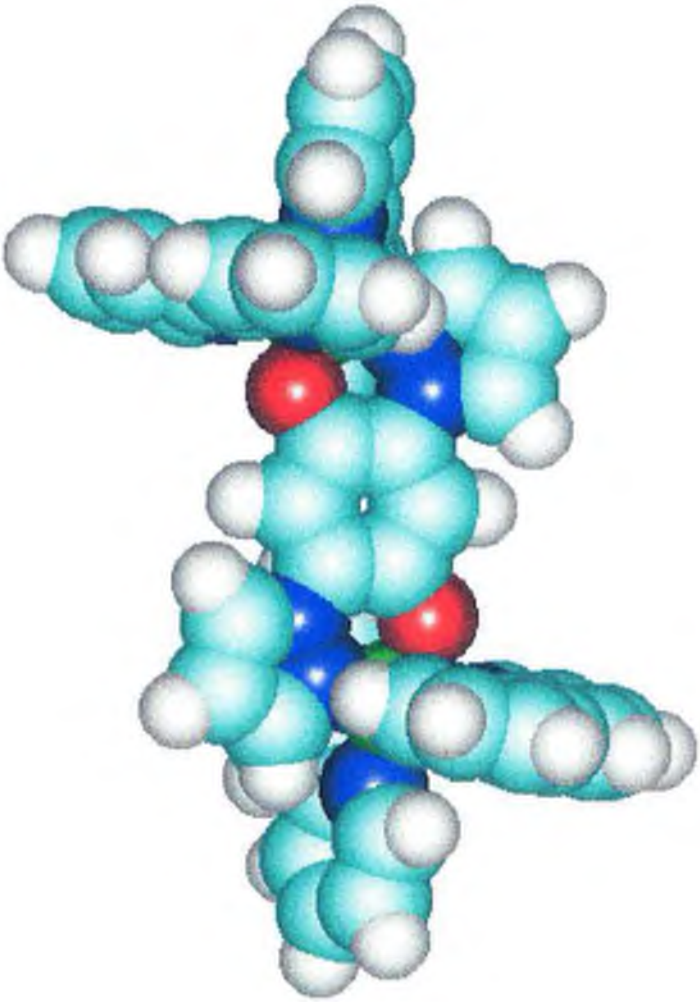

5.9(a) Computational model of $[(Ru(bpy)_2)_2(L8)]^{2+}$ *where pale blue = carbon, dark blue = nitrogen, red, = oxygen, white = hydrogen and green = ruthenium.*

A full assignment of the ^{1}Hnmr of $[(Ru(bpy)_2)_2(HL2)]^{3+}$ therefore was not possible. However, figure 5.9(a) shows the computational model of $[(Ru(bpy)_2)_2(HL2)]^{3+}$.

For $[(Ru(bpy)_2)_2(L8)]^{2+}$, structural elucidation was considerably easier. No geometric isomers were formed and the structure is completely symmetric, this point is illustrated exceedingly well by the computational model for this species, see figure 5.9(b). The symmetry (C_{2v}) of this complex is also apparent in its ^{1}Hnmr, only 4 resonances (each integrated for 2 protons) are observed for the coordinated ligand, these shifts are shown in figure 5.8(b) in the ^{1}Hnmr of the deuterated analogue. Employing the numbering system described in chapter 4, the hydroquinone protons, H^6 and H^3 are observed as a singlet at 6.1 ppm (7.27 free ligand), pyrazole $H^{3'/3''}$ is at 6.4 ppm (free ligand = 7.78 ppm), and $H^{4'/4''}$ appears as a triplet at 6 3 (6.57 free ligand), and $H^{5'/5''}$ appears as a doublet at 7.9 ppm (8.24 free ligand). It is evident that in each instance dinuclear coordination produces an upfield shift in the ligand resonances for $[(Ru(bpy)_2)_2(L8)]^{2+}$. This is particularly so for the hydroquinone protons which shift by -1.17 ppm on coordination and the pyrazole $H^{3/3''}$ protons which change by -1.38 ppm. The large shifts in these cases are due to the proximity of these protons to the coordinating sites and the amount of back donation from the ruthenium(II) centre to the ligand.

5.3.2 Photophysical and electronic properties.

The spectrum shown in figure 5.10 is of complex $[(Ru(bpy)_2)_2(L8)]^{2+}$, and is representative of the spectra of these complexes. The λ_{max} is around 480 nm and an intense shoulder is observed at around 560 nm which tails to approximately 800 nm.

The electronic and photophysical properties of the dinuclear complexes are shown in table 5.1.

Table 5.1. Electronic and photophysical properties

Complex	**Absorbance**	**Emission**	**λ_{max}**	**τ (ns)**		**ϕ_{em}**
	λ_{max} nm	**(nm)**				
	(ε*)	**RT**	**77K**	**RT**	**77K**	
$[(Ru(bpy)_2)_2(HL2)]^{3+}$	479 (0.74)	660	620	108	3860	1.1 x10^{-4}
$[(Ru(bpy)_2)_2(L8)]^{2+}$	480 (0.83)	660	620	93	4390	1.4 x10^{-6}
$[(Ru(bpy)_2)_2(bpt)]^{3+}$	453 (1.85)^{A}	648	608	100	3600	2 x10^{-3}

*Values in parenthesis are e_{max} x 10^{-4}. ^{A}Values taken from ref. [18].

Visually, the compounds are black/brown, therefore, like their mononuclear analogues, they possess intense broad spectrum visible absorbances. Making them possible candidates as solar sensitiser materials.

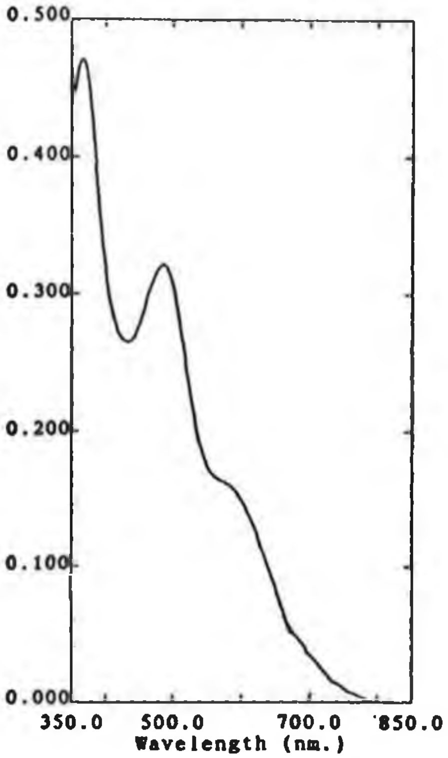

Figure 5.10. Absorbance spectra for $[(Ru(bpy)_2)_2(L8)]^{2+}$ in acetonitrile.

Unlike $[(Ru(bpy)_2)_2(bpt)]^{3+}$ there is very little difference between the spectra of the mono and dinuclear complexes. In $[(Ru(bpy)_2)_2(bpt)]^{3+}$ as a result of the reduction of electron density "experienced" by each metal in the dinuclear complex, the spectra is blue shifted by approximately 30 nm with respect to the mononuclear analogue. The absence of significant change in the spectra of the O,N dimer $[(Ru(bpy)_2)_2(L2)]^{3+}$ is associated with the fact that the phenolate is remote from the second metal centre, and its donor ability remains largely unaffected.

The same argument applies to $[(Ru(bpy)_2)_2(L8)]^{2+}$, the influence of the binding hydroxylates is largely unaffected by complexation of a second metal.

In mono and binuclear ruthenium complexes bound to quinone moieties the long wavelength shoulder in the electronic spectra of these complexes has been attributed to a π-(catecholate(or phenolate))-π^*(bpy) transition [30], and the possibility exists that this is the transition observed at long wavelengths for $[(Ru(bpy)_2)_2(L2)]^{3+}$, and in fact all its mononuclear isomers. If this is the correct assignment for this transition, then in fact what would be expected is an increase in intensity of this transition in the dimer with respect to the monomer. In fact the molar extinction coefficients of both mono and dinuclear complexes are identical in $[(Ru(bpy)_2)_2(L2)]^{3+}$.

What is particularly important, is the fact that the complexes discussed here all emit, the intensity of emission at room temperature is low, nonetheless the lifetimes are almost identical to that of $[(Ru(bpy)_2)_2(bpt)]^{3+}$. At low temperature the emissions are particularly intense, with lifetimes approaching 4 μs. Interestingly, the emission wavelengths, unlike the associated absorbances, exhibit a blue-shift of approximately 20 nm which is consistent with normal changes observed, for example, in bpt mono and dinuclear complexes [47]. Emissions are also at wavelengths which would imply overlap between the emission and low energy tail of the absorbance spectra, this is the case for both mono and dinuclear complexes discussed here. This would imply that the long wavelength shoulders observed for these complexes are not associated with the emission, and in fact the excitation spectra confirm this, since they indicate that absorbances around 450-490 nm are associated with the emission. Excitation at wavelengths longer than 490 nm produce only very weak emission. The excitation and emission spectra for the O,N complexes are red-shifted with respect to $[(Ru(bpy)_2)_2(bpt)]^{3+}$ which is what is expected for O-donor ligands, on the basis of their weaker Δ_o splitting ability. However, that the very long wavelength shoulder is not responsible for emission implies that it is not a $Ru(t_{2g})$-π^*(bpy) transition. Therefore it seems more probable that the long wavelength transition in these complexes is associated with a (hydroquinone)π-π^*(bpy) transition for the pyrazole-hydroquinone complexes, and a (phenolate)π-π^*(bpy) transition for the O,N H_2L2 complexes. Resonance Raman should conclusively resolve this assignment for these complexes.

5.3.2 Temperature dependence and photochemical stability.

Temperature dependence followed Arrhenius behaviour.

$$1/\tau = k_o + A\exp(-E_a/kT) \qquad (5.11)$$

Table 5.2 displays the data from temperature dependent luminescent studies of the complexes discussed.

For $[Ru(bpy)_3]^{2+}$, E_a represents the energy of activation to the deactivating ^3MC state, and A represents the rate of radiationless deactivation from this state. It is well established that $[Ru(bpy)_3]^{2+}$ is a photoactive species [48, 49], and the E_a and A values for this species are representative of complexes that are particularly susceptible to photochemically induced decomposition.

Table 5.2 Temperature dependent luminescence data for dinuclear complexes.

Complex	**Ea (cm^{-1})**	**A (s^{-1})**	**k_0 (s^{-1})**	**k_{nr} (s^{-1})**	**k_r (s^{-1})**
$[Ru(bpy)_3]^{2+*}$	3960	1.3 x 10^{14}	5.6 x10^5	1.3 x10^5	8 x10^4
$[(Ru(bpy)_2)_2(HL2)]^{3+}$	950	2.72 x10^{12}	1.29 x10^6	1.28 x10^6	2.51 x10^3
$[(Ru(bpy)_2)_2(L8)]^{2+}$	1380	6.99 x10^{12}	1.25 x10^6	1.25 x10^6	45.2
$[(Ru(bpy)_2)_2(bpt)]^{3+*}$	3200	8.2 x10^{13}	2.4 x10^5	2.4 x10^5	3.6 x10^4

* Values taken from reference [18], determined.

As a result of the distribution of the negative charge on the triazolate bridge, between both metal centres, in $[(Ru(bpy)_2)_2(bpt)]^{3+}$, this complex behaves in a way similar to the its protonated mononuclear analogues. Since in both complexes the strong σ-donation to the metal, and hence destabilisation of t_{2g}, is reduced and facile population of the destructive ^{3}MC states occurs at temperatures above 250 K. Therefore, like $[Ru(bpy)_3]^{2+}$, the temperature dependent data for $[(Ru(bpy)_2)_2(bpt)]^{3+}$ represents a compound which is photochemically unstable. The temperature dependent luminescent behaviour of the O,N coordinated dimers discussed, is displayed in figure 5.11.

Compared with the behaviour of their mononuclear analogues, the dinuclear complexes exhibit a marked temperature dependence at temperatures above 220 K. As described in chapter 4, the mononuclear complexes $[Ru(bpy)_2(L8)]^+$, and $[Ru(bpy)_2(o,nHL2)]^+$ show little temperature dependence, and are essentially photostable complexes.

However, despite their temperature dependence relative to their monomeric analogues, the dinuclear complexes show less temperature dependence relative to the bpt dimer and $[Ru(bpy)_3]^{2+}$.

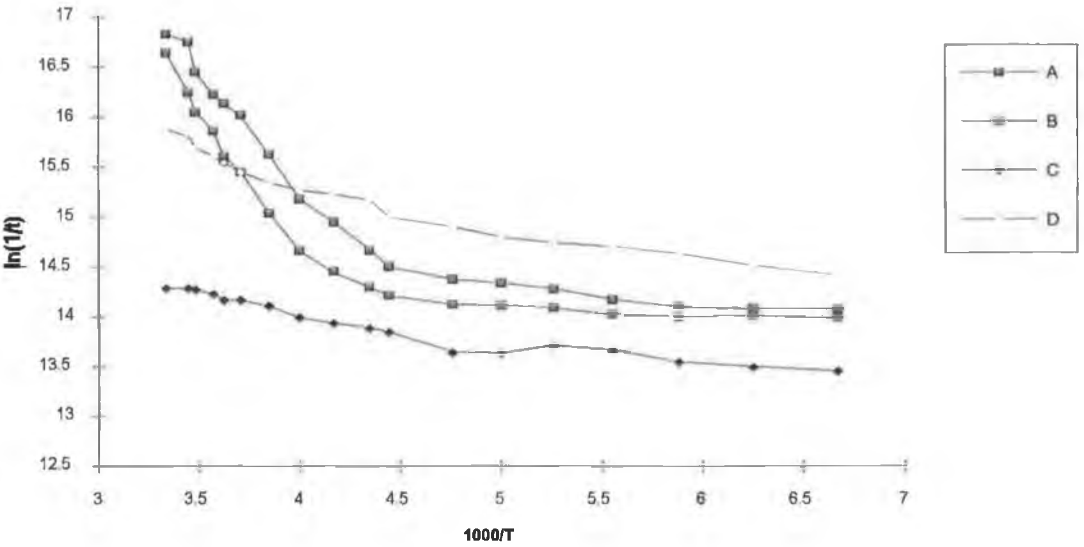

Figure 5.11. Temperature dependent behaviour of the dinuclear complexes and their analogous monomers, where A = $[(Ru(bpy)_2)_2(L8)]^{2+}$, *B =* $[(Ru(bpy)_2)_2(L2)]^{3+}$, *C =* $[Ru(bpy)_2(L8)]^{+}$, *and D =* $[Ru(bpy)_2(o,nHL2)]^{+}$.

E_a for $[Ru(bpy)_2(L8)]^+$, and $[Ru(bpy)_2(O,NL2)]^+$ are 1380 and 950 cm^{-1} respectively, with A of 6.99 $x10^{12}$, and 2.72 $x10^{12}$ s^{-1} respectively. Whereas $[(Ru(bpy)_2)_2(bpt)]^{3+}$ and $[Ru(bpy)_3]^{2+}$ possess E_a values greater than 3000 cm^{-1}, and A values around 1 $x10^{13}$ s^{-1}. This is suggestive of intermediate behaviour on the part of the O,N dimers where an equilibrium exists between electron transfers between the ^{3}MC and ^{3}MLCT states.

In both cases, the perturbation of photophysical properties caused by substitution of a second metal species is evident. The extent of perturbation on coordination of a second metal, in particular, in the case of $[Ru(bpy)_2(O,NL2)]^+$ is not as strong as dimerisation of for example, bpt. The smaller perturbation in each case may be a result of the particularly strong σ-donor ability of the hydroxylate sites. In $[Ru(bpy)_2(O,NL2)]^+$, although both metals share the triazolate bridge, the O,N coordinated Ru(II) centre does not require the same extent of triazole electron density as the N,N coordinated side Therefore, addition of a second metal causes significantly smaller changes in the photophysical properties of the complex by comparison with the bpt complex where the major source of σ-donation and destabilisation of the metal levels is shared roughly equally between both metals. The same argument may be applied to H_2L8, it contains two strong σ-donor sites, the pyrazoles, remote from one another and the metal's common bridge the hydroquinone, contains two negative sites. This provides the ruthenium with considerable electron density, capable of maintaining two metal centres.

5.3.3 Electrochemistry and Spectroelectrochemistry.

The electrochemical data for the complexes discussed are shown in table 5.3. Figure 5.12 and 5.13 show the electrochemistry of the dinuclear complexes discussed. Each complex exhibits four reductions associated with the bipyridyls.

In each instance two reversible oxidations are observed which are associated with the oxidation of $Ru^{(III)/(II)}$. In the case of $[(Ru(bpy)_2)_2(L2)]^{3+}$ one irreversible oxidation at 1.44V, and two irreversible oxidations for $[(Ru(bpy)_2)_2(L8)]^{2+}$ at 1.0 and 1.52 V are observed. These are tentatively assigned as ligand-based oxidations most likely associated with the bound hydroxyl groups. In each instance, the oxidation potentials for O^- are very anodic. This may be associated with the fact that they are bound to Ru(III) whose oxidation precedes them. The hydroxylate groups are capable of stabilisation of ruthenium in high oxidation [50] states but will themselves become difficult to oxidise since they are donating so much of their electron density to the oxidised metals.

Table 5.4 Electrochemical data for dinuclear complexes.

Complex	Oxidation potentials (V)		Reduction potentials (V)
	$Ru^{(III)}/Ru^{(II)}$	Ligand based	
$[(Ru(bpy)_2)_2(HL2)]^{3+}$	0.27, 1.0	1.44	-1.51, -1.80
$[(Ru(bpy)_2)_2(L8)]^{2+}$	0.10, 0.55	1.0, 1.52	-1.37, -1.50, -1.64, -1.83
$[(Ru(bpy)_2)_2(bpt)]^{3+}$	1.04, 1.34	-------	-1.62, -1.67, -2.23, -2.33

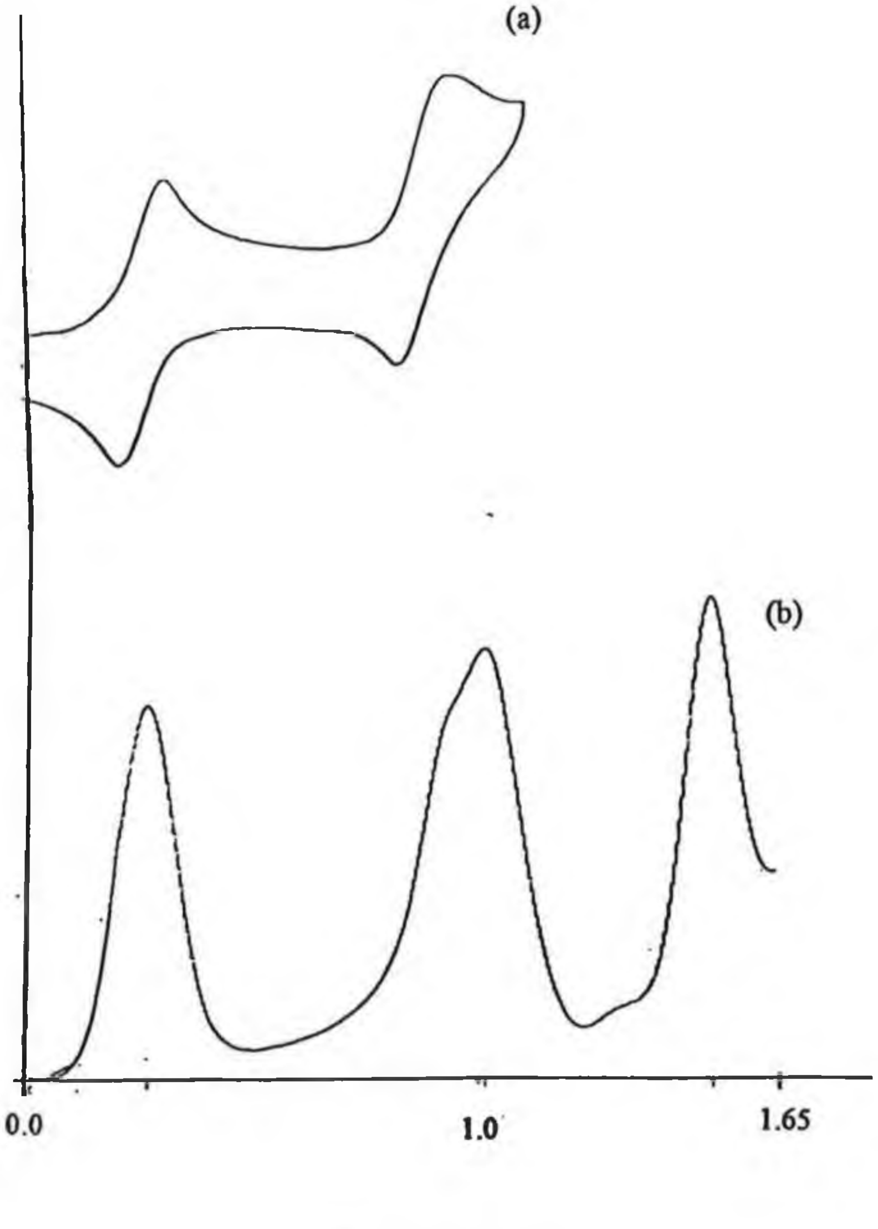

Figure 5.12, Electrochemistry of $[(Ru(bpy)_2)_2(HL2)]^{3+}$ *in acetonitrile (a) Cyclic voltammetry (b) differential pulse polarography.*

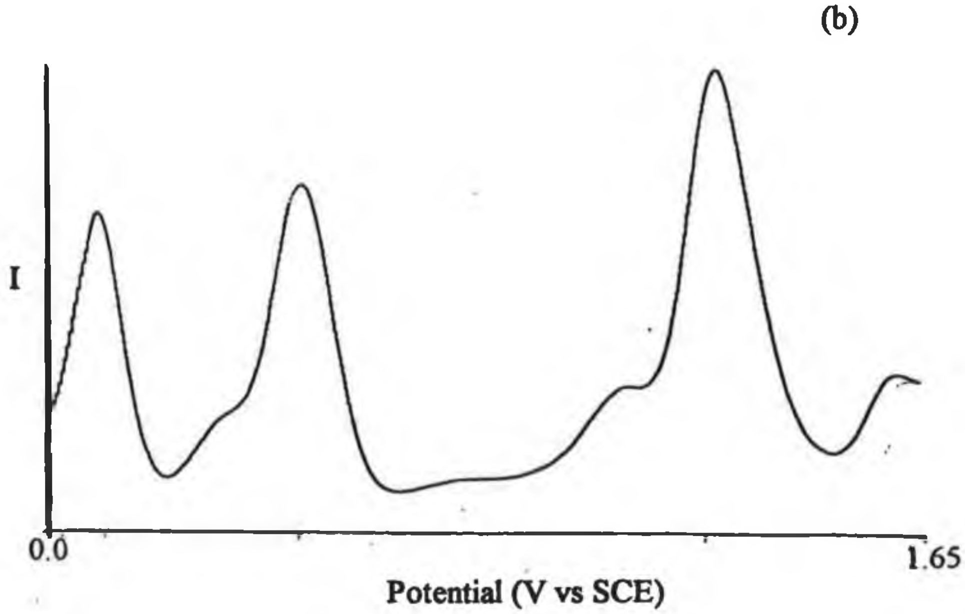

Figure 5.13, Electrochemistry of $[(Ru(bpy)_2)_2(L8)]^{2+}$ *in acetonitrile (a) Cyclic voltammetry (b) differential pulse polarography.*

For the hydroquinone-pyrazole complex $[(Ru(bpy)_2)_2(L8)]^{2+}$, discussion is complicated by the fact that there is more than one possible interpretation. In the first interpretation it is presumed that the less anodic oxidations are attributed to the two metal oxidations, whereas in the other approach, these processes may be attributed to the hydroquinone ligand. In the first instance, the former approach will be taken, while discussing both $[(Ru(bpy)_2)_2(L8)]^{2+}$ and $[(Ru(bpy)_2)_2(HL2)]^{3+}$. The alternative interpretation of the electrochemistry for $[(Ru(bpy)_2)_2(L8)]^{2+}$ will then be discussed.

In both dinuclear complexes there is considerable separation in the oxidation potentials of the two metals. This is particularly significant in $[(Ru(bpy)_2)_2(L8)]^{2+}$, since separation of such magnitude (>400 mV), of the metal oxidations in a symmetric complex implies strong communication between the two metal centres. Whereas for complex $[(Ru(bpy)_2)_2(HL2)]^{3+}$ the large difference in metal oxidation potentials may simply be due to the asymmetry of the environments of the metal centres.

In general separation of oxidation potentials in such dinuclear complexes may be attributed to;

(i) Electrostatic effects, whereby the increased positive charge on the complex as a result of the initial oxidation causes an anodic shift in the second metal oxidation.

(ii) Asymmetry in coordination sites or in the nature of the metal, (in fact the induced asymmetry on creation of a M(II)-M(III) system, which is enhanced by the different solvation shells on each end of the molecule).

(iii) Delocalization effects, communication, via for example, extension of the dπ system through the bridging π levels, means that the reduced electron density on the oxidised metal is compensated for, by delocalization of the electron density on the reduced metal, which itself becomes more difficult to oxidise.

(iv) Statistical effects, since the first oxidation can lead to either M(II)-M(III) or M(III)-M(II).

The stability of the mixed valence complex towards redox dissociation is expressed by K_c, the comproportionation equilibrium constant (5.12) [2], which may be calculated from (5.13).

$$2[Ru - LL - Ru]^{n+} \overset{K_c}{\rightleftharpoons} [Ru - LL - Ru]^{(n+1)+} + [Ru - LL - Ru]^{(n-1)+} \quad (5.12)$$

Where $$\log(K_c) = \frac{\Delta E_{1/2}}{0.059} \quad (5.13)$$

The $\Delta E_{1/2}$ and K_c values for the complexes discussed here are shown in table 5.4.

Table 5.5. Electrochemical stability of dimers in acetonitrile at 298K.

Complex	**$\Delta E_{1/2}$ (V)**	**K_c**
$[(Ru(bpy)_2)_2(HL2)]^{3+}$	0.730	2.36×10^{12}
$[(Ru(bpy)_2)_2(L8)]^{2+}$	0.450	4.24×10^{7}
$[(Ru(bpy)_2)_2(bpt)]^{3+}$	0.300	1.22×10^{5}

In order for an intervalence transition to be visible the value of K_c must be favourable. The statistical limit for the K_c value is 4, below which the intervalence state approaches instability and intervalence absorptions are unlikely [4]. This value reflects the fact that the values obtained for the dinuclear complexes discussed here, are very large. $[(Ru(bpy)_2)_2(bpt)]^{3+}$ forms a stable class II mixed valence ion, it's K_c value is large and it is deemed to exhibit strong communication between the metal centres in the mixed valent state [19].

The K_c value for $[(Ru(bpy)_2)_2(HL2)]^{3+}$ is extremely high. However, it seems likely that a significant contribution to K_c for $[(Ru(bpy)_2)_2(HL2)]^{3+}$ comes from the asymmetry of the molecule in question. SEC of the mononuclear complex (E_{ox} = 0.35 V) established the fact that the first oxidation occurs on the O-coordinated side of the molecule, since oxygen, as a result of it's strong σ-donor ability stabilises the Ru(III) state. In the mononuclear N,N coordinated complex E_{ox} occurs at approximately 1V, therefore the difference between the two mononuclear complexes is already 0.65 V, indicating that the asymmetry of $[(Ru(bpy)_2)_2(HL2)]^{3+}$ is indeed the strongest contributing factor to its unprecedented K_c.

$[(Ru(bpy)_2)_2(L8)]^{2+}$ presents quite a different situation, since this molecule is completely symmetric, and yet again, its K_c value is remarkably high. In fact a K_c value of 4.0 x10^7 was recorded for a class III complex $[Ru(NH_3)_5]_2L\text{-}L^{5+}$,[2], where L-L is shown in figure 5.12.

Figure 5.12. Bridging ligand for class III complex $[Ru(NH_3)_5]_2L\text{-}L^{5+}$ *[2].*

Spectroelectrochemistry in the vis/NIR region was carried out on the complexes discussed. The results of this work are shown in figure 5.14 and 5.15. On oxidation of the first metal in $[(Ru(bpy)_2)_2(HL2)]^{3+}$ the long wavelength visible shoulder disappears, implying that the oxygen bound metal is oxidised, and two overlapping bands centred at 832 nm and 1050 nm grow in. These two bands are maintained until 1V when the band at 1050 nm starts to decrease in intensity, along with the MLCT band in the visible. The 1050 nm absorbance persists between the oxidation of the first and second metal oxidations, it is assigned as an intervalence (IT) band. The overlapping band at 832 nm is assigned as the LMCT band since this absorbance persists throughout the potentials scanned, once the initial metal oxidation has occurred. Previous reports of ligand to metal charge transfer of this nature have been reported [51], for $[(Ru(bpy)_2)_2(bpt)]^{3+}$, this band occurs around 720 nm [19], and experiences a blue shift on oxidation of the second metal centre [8]. In $[(Ru(bpy)_2)_2(HL2)]^{3+}$ the band is red shifted with respect to $[(Ru(bpy)_2)_2(bpt)]^{3+}$, also no change is observed on oxidation of the second metal. Furthermore the absorbance is broader than that in $[(Ru(bpy)_2)_2(bpt)]^{3+}$, although width is difficult to define as a result of the overlap with the IT band. This may imply that the LMCT is of a different source to that of $[(Ru(bpy)_2)_2(bpt)]^{3+}$ where the charge transfer is expected to originate from bpy. In $[(Ru(bpy)_2)_2(HL2)]^{3+}$ it is possible that the charge transfer originates from the phenol moiety, since it is considerably easier to oxidise than either the triazole bridge or the bipyridyl moieties. As a result of the asymmetry of $[(Ru(bpy)_2)_2(HL2)]^{3+}$ ΔE (the asymmetry induced energy difference between the two metal centres) is estimated to be large, hence the IT band is rather more blue shifted than is usual for more symmetric species [19, 13] and this effect has been noted elsewhere for similarly asymmetric complexes [53]

The SEC of $[(Ru(bpy)_2)_2(L8)]^{2+}$ reveals the grow-in of an unusually intense band at 1400 nm from 0.05V which is maintained then between potentials of 0.2V and 0.55V (vs SCE). At 0.55V an intense absorbance appears at 1000 nm which continues to increase in intensity as the MLCT and band at 1440 nm collapse. The band at 1400 nm is assigned therefore, as an IT band, and that at 1000 nm as a LMCT absorbance. Interestingly, although considerably more intense, the LMCT is centered at roughly the same wavelength as that in $[(Ru(bpy)_2)_2(HL2)]^{3+}$ and is roughly the same width. This may suggest that the LMCT originates from the same source in both complexes, namely from a negative hydroxylate. The data obtained from applying the Hush analyses (equation 5.6 to 5.8) to the IT bands of $[(Ru(bpy)_2)_2(HL2)]^{3+}$ and $[(Ru(bpy)_2)_2(L8)]^{2+}$ is shown in table 5.5 along with the data reported for $[(Ru(bpy)_2)_2(bpt)]^{3+}$ [19].

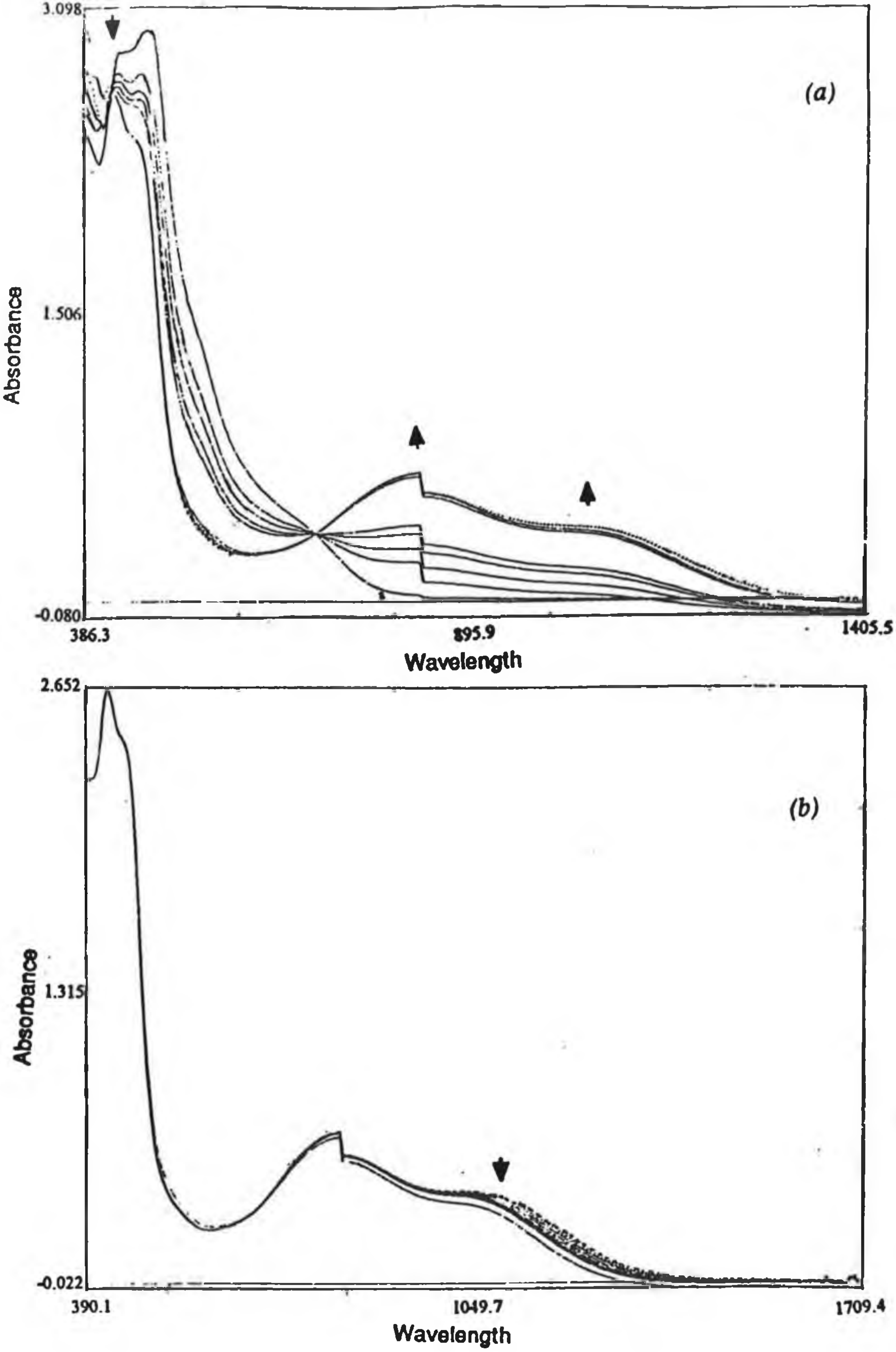

Figure 5.14. Spectroelectrochemistry of $[(Ru(bpy)_2)_2(HL2)]^{3+}$ *(a) 0.0V to 1.0V, (b) 1.0V to 1.2V.*

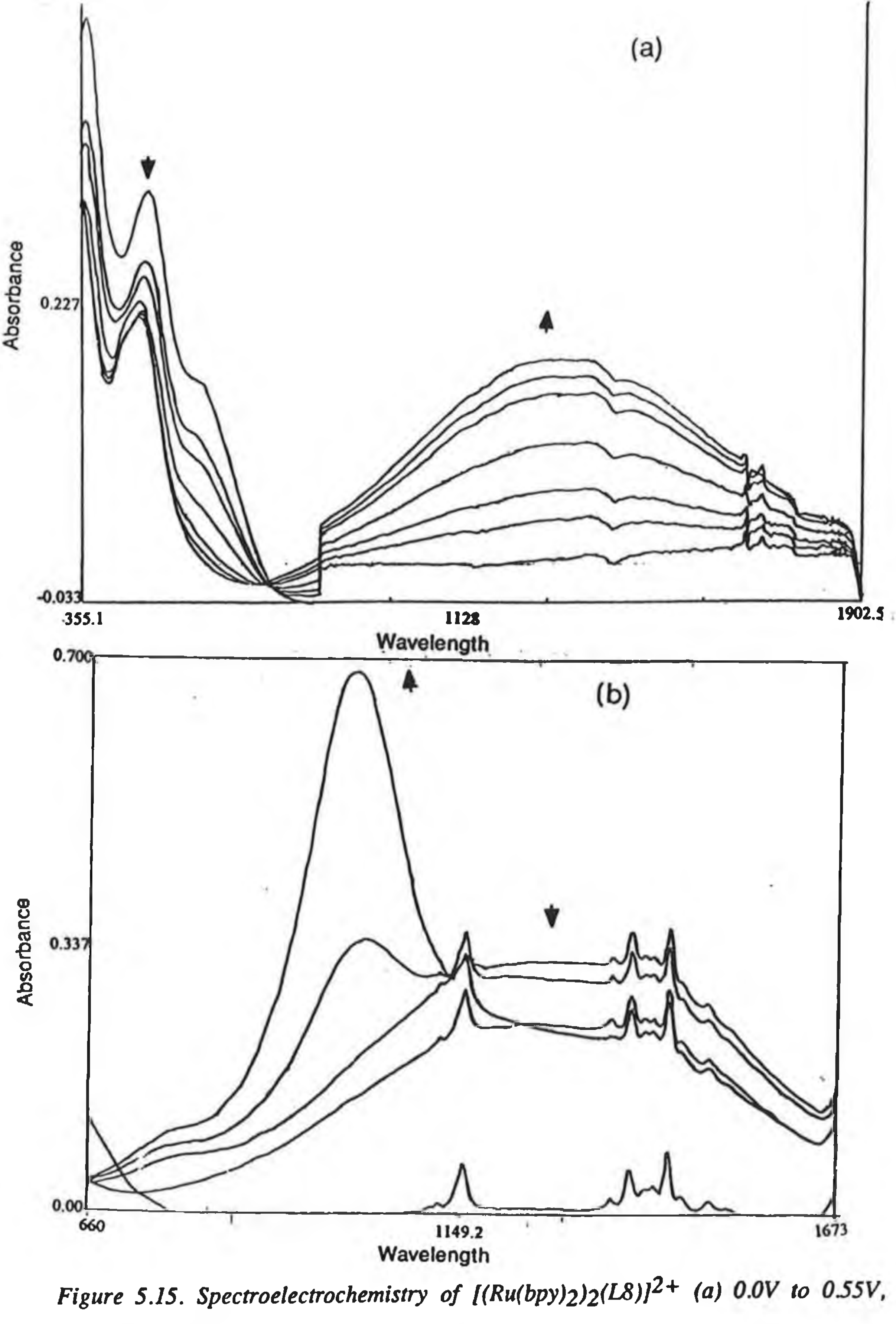

Figure 5.15. Spectroelectrochemistry of $[(Ru(bpy)_2)_2(L8)]^{2+}$ *(a) 0.0V to 0.55V, (b) 0.55V to 0.9V.*

Table 5.5 Optical properties of the intervalence transition of the mixed valence complexes.

Complex	**E_{on}** **cm^{-1}**	**ε_{max}** **$M^{-1}cm^{-1}$**	**α^{2*}**	**$\Delta\upsilon_{1/2}$ exp.** **cm^{-1}**	**$\Delta\upsilon_{1/2}$ calc.** **cm^{-1}**
$[(Ru(bpy)_2)_2(HL2)]^{3+a}$	9524	1287	0.005	3226	3676
$[(Ru(bpy)_2)_2(L8)]^{3+\ a}$	6944	4807	0.012	4112	4005
$[(Ru(bpy)_2)_2(L8)]^{3+\ b}$	7870	8338	0.014	3154	4264
$[(Ru(bpy)_2)_2(bpt)]^{3+a}$	5556	2400	0.016	3300	3580

a : Carried out in acetonitrile.

b : Carried out in dichloromethane.

* Estimated error for α^2 is 10%.

From figure 5.2, the energy of the optical transition is related to the energy gradient between the minima of states A-B and A^+-B^- (the relative values for which are obtained from the asymmetry factor ΔE, which for symmetric species is 0), and the reorganisational energy as described in equation (5.4). The phenolate complex $[(Ru(bpy)_2)_2(HL2)]^{3+}$ exhibits the highest energy transition (E_{op}) of the complexes discussed here, and this is most likely due to the contribution from the asymmetry factor, i.e. the energy gradient. For the symmetric species $[(Ru(bpy)_2)_2(L8)]^{2+}$, the optical transition energy is influenced solely by reorganisational parameters, since $\Delta E = 0$.

The asymmetry ΔE, of $[(Ru(bpy)_2)_2(bpt)]^{3+}$ is calculated to be 100 mV [52], on the basis of the difference in the $N^{1'}$ $N^{4'}$ coordination sites based on the differences in electrochemical potentials of the OsRu, RuOs complexes. The mixed metal RuOs dimers based on $[(Ru(bpy)_2)_2(HL2)]^{3+}$ have yet to be prepared, however, the differences in this complex between oxidation potentials for the mixed metal complex in which the Os is O,N and N,N bound is expected to be at least 400 mV. In order to estimate a value for $[(Ru(bpy)_2)_2(HL2)]^{3+}$, the assumption, is that the reorganisational parameters for electron transfer in $[(Ru(bpy)_2)_2(HL2)]^{3+}$ and the symmetric $[(Ru(bpy)_2)_2(L8)]^{2+}$ will be similar, since $[(Ru(bpy)_2)_2(L2)]^{3+}$ is triazole bridged like $[(Ru(bpy)_2)_2(bpt)]^{3+}$, but is O,N coordinated like $[(Ru(bpy)_2)_2(L8)]^{2+}$, the reorganisational energy for $[(Ru(bpy)_2)_2(HL2)]^{3+}$ is estimated to be an average of λ for the L8 and bpt dimers. On this assumption λ is estimated to be 3678 cm^{-1} for $[(Ru(bpy)_2)_2(L2)]^{3+}$, and ΔE for $[(Ru(bpy)_2)_2(HL2)]^{3+}$ is calculated to be 460 mV. In principle ΔE may be determined from equation (5.14).

$$\Delta E = \frac{E_{op} - (\Delta \nu_{1/2})^2}{2310} \qquad (5.14)$$

Employing this equation, the ΔE was estimated to be 560 mV, which is in relatively good agreement with the former, however, since results employing this equation have been found to be largely erroneous [2], 460 mV is employed in further calculations for $[(Ru(bpy)_2)_2(HL2)]^{3+}$ until further synthesis allows a more accurate estimate of ΔE to be made.

Comparison of the calculated band width at half height with that observed, provides information on the nature of the interaction between the metal centres. If the measured bandwidth correlates well with the calculated bandwidth (equation (5.5)) the system is valence trapped (localised). If the band is too narrow the species is delocalised and the description of the system should be $Ru^{2.5}$ - $Ru^{2.5}$. In acetonitrile for all the dinuclear species described the $\Delta\upsilon_{1/2}$calc. correlates well with $\Delta\upsilon_{1/2}$obs., implying the electron is valence trapped, and these species are class II complexes.

The remarkably intense IT transition for $[(Ru(bpy)_2)_2(L8)]^{2+}$ as well as it's high K_c value, implies large degree of delocalization. The calculated band width is larger than the observed band width in acetonitrile which implies that the metal electron density is valence trapped between the two metal centres. The extent of delocalisation α^2 is comparable to that observed for $[(Ru(bpy)_2)_2(bpt)]^{3+}$, which is without doubt a valence trapped species, although with strong interaction between the two metal centres, as a result of what is thought to be a hole transfer (possibly superexchange) mechanism across the negative triazole bridge.

Examination of the emission spectra of the mixed valence state of $[(Ru(bpy)_2)_2(HL2)]^{3+}$ revealed that the emission intensity increased significantly in the mixed valence state (see figure 5.16) this was accompanied by an doubling in luminescent lifetime from 108 ns to 200 ns. This was an unexpected result since electron or energy transfer would be expected between the coupled metal centres in the complex.. The increased emission of the mixed valence species, suggests that the M-M centres are not communicating in the excited state. Ordinarily, in a communicating M(II)-M(III) centre, energy transfer (5.15) or electron transfer (5.16) are expected to occur.

$$[(bpy)_2Ru^{II}\text{-LL-}Ru^{III}(bpy)_2]^{n+} \xrightarrow{hv} [(bpy)(bpy^{-})Ru^{III}\text{-LL-}Ru^{III}(bpy)_2]^{n+} \quad (5.15)$$

$$[(bpy)(bpy^{-})Ru^{III}\text{-LL-}Ru^{III}(bpy)_2]^{n+} \longrightarrow [(bpy)_2Ru^{III}\text{-LL-}Ru^{II}(bpy)_2]^{n+} \quad (5.16)$$

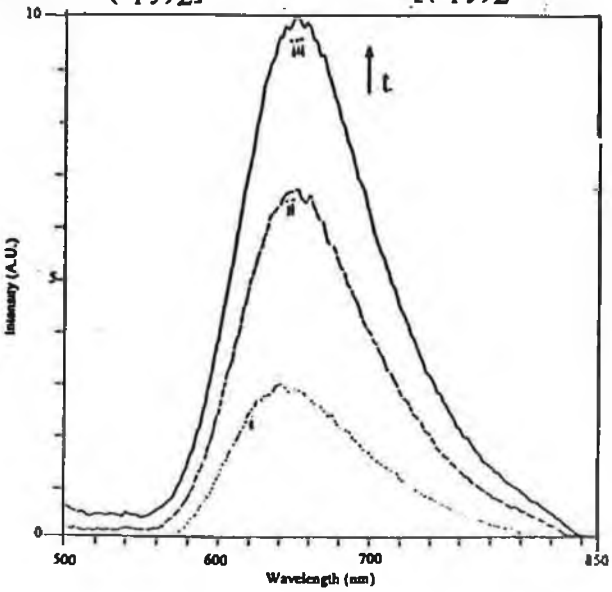

Figure 5.16 Emission spectroscopy of $[(Ru(bpy)_2)_2(HL2)]^{3+}$ in the (i) M(II)-M(II) state and (ii) and (iii) in the mixed valence state.

This is a very unusual situation, to our knowledge no other accounts exist of luminescent mixed valence compounds not to mention one in which the luminescence increases compared with the M(II)-M(II) complex. It is the N,N coordinated side of the molecule which is thought to be luminescing in this situation, since in the mixed valence species the O,N side is oxidised first, it would seem that for some reason, the small communication between the metal centres in the ground state become negligible in the excited state, allowing the N,N coordinated side to luminesce as though it were mononuclear.

The intervalence band of $[(Ru(bpy)_2)_2(L8)]^{2+}$ shows strong solvent dependence which further verifies the fact that this is not class III [2]. A strong blue shift in E_{op} occurs as well as a considerable increase in the intensity of the transition (ε_{max} almost doubles) in less polar dichloromethane, also $\Delta\upsilon_{1/2}$calc. exceeds $\Delta\upsilon_{1/2}$obs by more than 1000 cm^{-1}, suggesting delocalised behaviour. However, α^2 remains smaller than $[(Ru(bpy)_2)_2(bpt)]^{3+}$ implying that the intervalence state is still valence trapped.

The extent of delocalisation in $[(Ru(bpy)_2)_2(HL2)]^{3+}$ is small and comparison with the bpt dimer is a useful means of examining the influence of the phenolate on this species, since the triazolate forms the bridge in both complexes. From the point of view of distance, and available π-electron density, it is expected that the electron transfer would proceed via the triazole, and not the phenol. From the electrochemistry of the mononuclear complex, we know that the phenol stabilises ruthenium in the 3+ state. It is probably the fact that this state is stabilised that reduces the requirement for further stabilisation by delocalisation of electron density from the N,N coordinated Ru(II) side of the molecule. Since it is expected that the phenol will deprotonate when the ruthenium is oxidised [55]

The electronic coupling constants and thermal electron transfer parameters are displayed in table 5.7. For the calculation of k_{th}, equation 5.10 is employed in which the frequency factor υ_n is taken to be 5 x 10^{12} s^{-1} [2].

Table 5.7 Thermal properties of IT bands in MeCN at 298 K.

Complex	**ΔE (cm^{-1})**	**E_{th}* (J x10^{-20})**	**k_{th}* (s^{-1})**	**H_{AB}* (cm^{-1})**
$[(Ru(bpy)_2)_2(HL2)]^{3+}$	3678	6.39	9.03 x10^5	666
$[(Ru(bpy)_2)_2(L8)]^{2+}$	0	1.97	4.17 x10^{10}	745
$[(Ru(bpy)_2)_2(L8)]^{2+A}$	0	2.09	3.11 x10^{10}	916
$[(Ru(bpy)_2)_2(bpt)]^{3+}$	806.5	1.46	1.3 x 10^{11}	700

* Estimated errors are, H_{AB}, 10%, E_{th}, 10% and k_{th} 50%.

^{A} Values in dichloromethane.

The thermal electron transfer values for $[(Ru(bpy)_2)_2(L8)]^{2+}$ and $[(Ru(bpy)_2)_2(bpt)]^{3+}$ are clearly comparable. Further suggesting that $[(Ru(bpy)_2)_2(L8)]^{2+}$ is indeed a class II complex. As mentioned briefly, important verification of this comes from the solvent dependence displayed by this complex, it has been shown in the Creutz-Taube and other delocalised class III systems that the IT bands are largely solvent insensitive [2, 54]. This is because in delocalised systems, on the solvent reorganisational time-scale discrete Ru(II) and Ru(III) centres do not exist. The media dependence displayed by $[(Ru(bpy)_2)_2(L8)]^{2+}$ is manifested in both the band width and wavenumber of the absorbance, causing significant changes in many of the associated parameters. One of the most interesting differences is the change in observed bandwidth relative to the calculated bandwidth in the less polar solvent dichloromethane. However, although electronic coupling matrix, H_{AB} and degree of electronic delocalisation do increase for $[(Ru(bpy)_2)_2(L8)]^{2+}$ in dichloromethane, they remain indicative of a strongly coupled class II complex. The large coupling in this complex is possibly a function of the anionic nature of the bridge and strong ligand π interaction, expected in quinonoid species.

The analyses of the optical and thermal electron transfer in $[(Ru(bpy)_2)_2(HL2)]^{3+}$ are suggestive of a class II complex in which the metal-metal communication is weak. The large K_c value in this complex may be attributed in the main, to the complete asymmetry of the coordination sites. The weaker coupling in this species relative to $[(Ru(bpy)_2)_2(bpt)]^{3+}$ may be associated with the electronic stabilisation of the Ru(III) side (O,N) of the molecule by the strongly electron donating phenolate, since it is expected that the phenol will deprotonate on oxidation of the O,N metal [55].

Lever and co-workers and Pierpont and co-workers, postulated that in complexes of Ru and catecholate, extensive orbital mixing occurred between metal and ligand, which incidentally, they found decreased systematically on replacement of O-donors with N-donors [31-35]. Kaim and co-workers, described the synthesis and characterisation of the hydroquinone complexes shown in figure 5.6 [30]. Electrochemistry of these species was described in terms of unusually strong ligand mediated metal-metal interaction, whereby, the mixed valence state may be described as a resonance structure as shown in (5.17)

$$Ru^{(II)}\text{-}(SQ)\text{-}Ru^{(II)} \leftrightarrow Ru^{(II)}\text{-}(Q^{2-})\text{-}Ru^{(III)} \leftrightarrow Ru^{(2.5)}\text{-}(Q^{2-})\text{-}Ru^{(2.5)} \quad (5.17)$$

The K_c value for structure of figure 5.6(b) is 6.31×10^9 which is larger than that of $[(Ru(bpy)_2)_2(L8)]^{2+}$ by a factor of more than 100. However, the first oxidation and reduction potentials of $[(Ru(bpy)_2)_2(L8)]^{2+}$ and Kaim's complex are quite similar. However, in his interpretation Kaim associates both oxidations with those of the ligand and not the metal. As shown by equation (5.15), the strong metal-ligand delocalisation results in the creation of three possible states. What is most striking between the work reported here and that reported by Kaim is that the NIR spectroelectrochemistry of complex $[(Ru(bpy)_2)_2(L8)]^{2+}$ and that of the complex fig 5.6 (b) is almost identical. The long wavelength band at the first oxidation potential Kaim associated with Ru(dπ)-π(SOMO) transitions between the metal and the singly occupied molecular orbital (SOMO) of the semiquinone radical. The shorter wavelength band appearing on complete oxidation of the complex (called the LMCT here) Kaim assigned as Ru(dπ−π*) transition, if valid, this is an exceptionally low energy MLCT band. In Kaims interpretation, the second oxidation is associated with formation of the quinone, to produce the resonance structures shown in (5.18)

$$Ru^{(II)}\text{-}(Q)\text{-}Ru^{(II)} \quad \leftrightarrow \quad Ru^{(II)}\text{-}(SQ)\text{-}Ru^{(III)} \quad \leftrightarrow \quad Ru^{(III)}\text{-}(Q^{2-})\text{-}Ru^{(III)} \qquad (5.18)$$

Figure 5.15 shows the orbital configuration postulated to occur for the three oxidation states of the quinone in Kaim's complexes.

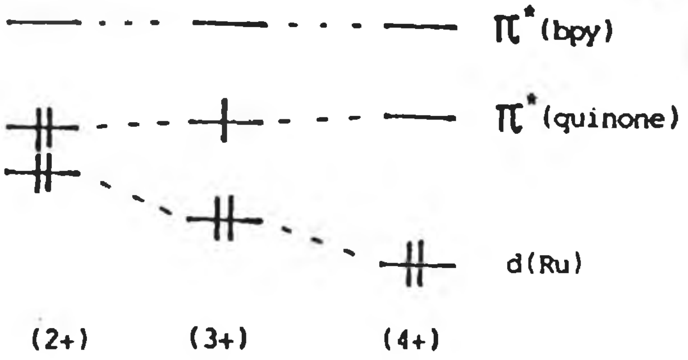

Figure 5.15. Simplified orbital diagram of the three different oxidation states of the system shown in figure 5.6 [30].

The verification of this extent of metal-ligand delocalisation was attempted by Kaim by employing EPR experiments in which as a result of extensive metal-ligand interaction, the assignment remains ambiguous. As a result of Levers and Pieronts work, there is little doubt that extensive orbital mixing occurs between metal and ligand in Ru-quinone complexes. Hence, the situation described by Kaim cannot be ruled out for

$[(Ru(bpy)_2)_2(L8)]^{2+}$ as a result of strong structural, electrochemical and spectroscopic similarities between his complexes and $[(Ru(bpy)_2)_2(L8)]^{2+}$. However, a few points are worth noting. Firstly, the K_c value for $[(Ru(bpy)_2)_2(L8)]^{2+}$ is lower than that of Kaim's complex. Secondly, application of Hush theory to $[(Ru(bpy)_2)_2(L8)]^{2+}$ suggests a complex in which the metal centres are strongly coupled but remain valence trapped, strong coupling is anticipated for a system bridged by a ligand such as hydroquinone which is capable of metal-ligand orbital mixing, since it should enhance super-exchange, however the complex is not delocalised. Thirdly, Kaim suggests resonance structures for his first and second oxidation states which involve the mixed-valent complexes, but makes assignments of spectral transitions based on the oxidation of the ligands alone and not LMCT or IT bands, which under resonance conditions could equally apply. Fourthly, since $[(Ru(bpy)_2)_2(L8)]^{2+}$ under mixed valence conditions exhibits emission, the first oxidation state cannot involve a semiquinone species, since this species will quench such luminescence, this implies that the first oxidation is metal based. Finally, $[(Ru(bpy)_2)_2(L8)]^{2+}$ exhibits strong solvent dependence which strongly suggests that this system is not delocalised.

5.4 Conclusion

From the values for α^2 and ε_{max} the interaction between the metal centres in $[(Ru(bpy)_2)_2(HL2)]^{3+}$ is considerably less than $[(Ru(bpy)_2)_2(L8)]^{2+}$. This is unexpected since the M-M distance in this complex $[(Ru(bpy)_2)_2(L2)]^{3+}$ is less than complex $[(Ru(bpy)_2)_2(HL2)]^{8+}$, and also the bridging ligand is a triazolate which is known to enhance electronic communication in other complexes [19]. The weak communication between the metals in $[(Ru(bpy)_2)_2(HL2)]^{2+}$, and the fact that luminesence increases in the mixed valence state, may be associated with the localised stabilisation of the Ru(III) state by the phenol ligand, which probably deprotonates on metal oxidation. The unusually large separation of metal redox potentials, and K_c for this complex would seem therefore, to be a result of the asymmetry of the compound.

These Ru(II) O,N co-ordinated complexes look promising as new sensitiser species for a number of reasons. Firstly, they exhibit strong absorbances over a broad visible spectrum. Secondly, both mononuclear and binuclear complexes are luminescent at room temperature. Thirdly, all of the complexes discussed show high levels of photostability.
The mixed valence binuclear complexes exhibit interaction between the metal centres. This interaction is particularly strong in $[(Ru(bpy)_2)_2(L8)]^{2+}$ where the metals are bound via anionic hydroxyls through a bridging hydroquinone. In this complex the extent of delocalization of the electron density between the mixed valence metals is dependent on the solvent, where interaction between the metal centres is enhanced in dichloromethane. The strong interaction in this complex is likely mediated by strong metal-ligand orbital mixing, however, Hush treatment and strong solvent dependence rule out delocalisation, and therefore any value in application of the same treatment as Kaim and co-workers on similar species (30).

5.5 References.

[1] C. Creutz, H. Taube, J. Am. Chem. Soc., 91, 3988, 1969.

[2] C. Creutz, Prog. Inorg. Chem., 30, 1, 1983.

[3] H. Taube, Science, 266, 1028, 1984.

[4] C. Joachim, J.P. Launay, J. Mol. Elec., 6, 37, 1990.

[5] N.S. Hush, Prog. Inorg. Chem., 3, 391, 1967.

[6] N.S. Hush, Electrochim. Acta, 13, 1005, 1968.

[7] J.E. Sutton, H. Taube, Inorg. Chem., 20, 3125, 1981.

[8] M. Haga, T. Matsumura-Inoue, S. Yamabe, Inorg. Chem., 26, 4148, 1987.

[9] J.T. Hupp, J. Am. Chem. Soc., 112, 1563, 1990.

[10] R.A. Marcus, N. Sutin, Biochim. Biophys. Acta, 811, 265, 1985.

[11] M.B. Robin, P. Day, Advan. Inorg. Chem. Radiochem., 10, 247, 1967.

[12] M.J. Powers, T.J. Meyer, J. Am. Chem. Soc., 102, 1289, 1980.

[13] M.M. Richter, K.J. Brewer, Inorg. Chem., 32, 2827, 1993.

[14] S.P. Best, R.J.H.Clark, R.C.S. McQueen, S. Joss, J. Am. Chem. Soc., 111, 548, 1989.

[15] K. Nozaki, T. Ohno, M. Haga, J. Phys. Chem., 96, 10880, 1992.

[16] C.R. Arana, H.D. Abruna, Inorg. Chem., 32, 194, 1993.

[17] B.E. Buchanan, R. Wang, J.G. Vos, R. Hage, J.G. Haasnoot, J. Reedijk, Inorg. Chem., 29, 3263, 1990.

[18] F. Barigelletti, L. De Cola, V. Balzani, R. Hage, J.G. Haasnoot, J. Reedijk, J.G. Vos, Inorg. Chem., 28, 4344, 1989.

[19] R. Hage, J.G. Haasnoot, J. Reedijk, R. Wang, J.G. Vos, Inorg. Chem., 30, 3263, 1991.

[20] R. Hage, J.G. Haasnoot, H.A. Niewenhuis, J. Reedijk, D.J.A. de Ridder, J.G. Vos, J. Am. Chem. Soc., 112, 9245, 1990.

[21] G. Giuffrida, G. Calogero, G. Gugliemo, V. Ricevuto, M. Ciano, S. Campagna, Inorg. Chem., 32, 1179, 1993.

[22] J.T. Hupp, T.J. Meyer, Inorg. Chem., 26, 2332, 1987.

[23] H.P. Hughes, D. Martin, S. Bell, J.J. McGarvey, J.G. Vos, Inorg. Chem., 32, 4402, 1993.

[24] P.H. Merrell, Inorg. Chim. Acta, 32, 99, 1979.

[25] J.C. Jeffery, M.D. Ward, J. Chem. Soc., Dalton Trans., 2119, 1992.

[26] J.C. Jeffery, E. Schatz, M.D. Ward, J. Chem. Soc., Dalton Trans., 1921, 1992.

[27] K.A. Goldsby, T.J. Meyer, Inorg. Chem., 23, 3002, 1984.

[28] A. Dei, D. Gatteschi, L. Pardi, Inorg. Chem., 29, 1442, 1990.

[29] S. Ernst, V. Kasack, C. Bessenbacher, W. Kaim, Z. Naturforsch, 426, 425, 1987.

[30] S. Ernst, P. Hanel, J. Jordanov, W. Kaim, V. Kasack, E. Roth, J. Am. Chem. Soc., 111, 1733, 1989.

[31] M. Haga, E.S. Dodsworth, A.B.P. Lever, Inorg. Chem., 25, 447, 1986.

[32] M. Haga, K. Isobe, S.R. Boone, C.G. Pierpont, Inorg. Chem., 29, 3795, 1990.

[33] H. Masui, A.B.P Lever, P.R. Auburn, Inorg. Chem., 30, 2402, 1991.

[34] S. Bhattacharya, C.G. Pierpont, Inorg. Chem., 31, 35, 1992.

[35] H. Masui, A.B.P. Lever, E.S. Dodsworth, Inorg. Chem., 32, 258, 1993.

[36] L.F. Joulie, E. Schatz, M.D. Ward, F. Weber, L.J. Yellowlees, J. Chem. Soc., Dalton Trans., 799, 1994.

[37] G.G. Sadler, N.R. Gorden, Inorg. Chim. Acta, 180, 271, 1991.

[38] C. Carriedo, N.G. Connolley, J. Organomet. Chem., 403, 359, 1991.

[39] J.V. Mondal, F.A. Schultz, T.D. Brennan, W.R. Scheidt, Inorg. Chem., 27, 3950, 1988.

[40] A. Das, J.C. Jeffery, J.P. Maher, J.A. McCleverty, E. Schultz, M.D. Ward, G. Wollerman, Inorg. Chem., 32, 2145, 1993.

[41] V.R.L. Constantino, L.F.C. deOliveira, P.S. Santos, H.E. Toma, Trans. Met. Chem., 19, 103, 1994.

[42] R. Hage, A.H.J. Dijkhuis, J.G. Haasnoot, R. Prins, J. Reedijk, B.E. Buchanan, J.G. Vos, Inorg. Chem., 27, 2185, 1988.

[43] D.P. Rillema, K.B. Mack, Inorg. Chem., 21, 3849, 1982.

[44] D.P. Rillema, G. Allen, T.J. Meyer, D. Conrad, Inorg. Chem., 22, 1614, 1983.

[45] S. Ernst, V. Kasack, W. Kaim, Inorg. Chem., 27, 1146, 1988.

[46] R. Hage, J.G. Haasnoot, J. Reedijk, R. Wang, E. Ryan, J.G. Vos, A.L. Spek, A.J.M. Duisenberg, Inorg. Chim. Acta, 174, 77, 1990.

[47] R. Hage, J.G. Haasnoot, D.J. Stufkens, T.L. Snoeck, J.G. Vos, J. Reedijk, Inorg. Chem., 28, 1413, 1989.

[48] J. Van Houten, R.J. Watts, Inorg. Chem., 17, 3381, 1978.

[49] B. Durham, J.V. Casper, J.K. Nagle, T.J. Meyer, J. Am. Chem. Soc., 104, 4803, 1982.

[50] D.A. Bardwell, D. Black, J.C. Jeffery, E. Schatz, M.D. Ward, *J. Chem. Soc., Dalton Trans.*, 2321, 1993.

[51] A. Juris, V. Balzani, F. Barigelletti, S. Campagna, P. Belser, A. von Zelewsky, *Coord. Chem. Rev..*, 93, 245, 1988.

[52] R. Hage, Ph.D. Thesis, Leiden University, The Netherlands, 1991.

[53] C. Creutz, P. Kroger, T. Matsubara, T.L. Netzel, N. Sutin, J. Am. Chem. Soc., 101, 5442, 1979.

[54] J. Poppe, M. Moscherosch, W. Kaim, Inorg. Chem., 32, 2640, 1993.

[55] M.J. Ridd, D.J. Gakowski, G.E. Sneddon, F.R. Keene, *J. Chem. Soc., Dalton Trans.*, 1949, 1992.

Chapter 6.

The influence of bipyridyl deuteration on the excited state properties of Ru(II)polypyridyl mixed ligand complexes.

6.1 Introduction.

Ligand deuteration, as a tool for the investigation the excited state of Ru(II)diimine compounds is relatively under-exploited. The reason for this may be the synthetic demands in traditional methodology of producing significant amounts of deuterated bipyridyl. In this short chapter, a simple one-pot method of deuteration of 2,2-bipyridyl is discussed. As well, the value deuteration represents in the structural elucidation of ruthenium polypyridyl complexes by ^{1}H nmr, where the bipyridyl protons act as interferents in the recognition of the resonances of the heteroligand. Also, the influence of deuteration on the excited state of complexes in which the excited state is bpy-based and on compounds where it is not is addressed. This discussion remains relatively superficial since complete analyses of the influence of deuteration on the complexes employed would require emission spectral analyses and fitting to the energy gap law, requiring the development of specialised software.

Although relatively uncommon in coordination chemistry, deuteration (and other isotope exchange) has been an important part of investigation into the excited states of organic compounds for many years [1]. One of the earliest reports of perdeuteration of Ru(II) polypyridyl complexes was made by Van Houten and Watts in 1970 [2], in which they described the synthesis of Ru(d_8-bpy)$_3$]Cl$_2$. They noted briefly the fact that deuteration of the free ligand dramatically increased luminescent lifetimes and coupled with solvent deuteration the lifetimes exhibited an even greater isotope effect. The influence of solvent they attributed to partial charge transfer to solvent (CTTS) in their excited state model. The following year this group reported on further experiments on [Ru(d_8-bpy)$_3$]Cl$_2$ and [Ru(h_8-bpy)$_3$]Cl$_2$ involving temperature dependent studies [3]. The model for temperature dependence employed by the authors possessed two terms to describe non-radiative decay, one they found to be strongly dependent on deuteration of ligands and solvent, the other almost entirely independent. The independent term was attributed to the non-radiative decay from d-d level. Since the d-d transition does not involve the bpys, and since it is a strongly internalised transition, solvent deuteration should have little bearing. Again, in this account although the photophysical differences between the protonated and perdeuterated complexes were described, little explanation of these differences was given. This report [3] does, however, serve to illustrate very elegantly the potency of isotope exchange as a means of probing the excited state in such complexes. The most prevalent application of ligand perdeuteration to date has been in investigations of the condition of localisation/delocalisation of the excited state electron in $[Ru(bpy)_3]^{2+}$. This has been investigated from two points of view. Firstly, from highly resolved emission spectra at low temperature in the solid state. Where, for example, in the work of Yersin and co-workers, protonated, perdeuterated and partially perdeuterated $[Ru(bpy)_3]^{2+}$, $[Os(bpy)_3]^{2+}$ and $[Ru(bpy)_2(bpz)]^{2+}$ were doped into single crystals of $[Zn(bpy)_3](ClO_4)_2$ [4-7]. Through their work, this group have found that information from the emission decay behaviour and vibrational satellites of E^{0-0} of these complexes leads to a clear distinction between localised and delocalised MLCT transitions to the lowest excited state. The appearance or absence of ligand centered vibrational modes belonging to the different types of ligands in these systems is vital evidence to the localised or delocalised nature of the excited state. Yersin et al found for example, that the highly resolved emission spectra of $[Ru(bpy)_2(bpz)]^{2+}$ contained only bpz-based vibrations. Whereas, in contrast, for the complexes containing a mixture of both perdeuterated and protonated bpys, e.g. $[Ru(d_8\text{-}bpy)_2(h_8\text{-}bpy)]^{2+}$, the ligand centered vibrations are due to both d_8-bpy and h_8-bpy, suggesting strongly that the electron is delocalised over all three ligands. The same results are observed for the osmium analogues. Electron hopping or tunnelling may be disregarded since the temperature at which these experiments were carried out (1.3K) is too low to provide energy to support this process.

Resonance Raman (rR) spectroscopy is the second area where deuteration of bipyridyls has proved important in the investigation into the localisation/delocalisation of the excited state. The results from this area, however, challenge those of the emission studies.

Examples come from the work of Kincaid et al [8-11], the results from these and other groups [12] studies concur that the electron is localised on one ligand only. This is derived from the fact that strongly enhanced modes are observed in transient rR for $[Ru(bpy)_3]^{2+}$ corresponding to bpy^- vibrations. In fact, through deuteration of the pyridine half of the pyridine-pyrazole ligand shown in figure 6.1, Kincaid et al have shown that the electron is further localised in $[Ru(bpy)_2(bpz)]^{2+}$ to the pyrazine half of the bpz moiety [9].

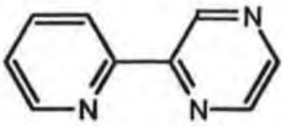

Figure 6.1. Pyridylpyrazine as described by Kincaid and co-workers [9].

That the results from solid state highly resolved emission spectroscopy and rRaman spectroscopy do not concur is given little discussion in the literature. However, findings in these publications may not be completely at odds, since the emission studies are carried out on a doped single crystal (i.e. in the solid state) and the rRaman studies are carried out in fluid solution. Examining the symmetry of, for example, $[Ru(bpy)_3]^{2+}$, in the ground state, the point group is D_3. In the excited state if the electron is localised on a single bpy, the point group if the molecule is reduced in symmetry to C_{2v}. If the electron is delocalised in the excited state there is no loss of symmetry and the point group remains D_3. It is obvious, therefore, that reduction of symmetry from D_3 to C_{2v} will result in the generation of a large dipole moment in the excited state which will require considerable solvent reorientation for stabilisation. Van Houten and Watts [3] associated the strong influence solvent deuteration bears on the excited state lifetime with charge transfer to solvent, whereby this CTTS interacts with the MLCT states lowering the energy of the transition. If solvent bears such a strong influence, it is conceivable that fluid, and in particular polar solvents may induce, or in some way catalyse the localisation of the electron on a single bpy, perhaps by creating a potential energy well for this state by solvent stabilisation. In glass media there is no solvent CTTS-MLCT interaction and solvent reorganisation around a polar intermediate is very slow, therefore the localisation of the electron may not be induced and the low polarity delocalised (higher symmetry) state is probably of lowest energy.

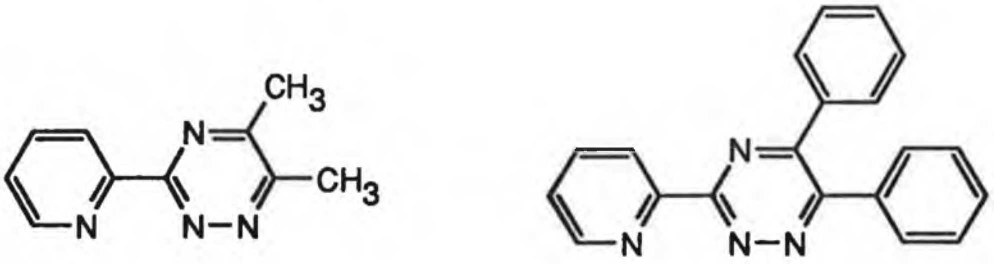

dmpt dppt

Figure 6.2. Structures of the triazine ligands discussed in the text [14].

6.2 Synthetic procedure.

6.2.1 Preparation of ligands:

Deuteration of 2,2-bipyridyl (d_8-bpy).

2,2-Bipyridyl (3g, 0.19M) was dissolved in D_2O which contained 1M NaOD. This was poured into a steel bomb and allowed to react over Pd-Charcoal (10% Pd) (1g) in the sealed bomb in an oven at 200°C for 8 days. After this period, the contents of the bomb were collected neutralised (DCl) and filtered hot to remove the Pd-Charcoal catalyst. The D_2O was vacuum distilled off the product which was collected and redissolved in fresh D_2O/NaOD. This was then further reacted over Pd-Charcoal under the conditions described for a week. The reactants and were then collected and filtered as described and the D_2O removed by distillation. The d_8-bpy was collected as an off-white crystalline solid which was recrystallised from hot D_2O. Yield was >80%. ^{1}Hnmr revealed 8 singlets, and in some instances (when reaction time was longer) no resonances at all, implying a very high extent of deuteration. IR revealed absorbances at 2250-2295 cm^{-1} attributed to C-D (str), by comparison with approximately 3000 cm^{-1} for C-H.

The preparation of the other ligands discussed in this chapter are described either in chapter 3, 4 HL1-HLx or HL3 or in case of the triazines (see figure 6.2 for structures) [13, 14].

6.2.2 Preparation of complexes.

Ru(d_8-bpy)$_2$Cl$_2$.

This complex was made according to the synthesis described in chapter 3.

All other complexes were synthesised in a similar manner to the synthetic procedure described in chapter 3 or in reference [13].

6.3 Results and discussion.

6.3.1 Synthetic procedure:

To date the most convenient synthetic procedure for deuteration of bipyridyl is the deuteration of a precursor, 2,2-bipyridyl-1,1-dioxide [15, 16], which is activated towards deuteration. This method which was first described by Cook *et al* [15], involves successive treatment of the di-N-oxide, with D_2O/NaOD, followed by reduction of the product with PCl_3. The deuteration of the dioxide is arduous by comparison with the simple one-pot synthesis described here, particularly since the di-N-oxide precursor itself requires preparation from 2,2-bipyridyl.

The synthesis described here employs mild reagents, NaOD/D_2O with Pd-charcoal as a catalyst and the starting material 2,2-bipyridyl is used directly . Although the reaction times are long, the work up is simple and the yields very high. The size of the reaction vessel would appear to be the only restriction to volume of reagents used, and it seems probable that this procedure could be also be applied to the deuteration of other ligands, opening up the opportunity for a wide variety of structural and photophysical elucidations.

6.3.2 ^{1}HNMR and structural analyses.

The fundamental motive behind the synthesis of the deuterated analogues of the complexes described was the deconvolution of ^{1}H nmr spectra. The aim was the elucidation of the structure of some of the more complicated complexes, in particular that of the unknown bpt complex described in appendix 1. To our knowledge there are very few other reports on the use of deuteration as a means of structural elucidation [16], and this scarcity of reports may be related to the fact that deuterated bpy is expensive, and that synthesis is not straight forward. Examples of the simplification of ^{1}Hnmr spectra obtained on deuteration is shown for some of the complexes discussed here in figure 6.3 (a)-(d).

In the instances of asymmetric mononuclear complexes, up to sixteen non-equivalent protons may arise from the bipyridyl moieties, and in dinuclear complexes 32, making complete unambiguous structural assignment to date, nigh on impossible. Deuteration of the bipyridyl results in the bipyridyl moiety appearing as low intensity singlet resonances in the ^{1}Hnmr thereby simplifying it to a large degree. Deuteration, coupled with nmr-COSY techniques provides a potent means of making a full assignment of the spectra, and hence an accurate assignment of complex structure. Figure 6.3 (a) shows, for example, the result of bipyridyl deuteration on the ^{1}H nmr COSY spectra of $[Ru(bpy)_2(H_2L1)]^+$. The spectral simplification is remarkable, and the ligand pyridyl is clearly easily assigned, most importantly, the hydroquinone is also completely unambiguous. It can be clearly seen from the deuterated spectra that long range coupling exists between the $H^{5"}$ and the H3" proton. This assignment had previously caused some confusion since a singlet was expected for H3", and coupling was not expected. In each instance, on deuteration, the bipyridyl resonances are reduced to low intensity singlets, and the ligand resonances, intense by comparison, are easily interpreted. For $[(Ru(bpy)_2)_2(H_2L8)]^+$ the four ligand resonances are clearly seen, only 4 shifts (2H) are observed since this complex is symmetric (belonging to the C_{2h} point group). This is rather exceptional for a dimer since even those, possessing symmetric ligands such as bpt often possess more than one geometric isomer. The singlet at approximately 6.1 ppm is clearly the hydroquinone protons (H^3, H^6). The remaining four, two doublets and triplets are those corresponding to the coordinated pyrazole species. Deuteration of $[(Ru(bpy)_2)_2(H_2L2)]^{3+}$ sadly did not yield the same clarification however it did verify that what it consists of is two geometric isomers. This procedure was also to verify the structures of the triazine complexes reported previously [15] since there had been some difficulty in their ^{1}Hnmr assignment.

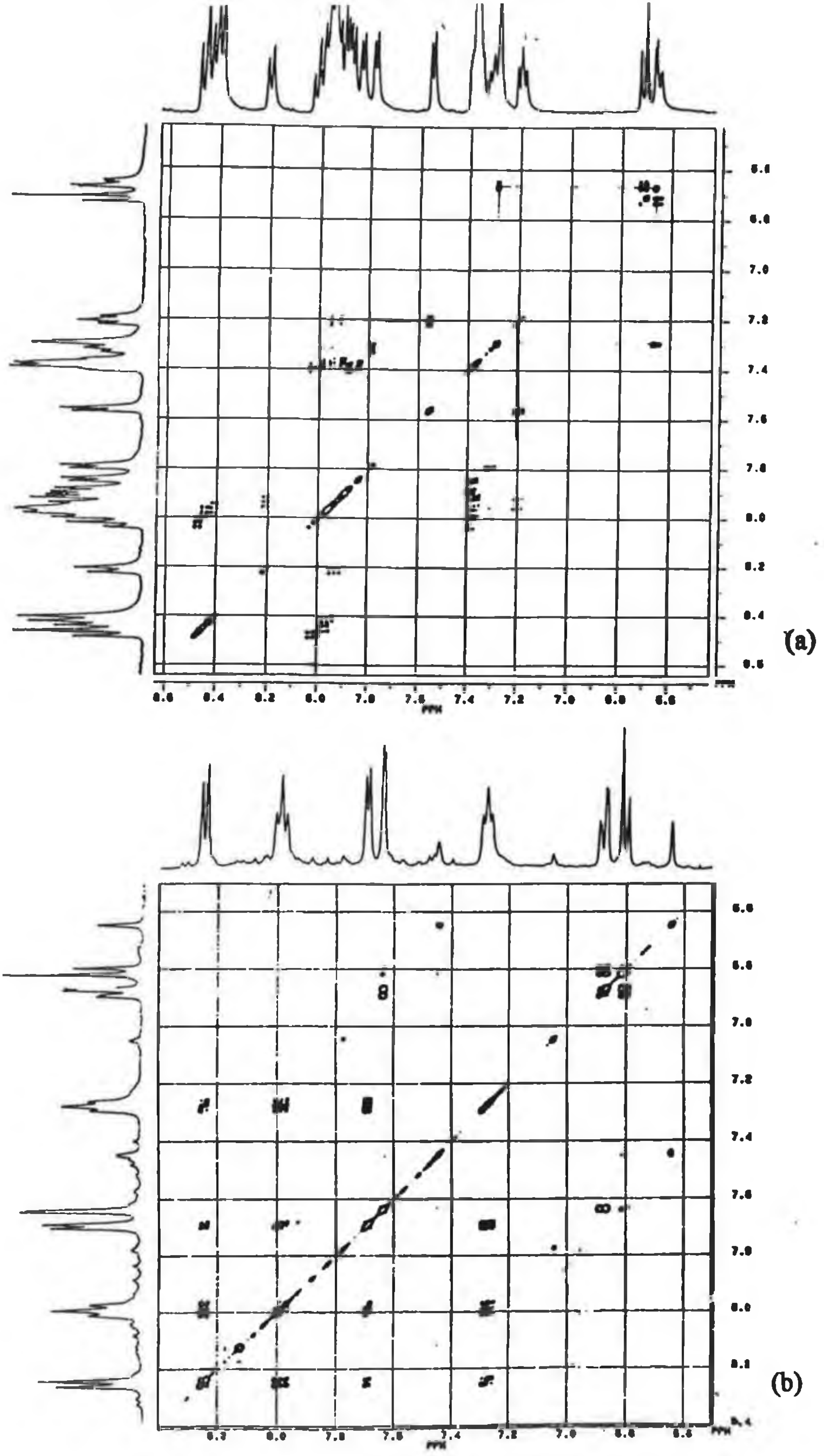

Figure 6.3(a) ^{1}Hnmr COSY of [Ru(bpy)$_2$(H$_2$L1)]$^+$ (above) and [Ru(d$_8$-bpy)$_2$(H$_2$L1)]$^+$ (below) in acetonitrile-d$_3$.

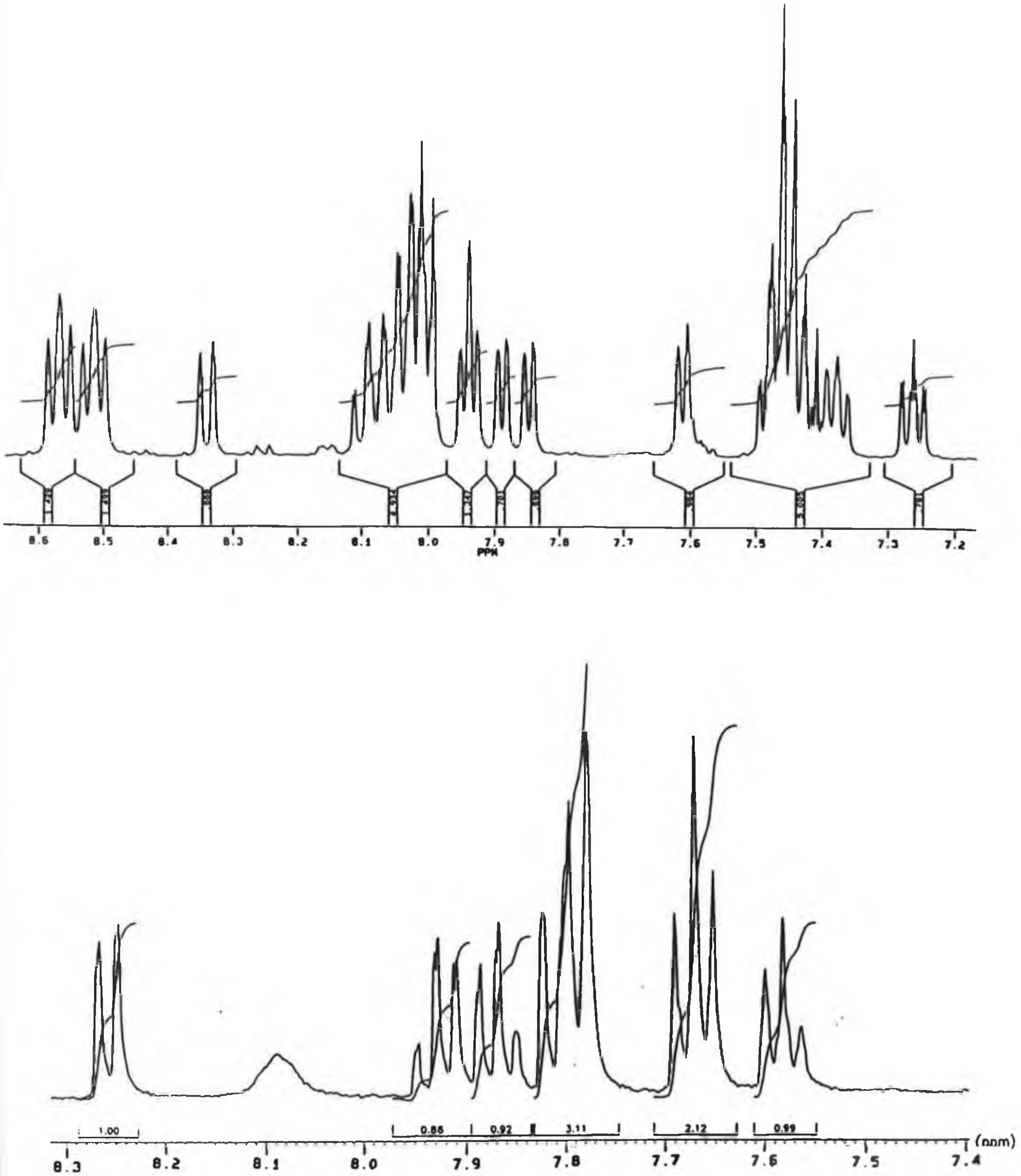

Figure 6.3(b) ^{1}Hnmr spectra of [Ru(bpy)$_2$(HL5)]$^+$ (above) and [Ru(d$_8$-bpy)$_2$(HL5)]$^+$ (below) in acetonitrile-d$_3$.

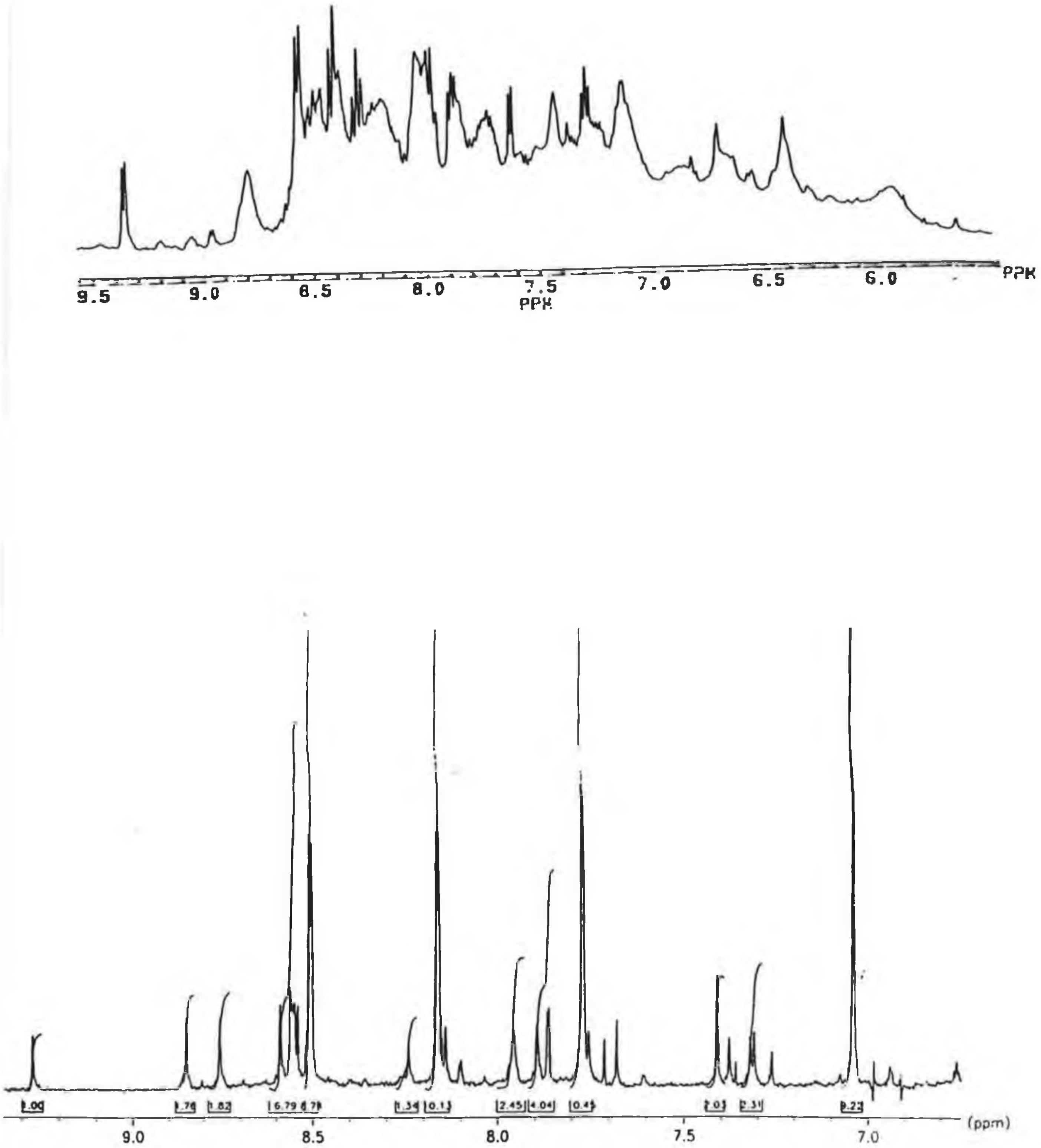

Figure 6.3(c) ^{1}Hnmr spectra of [Ru(bpy)$_2$(HL8)]$^+$ (above) and [Ru(d$_8$-bpy)$_2$(HL8)]$^+$ (below) in acetonitrile-d$_3$.

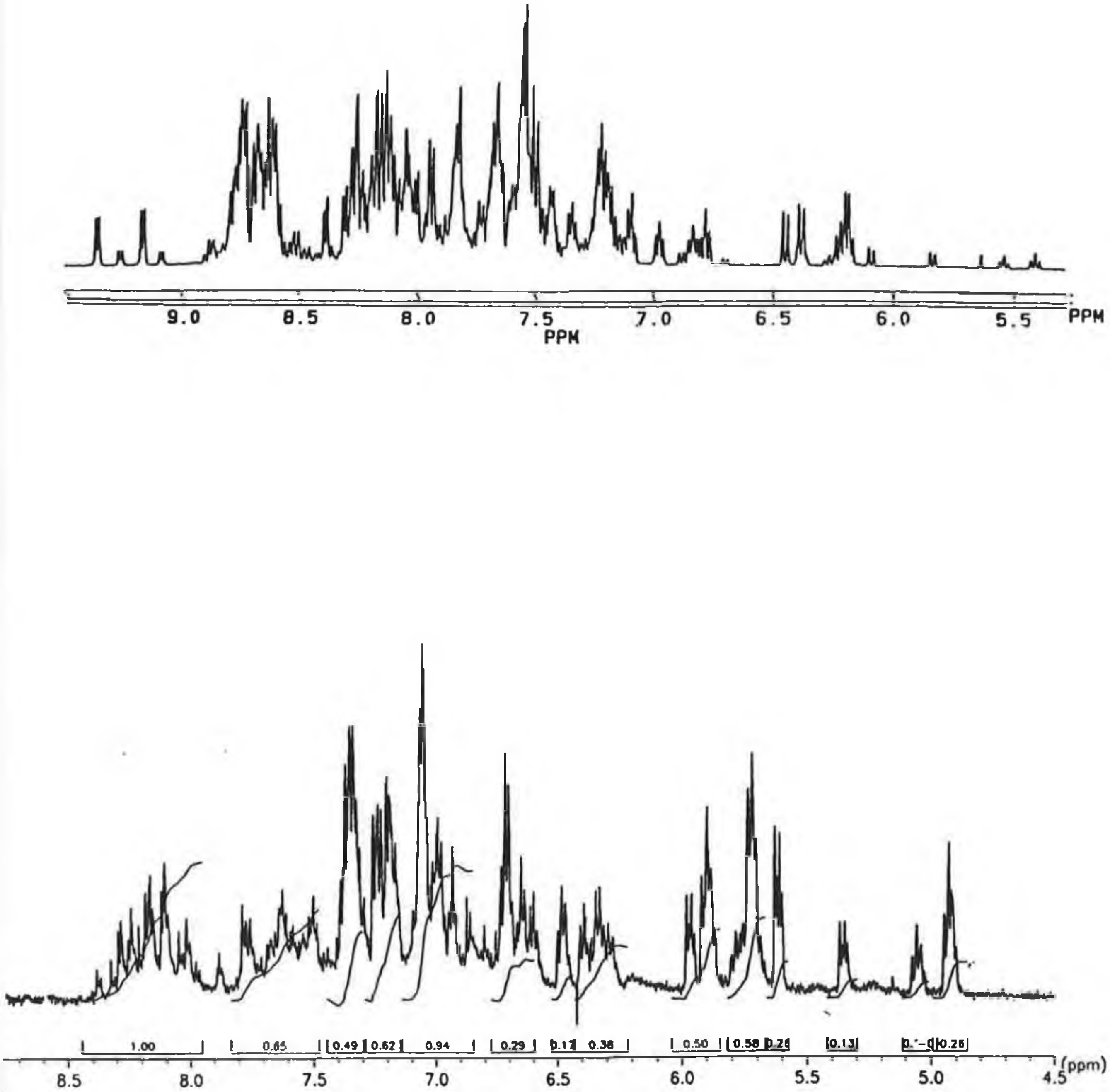

Figure 6.3(e) ^{1}Hnmr spectra of $[(Ru(bpy)_2)_2(HL2)]^{3+}$ (above) and $[(Ru(d_8\text{-}bpy)_2)_2(HL2)]^{+}$ (below) in acetonitrile-d_3.

6.3.3 Electronic properties and lifetimes.

Table 6.1. The absorption and emission properties of deuterated complexes in acetonitrile.

Complex	**Absorbance** λ_{max}**(nm) (logε)**	**Emission (nm)**		**Lifetimes (ns)**		**ϕem**
		RT	77K*	RT*	77K*	
$[Ru(d_8\text{-}bpy)_2H_2L1]^+$	474.5 (3.68))	672	608	324	4326	2.3×10^{-3}
$[Ru(h_8\text{-}bpy)_2H_2L1]^+$	475 (3.987)	672	614	160	3564	1.4×10^{-3}
$[Ru(d_8\text{-}bpy)_2H_3L1]^{2+}$	431 (3.80)	613	579	----	5517	4.5 x10-4
$[Ru(h_8\text{-}bpy)_2H_3L1]^{2+}$	430.5 (4.03)	613	577	----	4364	2.9×10^{-4}
$[Ru(d_8\text{-}bpy)_2HL4]^+$	480 (3.78)	685	621	245	3545	2.3×10^{-3}
$[Ru(h_8\text{-}bpy)_2HL4]^+$	482 (3.93)	672	623	140	2613	1.4×10^{-3}
$[Ru(d_8\text{-}bpy)_2H_2L4]^{2+}$	433 (3.87)	672	583	-----	5563	NA
$[Ru(h_8\text{-}bpy)_2H_2L4]^{2+}$	440	626	585	-----	6712	4.4×10^{-4}
$[Ru(d_8\text{-}bpy)_2L5]^+$	482 (3.87)	688	611	409	3471	4.0×10^{-3}
$[Ru(h_8\text{-}bpy)_2L5]^+$	482 (3.93)	690	615	225	2613	2.2×10^{-3}
$[Ru(d_8\text{-}bpy)_2HL5]^{2+}$	439 (3.98)	614	580	----	5724	4.4×10^{-4}
$[Ru(h_8\text{-}bpy)_2HL5]^{2+}$	440 (4.01)	658	589	-----	3073	NA
$[Ru(d_8\text{-}bpy)_2L8]^+$	571 (3.66)	685	605	714	NA	2.5×10^{-4}
$[Ru(h_8\text{-}bpy)_2L8]^+$	567 (3.76)	680	605	503	3099	1.8×10^{-4}
$[Ru(d_8\text{-}bpy)_2(dppt)]^+$	480	714	650	780	10090	9.41×10^{-4}
$[Ru(h_8\text{-}bpy)_2(dppt)]^{+*}$	475	712	651	1080	8600	9.43×10^{-4}
$[Ru(d_8\text{-}bpy)_2(dmpt)]^+$	445	664	610	90	5900	2.51×10^{-4}
$[Ru(h_8\text{-}bpy)_2(dmpt)]^{+*}$	443	663	612	97	5750	2.72×10^{-4}

^{W} All low temperature menasurements were carried out in ethanol/methanol (4:1 v/v) solution. * Values obtained from [14]. NA = value not available.

Table 6.1 displays the photophysical and electronic properties of the deuterated compounds discussed. For complexes containing numbered ligands (i.e. not the triazines), the most immediately obvious effect of deuteration is the dramatic increase in luminescent lifetime and quantum yield of luminescence by comparison with their protonated analogues, see table 6.1. This effect is seen through all complexes at both room temperature and 77K with the exception of the triazine complexes. The reason for the absence of change in these compounds will be discussed. For $[Ru(d_8\text{-bpy})_2L1]^+$ in acetonitrile at room temperature the lifetime is observed to be 324 ns as opposed to 160 ns for it's protonated analogue. This doubling of emission lifetime is perpetuated through the other numbered complexes, with quantum yields showing strong increases as well. The λ_{max} of emission and absorption of the complexes are not influenced to any significant extent by deuteration.

The strong influence deuteration bears on the luminescent behaviour of these complexes is related to the non-radiative relaxation of the excited state, k_{nr}. knr may derived from the following equations;

$$\tau = k_r + k_{nr}$$
$$\phi_{em} = k_r \tau$$
$$k_{nr} = \frac{1}{\tau_{77K}} - k_r$$

Table 6.2 show the photophysical parameters obtained for the complexes discussed with their protonated analogues.

It is apparent in each instance for complexes containing L1 to L8 that there is a decrease of k_{nr} observed on deuteration of the bipyridyls. This phenomena is associated with the slower vibrational relaxation of the excited electron on the bipyridyl.

Table 6.2; Photophysical parameters.

Complex	ϕ_{em}	k_r (s^{-1})	k_{nr} (s^{-1})
$[Ru(d_8\text{-}bpy)_2H_2L1]^+$	2.3×10^{-3}	7.1×10^3	2.24×10^5
$[Ru(h_8\text{-}bpy)_2H_2L1]^+$	1.4×10^{-3}	8.75×10^3	2.75×10^5
$[Ru(d_8\text{-}bpy)_2L5]^+$	4.0×10^{-3}	9.78×10^3	2.78×10^5
$[Ru(h_8\text{-}bpy)_2L5]^+$	2.25×10^{-3}	1×10^4	3.73×10^5

This is explained in terms of the contribution of the bpy C-H stretch and other modes to the vibrational relaxation of the excited state of the complex. If C-H vibrations are important as promoting modes for transition then the transition should be sensitive to deuteration, which is the case here. The importance of such promotional vibrations to the non-radiative decay of a luminescent complex is expressed by the energy gap law, equation 6.1.

$$\ln k_{nr} = \ln \beta - S_m - \frac{\gamma E_{oo}}{\hbar\omega_m} + S_L \frac{\omega_L}{\omega_M}(\gamma + 1) + \frac{b\chi}{\hbar\omega_M} \qquad (6.1)$$

Where

$$\beta = \left(C_k^2 \omega k\right)\left(p / 2\hbar\omega_M E_{oo}\right)^{1/2} \qquad (6.2)$$

$$\gamma = \ln\left(E_{oo} / \hbar\omega_M S_M\right) - 1 \qquad (6.3)$$

$$\pi = \left(\Delta\nu_{1/2}\right)^2 / \left(16 k_B T \ln 2\right) \qquad (6.4)$$

$$b = \left(k_B T / \hbar\omega_M\right)\left(g + 1\right)^2 \qquad (6.5)$$

$\Delta\upsilon_{1/2}$ is the full width at half maximum for the E^{o-o} and other components of the emission. ω_M and ω_L are the vibrational frequencies related to the bpy ring and Ru-N stretching modes, respectively. S_M and S_L are the vibrational coupling parameters related to the distortion in molecular coordinates relating to ω_M and ω_L, respectively. The factors E^{o-o} S_M and L, ω_M and L and $\Delta\upsilon_{1/2}$ may be estimated from emission spectral fitting based on the Franck-Condon analysis [17], since the required software was not available this was not carried out. Of course the most important notion derived from the energy gap law is the logarithmic dependence of knr on the excited state energy E^{o-o}. However, from equation 6.1 it is also apparent that bpy vibrational frequencies will play an important role, via the variables ω_M and S_M in the non-radiative transitions of a complex. The deuteration effect will depend on the influence the C-H has as a vibrational mode into which excited state energy is dissipated. In organic systems, where most of the theorising has evolved, there is debate over the importance of the C-H vibrations in non-radiative decay. According to Siebrands theory of non-radiative transition [18, 19], high energy anharmonic C-H stretching vibrations are the dominant promotional modes in non-radiative decay. This implies that the emission lifetime should be very sensitive to deuterium substitution. Since this will reduce the energy of the C-H stretching vibration from approximately 3000 cm^{-1} to approximately 2250 cm^{-1}. The importance of these modes has been disputed, since presumption of their dominance as acceptors of excited state energy was derived largely from the fact that they are the most energetic vibrational modes. Some evidence has emerged however that the C-C vibrations may have an equally if not more important role [20], and particularly in inorganic MLCT excited state complexes where it has been postulated that the C-H modes are only weakly involved as acceptor modes [21]. Nonetheless, the importance of the C-H stretching vibrations as promotional modes in non-radiative transitions are reflected in the changes in photophysical attributes on deuteration seen here. Furthermore, realising the impact deuteration has on the excited state lifetime of Ru(II) polypyridyl complexes, this technique may be employed as a simple means of determining the destination of the excited state electron in mixed ligand systems.

This brings us to the question of absence of influence of deuteration of bipyridyl in complexes [Ru(d_8-bpy)$_2$(dmpt)]$^+$ and [Ru(d_8-bpy)$_2$(dppt)]$^+$ (see figure 6.2).

Little change in photophysical behaviour is observed between the perdeuterated and protonated complexes of the triazines, in fact if anything the lifetimes are shorter in the deuterated analogues. From previous studies on these complexes, it has been established that the excited state is localised on the heteroligand and not on a bipyridyl [12]. Since in the complexes containing the triazole and pyrazole ligands, dramatic increases in lifetime and quantum yield are evident, the absence of isotope effect on [Ru(d_8-bpy)$_2$(dmpt)]$^+$ and [Ru(d_8-bpy)$_2$(dppt)]$^+$reflects the fact that the bipyridyls are merely spectator ligands in these complexes and not directly involved in the excited state of the complexes. This is very significant since, to date the elucidation of the destination of the excited state electron in such complexes has required a combination of acid-base, electrochemical and most importantly resonance raman spectroscopy. By deuteration of one of the ligand sets in a complex of unknown excited state, the nature of the excited state may be determined simply by observing the influence of isotopic exchange on the complex. If significant increases in emission lifetime and quantum yield are observed then the deuterated ligand is directly involved in the excited state, if small, negative or no change is observed in these parameters the deuterated ligand may presumed to be a spectator species.

6.3.4 The influence of deuteration on electrochemistry.

Since the electronic spectra of the deuterated complexes described show little change by comparison with their protonated analogues, little change is expected in their electrochemistry. In particular, no change is anticipated in the metal redox processes, if any influence is exerted it would be expected to occur in the reduction potentials of the complexes. Table 3 displays the electrochemical data of the deuterated complexes described.

Table 6.3. Electrochemical data for deuterated complexes, all values in volts vs SCE.

Complexes^A	Oxidations (V)	Reductions (bpy) (V)
$[Ru(d_8\text{-}bpy)_2(H_2L1)]^+$		-1.51, -1.72
$[Ru(d_8\text{-}bpy)_2(L4)]^+$	1.04	-1.58, -1.79
$[Ru(d_8\text{-}bpy)_2(L5)]^+$	0.92	-1.67, -1.86
$[Ru(d_8\text{-}bpy)_2(HL8)]^+$	0.4, 0.76, 1.33	-1.57, -1.85
$[(Ru(d_8\text{-}bpy)_2)_2(HL2)]^+$	0.286, 1.088, 1.52	-1.41, -1.67(2e-), -1.87

^{A} All electrochemistry (DPP) was carried out in acetonitrile under neutral conditions, protonation of the complexes leads to surface effects which obscure the bpy reductions, therefore protonated complexes were not measured.

As expected there is no difference (within experimental error) between the metal redox potentials of the protonated and perdeuterated complexes. Surprisingly, there are small but perceivable variances between the bipyridyl reductions in all complexes described. The best example of this influence is observed in the electrochemistry of the dinuclear complex, $[(Ru(d_8\text{-}bpy)_2)_2(HL2)]^+$. Figure 6.4 shows the reduction of this complex (a) when the bipyridyls are protonated and (b) when they are perdeuterated. In the protonated complex, because it is such an asymmetric complex (see chapter 4) the reductions waves of all four bpys are resolved. Whereas the deuterated analogue sees a shift in the bpy reductions resulting in an overlap of the 2nd and 3rd waves.

This unequivocally proves that deuteration bears an influence on the bipyridyl reduction potentials. However, these changes are so small as to create little observable change in the electronic spectroscopy of the complex. Nevertheless, differences are discernible between the protonated and perdeuterated complexes in terms of temperature dependent behaviour, as will be described in section 6.3.5.

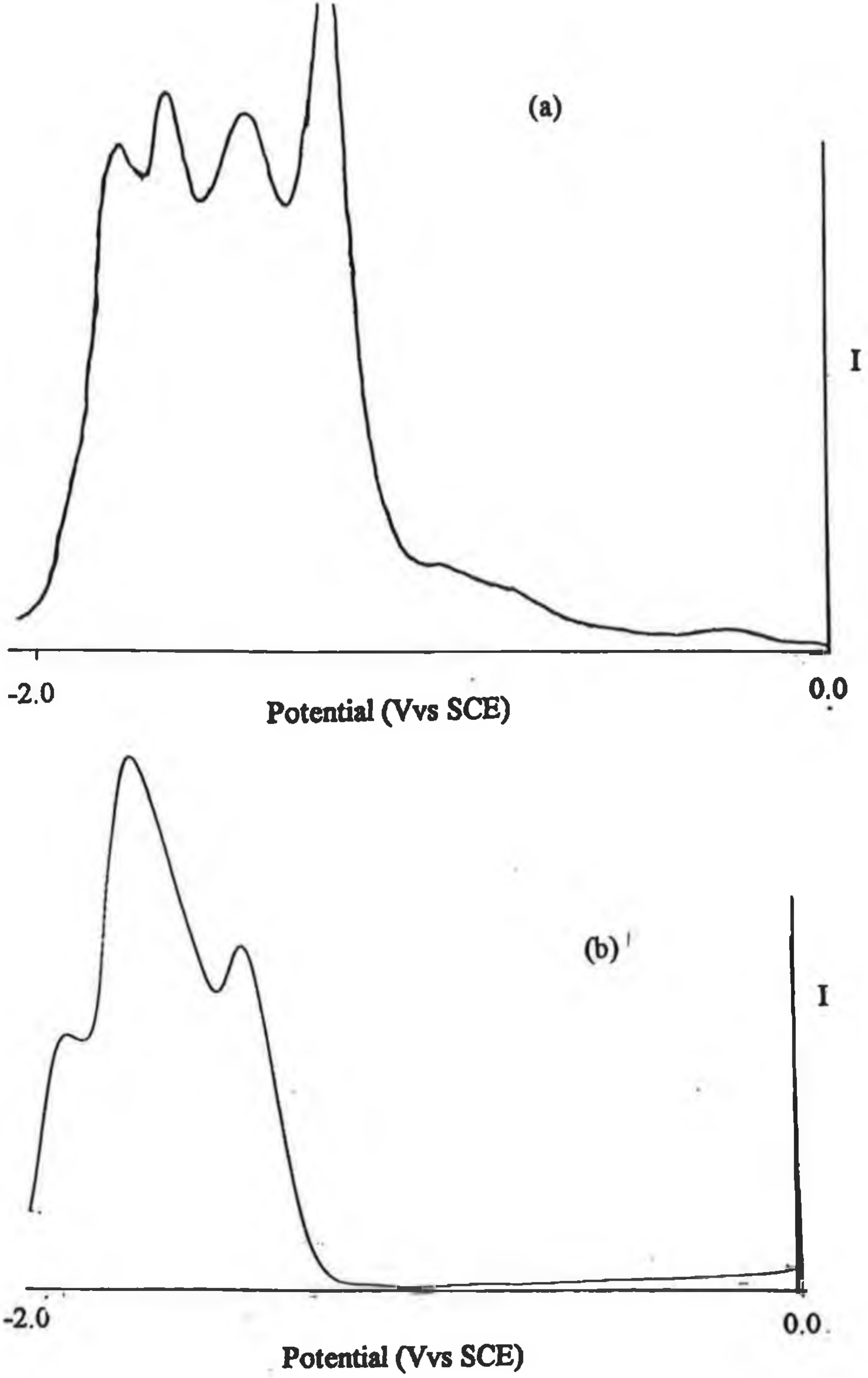

Figure 6.4. Differential pulse polarography of the reduction of (a) $[(Ru(h_8\text{-}bpy)_2)_2(HL2)]^+$ *and (b)* $[(Ru(d_8\text{-}bpy)_2)_2(HL2)]^+$*, in neutral acetonitrile, vs SCE.*

6.3.5. Temperature dependent lifetime studies.

As was described the temperature dependent lifetime behaviour was investigated in the region 150-300K and the data fitted to an Arrhenius plot (6.6).

$$\frac{1}{\tau_{obs}} = k_o + A\exp(-E_a / RT) \quad (6.6)$$

Table 6.4. Temperature dependent data.

Complex	**E_a (cm^{-1})**	**A (s^{-1})**	**k_o (s^{-1})**
$[Ru(d_8\text{-bpy})_2H_2L1]^+$	287	9.4 x10^7	1.4 x10^6
$[Ru(h_8\text{-bpy})_2H_2L1]^+$	113	6.7 x10^7	3.2 x10^7
$[Ru(d_8\text{-bpy})_2H_3L1]^{2+}$	1254	6.3 x10^{12}	5.2 x10^5
$[Ru(h_8\text{-bpy})_2H_3L1]^{2+}$	2928	4.5 x10^{13}	4.0 x10^6
$[Ru(d_8\text{-bpy})_2L5]^+$	529	6.8 x10^8	2.0 x10^6
$[Ru(h_8\text{-bpy})_2L5]^+$	362	3.6 x10^7	1.6 x10^6
$[Ru(d_8\text{-bpy})_2L8]^+$	839	8.7 x10^9	2.3 x10^7
$[Ru(h_8\text{-bpy})_2L8]^+$	235	9.3 x10^6	1.3 x10^6
$[Ru((d_8\text{-bpy})_2)_2L8]^{2+}$	784	1.6 x10^{10}	8.1 x10^5
$[Ru((h_8\text{-bpy})_2)_2L8]^{2+}$	1350	7.0 x10^{12}	1.3 x10^6

From comparison of the temperature dependent data of the perdeuterated and protonated complexes, it is apparent that there is quite a significant change in behaviour. Since deuteration reduces k_{nr} and increases emissive lifetime, some change in k_o was expected, however, as is apparent from the values in table 6.4, significant changes occurs in E_a and the preexponential factors as well. Examining $[Ru(d_8\text{-bpy})_2H_2L1]^+$, k_o is lower than it's protonated analogue (ko = 3.17 x10^7 s^{-1}), by a factor of 10. This is anticipated since $k_o = k_{nr} + k_r$, so the reduction of the radiative and non-radiative terms as described in table 2 are expected to reduce the value of k_o. The comparative temperature dependent lifetime profiles of $[\mathrm{Ru(d_8\text{-}bpy)_2H_2L1}]^+$ and $[\mathrm{Ru(h_8\text{-}bpy)_2H_2L1}]^+$ are displayed in figure 6.5.

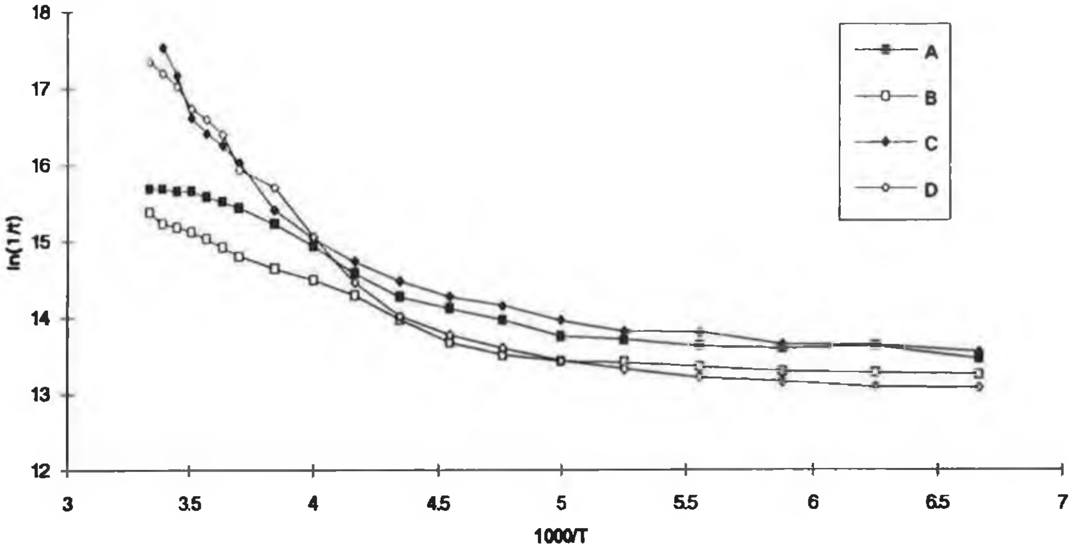

Figure 6.5. Temperature dependent plot of $[\mathrm{Ru(d_8\text{-}bpy)_2H_2L1}]^+$ *and* $[\mathrm{Ru(h_8\text{-}bpy)_2H_2L1}]^+$ *in both neutral and acidic media.* $A = [\mathrm{Ru(h_8\text{-}bpy)_2H_3L1}]^{2+}$ *in acidic alcohol,* $B = [\mathrm{Ru(d_8\text{-}bpy)_2H_3L1}]^{2+}$ *in acidic alcohol,* $C = [\mathrm{Ru(h_8\text{-}bpy)_2H_2L1}]^+$ *in neutral alcohol,* $D = [\mathrm{Ru(d_8\text{-}bpy)_2H_2L1}]^+$ *in neutral alcohol.*

What is immediately apparent, is that for complexes in neutral media the profiles of the plots of both protonated and perdeuterated complexes are almost identical except that the ln(1/τ) values are higher for the protonated complex, as a result of their shorter luminescent lifetimes. This means that at no point do the two plots converge, this is reflected in the lower k_0 of the perdeuterated complex.

For the complexes in acidic media, i.e. when their triazoles are protonated, the behaviour is revealing. At low temperature the curves have a relationship similar to that of the complexes in neutral media, i.e., similar but non-convergent behaviour. However, at high temperature the two curves overlap, and little difference is observed. This is because at high temperature in these complexes the dominant pathway for radiationless deactivation is via the d-d or ^{3}MC state. This means that the contribution to the k_{nr} from the bpy vibrations is mitigated by decay from ^{3}MC and hence the deuterium effect becomes less meaningful at high temperatures.

The preexponential factor is slightly higher in $[Ru(d_8\text{-}bpy)_2H_2L1]^+$ than $[Ru(h_8\text{-}bpy)_2H_2L1]^+$, and there is a quite significant increase in the activation energy of the deuterated complex. Since the estimated error for the temperature dependent data is ± 10%. These changes may be regarded as real. E_a in the instance where A is small (i.e. < 1 x 10^{10} s-1 reflects the energy of activation to the fourth MLCT state which is regarded to be largely singlet in nature [22]. It would seem that deuteration of bpy increases the energy difference between the ^{3}MLCT-*^{1}MLCT, and it would seem that this is a trend persistent throughout the monomeric complexes. The reason for this increase in the energy of the fourth MLCT (not forgetting that this could equally be a decrease in the energy of the three ^{3}MLCT) is unclear, since no change of wavelength is perceived in the electronic spectra of the complexes. However, no change can really be expected since, as in the case of $[Ru(d_8\text{-}bpy)_2H_2L1]^+$ and $[Ru(h_8\text{-}bpy)_2H_2L1]^+$, the energy change is only 174 cm^{-1}, and hence would represent an infinitesimal change, well outside experimental error on the spectroscopic equipment employed. This change in all the monomeric complexes, does not however predict a significant change in the photostability of the complexes.

For the complexes in acidic media, the difference between k_o for the protonated and deuterated complexes is considerably smaller. As was described from figure 3, this is the result of the onset of thermal population the of ^{3}MC state, resulting in a reduction of the deuterium effect on k_{nr}. However, significant differences are discerned between the activation energies, 1250 cm^{-1} for $[(Ru(d_8\text{-}bpy)_2)(H_3L1)]^{2+}$ and 2930 cm^{-1} for $[(Ru(h_8\text{-}bpy)_2)(H_3L1)]^{2+}$, and the prefactors 6.3 x10^{12} for $[(Ru(d_8\text{-}bpy)_2)(H_3L1)]^{2+}$ and 4.5

x10^{13} for $[(Ru(h_8\text{-}bpy)_2)(H_3L1)]^{2+}$. In this case where the triazole is protonated, E_a represents the activation energy for internal conversion between ^{3}MLCT and ^{3}MC. Perdeuteration has reduced the complex to an intermediate position of equilibrium between ^{3}MC and ^{3}MLCT, as opposed to rapid population and decay from the ^{3}MC state. This should be manifested by a reduction in photochemical activity of the deuterated complex. That E_a and A increase in the deuterated complex by comparison with the protonated analogue when the triazole is deprotonated and decrease with respect to it's analogue when the triazole is protonated suggests that it is the fourth singlet MLCT that is increased in energy on deuteration and not a reduction in the energy of the triplet excited state manifold, since if this were the case the ^{3}MLCT-^{3}MC state would be observed to increase in energy on deuteration in the complexes in acidic media.

The temperature dependent lifetimes were also measured for the deuterated dimeric complex $[(Ru(d_8\text{-}bpy)_2)(L8)]^{2+}$. Comparison with the data obtained in chapter 5, reveals that as expected k_0 decreases, and interestingly E_a and A also decrease. In fact A decreases by a factor of nearly 200. This change may significant enough to induce a change in photochemical behaviour. As was described, if ^{3}MC and ^{3}MLCT states are in equilibrium, the energy gap is usually between 800 and 2000 cm-1 and the preexponential factor is 10^{10} to 10^{12}. In the protonated complex the Ea and A are on the farther end of the scale and the perdeuterated possess values on the lower end which would suggest that some difference in photochemical lability may be perceived.

Figure 6.5 shows the 1/t vs 1000/T plots for the L8 dimer in both the perdeuterated and protonated condition.

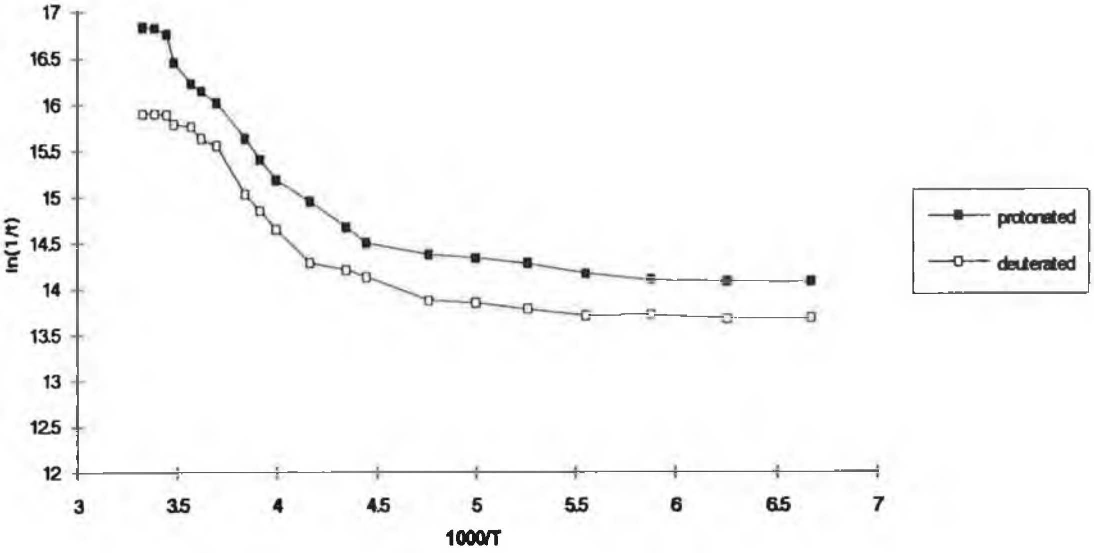

Figure 6.6. Temperature dependent behaviour of $[(Ru(d_8\text{-}bpy)_2)(L8)]^{2+}$ *and* $[(Ru(h_8\text{-}bpy)_2)(L8)]^{2+}$ *in ethanol/methanol.*

In the lower temperature range the temperature dependent curves are similar although as expected the deuterated complex shows overall lower ln(1/t) values. At higher temperatures the curves are different, with stronger temperature dependence exhibited by $[(Ru(d_8\text{-}bpy)_2)(L8)]^{2+}$.

6.4 Conclusions

In the preceding chapter a simple one pot reaction for the deuteration of 2,2-bipyridyl is discussed. This is a high yield synthesis, allowing the production of large amounts of $Ru(d_8\text{-}bpy)_2Cl_2$. One of the prime values of $Ru(d_8\text{-}bpy)_2Cl_2$ is that the ^{1}Hnmr of complexes in which the bipyridyl resonances obscured those of the heteroligand and therefore hindered structural assignment. Throughout this thesis bipyridyl deuteration has proved very valuable in structural elucidation, in particular in the novel pyrazole hydroquinone and dinuclear complexes.

The deuterium effect is discussed in terms of the electronic spectra and luminescent lifetimes of the Ru(II) complexes. Large increases (doubling in some cases) of the luminescent lifetime and quantum yield of emissions are observed. This is associated with the reduction of vibrational energy of the C-D stretching modes with respect to C-H, that are part of the bipyridyl acceptor modes in vibrational relaxation of the complex's excited state. The effect of deuterium substitution on the emissive behaviour of the complexes discussed, is described by the energy gap law (1), where the influence of the bpy vibrations and the molecular distortions they cause, are related directly to k_{nr}, the rate of non-radiative decay.

Interestingly, the complexes in which the heteroligand is triazine are not influenced by deuteration, lifetime and quantum yield remain essentially unchanged from their protonated analogues. This is associated with the fact that in these complexes the bpys act as spectator ligands, while the excited state rests on the triazine. This would suggest that deuteration, (with it s now simple synthesis) could be used as a convenient means of determining the site of the excited state in mixed ligand systems. It could be used alone or in conjunction with other techniques such as excited state pK_a or rRaman.

The influence of bpy deuteration is discussed in terms of electrochemistry, where no change is observed in the redox potentials of the metal based oxidations. Some change is observed however in the bipyridyls reduction, this change is small, but is proved unequivocally to exist. The temperature dependence of the deuterated complexes interestingly, show quite significant change in k_0, E_a and A values. The change in k_0 is anticipated since it is directly correlated with k_{nr}. The changes in particular in E_a suggest that deuteration of bpys is associated with changes in the ^{3}MLCT energy. That deuteration is capable of changing E_a, and A, suggests it is capable of influencing to some extent the photolability of a complex. This is particularly the case with $[(Ru(d_8\text{-}bpy)_2)(L8)]^{2+}$ where perdeuteration of bpy would seem to change the class of behaviour of the complex. From one with in which deactivation of from ^{3}MC is rapid relative to the back electron transfer from ^{3}MC to ^{3}MLCT to one where ^{3}MC and ^{3}MLCT state are in equilibrium and back electron transfer competes with deactivation from ^{3}MC. Such a difference should be manifested in the photochemistries of the two analogous compounds.

6.5 References.

[1] J.B. Birks, Photophysics of Aromatic Molecules, Wiley Interscience, Chichester, 1970.

[2] J. van Houten, R.J. Watts, *J. Am. Chem. Soc.*, 97, 13, 3843, 1975.

[3] J. van Houten, R.J. Watts, *J. Am. Chem. Soc.*, 98, 16, 4853, 1976.

[4] H. Yersin, D. Braun, Chem. *Phys. Lett.*, 179, 85, 1991.

[5] P. Huber, H. Yersin, *J. Am. Chem. Soc.*, 97, 12705, 1993.

[6] P. Huber, H. Yersin, H. Wiedenhofer, *Coord. Chem. Rev.*, 132, 35, 1994.

[7] D. Braun, P Huber, J. Wudy, J. Schmidt, H. Yersin, *J. Phys. Chem.*, 1994, in press.

[8] D.P. Strommen, P.K. Mallick, G. D. Danzer, R. S. Lumpkin, J.R. Kincaid,

[9] G.D. Danzer, J.R. Kincaid, *Spring. Proc. Phys.*, Ed. H. Takahashi, 68, 117, 1992.

[10] P.K. Mallick, G.D. Danzer, D.P. Strommen, J.R. Kincaid, *J. Phys. Chem.*, 92, 5628, 1988.

[11] G.D. Danzer, J.A. Golus, D.P. Strommen, J.R. Kincaid, *J. Raman, Spect.*, 1, 21, 1990.

[12] M.K. De Armond, M.L. Myrick, *Acc. Chem. Res.*, 22, 364, 1989.

[13] R. Hage, J.H. van Diemen, G. Ehrlich, J.G. Haasnoot, D.J. Stufkens, T.L. Snoeck, J.G. Vos, J. Reedijk, *Inorg. Chem.*, 29, 988, 1990.

[14] H. Hughes, Ph.D. Thesis, Dublin City University, 1993.

[15] M.J. Cook, A.P. Lewis, G.S.G. McAuliffe, V. Skarda, A.J. Thomson, J.L. Glasper, D.J. Robbins, J. Chem. Soc., Perkin Trans. II, 1293, 1984.

[16] S. Chirayil, R.P. Thummel, Inorg. Chem., 28, 813, 1989.

[17] J.V. Casper, T.D. Westmorland, G.H. Allen, P.G. Bradley, T.J. Meyer, W.H. Woodruff, *J. Am. Chem. Soc.*, 106, 3492, 1984.

[18] W. Siebrand, *J. Chem. Phys.*,46, 440, 1967.

[19] W.Siebrand, *Chem. Phys.*, 55, 5843, 1971.

[20] G. Dujardin, S. Leach, *Faraday Discuss.* 75, 23, 1983.

[21] E.M. Kober, J.V. Casper, R.S. Lumpkin, T.J. Meyer, *J. Phys. Chem.*, 90, 3722, 1986.

[22] E.M. Kober, T.J. Meyer, *Inorg. Chem.*, 21, 3967, 1982.

Chapter 7

Final remarks and Future work.

The work in this thesis may conveniently be split into several categories, firstly, an investigation into new synthetic methods for creation of hydroquinone and quinone pyridyltriazole ligands, and an examination into the intramolecular processes the addition of these, and phenolic, electroactive moieties cause in the ruthenium polypyridyl complexes they produce. In particular, investigation of these complexes is carried out with a view to determining whether the properties they possess merit portrayal of these complexes as abiotic systems capable of mimicking, and therefore perhaps shedding light on, some of the unit functions of the photosynthesis. Employing hydroquinone and phenolate ligands attached to strong σ-donor ligands the creation and characterisation of a series of novel O,N coordinated mono and dinuclear complexes was undertaken. The most important results bearing in mind this work outline were.

(i) Electrochemically induced intramolecular proton transfer in $[Ru(bpy)_2(H_2L1)]^+$.
$[Ru(bpy)_2(H_2L1)]^+$, through electro and spectroelectrochemical experimentation was found to exhibit a reversible, electrochemically induced proton transfer between a hydroquinone hydroxyl and the adjacent triazole ring. This transfer would seem to occur intramolecularly across a H-bridge between the hydroquinone and triazole. This process may viewed as a simple model of the protonmotive cycle in the photosynthetic centre.

(ii) Intramolecular electron transfer in Ru(II) pyridyl triazole complexes containing phenolate, hydroquinone and quinone moieties.
At high pH slow intramolecular electron transfer was observed in these complexes. These transfers are associated with reductive quenching of the Ru(III)-$(bpy^-)^*$ excited state by the pendent phenolate, anionic hydroquinone or semiquinone species formed at high pH from the neutral ligands. These electron transfers are particularly interesting since they occur between the excited ruthenium centre and pendant quenching groups on remote

The work in this thesis may conveniently be split into several categories, firstly, an investigation into new synthetic methods for creation of hydroquinone and quinone pyridyltriazole ligands, and an examination into the intramolecular processes the addition of these, and phenolic, electroactive moieties cause in the ruthenium polypyridyl complexes they produce. In particular, investigation of these complexes is carried out with a view to determining whether the properties they possess merit portrayal of these complexes as abiotic systems capable of mimicking, and therefore perhaps shedding light on, some of the unit functions of the photosynthesis. Employing hydroquinone and phenolate ligands attached to strong σ-donor ligands the creation and characterisation of a series of novel O,N coordinated mono and dinuclear complexes was undertaken. The most important results bearing in mind this work outline were.

(i) Electrochemically induced intramolecular proton transfer in $[Ru(bpy)_2(H_2L1)]^+$.
$[Ru(bpy)_2(H_2L1)]^+$, through electro and spectroelectrochemical experimentation was found to exhibit a reversible, electrochemically induced proton transfer between a hydroquinone hydroxyl and the adjacent triazole ring. This transfer would seem to occur intramolecularly across a H-bridge between the hydroquinone and triazole. This process may viewed as a simple model of the protonmotive cycle in the photosynthetic centre.

(ii) Intramolecular electron transfer in Ru(II) pyridyl triazole complexes containing phenolate, hydroquinone and quinone moieties.
At high pH slow intramolecular electron transfer was observed in these complexes. These transfers are associated with reductive quenching of the $Ru(III)\text{-}(bpy^-)^*$ excited state by the pendent phenolate, anionic hydroquinone or semiquinone species formed at high pH from the neutral ligands. These electron transfers are particularly interesting since they occur between the excited ruthenium centre and pendant quenching groups on remote

spectator ligands. These electron transfers appear to occur via the triazolate bridge most likely via hole transfer mechanism. The result is a stable charge separated state which from transient absorption spectra appears to exist for several microseconds. Significantly, these electron transfer processes persist at cryogenic temperatures, and exhibit minimum temperature dependence at all but the lowest temperatures.

This means that these complexes may indeed be regarded as simple abiotic models for photosynthesis. This is particularly true of $[Ru(bpy)_2(H_2L1)]^+$ which exhibits a reversible intramolecular proton transfer involving a hydroquinone moiety, It exhibits light induced intramolecular electron transfer leading to a stable, long lived charge separated state, and proton transfers.

(iii) Novel O,N coordinated complexes as possible solar sensitiser material.

The creation of novel O,N coordinated complexes, which are photostable, possess a wide visible absorbance range, and are emissive at both room and cryogenic temperatures. Literature reports of O,N coordinated complexes are relatively uncommon, and all such mononuclear species reported to date do not exhibit luminescence either at ambient or low temperatures. This makes these complexes strong candidates as sensitisers in solar cells, with one important exception, as a result of the cathodically shifted metal oxidations in these complexes they cannot be applied in the current Graetzel cell.

(iv) O,N coordinated dinuclear complexes with triazolate and hydroquinone bridges.

Like their mononuclear analogues, these species absorbance over a wide visible range, and are emissive at both room and cryogenic temperatures. They show considerable K_c values but for different reasons; the $[(Ru(bpy)_2)_2(HL2)]^{3+}$ complex is totally asymmetric and exhibits weakly coupled class II behaviour. $[(Ru(bpy)_2)_2(L8)]^+$ as a result of the intervening hydroquinone bridge, exhibits strong metal-metal coupling in what remains a class II complex. Strong metal-ligand orbital mixing and possibly interaction of negative hydroxylate groups, enhance the super-exchange (electron-hole) transfer process in

$[(Ru(bpy)_2)_2(L8)]^{2+}$. One of the most interesting findings of these investigations has been the increase of emission intensity on oxidation of $[(Ru(bpy)_2)_2(L2)]^{3+}$ to its mixed valence analogue, to date no other reports of such a phenomena have been made for a class II complex.

(v) Deuteration of bipyridyl as a means of determining the location of the excited state.

A novel one-pot synthesis of d_8-bipyridyl is described as well as the influence deuteration has over the excited state of a $[Ru(d_8\text{-}bpy)_2(LL)]^{n+}$ complex. Complexes in which the bipyridyl possesses the excited state electron and those in which bpy is a spectator ligand were prepared. Deuteration of a ligand responsible for the excited state causes a significant increase in luminescence lifetime and quantum yield as a result of the decreased energy of the C-D vibration in the non-radiative decay pathway. It was observed that for complexes in which bpy directly participates in the excited state deuteration caused these increases in radiative behaviour, yet no change in behaviour was observed in complexes where the heteroligand possesses the LUMO. Bipyridyl deuteration would therefore appear to be a straightforward means of determining the source of the LUMO in mixed ligand complexes.

The results described here have also raised a number of questions and suggested experiments which should be addressed in the future;

I One of the major concerns regarding chapter 3 is the nature of the quenching moieties for the complexes at high pH, this is particularly relevant for $[Ru(bpy)_2(L3)]^+$ which is thought to be semiquinone, and the nature of the intermediates in the charge separated state. Transient absorption spectroscopy suggests that the for $[Ru(bpy)_2(L1)]$ the intermediate is predominantly semiquinone and quinone for $[Ru(bpy)_2(L3)]^+$. EPR spectroscopy, therefore, is a vital experiment for elucidation of the nature of the quenching species.

II The catecholate ligand H_3L6 possesses two coordinating sites one N,N in nature and one O,O. Both mononuclear complexes have been prepared, and have been found to possess considerably different properties. Employing $[Ru(bpy)_2(H_2L6)]^+$ this complex has the potential to act as a bridging species in a variety of mixed metal supramolecular complexes, as a result of the remarkable coordinating ability of the catecholate. In fact preliminary experiments in which controlled concentrations of Fe(III) were added to a sample of $[Ru(bpy)_2(H_2L6)]^+$ suggest that binding readily occurs.

III. Verification of the nature of $[Ru(bpy)_2(HL7)]^+$ requires EPR. It is thought from ^{1}Hnmr and electrochemistry of this complex that the hydroquinone is in a semiquinone state. This could be confirmed quite simply employing EPR.

IV Spectroelectrochemistry of $[Ru(bpy)_2(HL8)]^+$ suggests that the first oxidation potential is the $Ru^{(III)/(II)}$ couple and by inference it was assumed that this was the case for $[Ru(bpy)_2(HL7)]^+$ and $[Ru(bpy)_2(HL9)]^+$. Verification of this assignment could be made from the electrochemistry of the Os analogues of these complexes. Preliminary studies on $[Os(bpy)_2(HL8)]^+$ show that what is assigned as the metal couple is cathodically shifted and that the Os in air is in the 3+ state. This corroborates the assigned electrochemistry, however further work is required.

V For $[((Ru(bpy)_2)_2(L8)]^{2+}$ the Kaim interpretation appears to be largely non-applicable to these systems. However, the extent of ligand-metal orbital mixing in the mixed valence complex is of interest. Resonance Raman and transient resonance Raman and EPR, are techniques which should provide interesting insight into the M-M interaction of this complex.

VI Attempts at the preparation of $[((Ru(bpy)_2)_2(L9)]^{2+}$ were made, however, unlike $[((Ru(bpy)_2)_2(L8)]^{2+}$ as a result of isomer formation, this complex requires time consuming purification. The IT properties of this complex, as a result of the asymmetry induced by steric hindrance, and hence orbital discontinuity, are expected to be different to $[((Ru(bpy)_2)_2(L8)]^{2+}$. A comparative study of $[((Ru(bpy)_2)_2(L8)]^{2+}$ and

$[((Ru(bpy)_2)_2(L9)]^{2+}$ should provide valuable insight into the influence of orientation on electron transfer properties in mixed valence complexes.

Appendices

Appendix I One-pot synthesis of bpt and elucidation of a novel bpt-hydroquinone co-crystal.

The synthesis of H_3L1 is described in chapter 3, section 3.2.1. Direct reaction of this ligand with $Ru(bpy)_2Cl_2$ had for some time been found to result in the formation of two mononuclear and one dinuclear complexes[1]. Apart from $[Ru(bpy)_2(H_2L1)]^+$ the remaining monomer and the dimer were assigned as O,N coordinated species. However, absence of appropriate electrochemistry, electronic properties, and the fact that the same complex is a biproduct when the catechol ligand H_3L6 was prepared in an analogous manner to H_3L1, were compounded when preparation of the deuterated complex verified that the O,N complexes are not the unknown. Furthermore, preparation of $[Ru(bpy)_2(H_2L1)]^+$ directly from the deprotected ligand produced only one product. The mononuclear and dinuclear complexes occurred as a result of the presence of an impurity formed as a side-product during ligand synthesis.

Initial difficulty in recognising this fact came as a result of the ^{1}Hnmr spectra of this ligand, which exhibited no extra discernible shifts as a result of impurity. What was evident, however, was that the integration of the peaks was incorrect (figure A1.1). This side product was isolated from the hydroquinone synthesis and analysed. Mass spectra, melting point, and comparative IR were carried out, combined with the ^{1}Hnmr of the unknown and deuterated unknown mononuclear complex. From this it was concluded that the unknown ligand was either dpa or bpt (figure A1.2).

Synthesis of dpa (dipyridylazine) was subsequently carried out by reaction of equimolar volumes of hydrazine monohydrate and 2-pyridinecarboxaldehyde. This immediately ruled out this ligand as the unknown, since the C-H protons appearing at around 2-3 ppm were absent in the unknown ligand, also the mass spectra and IR did not correlate. Furthermore, the properties of the resulting complexes were totally dissimilar.

---

[1] R. Wang, Ph.D thesis, D.C.U, 1991.

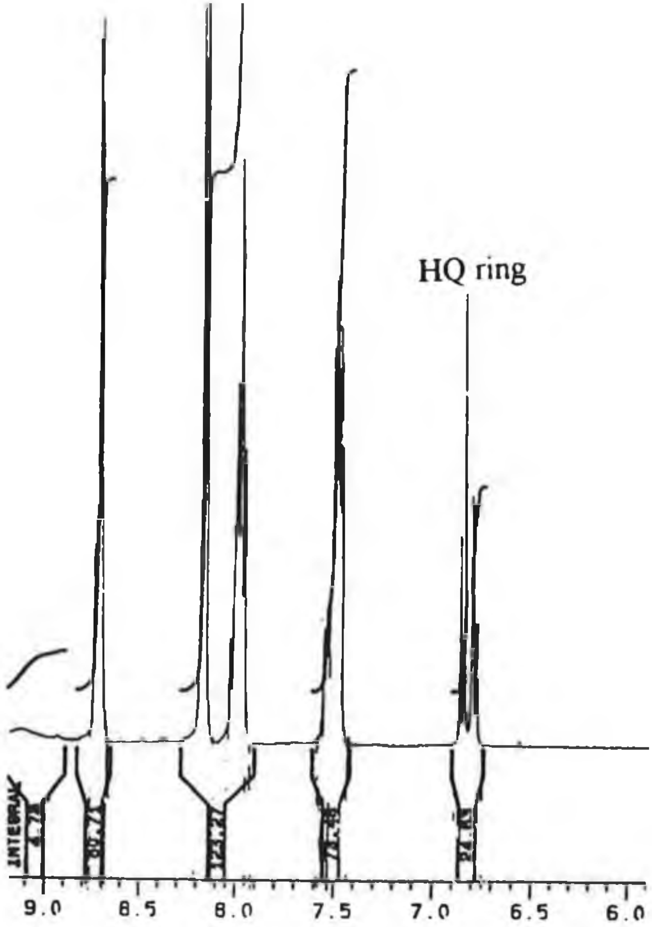

Figure A1.1. ^{1}Hnmr of product from hydroquinone synthesis

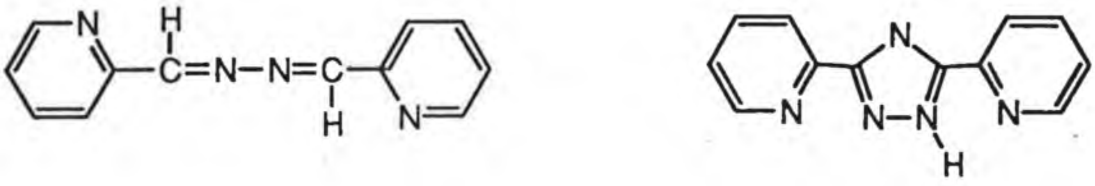

dpa **bpt**

Figure A1.2. Structures of dpa and bpt ligands.

Therefore, the side product from the hydroquinone ligand synthesis was determined to be bpt, with one problem, although the mass spectra was correct for bpt (with a molecular ion of 223.086), the C.H.N analyses was too high in C and H and the ^{1}H nmr for the unknown exhibited a broad (4H) singlet at approximately 6.5 ppm, which is absent in bpt, also the melting point of the unknown material was extremely sharp but 5^{o}C too high for bpt. These problems were resolved by the crystallography of a single crystal of the side-product material.

Isolation of a single crystal of the isolated side-product was obtained by slow cooling of a dilute solution of the material in hot ethanol/water (1:1, v/v). The result of crystallographic analyses is shown in figure A.1.4. A co-crystal which had formed between residual hydroquinone and the reaction side product bpt, showing some remarkable H-bonding features. Other reports of co-crystals have been made[2]. The structure, from its melting point exhibits remarkable stability as a result of these H-bridges there are three points of H-bonding observed for each unit. One between the triazole proton and a hydroxyl oxygen, two between the O-H and pyridyls the two types of H-bridge occurring in two different planes. There is also electrostatic interaction of π-electron density between the hydroquinone and bpt as a result of intermolecular stacking of pairs of molecules. The result is the beautiful three dimensional herring bone pattern shown in figure A.1.4, with the crystallographic data appended to the end of appendix I. The strength of this structure was such that ^{1}Hnmr of the compound at different dilutions showed no response of the OH proton, and as described the melting point is sharp and high.

From crystal structure therefore, absolute verification of the formation of bpt was obtained. Formerly, the synthesis of the bpt ligand involved several steps and by refining this side reaction, the process may be reduced to one step. The hydroquinone synthesis is inefficient as a result of low yields for the hydrazinolysis of the hydroquinol ester. The result is that on addition of the hydroquinol hydrazide to the methyl-2-picolinimidate, unreacted hydrazide is available to react with the picolinimidate, to produce III shown in scheme A1.1. It was observed that cyclisation of H_3L1 in a beaker without solvent lead to the production of a basic, ammonical smelling gas, (whereas only H_2O is expected) and

---

[2] C.B. Aakeroy, K.R. Seddon, Chem. Soc. Rev. 397, 1993.

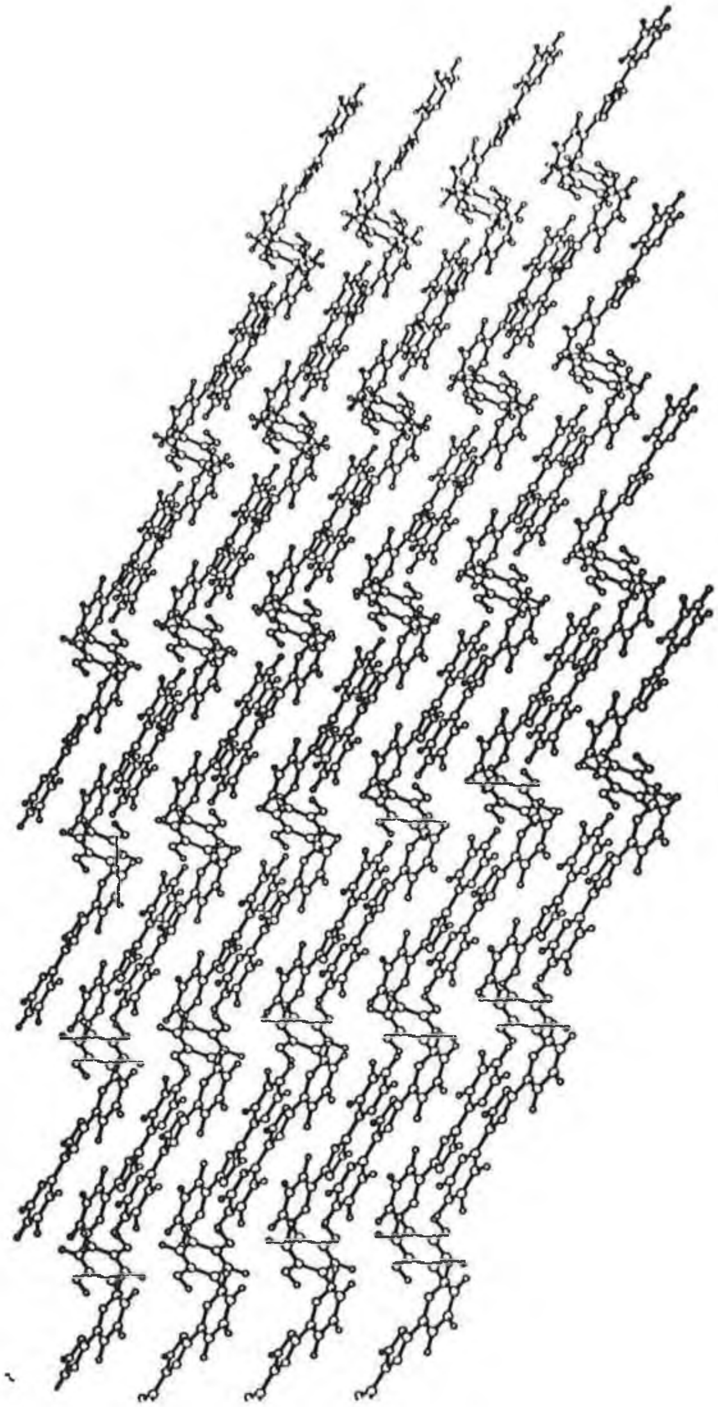

Figure A1.4. Repeating structure of the hydroquinone-bpt co-crystal.

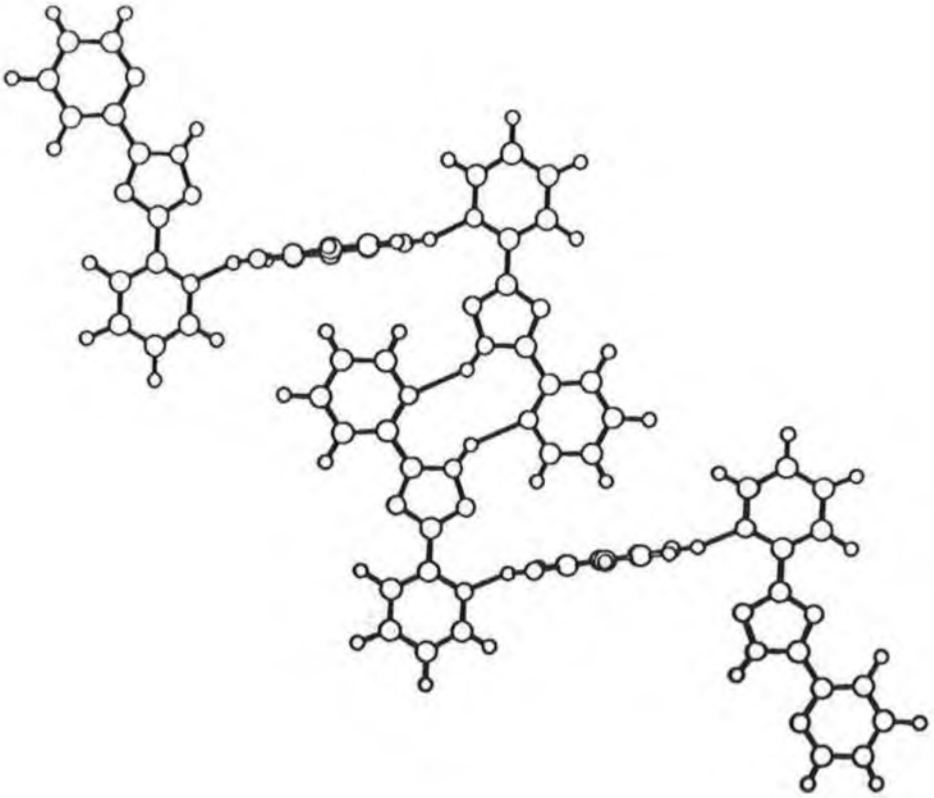

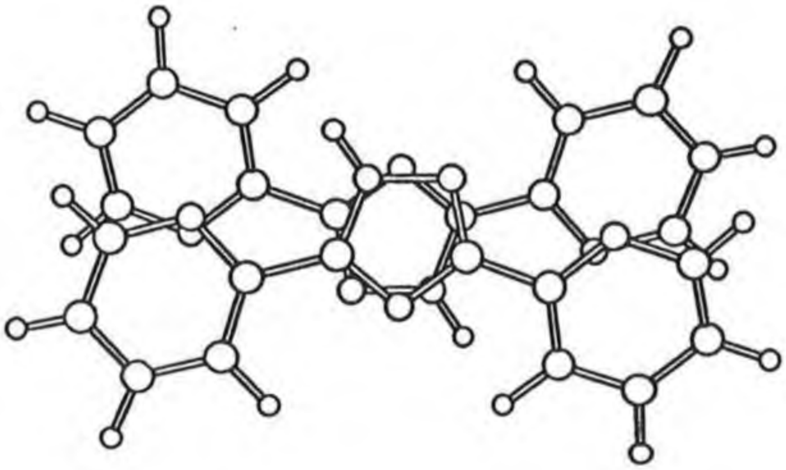

Figure A1.4. Unit cells showing interaction between the hydroquinone and triazole and π-packing between the triazoles, in the hydroquinone-bpt co-crystal.

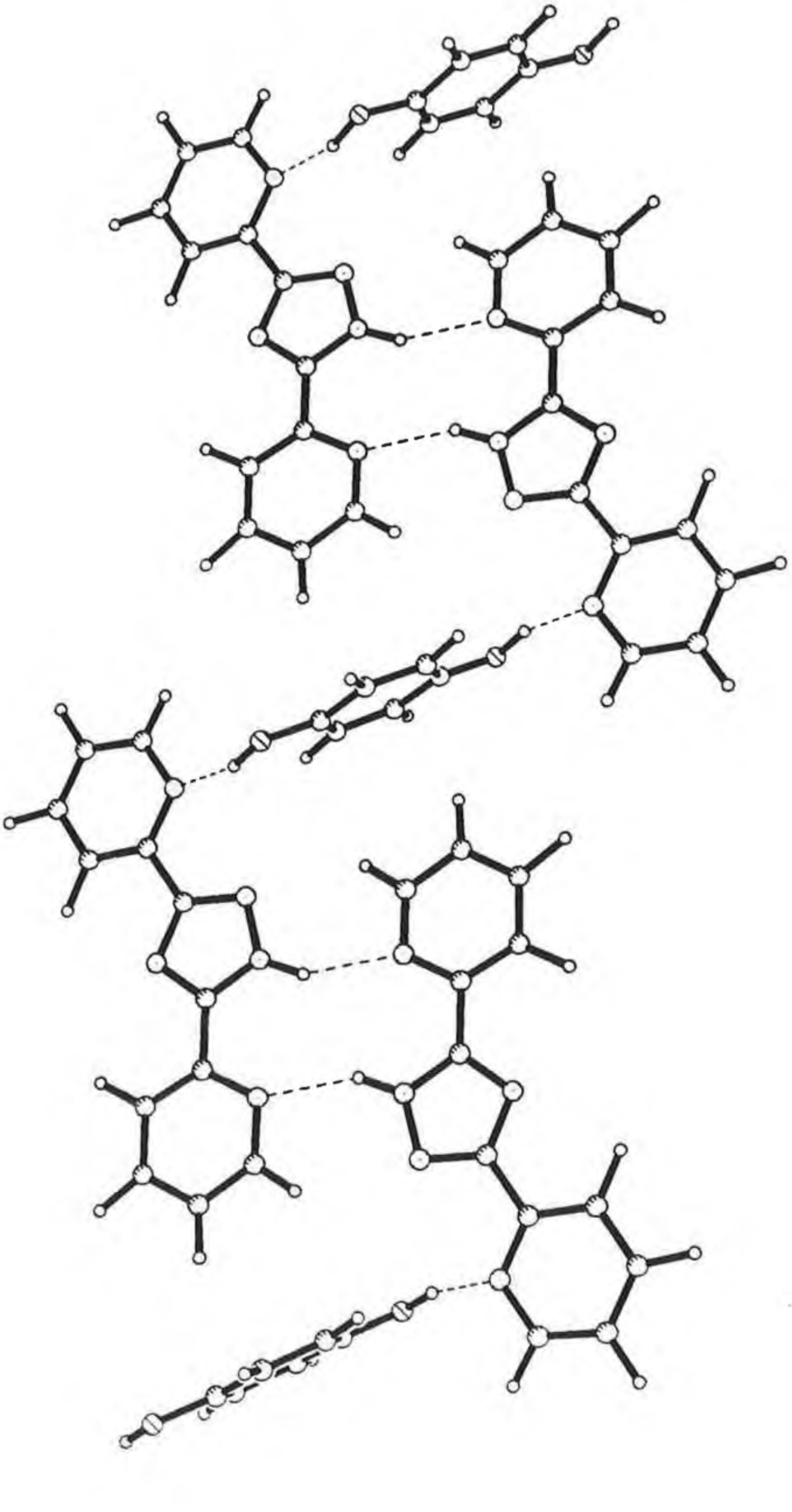

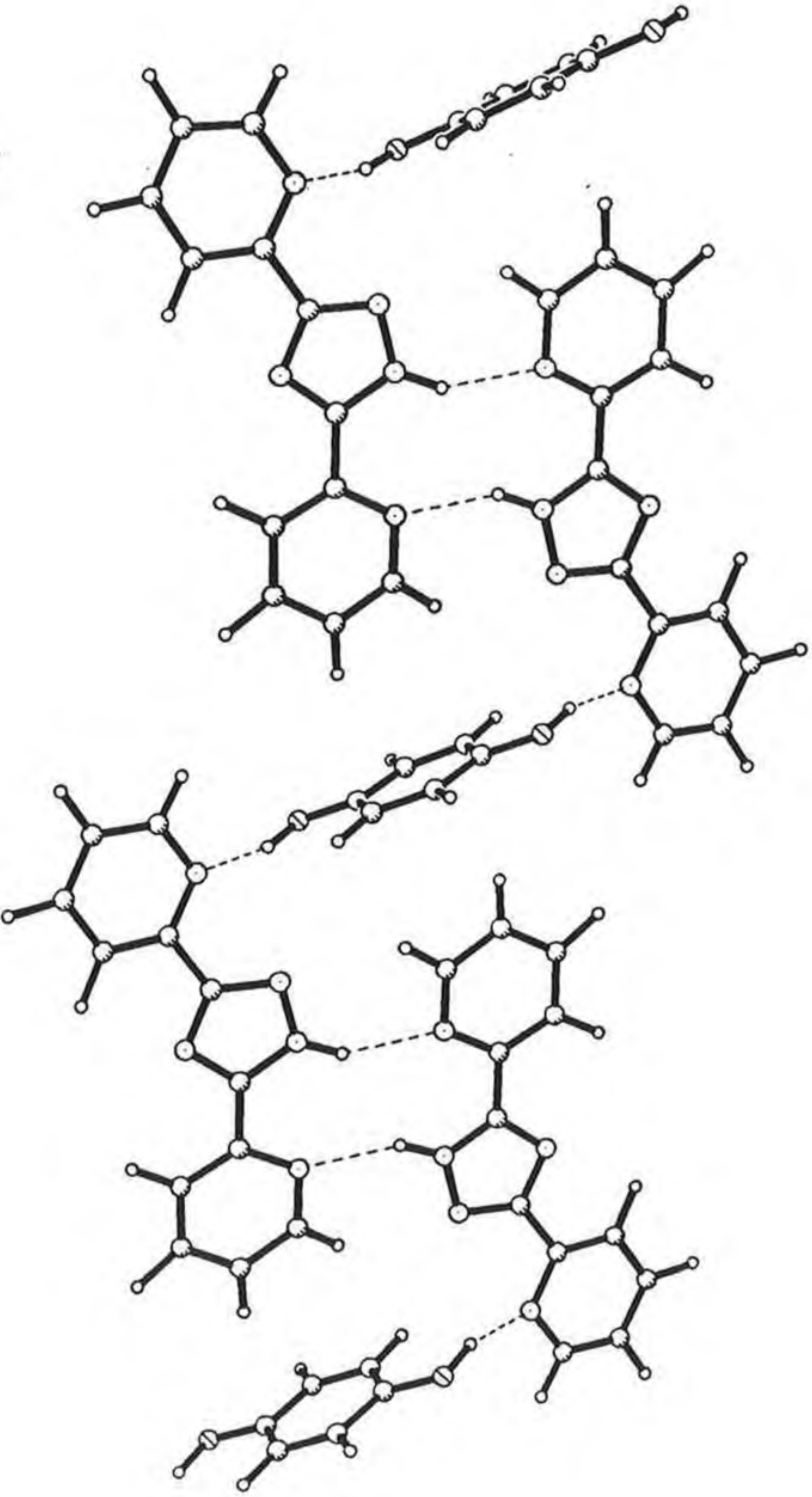

Table 1. Crystal data and structure refinement for 1.

Identification code	bptdub
Empirical formula	$C_{15}H_{12}N_5O$
Formula weight	278.30
Temperature	293(2) K
Wavelength	0.71073 Å
Crystal system	Triclinic
Space group	P-1
Unit cell dimensions	a = 7.3220(10) Å α = 105.060(10)^{o} b = 7.6710(10) Å β = 92.140(10)^{o} c = 13.2160(10) Å γ = 110.000(10)^{o}
Volume	667.03(14) Å^3
Z	2
Density (calculated)	1.386 Mg/m^3
Absorption coefficient	0.093 mm^{-1}
F(000)	290
Crystal size	0.34 x 0.19 x 0.65 mm
θ range for data collection	2.92 to 25.00^{o}
Index ranges	$0 \le h \le 8$, $-8 \le k \le 8$, $-15 \le \ell \le 15$
Reflections collected	2513
Independent reflections	2312 (R_{int} = 0.0150)
Refinement method	Full-matrix least-squares on F^2
Data / restraints / parameters	2312 / 0 / 190
Goodness-of-fit on F^2	1.037
Final R indices [$I>2\sigma(I)$]	R1 = 0.0478, wR2 = 0.1069
R indices (all data)	R1 = 0.0757, wR2 = 0.1234
Largest diff. peak and hole	0.165 and -0.221 eÅ^{-3}

Table 1. Crystal data and structure refinement for 1.

Identification code	bptdub
Empirical formula	$C_{15}H_{12}N_5O$
Formula weight	278.30
Temperature	293(2) K
Wavelength	0.71073 Å
Crystal system	Triclinic
Space group	P-1
Unit cell dimensions	a = 7.3220(10) Å α = 105.060(10)° b = 7.6710(10) Å β = 92.140(10)° c = 13.2160(10) Å γ = 110.000(10)°
Volume	667.03(14) $Å^3$
Z	2
Density (calculated)	1.386 Mg/m^3
Absorption coefficient	0.093 mm^{-1}
F(000)	290
Crystal size	0.34 x 0.19 x 0.65 mm
θ range for data collection	2.92 to 25.00°
Index ranges	$0 \leq h \leq 8$, $-8 \leq k \leq 8$, $-15 \leq \ell \leq 15$
Reflections collected	2513
Independent reflections	2312 (R_{int} = 0.0150)
Refinement method	Full-matrix least-squares on F^2
Data / restraints / parameters	2312 / 0 / 190
Goodness-of-fit on F^2	1.037
Final R indices [$I>2\sigma(I)$]	R1 = 0.0478, wR2 = 0.1069
R indices (all data)	R1 = 0.0757, wR2 = 0.1234
Largest diff. peak and hole	0.165 and −0.221 $eÅ^{-3}$

Table 2. Atomic coordinates [x 10^4] and equivalent isotropic displacement parameters [$Å^2$ x 10^3] for 1. U(eq) is defined as one third of the trace of the orthogonalized U_{ij} tensor.

	x	y	z	U(eq)
C(1)	1395(3)	5512(3)	3898(2)	45(1)
C(2)	898(4)	3582(3)	3325(2)	55(1)
C(3)	1104(4)	3140(4)	2272(2)	59(1)
C(4)	1727(4)	4632(4)	1818(2)	58(1)
N(5)	2191(3)	6510(3)	2348(2)	47(1)
C(6)	2040(3)	6922(3)	3385(2)	37(1)
C(7)	2629(3)	8978(3)	3987(2)	37(1)
N(8)	3607(3)	10410(3)	3598(1)	44(1)
N(9)	2269(3)	9554(2)	4994(1)	40(1)
N(8')	3874(3)	12002(3)	4425(1)	42(1)
C(7')	3073(3)	11471(3)	5247(2)	37(1)
C(6')	3079(3)	12819(3)	6260(2)	37(1)
N(5')	3830(3)	14726(3)	6343(2)	44(1)
C(4')	3818(4)	15948(3)	7269(2)	51(1)
C(3')	3093(4)	15360(4)	8125(2)	50(1)
C(2')	2336(4)	13412(4)	8027(2)	49(1)
C(1')	2330(3)	12111(3)	7080(2)	45(1)
C(1S)	5118(4)	9118(3)	774(2)	47(1)
C(2S)	3407(4)	9395(3)	537(2)	43(1)
C(3S)	3289(4)	10287(3)	-237(2)	47(1)
O(4S)	1790(3)	8798(3)	1032(1)	58(1)

Table 4. Anisotropic displacement parameters [$Å^2 \times 10^3$] for 1.

The anisotropic displacement factor exponent takes the form:

$-2\pi^2$ [$(ha^*)^2U_{11}$ + ... + $2hka^*b^*U_{12}$]

	U11	U22	U33	U23	U13	U12
C(1)	47(1)	30(1)	52(1)	12(1)	7(1)	7(1)
C(2)	53(2)	36(1)	70(2)	17(1)	5(1)	9(1)
C(3)	54(2)	34(1)	78(2)	2(1)	0(1)	14(1)
C(4)	68(2)	47(2)	52(2)	0(1)	11(1)	21(1)
N(5)	57(1)	37(1)	43(1)	7(1)	11(1)	14(1)
C(6)	36(1)	31(1)	41(1)	9(1)	7(1)	10(1)
C(7)	41(1)	31(1)	38(1)	11(1)	6(1)	12(1)
N(8)	58(1)	29(1)	37(1)	7(1)	9(1)	9(1)
N(9)	47(1)	31(1)	39(1)	11(1)	9(1)	11(1)
N(8')	59(1)	25(1)	38(1)	10(1)	10(1)	9(1)
C(7')	40(1)	31(1)	39(1)	11(1)	5(1)	10(1)
C(6')	38(1)	32(1)	39(1)	10(1)	4(1)	11(1)
N(5')	55(1)	30(1)	40(1)	8(1)	12(1)	10(1)
C(4')	66(2)	33(1)	46(2)	6(1)	15(1)	12(1)
C(3')	55(2)	45(2)	42(1)	5(1)	10(1)	15(1)
C(2')	54(2)	48(2)	42(1)	13(1)	11(1)	16(1)
C(1')	51(2)	39(1)	45(1)	16(1)	9(1)	11(1)
C(1S)	59(2)	46(1)	39(1)	16(1)	4(1)	20(1)
C(2S)	54(2)	38(1)	33(1)	8(1)	10(1)	14(1)
C(3S)	53(2)	48(1)	42(1)	14(1)	4(1)	18(1)
O(4S)	63(1)	66(1)	55(1)	29(1)	22(1)	25(1)

Table 3. Bond lengths [Å] and angles [°] for 1.

C(1)-C(6)	1.381(3)	C(1)-C(2)	1.388(3)
C(2)-C(3)	1.371(4)	C(3)-C(4)	1.378(4)
C(4)-N(5)	1.344(3)	N(5)-C(6)	1.343(3)
C(6)-C(7)	1.471(3)	C(7)-N(8)	1.329(3)
C(7)-N(9)	1.355(3)	N(8)-N(8')	1.361(2)
N(9)-C(7')	1.326(3)	N(8')-C(7')	1.342(3)
C(7')-C(6')	1.463(3)	C(6')-N(5')	1.348(3)
C(6')-C(1')	1.385(3)	N(5')-C(4')	1.337(3)
C(4')-C(3')	1.382(3)	C(3')-C(2')	1.372(3)
C(2')-C(1')	1.382(3)	C(1S)-C(2S)	1.378(3)
C(1S)-C(3S)#1	1.392(3)	C(2S)-O(4S)	1.372(3)
C(2S)-C(3S)	1.386(3)	C(3S)-C(1S)#1	1.392(3)

C(6)-C(1)-C(2)	119.0(2)	C(3)-C(2)-C(1)	118.9(2)
C(2)-C(3)-C(4)	118.4(2)	N(5)-C(4)-C(3)	124.1(2)
C(6)-N(5)-C(4)	116.7(2)	N(5)-C(6)-C(1)	122.9(2)
N(5)-C(6)-C(7)	117.4(2)	C(1)-C(6)-C(7)	119.7(2)
N(8)-C(7)-N(9)	114.9(2)	N(8)-C(7)-C(6)	122.7(2)
N(9)-C(7)-C(6)	122.4(2)	C(7)-N(8)-N(8')	101.9(2)
C(7')-N(9)-C(7)	103.2(2)	C(7')-N(8')-N(8)	110.3(2)
N(9)-C(7')-N(8')	109.7(2)	N(9)-C(7')-C(6')	125.6(2)
N(8')-C(7')-C(6')	124.7(2)	N(5')-C(6')-C(1')	123.0(2)
N(5')-C(6')-C(7')	117.2(2)	C(1')-C(6')-C(7')	119.8(2)
C(4')-N(5')-C(6')	116.8(2)	N(5')-C(4')-C(3')	123.8(2)
C(2')-C(3')-C(4')	118.7(2)	C(3')-C(2')-C(1')	119.0(2)
C(2')-C(1')-C(6')	118.8(2)	C(2S)-C(1S)-C(3S)#1	120.6(2)
O(4S)-C(2S)-C(1S)	122.5(2)	O(4S)-C(2S)-C(3S)	118.2(2)
C(1S)-C(2S)-C(3S)	119.3(2)	C(2S)-C(3S)-C(1S)#1	120.1(2)

Symmetry transformations used to generate equivalent atoms:

#1 -x+1,-y+2,-z

Table 5. Hydrogen coordinates (x 10^4) and isotropic displacement parameters ($Å^2$ x 10^3) for 1.

	x	y	z	U(eq)
H(1)	1307(3)	5914(3)	4794(2)	54
H(2)	339(4)	2509(3)	3806(2)	66
H(3)	690(4)	1605(4)	1802(2)	71
H(4)	1900(4)	4360(4)	1020(2)	70
H(8')	4550(3)	13341(3)	4417(1)	51
H(4')	4317(4)	17439(3)	7402(2)	61
H(3')	3068(4)	16434(4)	8810(2)	60
H(2')	1941(4)	12966(4)	8806(2)	58
H(1')	1733(3)	10498(3)	7012(2)	55
H(1S)	5305(4)	8534(3)	1382(2)	57
H(3S)	1965(4)	10447(3)	-385(2)	57
H(4S)	2136(3)	8181(3)	1604(1)	70

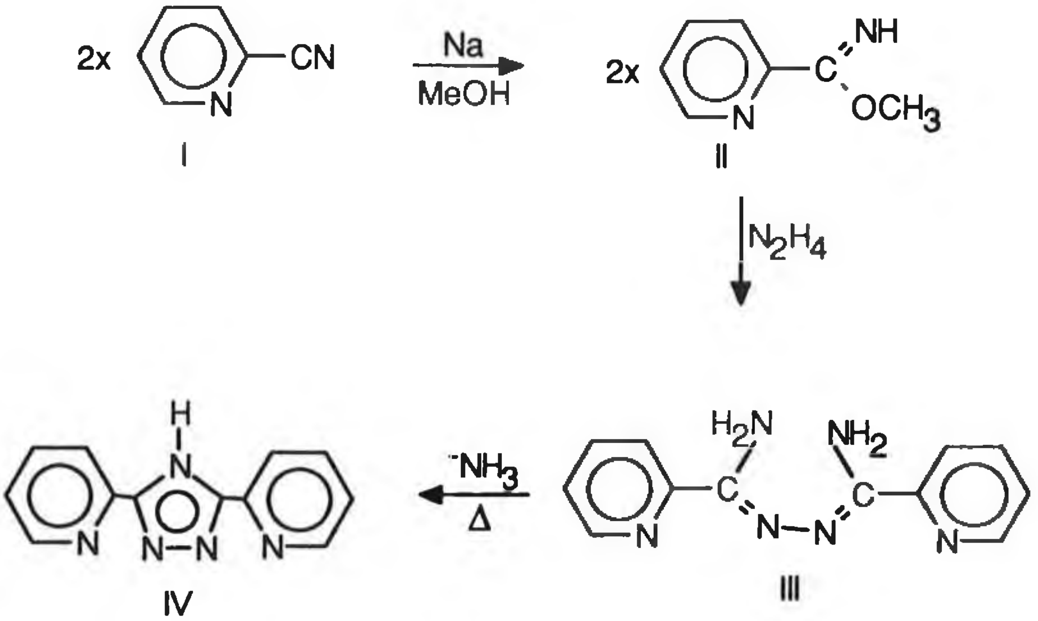

Scheme A1.1, suggested scheme for synthesis of bpt.

This scheme was tested by attempting the synthesis of bpt as suggested in this scheme, by reacting 2 molar equivalents of methyl-2-picolinimidate with hydrazine in methanol. The result was a bright yellow solid, which was collected and cyclized dry in a beaker at 200°C. The result was a greater than 80% yield of bpt. This method is a considerable improvement on the original method which was, as described multi-step but also produced yields of around 26%[3].

---

[3] R. Hage, Ph.D thesis Leiden University, 1991.

Appendix II O,O coordinated catecholic complex.

The reaction leading to formation of [Ru(bpy)$_2$(H$_2$L6)], when carried out under basic condition, and under an inert atmosphere leads to the formation of [Ru(bpy)$_2$(o,oL6)], figure A.2.1.

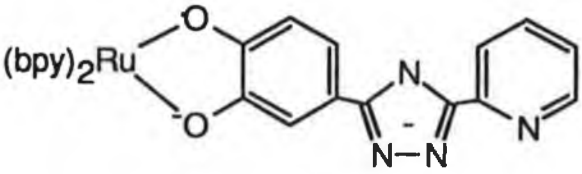

Figure A.2.1. [Ru(bpy)$_2$(o,oL6)]$^+$.

Structural elucidation of this complex is based mainly on C.H.N and electronic properties of these complexes, which will be discussed. ^{1}Hnmr studies were made impossible by the extensive broadening of the bands in the region 7.0 to 9.4 ppm, undoubtedly caused by the presence of paramagnetic species. The complex was deemed pure by both elemental[4] and HPLC analyses. The elemental analyses, and IR did not indicate the presence of counter-ion, implying the complex is neutral. This correlates well with the observed NMR, since the catecholate complex in the presence of either a Ru(III) centre or semiquinone would be expected to carry no charge. It is therefore also apparent that the triazole in this complex must be deprotonated. The infrared spectra of [Ru(bpy)$_2$(o,oL6)], carried out in KBr exhibits a peak at 1464 cm^{-1}, which is characteristic of coordinated semiquinone[5]. This indicates that the paramagnetic interference in the ^{1}Hnmr is not simply a paramagnetic impurity. The paramagnetic nature of the complex, is however, difficult to define. Catecholates as a result of their strong σ-donor ability (because of their high

---

[4] Anal. calc. for [RuC$_{33}$H$_{23}$N$_8$O$_2$.2H$_2$O]; C, 56.57; H, 3.88; N, 15.99 %. Anal. found C, 56.37; H, 3.88, N, 15.10 %.

[5] A.P.B. Lever, P.R. Auburn, E.S. Dodsworth, M. Haga, W. Liu, M. Melnik, W.A. Nevin, J. Am. Chem. Soc., 110, 8076, 1988.

basicity), will stabilise the higher oxidation states of coordinated metals. As a result of the extensive mixing of metal and ligand orbitals[6] in such complexes, it is expected that the resonance structures (A.2.1) apply as a more accurate description of the molecule, (where SQ = semiquinone, and Cat = catecholate).

$$[Ru^{(II)}(bpy)_2SQ] \longleftrightarrow [Ru^{(III)}(bpy)_2Cat] \qquad (A2.1)$$

Where contributions from both Ru(III) and the semiquinone radical are responsible for the paramagnetism observed in the ^1H nmr of $[Ru(bpy)_2(o,oL6)]$.

This complex, is dark brown in colour and its electronic spectra exhibits two absorptions in the visible region. Figure A.2.2, shows the visible spectra of $[Ru(bpy)_2(o,oL6)]$ in neutral acetonitrile.

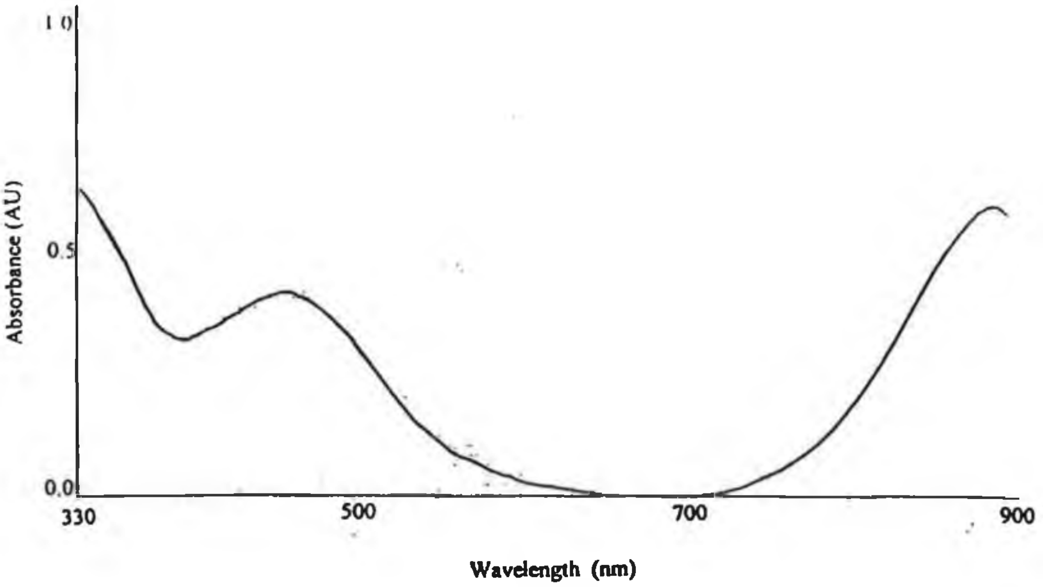

Figure A.2.2. Electronic absorption spectra of $[Ru(bpy)_2(o,oL6)]^+$ in neutral MeCN.

In neutral media λ_{max} is an intense absorbance at 895 nm with a second visible absorbance observed at 460 nm. In order to ascertain the nature of these transitions

---

[6] A.P.B. Lever, H. Masui, R.A. Metcalfe, D.J. Stufkens, E.S. Dodsworth, P.R. Auburn, *Coord. Chem. Rev.*, 125, 317, 1993.

resonance Raman spectra was carried out. Figure A.2.3 (a) and (b) show the resonance Raman spectra for [Ru(bpy)$_2$(o,oL6)] excited at 840 and 457.9 nm respectively. By exciting at these wavelengths Raman active vibrational features relating to the sites responsible for the visible absorbances at these wavelengths are expected to be enhanced. The spectrum resulting from excitation at 457.9 nm shows peaks marked * all corresponding to bipyridyl vibrations and the transition at 460 nm is therefore assigned as a Ru(dπ)-bpy(π*), MLCT transition. The spectra obtained at 840 nm is entirely different with the more important peaks observed at 531 (s), 587 (s), 1061 (w) and 1121 (w) cm^{-1}. Comparison with reports of resonance Raman on similar O,O coordinated catechol Ru(bpy)$_2$ complexes, reveal that the features observed are very similar[7]. The lower energy bands at 531 and 587 cm^{-1} are assigned as Ru-O stretching modes. Similar bands observed by Lever and co-workers[6] were found to be coupled to ring deformation modes of a coordinated semiquinone. Therefore, the strong band at 895 nm is assigned as a Ru(dπ)-sq(3b$_1$), where 3b1 is essentially a semiquinone π* level, its position and intensity correlate well with other related complexes[5].

[Ru(bpy)$_2$(o,oL6)],exhibits acid-base behaviour which is reflected in the absorption spectra in a red-shift of the two visible absorbances to 640 and 424 nm respectively. These spectral changes appear to be reversible when low concentrations of acid are used (pH 4 or 5).

[Ru(bpy)$_2$(o,oL6)] exhibits a very weak emission at 658 nm (ϕ_{em} = 4.35 x 10^{-4}),when excited with light of λ <460nm, which possess a lifetime of less than 80 ns in degassed acetonitrile. Structured emission is observed at 77K at 617 nm with a lifetime of 4140 ns. The excitation spectra for this emission correlates adequately with the absorbance at 465 nm. The short-lifetime and weak intensity of this process is most likely associated with intramolecular quenching of the excited state by the semiquinone which is strongly

---

[7] D.J. Stufkens, Th.L. Snoeck, A.B.P. Lever, *Inorg. Chem.*, 27, 953, 1988.

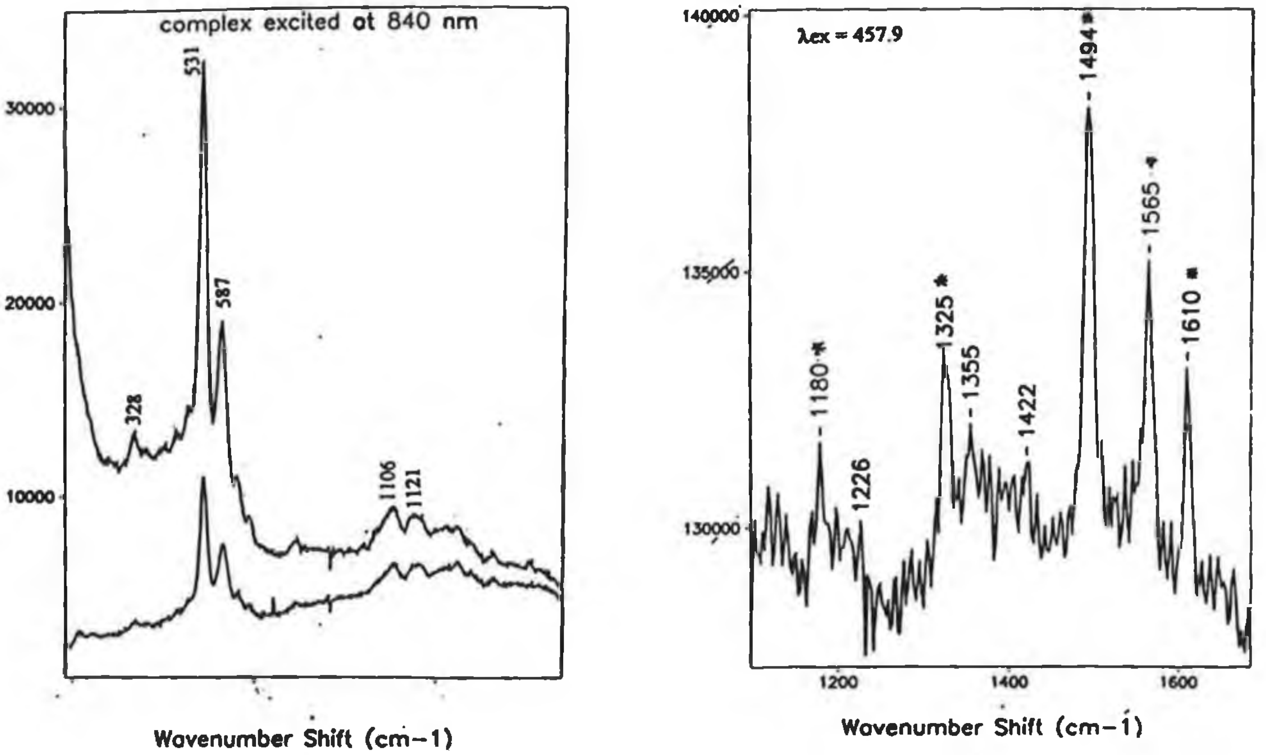

*Figure A2.3 Resonance raman of [Ru(bpy)$_2$(o,oL6)] in acetone excited at (a) 840 nm and (b) 457.9 nm * = bpy vibrations.*

temperature dependent. Protonation of the complex causes almost complete extinction of emission properties.

Temperature dependent luminescent behaviour was studied and analysed according to methods described in the preceding chapters. The following data were obtained, E_a = 1067 cm^{-1}, A = 3.42 $x10^{11}$ s^{-1}, k_o = 1.19 $x10^7$ s^{-1}. These results indicate that the population of a ^{3}MC state which is in equilibrium with the reverse electron transfer to ^{3}MLCT state.

The electrochemistry of [Ru(bpy)$_2$(o,oL6)] is shown in figure A.2.3.

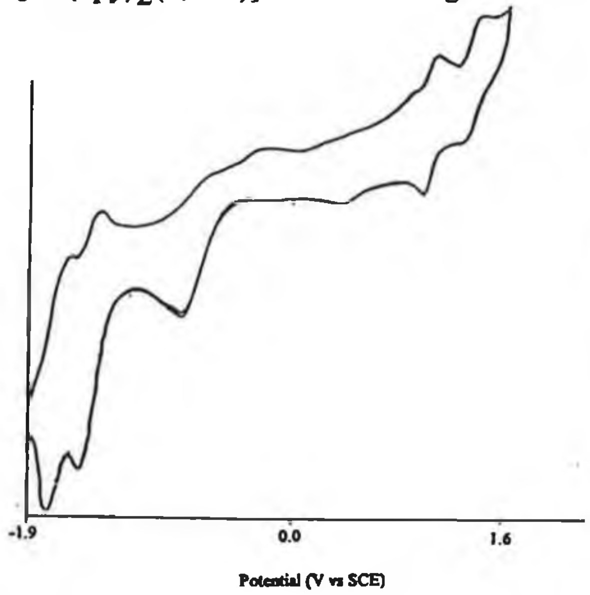

Figure A.2.3. Cyclic voltammogram of [Ru(bpy)$_2$(o,oL6)]$^+$ in neutral MeCN.

Two reversible bipyridyl reductions are observed at -1.49 and -1.82 V (vs SCE). The reversible metal (Ru$^{(III)/(II)}$) oxidation is observed at 1.04 V ($E_{1/2}$ = 0.982V). This immediately implies that the coordinating catechol is not in the catecholate state, since as with the O,N coordinated monomers described in chapter 4, the Ru$^{(III)}$ state would be stabilised under such circumstances. An oxidation is also observed at 1.40 V, which is thought to be ligand based, possibly associated with quinone formation. Application of cathodic potential to [Ru(bpy)$_2$(o,oL6)] from 0V (i.e. without prior oxidation) shows an irreversible reduction at 0.845V, which is most likely associated with the SQ $\rightleftharpoons$ Q couple. Thus further verifying that the complex is in the semiquinoid state.

From the data above it can be concluded that reaction of H_3L6 with $Ru(bpy)_2Cl_2$ creates a neutral O,O coordinated complex,$[Ru(bpy)_2(o,oL6)]$, in which the ligand exists in the semiquinoid state. The semiquinone is presumably stabilised by the low oxidation state of the ruthenium in this complex, as evidenced by the anodic oxidation potential of the $(Ru^{(III)/(II)})$ relative to the O,N coordinated complexes of the preceding chapters. The complex exhibits acid-base characteristics, presumably associated with the triazole and possibly also the catechol. It also exhibits a low intensity and short lived emission, which exhibits moderate temperature dependence. That the emission is weak suggests that the semiquinone is quenching the excited state.